# Anatomie et physiologie des voies de sortie du cervelet chez le rongeur

Hind Baba Aïssa

PSL
UNIVERSITÉ PARIS

THÈSE DE DOCTORAT
DE L'UNIVERSITÉ PSL

Préparée à l'École Normale Supérieure

# Anatomie et physiologie des voies de sortie du cervelet chez le rongeur


Soutenue par
**Hind BABA AÏSSA**


Le 1er avril 2021

Ecole doctorale n° 158
**ED3C**

Spécialité
**Cerveau, Cognition, Comportement**

Composition du jury :

| | |
|---|---|
| Laurent, BOURDIEU<br>DR-HDR, IBENS | *Président* |
| Isabelle, FEREZOU<br>CR-HDR, UNIC | *Rapporteur* |
| Sylvain, CROCHET<br>CR, EPFL | *Rapporteur* |
| Matilde, CORDERO-ERAUSQUIN<br>CR, INCI | *Examinateur* |
| Daniela, POPA<br>DR-HDR, IBENS | *Directeur de thèse* |
| Clément, LENA<br>DR-HDR, IBENS | *Directeur de thèse* |

ENS | PSL

# SOMMAIRE

*« Le plus beau des métiers, c'est de vivre sa passion. »*

*François Salvat de Montfort*

À Renée et Armand,
Le souvenir de votre affection et générosité guident chacun de mes pas.

# Remerciements

Je tiens tout d'abord à remercier les membres de mon jury de thèse, qui ont pris le temps (précieux en recherche) de lire ce manuscrit et de m'apporter leur expertise. En particulier je souhaite remercier mes deux rapporteurs Isabelle et Sylvain, qui ont lu ma thèse et rédigé leurs rapports en un temps record ! Laurent, merci d'avoir accepté d'être président du jury, mais aussi de ta gentillesse et de ton soutien pendant ces années passées à l'IBENS, qui m'ont été d'un grand secours. Merci à Matilde Cordero-Erausquin, qui a accepté de rejoindre ce jury malgré une notification de toute dernière minute.

Ce deuxième paragraphe de remerciement risque d'être le plus long, puisqu'il concerne mes deux directeurs de thèse, qui ont probablement été les acteurs principaux de ma thèse, Daniela et Clément. Avoir deux directeurs de thèse, surtout travaillant dans la même équipe, ce n'est pas commun, et aurait pu être la recette du désastre. Je suis heureuse de pouvoir dire que (malgré les nombreuses mises en garde), j'ai eu une chance infinie de bénéficier de ce co-encadrement. J'ai pu profiter des forces de chacun, de leur soutien et de leur confiance. Dans cette grande aventure humaine qu'est la thèse, dans les moments difficiles comme dans les moments exaltants, j'ai pu compter sur votre présence et je vous en remercie.

Je vais commencer par remercier Daniela, puisque le début de ma thèse a été principalement sous sa supervision. Dans ces débuts en recherche, pleins d'incertitudes, de découverte et d'apprentissage, tu as su encadrer mon enthousiasme, alléger mes angoisses et orienter mon projet. Tu as une force de travail et une capacité à optimiser les expériences qui m'ont inspiré et permis de démarrer ma thèse à grande vitesse. Tu n'as jamais fléchi dans la confiance que tu avais de mes capacités et dans ce projet, et ça m'a donné la force d'avancer. Dans les conférences, nationales ou internationales, ou dans les comités de thèse, tu as été ce visage souriant et encourageant auquel je me raccrochais quand je sentais l'incertitude monter, et je ne t'en remercierai jamais assez. Je retiendrais nos moments de fou rire, la joie que tu exprimais à chacune de mes réussites, les paroles encourageantes dans mes échecs et ton soutien sans faille. En particulier de ce moment en

début de troisième année, où tu m'as donné mon envol en mettant fin à nos réunions du lundi matin (tout en me gardant mon créneau au cas où), en me disant « tu es grande maintenant, tu gères très bien, mais je suis toujours là si tu as besoin. ». J'ai été très heureuse que tu sois ma directrice de thèse, et j'espère que nous continuerons à collaborer dans le futur !

S'il a toujours été présent, c'est surtout sur la seconde moitié de thèse que Clément est intervenu dans ma supervision. A ce moment où il fallait faire sens de la « terrachié » de datas produites (selon ton expression), tu m'as appris à former mon esprit scientifique, à exploiter la littérature et à fouiller mes données. Tu as su guider ma réflexion sans m'imposer la tienne, et tu as toujours eu à cœur de me pousser à toujours mieux faire, quitte à me mettre un coup de pied aux fesses de temps en temps ! Notamment à la fin de chacune de mes présentations, en me disant, « c'était parfait, mais on va revoir deux/trois choses », pour finir par détruire méthodiquement chacune de mes diapos (pour mieux les reconstruire !). Je te taquine avec cela, mais je t'en suis tellement reconnaissante. Tu ne m'as pas laissée me reposer sur mes acquis, mais tu avais la conviction que j'avais toujours la capacité de mieux faire. Tu n'as jamais été avare de ton temps que ce soit pour des discussions scientifiques, ou nos digressions de fin de journée à parler du monde, de la vie, de tout et de rien. Je te remercie de ta patience (notamment face à groumpf), de ton humanité, de ta main tendue dans les moments difficiles, et des moments de rire partagés. Je ne saurais jamais assez te dire combien nos discussions et ta confiance inébranlable en moi ont joué dans ce long parcours initiatique qu'est la thèse. Je suis heureuse d'avoir eu la chance de t'avoir pour directeur de thèse et j'espère que nous trouverons toujours le temps de parler de science, de la vie, de tout et de rien !

Je souhaitais adresser un salut particulier aux deux membres de mon comité de thèse, Sylvain Crochet et Dan Shulz. Avec gentillesse, ils ont au cours de ma thèse challengé ma réflexion et veillé à mon évolution. Je vous en remercie, ces comités de thèse ont été des moments charnières, et vos réflexions m'ont permis de pousser plus loin celle sur mon projet.

Il me faut aussi remercier l'ensemble de l'équipe NBC, ses membres présents comme ses membres passés. Au commencement il y eu Sébastien, mon binôme. A nous deux, nous

avons trouvé le POm et défriché l'ensemble de ce projet. Ça a été un plaisir de travailler avec toi. Il y eut aussi Julie, qui au début de ma thèse me fit partager son expérience et me soutint dans les moments difficiles. Je suis très chanceuse d'avoir pu travailler avec toi, un peu triste que tu sois partie, mais très heureuse de pouvoir toujours partager mes aventures au téléphone ! Il y a eu les cavalières de l'apocalypse aussi et nos fous rires qui ont égayé mon début de thèse. Je ne peux pas ne pas mentionner Aurélie, mon binôme, avec qui nous avons tout partagé pendant des années, notamment le « one drink and we go home ». Jimena, depuis ce premier congrès à Bordeaux où nous étions aussi perdues l'une que l'autre, notre amitié n'a cessé de croître, et j'ai adoré collaborer avec toi. Bérénice, que dire, nous avons le même grain de folie. Tu as été un soutien immense et une amie formidable. Il y aussi eu mes stagiaires, que j'ai eu un plaisir infini à encadrer : Andréa, Tim, Giovanni. Enfin, chaque membre de l'équipe, qui ont rendu ces années de thèse merveilleuses et pleines de fous rires, Thibault, Romain F et Romain S, Idriss, Nolwenn, Guillaume. Merci !

J'ai une pensée affectueuse pour les cérébelliqueux et la team de l'Apocalypski, Victor, Marie, Alan, Willou. Nos moments de folie et de discussion ont égayé ces années de thèse. Victor en particulier, merci de ces temps de chirurgie ponctué par des chansons disney chantées à tue-tête. Willou, comme tu le sais, nous aimons tous les deux l'oignon, alors au pas camarade !

Une thèse, c'est aussi une vie au sein d'un Institut, dont chaque membre contribue aux petits moments de bonheur. J'oublierai peut-être de tous vous nommer, mais chacun d'entre vous a contribué à rendre mon passage à l'IBENS plus agréable. De l'administration : Virginie, Béatrice, Karine, Julien, Olga, Nadège : merci de votre aide, efficacité et fous rires. De SPIBENS : Nora, Yves, Victor, pour cette énergie déployée à faire revivre l'association ! Gérard, pour ton humour et ta patience quand on venait se réfugier dans ton bureau, pour ta pédagogie et ta passion à nous enseigner l'électronique, je ne te remercierai jamais assez ! De même, Caroline, merci pour ta patience et ta gentillesse, je n'aurai probablement réussi autant de chirurgies sans ton aide ! Des partenaires de pause et de fins de journée chez Youssef : Ioana, Anthony, Dimitri, Souraya, Justine, Jérôme, Thierry, Nadia, merci pour tous ces moments partagés, pour toutes ces séances de bitchage et de célébration ! A mon

Allemand préféré et partenaire de conférence, Ludo, ainsi qu'à ses acolytes strasbourgeois, je tire mon chapeau, en espérant vous retrouver longtemps sur le chemin de la recherche !

Je ne peux pas parler de ma thèse sans remercier Youssef, Mangala et Yaya. Youssef, tu m'as accueilli les bras ouverts, tu nous as offert un refuge près du laboratoire, sans jamais de jugement. Tu as toujours été prêt à nous engueuler et à nous réconforter. Merci d'être qui tu es !

Des remerciements particuliers doivent aller à Pénélope, Lola et Léa. A travers nos dix ans d'amitié, nous avons aussi parcouru les études supérieures pour arriver au diplôme final. Merci de cette aventure, qui j'espère continuera longtemps. Vous êtes et avez toujours été mon petit cocon de bonheur, de rire et de confort dans les moments difficiles.

Enfin, je tiens à remercier ma famille, qui a supporté depuis presque 30 ans mes humeurs, mes passions, mes désespoirs et mes joies. En particulier, Maman, merci. Les mots ne suffisent pas à exprimer ce que je te dois et combien je t'aime. Je n'aurai pas réussi ce parcours là sans ton soutien sans faille, ton écoute et ta patience, ton aide en tous points. Faire des études supérieures est un privilège que vous m'avez offert et je vous en suis infiniment reconnaissante.

Enfin, je vais remercier les petits animaux qui ont aidé ma thèse. Mes chats, Loukoum et Cara, dont voir la petite bouille à la fin d'une dure journée a toujours été un bonheur. Enfin, à toutes les souris qui ont fait partie de mes expériences, et sans qui aucun des résultats de cette thèse n'auraient été possible.

# Avant-propos

Mon intérêt pour le cerveau remonte à mon adolescence, lorsque je découvris fascinée la psychologie de Freud, et son « interprétation des rêves ». Très vite, je perçus les limites de ce domaine, où toutes les théories se justifient par elle-même, à défaut d'un substrat scientifique solide. Plus tard, mes études me portèrent vers la biologie où je fis connaissance avec la physiologie humaine et animale, et les principes de base de la Neuroscience. La notion de potentiel d'action et de transmission électrique d'information entre neurones piqua mon intérêt, et me poussa à choisir plusieurs cours de neurosciences à l'Université de Chicago, au cours desquels un professeur nous parla des Brain Machines Interfaces (BMI). Ce fut comme une révélation, une plongée dans un monde proche de la science-fiction : les Hommes pouvaient contrôler des bras robotiques à l'aide d'électrodes implantées dans le cerveau ! Mais voilà, un problème majeur subsistait dans ce domaine : jusqu'à présent, il a été pratiquement impossible d'implémenter un retour sensoriel, rendant l'apprentissage de l'utilisation de ces interfaces extrêmement complexe. Je découvris alors le fossé existant dans les systèmes sensorimoteurs, entre la compréhension de l'exécution motrice, et celle de l'intégration sensorimotrice. Je fis connaissance alors plus avant avec les systèmes sensoriels et notamment celui des vibrisses du rongeur, et chemin faisant, mon chemin croisa celui du cervelet. Dans les grandes théories motrices du cervelet, à travers son rôle présumé de suppression des informations sensorielles attendues, je vis un moyen d'explorer un champ nouveau de connaissance. J'ai donc pu au cours de ma thèse commencer à comprendre l'implication du cervelet dans les processus sensoriels. Loin d'assouvir ma soif de connaissance, le nombre de questions soulevées à chaque début de réponse a aiguisé mon envie d'en savoir plus. J'ai aussi eu la chance au cours de cette thèse de découvrir le cervelet en lui-même, les nombreux champs d'étude dans lequel il est impliqué, et la communauté vibrante qui l'étudie. J'espère que le travail que je présente dans cette thèse traduira l'enthousiasme et la passion que j'ai éprouvé durant ces cinq années.

# Introduction générale

## 1 : Le cervelet

### 1.1 Histoire du cervelet et de sa fonction

Si le cerveau a toujours intrigué et que sa fonction est restée obscure jusqu'aux temps moderne, la neuroanatomie a très tôt nommé la plupart des structures cérébrales décelables à l'œil nu. Ainsi, les termes de *dura mater* et *pia mater* furent déterminés par les anatomistes Alexandrins du premier siècle de notre ère tels que Rufus et Ephesus, et conservés jusqu'à présent. Il est intéressant de noter que le cervelet lui, s'il a été identifié précocement comme une structure cérébrale définie, a connu plusieurs dénominations ('parencéphale' par Galien et Nicolo de Reggio, 'puppi' par Constantin l'Africain), avant de trouver son appellation commune de 'petit cerveau' dans les années 1500 avec Magnus Hundt (Voogd and De Zeeuw, 2020). Parmi les écrits historiques qui évoquent le cervelet, nous pouvons retenir en particulier ceux de Galien (129 AD – 200/216 AD), médecin et philosophe de la Rome antique et de ses multiples traducteurs qui construisirent leur vision du cerveau sur son travail, ainsi que ceux de Vesalius (1514 AD-1564 AD) anatomiste et médecin italien de la Renaissance, qui connaissant les travaux de Galien eut l'audace de critiquer nombre de ses conclusions, notamment sur l'anatomie du cervelet. Les premières observations du cervelet se firent chez les animaux, chez qui il n'est pas recouvert par le cortex et est donc observable par une dissection depuis le sommet du crâne. Galien le décrit ainsi comme occupant un espace allant de la position postérieure du foramen à la suture lambdoïde, description réfutée par Vesalius, qui ayant pratiqué la dissection du cerveau chez l'humain, avait pu observer que le cervelet n'occupait que la moitié de cet espace, jusqu'à la moitié de l'occiput (Glickstein, Strata and Voogd, 2009). La description anatomique du cervelet se fit de plus en plus précise à partir de la Renaissance, grâce à plusieurs facteurs : l'émergence de nouvelles techniques de dissection, telles que celles introduites par Constant Varole et consistant à observer le cerveau en passant par la base du crâne et non plus par le sommet (lui permettant de découvrir le *pons*, aussi appelé pont de Varolius); une plus grande liberté quant à la dissection humaine succédant au ban longtemps imposé par la religion catholique, avec l'émergence de chaires d'anatomie

médicale notamment dans les grandes universités italiennes ; un peu plus tardivement, au 19ème siècle, grâce à un recours accru à l'expérimentation animale et à l'anatomie comparée.

En dépit de détails anatomiques tâtonnants mais relativement exacts, ces auteurs antiques et modernes firent des prédictions étonnamment perspicaces quant à la fonction du cervelet (Schmahmann, 2016). Ainsi, Galien postulait que le cervelet donnait de la force aux nerfs moteurs, tandis que Nemesius et Albertus Magnus suggéraient que c'était un centre de la mémoire. Nous retrouvons encore Varolius qui émettait l'hypothèse que le cervelet contrôlait des fonctions sensorielles telle que la sensibilité inconsciente. Ce n'est qu'au début du 19ème siècle que la fonction du cervelet commença à réellement être comprise, notamment grâce à un recours accru à l'expérimentation animale. Ainsi en 1809, Luigi Rolando, inspiré par deux idées nouvelles de son époque : les contractions musculaires produites par des impulsions électriques décrites par Luigi Galvani et la création d'une batterie produisant de l'électricité par Alessandro Volta, procéda à l'ablation du cervelet d'une chèvre. Son idée était que la structure la plus proche d'une batterie de l'époque, avec son organisation en *folia*, en feuillets, était le cervelet. La cérebellectomie de la chèvre, exécutée avec des méthodes chirurgicales non stériles, produisit une paralysie de l'animal suivie rapidement de sa mort, conduisant Rolando à conclure que le cervelet était responsable de l'initiation du mouvement. Cette conclusion fut battue en brèche quelques années plus tard par Marie-Jean-Pierre Flourens, professeur de physiologie au Collège de France, qui observa que le mouvement restait possible sur les animaux privés de cervelet, même si la balance était fortement affectée. Il émit l'hypothèse neuve en physiologie que le cervelet ne serait pas responsable de l'initiation du mouvement, mais coordonnerait les « mouvements voulus par d'autres parties du système nerveux » (Coco and Perciavalle, 2015). Il fallut attendre la seconde moitié du 19ème siècle et l'utilisation accrue d'antiseptiques pour résoudre les problèmes de mortalité post-chirurgicale liés à l'expérimentation animale, afin de distinguer les symptômes dus à l'impact de la chirurgie de ceux liés à l'ablation du cervelet. Ainsi, l'intuition de Florens fut confirmée par Luigi Luciani en 1891, par son observation d'une triade de symptômes : asthénie, atonie et astésie, indubitablement d'origine cérébelleuse, chez un chien ayant survécu à une cérébellectomie. Dans le même temps, en 1894, le neuroscientifique espagnol et futur lauréat Nobel, Ramon y Cajal publia ce qui est considéré comme le premier livre référence de neuroanatomie, avec une description nette du cervelet et des cellules de Purkinje.

## 1.2. Anatomie et physiologie du cervelet

A partir des travaux de Cajal, une vision plus complète de l'anatomie très particulière du cervelet s'est construite. Il est intéressant de noter que le cervelet est une structure particulièrement conservée au cours de l'évolution et une caractéristique majeure du cerveau postérieur chez les vertébrés. Classiquement comparé au cerebrum, le cervelet, situé dans la partie postérieure du crâne, est généralement plus petit que le cerebrum, et adopte une forme de sphère plate. Il est retrouvé chez des vertébrés aussi loin phylogénétiquement de l'humain que la lamproie ou les poissons cartilagineux (**Figure 1.A.**). Les différences majeures entre les multiples classes de vertébrés concernent principalement l'apparition de nouvelles classes de neurones inhibiteurs, de plusieurs noyaux cérébelleux profonds, ainsi qu'une complexification des follicules cérébelleux et une extension du cortex cérébelleux, notamment en rapport avec l'évolution du cerebrum (Herculano-Houzel, 2010). Du fait de cette diversité, il convient ici de restreindre la description du cervelet à la classe des mammifères supérieurs, et plus spécifiquement les rongeurs, modèle animal le plus exploité en science (Hodos, 2009).

### 1.2.1 Histologie

#### 1.2.1.1 Phylogénie

Le cervelet du rongeur a l'avantage d'avoir globalement une anatomie externe typique de la plupart des mammifères. Ainsi, chez le rat et la souris, le cervelet est situé dans la fosse crâniale postérieure, formant le plafond du quatrième ventricule (**Figure 2.A**). Il est composé de deux hémisphères latéraux joints par le vermis, et a été historiquement subdivisé en trois lobes -antérieur, postérieur et flocculonodulaire (**Figure 2.B**). Il est attaché au tronc cérébral par trois paires de pédoncules cérébelleux, qui sont de larges réseaux de fibres, qui portent les afférents et efférents cérébelleux. Une des particularités du cervelet chez les mammifères supérieurs est de comprendre entre 50 et 80% des neurones du système nerveux central pour 10% de la masse totale, contre environ 20% de neurones pour 80% de la masse dans le cortex cérébral (*The Mouse Nervous System*, 2012).

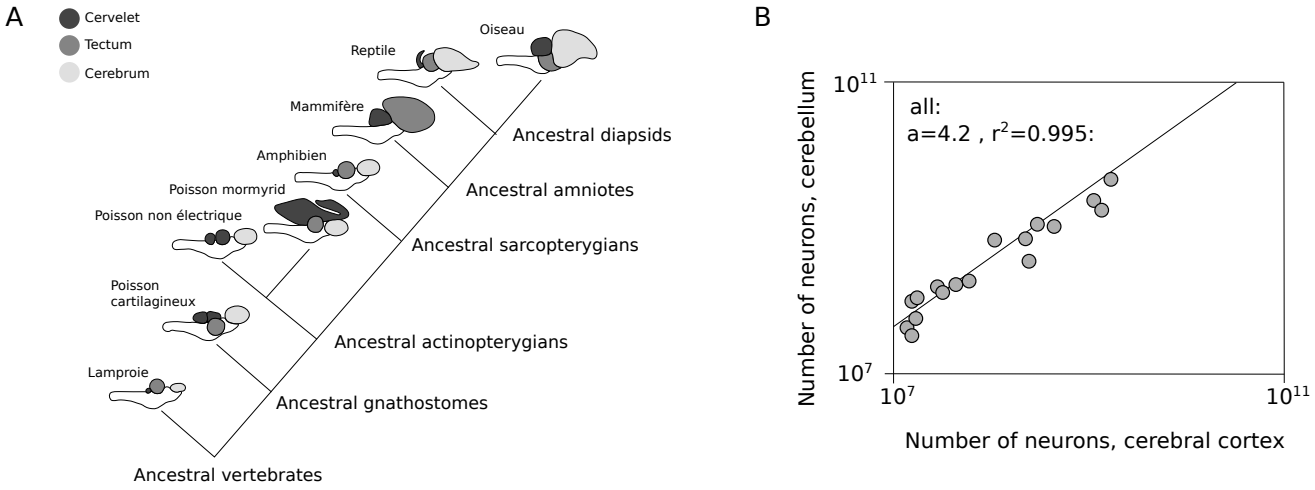


***Figure 1. Le cervelet dans l'évolution***

***A.*** *Cladogramme de l'évolution des vertébrés montrant le changement de forme et de taille du cervelet dans différentes classes de vertébrés. La représentation des cerveaux a été ramené à proportions équivalentes pour faciliter la comparaison de taille. (Reproduit de Hodos et al. 2009)*

***B.*** *Rapport proportionnel de l'évolution du nombre de neurones dans le cervelet et le cortex cérébral des mammifères. Le nombre de neurones dans le cervelet et le cortex cérébral covarie selon une fonction linéaire à travers toutes les espèces de mammifères. (Reproduit de Herculano-Houzel 2010)*

#### 1.2.1.2 Le cortex cérébelleux

L'apparence du cervelet présente des similarités avec celle du cerebrum. Sa division histologique classique présente deux compartiments : une surface en feuillets repliée en de nombreux follicules et fissures dénommée cortex cérébelleux et des noyaux cérébelleux profonds en-dessous (**Figure 2.C**).

La matière grise du cortex cérébelleux se subdivise en 3 couches à la différence du cortex cérébral qui en possède généralement 6 : une externe, la couche moléculaire, une intermédiaire, la couche de cellules de Purkinje, et une interne, la couche granulaire (**Figure 2.D**).

- La couche granulaire contient de très nombreuses cellules, les cellules en grain, densément disposées à la base du cortex cérebelleux. Ces petites cellules composent la majeure partie des neurones du cervelet et étendent leurs axones jusqu'à la couche moléculaire, où elles forment des fibres parallèles synapsant sur les dendrites des cellules de Purkinje, des cellules en étoile et cellules en panier. Les cellules de Golgi sont aussi trouvées dans cette couche granulaire, recevant des projections des fibres moussues, et projetant en retour des projections inhibitrices sur les dendrites des cellules en grain.

- La couche moléculaire quant à elle, regroupe principalement les axones des cellules granulaires et les dendrites des cellules de Purkinje. Elle est donc principalement synaptique, avec la présence en superficie de cellules inhibitrices : les cellules en étoile et les cellules en panier, qui font synapse respectivement dans une ou plusieurs bandes de cellules de Purkinje.
- La couche de cellule de Purkinje, qui a la spécificité d'être une couche mono-cellulaire de corps de cellules de Purkinje alignés. Ces cellules présentent une morphologie unique dans le système nerveux central, avec de denses arborescences dendritiques en 2D, organisées parallèlement au sein de la couche de Purkinje, ce qui a une importante incidence fonctionnelle. Les axones de ces cellules à transmission GABA projettent à travers la couche granulaire pour faire synapse dans les noyaux cérébelleux profonds.

#### 1.2.1.3 Les noyaux cérébelleux profonds

L'unique sortie du cortex cérébelleux est composée par les axones des cellules de Purkinje, venant se terminer dans les noyaux cérébelleux profonds (DCN). Cette projection GABAergique avec un fort tonus inhibe ainsi les cellules des noyaux profond (mais aussi vestibulaires, système non abordé ici). Ceux-ci sont au nombre de quatre paires, répartis ainsi sur un axe médio-latéral : le noyau fastigial, le noyau interposé antérieur et postérieur – chez l'humain composant deux noyaux distincts : le globose et l'emboliforme, et le noyau denté ou latéral. De plus, une partie des cellules de Purkinje projettent vers les noyaux vestibulaires. Si les Purkinje sont la seule sortie du cortex cérébelleux, les noyaux cérébelleux profonds et vestibulaires représentent la sortie de l'ensemble du cervelet. On observe notamment une convergence importante des cellules de Purkinje sur les neurones des noyaux profonds, estimée chez le chat à 26 pour 1 (Palkovits *et al.*, 1977) et 40 pour 1 chez la souris (Person and Raman, 2011).

- Le noyau fastigial (FN) est le plus médial des noyaux cérébelleux. Il reçoit des entrées du vermis et des afférents cérébelleux portant les informations vestibulaires, sensorielles proximales, auditrices et visuelles. Il projette en retour vers les noyaux vestibulaires, la formation réticulée et le thalamus.
- Le noyau interposé (IP), positionné latéralement par rapport au noyau fastigial, reçoit des entrées de la zone intermédiaire des hémisphères cérébelleux ainsi que des

afférents cérébelleux comprenant les informations spinales, somatosensorielles périphériques, auditrices, visuelles. Il projette au noyau rouge contralatéral et au thalamus.

- Le noyau denté (DN) est le plus latéral des noyaux cérébelleux profonds et reçoit pour sa part des projections depuis les hémisphères cérébelleux latéraux ainsi que des informations depuis le pons. Il projette vers le noyau rouge contralatéral ainsi que vers plusieurs zones du thalamus ventral.

Une caractéristique commune des DCN est la décharge spontanée de ses neurones, qui s'élève à plusieurs dizaines de Hertz in vivo comme in vitro, en l'absence d'entrée synaptique. Cependant, il existe une grande hétérogénéité au sein des neurones des DCN, tant en termes de morphologie que de propriétés électrophysiologiques. Les neurones des DCN ont au départ été classés en fonction de leur morphologie et de leur taille en six types différents, avant qu'une classification plus fonctionnelle émerge. Celle-ci se base sur les connexions et le type de neurotransmetteur des neurones, différentiant ainsi les petits et grands neurones de projection glutamatergiques, des petits neurones inhibiteurs (GABAergiques et glycinergiques) de circuiterie locale. Les neurones GABA présentent en moyenne une taille significativement inférieure à la population de neurones de projection glutamatergique. Dans leurs projections, les neurones GABA participent à la fois à un réseau d'inhibition local au sein des DCN, sous contrôle des cellules de Purkinje, mais aussi à une voie de projection inhibitrice vers l'olive inférieure. Les neurones de projection glutamatergiques constituent eux la voie de communication du cervelet vers le reste du système nerveux. Cependant, d'un point de vue électrophysiologique, les petites cellules glutamatergiques présentent des caractéristiques communes avec les neurones à transmission GABA, notamment celle de présenter une plus grande adaptabilité à la fréquence de stimulation (Uusisaari, Obata and Knöpfel, 2007). Les neurones de projection glutamatergiques quant à eux se présentent plutôt comme des traducteurs linéaires de la fréquence de décharge, comme il est généralement présumé dans les modèles de fonctionnement cérébelleux.

Cette entreprise de classification des cellules des DCN présente une importance non négligeable dans la conception du fonctionnement du cervelet. Ainsi, les DCN sont considérés dans les modèles de fonctionnement cérébelleux comme un simple relais, dont l'activité tonique est inhibée par les projections des cellules de Purkinje. Or, la présence de neurones

GABA locaux, qui reçoivent aussi des projections des Purkinje ouvre la possibilité qu'il existe un phénomène de désinhibition de populations spécifiques des DCN *via* l'activité des Purkinje, ouvrant un champ de complexité nouveau. De surcroît, les DCN constituent une zone d'intégration non négligeable, puisqu'ils reçoivent des entrées de tous les afférents cérébelleux, de la moelle épinière, du tronc cérébral et de l'olive inférieure, et les intègrent à l'activité des Purkinje pour constituer la voie de sortie du cervelet.

En sus de la description classique des zones de projection à la sortie du cervelet, ces dix dernières années ont aussi vu l'émergence de nouvelles zones de projection depuis ces noyaux cérébelleux profonds. Ainsi, il a été montré que ces trois noyaux projetaient en réalité tous dans de multiples zones du thalamus. Il a été démontré par exemple que le fastigial projette au thalamus dorsolatéral (Bohne *et al.*, 2019) ainsi qu'au thalamus médiodorsal (Çavdar *et al.*, 2014). Il est assez intéressant de voir qu'un effort d'identification des neurones *via* des marqueurs moléculaires fait apparaître différentes populations de neurones dans les DCN, dont les connections se font dans des circuits parallèles tant en regard des Purkinje qu'en regard de leurs projections en aval (Fujita, Kodama and Lac, 2020).

Il est à noter que l'intérêt de la communauté neuroscientifique a longtemps été portée sur le cortex cérébelleux et son organisation très stéréotypée, et assez peu sur les noyaux cérébelleux profonds. Cette organisation en un circuit à peu de types neuronaux (**Figure 3**) et reproduit dans tout le cortex cérébelleux suggérait que cette zone du cerveau serait la clé du lien entre computation neuronale et sortie comportementale. Cependant il apparaît de plus en plus évident que notre compréhension des mécanismes sous-tendant le fonctionnement du cervelet est limitée par notre méconnaissance des relations internes et externes du cervelet.

Ainsi, les efforts récents d'analyse des propriétés électrophysiologiques, moléculaires, morphologiques des noyaux cérébelleux profonds ouvre plusieurs champs d'investigation à approfondir pour faire évoluer notre compréhension du cervelet : 1 – quant à l'organisation précise des projections depuis le cortex cérébelleux vers les différents noyaux cérébelleux 2- regardant les différents types cellulaires présents au sein des noyaux cérébelleux 3- en regard des zones de projection des noyaux cérébelleux profond. L'organisation précédemment énoncée, si elle n'est pas erronée, offre une représentation partielle de la réalité de la cytoarchitecture de la sortie du cervelet. Comme nous le verrons dans la section liée à mes

résultats, je me suis attachée au cours de ma thèse à tenter de détailler les zones de projection des noyaux, et plus particulièrement celles du noyau latéral.

### 1.2.2 Organisation fonctionnelle du cervelet

L'organisation fonctionnelle du cervelet a été et est encore source de débat au sein de la communauté cérébelleuse, menant à plusieurs systèmes de classification fonctionnelle du cervelet abordés succinctement dans cette section. En dépit de cette variété de classification, le microcircuit du cortex cérébelleux est très similaire sur l'ensemble de la surface du cortex, avec des mécanismes physiologiques reproductibles et similaires qui constituent la base des théories cérébelleuses.

Une des organisations les plus anciennes est celle référant à l'ordre d'apparition phylogénétique des structures cérébelleuses. Elle se divise ainsi en 3 parties projetant chacune à un noyau cérébelleux (**Figure 2.B**).

- Le vestibulocervelet : Aussi appelé archéocervelet ou paléocervelet, il est composé du lobe flocculonodulaire ou lobule X, et assure les fonctions d'équilibre, de balance et d'orientation spatiale. Il reçoit des afférents vestibulaires primaires, ainsi que des entrées visuelles depuis le colliculus supérieur et le pons. Il projette majoritairement sur les noyaux vestibulaires.
- Le spinocervelet : composé du vermis et du paravermis, reçoit des entrées périphériques sensorielles et proprioceptives depuis la moelle épinière, et les noyaux trigéminaux. Il projette vers le noyau fastigial, qui en retour envoie des projections vers les structures du tronc cérébral impliquées dans la locomotion (formation réticulaire ventromédiale) et l'équilibre (noyaux vestibulaires). Il contacte aussi le noyau interposé antérieur qui fait la liaison avec le noyau rouge et le thalamus ventrolatéral, puis le cortex moteur.
- Le cérébrocervelet : composé des hémisphères latéraux du cortex cérébelleux, il est le plus récent dans l'évolution et reçoit principalement des entrées depuis le néocortex via le noyau pontique. Il projette ensuite vers le noyau rouge parvocellulaire ansi que sur les noyaux dentés bilatéraux, qui envoient en retour des projections ascendantes vers les aires corticales motrices primaires et secondaires.

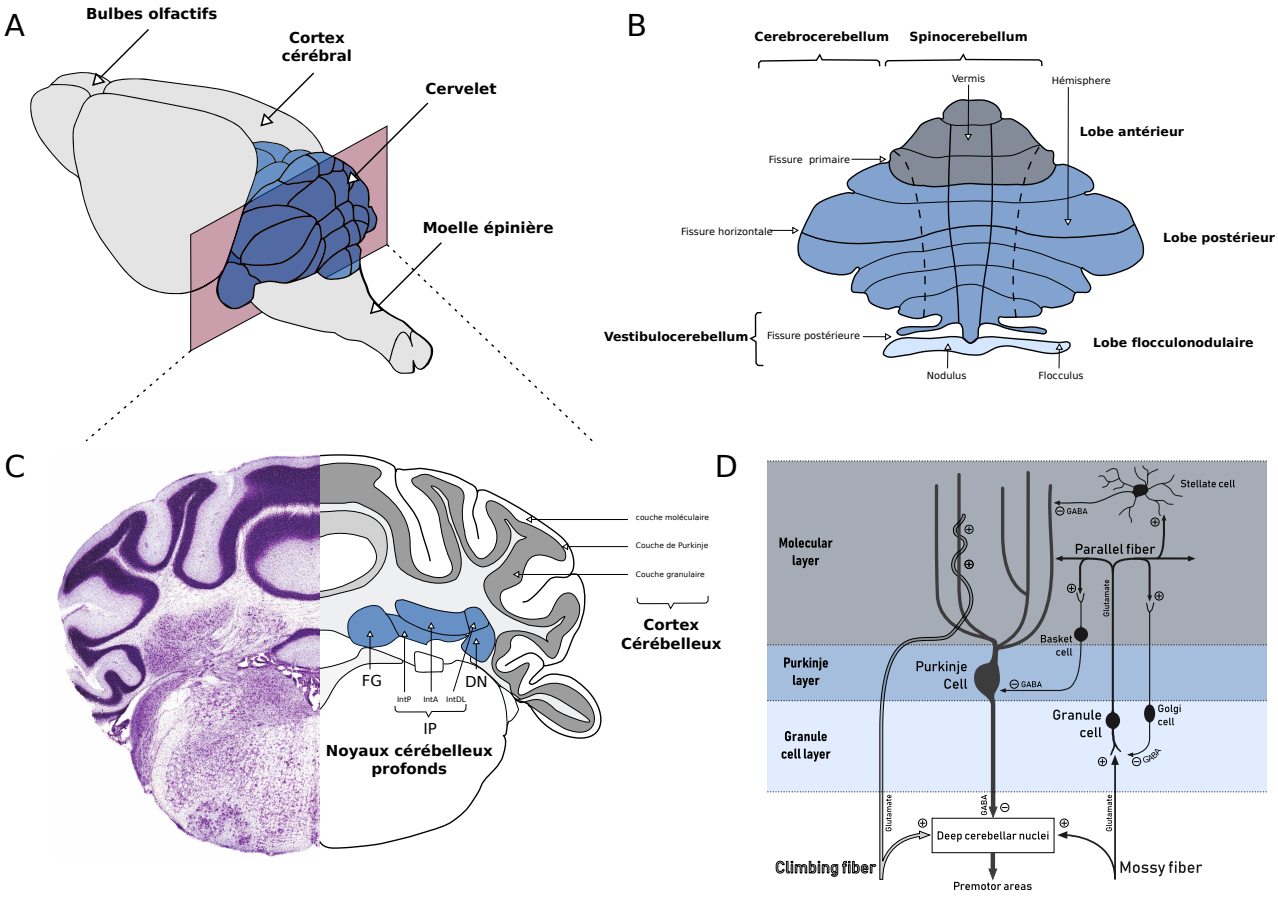


***Figure 2. Anatomie générale du cervelet***

***A.*** *Représentation des différentes parties d'un cerveau de souris. Le cervelet (en bleu) est positionné à l'arrière du cerveau, formant le plafond du 4$^{ème}$ ventricule. Sont aussi représentés les hémisphères du cortex cérébral, les bulbes olfactifs et le départ de la moelle épinière.*

***B.*** *Représentation de la surface du cervelet déroulée. Les hémisphères cérébelleux sont reliés par le vermis. A droite est représentée la délimitation initiale des lobes cérébelleux, définis anatomiquement par les 3 fissures les plus importantes du cervelet, les fissures primaire, horizontale et postérieure. Est aussi représentée la dénomination anatomo-fonctionnelle du cervelet. Le spinocervelet comprend le vermis et le paravermis, le cérébrocervelet comprend les hémisphères cérébelleux latéraux, tandis que le vestibulo-cervelet comprend le nodulus et le flocculus.*

***C.*** *Coupe coronale d'un cervelet murin. A gauche, révélation des structures anatomiques du cervelet à la teinture au Nissl. A droite, la délimitation présentée dans les atlas des principaux composants anatomiques du cervelet. En bleu sont représentés les trois noyaux cérébelleux profonds.* ***FG****= noyau fastigial aussi appelé noyau médian.* ***IP****= noyau interposé, avec ses multiples délimitations (****IntP****= interposé postérieur,* ***IntA****= interposé antérieur,* ***IntDL****= bosse dorsolatérale de l'interposé).* ***DN****= noyau denté aussi appelé noyau latéral. Le cortex cérébelleux suit des indentations appelées foliations, avec les couches moléculaire et granulaire en traçant le dessin. La couche de cellules de Purkinje, très fine se situe entre ces deux couches.*

***D.*** *Schéma du microcircuit du cortex cérébelleux, avec ses cellules principales et ses entrées/projections. Les fibres grimpantes (climbing fibers) et fibres moussues (mossy fibers) projettent à la fois au cervelet et aux noyaux cérébelleux profonds. Les fibres grimpantes synapsent directement sur les dendrites des cellules de Purkinje, tandis que les fibres moussues empruntent la voie passant par les cellules granulaires et éventuellement les interneurones de la couche moléculaire. Une convergence d'entrées excitatrices sur les cellules de Purkinje se fait via les fibres grimpantes et via la voie directe des cellules de granulaires. Les entrées inhibitrices sont indirectes via les cellules en panier (basket cells) et les cellules en étoile (stellate cells). Les cellules de Purkinje exercent ensuite une projection inhibitrice sur les noyaux cérébelleux profonds, qui contactent ensuite les structures prémotrices (et autres).*

Cette organisation fonctionnelle globale ne fait plus consensus au sein de la communauté cérébelleuse, notamment du fait de l'avancement des techniques d'électrophysiologie et de marquages biochimique et génétique. Ainsi, d'autres classifications existent, séparant le cervelet en module, zone et microzone (**Figure 3** et **Figure 4**). Ces organisations se sont, dans un premier temps, fondées sur les afférents sensoriels du cervelet.

Il existe deux sources d'entrées principales au cervelet : les fibres moussues et les fibres grimpantes. Les fibres grimpantes prennent origine dans l'olive inférieure, composée de plusieurs noyaux dans le tronc cérébral. Ceux-ci comprennent un vaste réseau de sous-noyaux dont les entrées ne sont pas toutes connues, mais incluant des projections indirectes depuis le néocortex (Allen and Tsukahara, 1974). Les zones longitudinales de cellules de Purkinje définies par ces entrées de fibres grimpantes sont la base de l'organisation modulaire du cortex cérébelleux définie notamment par Voogd et Bigarré, qui définit quatre grands modules du cortex cérébelleux, de A à D. Ces fibres grimpantes projettent à la fois au cortex cérébelleux et aux noyaux cérébelleux via des collatérales.

Les fibres moussues quant à elles peuvent être divisées en deux sous-groupes : une division majeure de ces fibres provient des noyaux pontiques, qui reçoivent elles-mêmes des projections depuis le néocortex via des collatérales du tractus pyramidal (Serapide *et al.*, 2001); l'autre division provient de la moelle épinière et des noyaux du tronc cérébral (Voogd and Ruigrok, 2012), incluant les noyaux trigéminaux et relayent les informations sensorielles directement depuis la périphérie. Ces fibres projettent aux cellules granulaires du cortex cérébelleux, qui en retour projettent aux cellules de Purkinje via les fibres parallèles.

L'étude séparée de ces deux sources d'entrées du cervelet a donné lieu à une multitude de classifications anatomo-fonctionnelles du cervelet. Il existe cependant une idée commune qui est celle d'une organisation modulaire du cervelet : celui-ci est décrit comme une répétition de microcircuits associés en parallèles, et formant des sous-unités fonctionnelles dans le traitement d'informations (Voogd, 2011). Les modules cérébelleux combinent les cellules de Purkinje avec les projections depuis l'olive inférieure et vers les noyaux cérébelleux profonds qui leur sont associés (**Figure 4.A**). Au sein de ces modules, les zones parasagittales désignent la partie corticale des modules cérébelleux : ces bandes longitudinales de cellules de Purkinje reçoivent des entrées d'une population donnée de neurones de l'olive inférieure, et projettent à des sous-régions des noyaux cérébelleux. Cette topographie issue donc des fibres grimpantes suggère un traitement parallélisé des informations, cependant un

traitement associatif des informations, impliquant plusieurs zones adjacentes a été montré. Une identification à l'aide d'injections anatomiques plus précises dans l'olive inférieure a permis la définition de zones anatomiques plus sensibles, et plus fines : les microzones anatomiques (Sugihara and Shinoda, 2004).

En sus de cette organisation modulaire du cervelet définie par les fibres grimpantes, il existe aussi une organisation topographique issue des fibres moussues. A la différence des fibres grimpantes qui ne ciblent qu'une ou deux bandes parasagittales, les fibres moussues peuvent contacter plusieurs zones à la fois (Apps and Hawkes, 2009). Les fibres moussues envoient ainsi des collatérales dans plusieurs lobules du cervelet à la fois, permettant ainsi la convergence au niveau d'une cellule granulaire de fibres moussues portant des informations sensorielles d'origines multiples (Chabrol *et al.*, 2015). A travers les fibres moussues, il existe ainsi une somatotopie fracturée au sein du cervelet (**Figure 4.B**), où une modalité sensorielle en provenance d'une région du corps peut se retrouver dans plusieurs lobules cérébelleux, sans continuité entre ces lobules. Cette redondance des fibres moussues permet d'enrichir l'encodage au sein des boucles fermées olivo-cortico-nucléaires, en fournissant le substrat pour combiner des informations d'origine variée. Il est à noter qu'il peut exister une convergence dans les champs récepteurs des fibres grimpantes et des fibres moussues, notamment observée dans le cadre de stimulations tactiles (Brown and Bower, 2001). Cette convergence enrichit les théories du fonctionnement cérébelleux, en suggérant que les fibres grimpantes porteraient une information somatosensorielle pré-traitée (potentiellement la copie motrice efférente), tandis que les fibres moussues apporteraient l'information sensorielle immédiate depuis la même région du corps, permettant la comparaison de ces deux sources d'information au sein du microcircuit cérébelleux (Apps and Hawkes, 2009). C'est cette convergence qui donne la définition de microzones fonctionnelles de cellules de Purkinje.

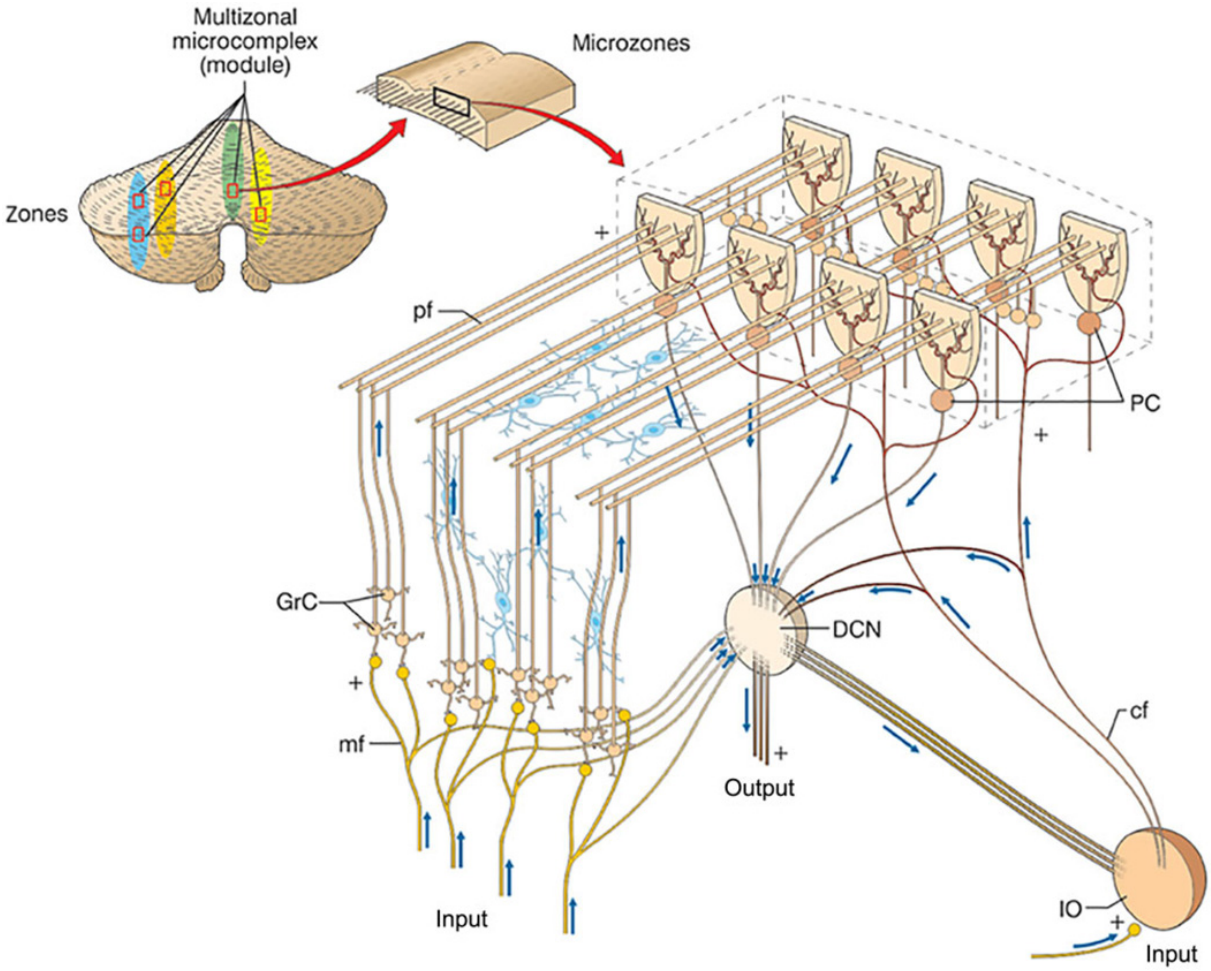


***Figure 3. Organisation fonctionnelle du cervelet en modules et microzones.***

*Le schéma montre ici une représentation aplanie du cervelet. 4 zones sont indiquées en couleur (en haut à gauche), chacune contenant des microzones formant des microcomplexes multizonaux. Les microzones ont une structure de base reproduite à droite. Une microzone est définie comme un groupe de l'ordre de 1000 cellules de Purkinje ayant les mêmes champs récepteurs somatotopiques. Ces cellules de Purkinje sont réparties dans une longue et étroite bande, perpendiculaire aux foliations corticales, de sorte que les dendrites des cellules de Purkinje sont aplaties dans la même direction que l'étendue de la microzone et traversées perpendiculairement par les fibres parallèles. Les fibres grimpantes innervent généralement des cellules de Purkinje de la même microzone, permettant ainsi de les synchroniser. Les cellules de Purkinje d'une même microzone envoient toutes leurs axones à la même petite population de cellules au sein des noyaux cérébelleux profonds.*

***mf=** fibre moussue**. GrC**= cellules granulaires**. DCN**= noyaux cérébelleux profonds. **IO**= olive inférieure**. Cf**= fibre grimpante**. pf**= fibre parallèle. **PC**= cellules de Purkinje*

***From D'Angelo et Casali 2012***

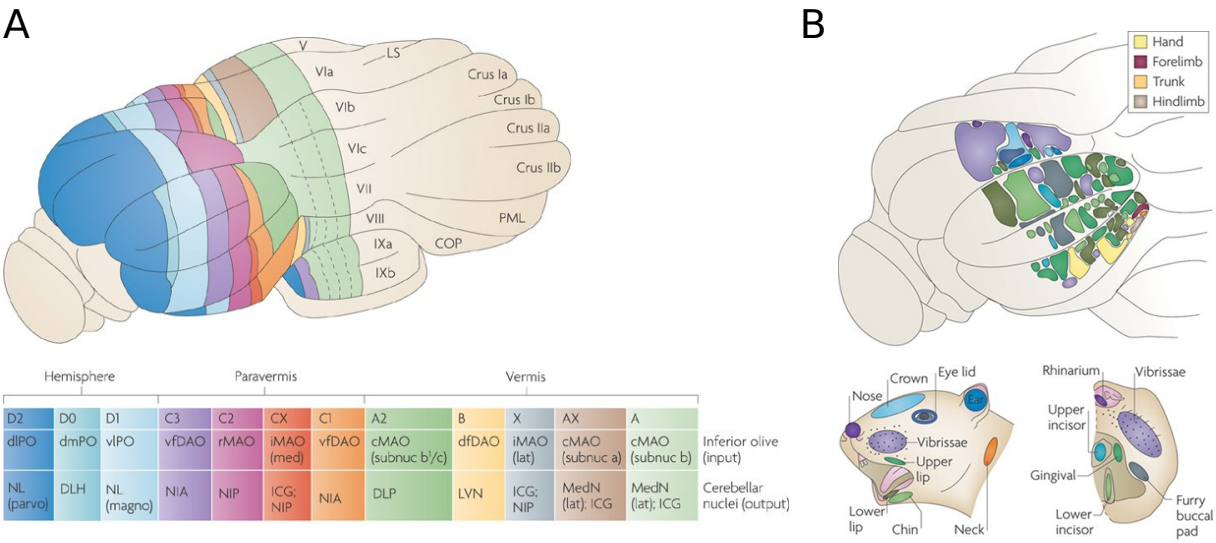


***Figure 4. Organisation anatomo-fonctionnelle du cervelet selon la distribution des fibres moussues et fibres grimpantes.***

***A.*** *Vue dorso-postérieure d'un cervelet de rat indiquant la position approximative des bandes longitudinales à la surface du cortex cérébelleux. Chaque zone longitudinale est définie par ses projections des fibres grimpantes depuis l'olive inférieure, ainsi que sa sortie corticonucléaire. En bas, un diagramme simplifié présente le nom de chaque zone, sa localisation, ainsi que son origine dans l'olive inférieure et sa projection dans les noyaux cérébelleux profonds.*

***B.*** *Vue dorso-postérieure d'un cervelet de rat indiquant la distribution spatiale des champs récepteurs enregistrés dans la couche granulaire en réponse à une stimulation mécanique de différentes zones du corps. La représentation à plusieurs endroits non continus dans le cortex cérébelleux de la même zone du corps produit ainsi une somatotopie fracturée, avec des zones de taille variable.*

***From Hawkes and Apps 2009***

### 1.3 Fonctionnement du cervelet : les théories cérébelleuses

Cette organisation en microcircuit du cortex cérébelleux a fasciné les neuroscientifiques depuis sa découverte : cette régularité dans l'organisation du cortex cérébelleux suggère un mécanisme computationnel récurrent qui permettrait au cervelet de réguler la sortie comportementale. Pour comprendre la fonction du cervelet, il convient dans un premier temps d'observer les impacts fonctionnels des lésions cérébelleuses. Nous verrons ensuite brièvement quelles théories coexistent quant aux computations neuronales dont sont responsables le cervelet.

#### 1.3.1 Quand le cervelet dysfonctionne

Depuis les travaux de Florens, l'impact du dysfonctionnement cérébelleux a été détaillé plus finement. Chez l'humain, les sources de dysfonction du cervelet peuvent avoir plusieurs origines : développementales, traumatiques ou encore dégénératives. Dans la plupart de ces cas, et notamment sur les lésions traumatiques, les symptômes moteurs sont très marqués et rendent l'évaluation d'autres aspects du comportement difficile.

La terminologie du syndrome cérébelleux a d'abord inclus principalement des déficits moteurs. Les travaux de Gordon Holmes sont souvent cités comme ayant la plus grande influence sur notre compréhension des symptômes cliniques et des signes de lésions cérébelleuses, plus généralement regroupés sous le terme d'ataxie. Celui-ci se réfère initialement à un manque de coordination (manque d'ordre en grec), et est défini plus généralement comme une coordination déficiente des mouvements volontaires, généralement causée par une lésion cérébelleuse ou une déficience dans les entrées vestibulaires ou proprioceptives (Ashizawa and Xia, 2016). Ces ataxies peuvent être d'origine traumatiques ou être le résultat d'une dégénérescence progressive comme dans les ataxies spinocérébelleuses d'origine génétique. Les dysfonctions motrices d'origine cérébelleuse peuvent ainsi prendre plusieurs formes cliniques, incluant une instabilité oculaire (nystagmus), une perturbation des mouvements dirigés avec une décomposition du mouvement et un tremblement d'intention. La variabilité des symptôme moteurs est généralement inhérente à la localisation du dommage cérébelleux. Ainsi, les lésions du lobe flocculonodulaire entraîneront spécifiquement un nystagmus (Patel and Zee, 2015). Les dystonies représentent la forme la plus commune de désordres moteurs et de tremblements, causés par la co-contraction de muscles antagonistes. Elles ont été initialement liées à un dysfonctionnement des ganglions de la base mais de nombreuses études ont révélé une implication notable du cervelet dans cette pathologie (Calderon *et al.*, 2011; Nikolov *et al.*, 2019).

Le lexique des atteintes cérébelleuses a été enrichi ces trente dernières années par une implication du cervelet dans la régulation de fonctions cognitives, affectives, linguistiques et perceptuelles (Schmahmann, 1991; Timmann and Daum, 2007), même si le détail de ces affections a été moins poussé que dans la quantification motrice, notamment en raison des limitations liées à l'expérimentation animale dans les processus cognitifs. Ainsi, un syndrome cognitivo-affectif cérébelleux a été décrit par le Dr Schmahman et inclut une large variété de symptômes : un déficit dans les fonctions exécutives telles que la planification, les performances linguistiques, et des changements dans la personnalité ou la gestion des émotions, dépendants du site et de l'origine de la lésion (Stoodley *et al.*, 2016). Ces observations cliniques ont mené à l'idée de l'existence d'une « dysmétrie » cognitive, similaire à la dysmétrie motrice, liée à des dysfonctions du circuit cérébello-thalamo-cortical

(Schmahmann, 1991). De surcroît, le cervelet a été impliqué dans une variété de maladie psychiatriques telles que la schizophrénie et l'autisme (Wang, Kloth and Badura, 2014).

### 1.3.2 Théories du contrôle moteur et modèles internes du cervelet

Si ce panel d'affections cérébelleuses inclut des symptômes moteurs et cognitifs, c'est principalement les fonctions sensorimotrices qui ont donné naissance aux grandes théories du fonctionnement cérébelleux, notamment du fait de la lisibilité comportementale chez l'animal des systèmes sensori-moteurs.

Ainsi le cervelet est nécessaire pour la fluidité des mouvements volontaires dirigés (Thach, Goodkin and Keating, 1992; Cerminara *et al.*, 2015). L'exécution de mouvements volontaires requiert une planification motrice afin d'obtenir le mouvement désiré de manière exacte. Cependant, des mouvements rapides et coordonnés du bras par exemple ne peuvent pas être exécutés uniquement à l'aide d'un simple rétro-contrôle, c'est-à-dire en « lisant » à chaque instant le résultat de l'action motrice et en le corrigeant, notamment du fait que les boucles de rétro-contrôle biologiques sont trop lentes et ont un gain trop faible. En effet, les propriétés mécaniques et neurales nécessaires à une gestion en *feedforward* du mouvement afin d'atteindre le point d'équilibre désiré nécessitent notamment une forte résistance mécanique aux perturbations, qui n'a pas été observée expérimentalement (Wolpert, Miall and Kawato, 1998). De plus, le retour sensoriel lorsqu'il arrive aux centres de contrôle moteur est déjà trop en retard par rapport au contexte : il y aurait ainsi un décalage de plusieurs dizaines de millisecondes entre l'exécution du mouvement et l'intégration de ses conséquences dans le but de le corriger. Il faut donc ainsi pouvoir prédire les conséquences sensorielles d'une action, permettant au contrôle moteur de se baser sur une estimation de l'état actuel de l'organisme et de son environnement. Cette prédiction de l'état sensoriel sur la base de la commande motrice permettrait ainsi de se prémunir du décalage lié au système sensoriel (**Figure 5.A**). Il a notamment été observé que le système nerveux central est capable de se départir de cette contrainte temporelle sur la base des symptômes liées aux lésions cérébelleuses. Il a donc été postulé que le cervelet assume cette fonction. Ainsi, des mouvements fiables requièrent une coordination temporelle précise entre différents muscles, et une disruption de cette temporalité est une des caractéristiques phares de l'ataxie cérébelleuse (Moberget and Ivry, 2016).

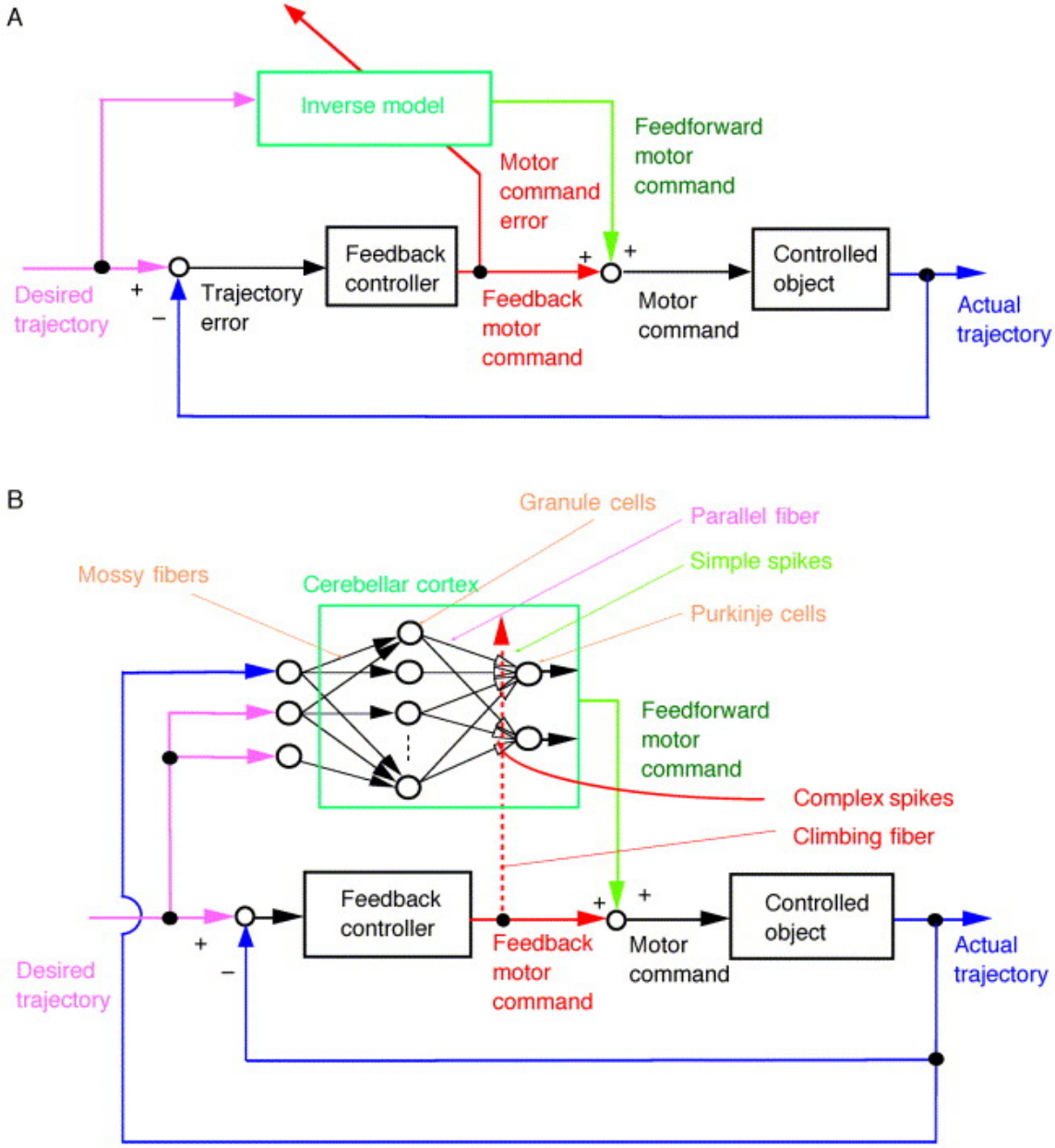


***Figure 5. Modèle d'apprentissage interne du cervelet***

***A.****Conception générale du modèle combinant modèle inverse et rétro-contrôle.* ***B.*** *Application de ce modèle dans le cervelet. L'objet contrôlé ici est une zone du corps ou un groupe musculaire. Le modèle inverse implémenté dans le cortex cérébelleux permet la traduction de la trajectoire désirée (en rose) en la commande motrice nécessaire pour atteindre la trajectoire. La commande motrice finalement envoyée est retraduite par un rétro-controlleur, le cortex moteur, et envoyée au cervelet, permettant la comparaison avec les entrées sensorielles produites effectivement par la commande motrice. Cela permet un apprentissage au sein du cortex cérébelleux.*

***From Wolpert et al. 1998***

Le cervelet est un centre majeur de convergence des informations périphériques et cérébrales. Les informations sensorielles périphériques de tout le corps, ainsi que les informations auditives, visuelles et vestibulaires parviennent au cervelet directement. De plus, le tractus pyramidal envoie des collatérales au cervelet, portant une copie de la commande motrice envoyée à la moelle épinière depuis le néocortex, et est appelée copie motrice efférente (Wolpert, Miall and Kawato, 1998; Bastian, 2006). A partir de la combinaison de ces informations, et grâce à l'organisation de son microcircuit, le cervelet est alors pensé comme effectuant un apprentissage supervisé en implémentant une combinaison de modèles internes (« forward » ou en-avant et inverse). Cette théorie est supportée par les données neurophysiologiques du paraflocculus ventral chez le singe, dans le suivi du réflexe vestibulo-oculaire (Shidara *et al.*, 1993). Le cervelet apprend ainsi à prédire les conséquences d'une action – modèle en-avant, qu'il compare au retour sensoriel immédiat pour assurer une correction motrice en cas d'erreur (Ito, 1984; Wolpert, Miall and Kawato, 1998; Doya, 1999). Cette correction s'effectuerait ensuite à travers des projections vers les aires motrices primaires et secondaires (Allen and Tsukahara, 1974). Au sein du cortex cérébelleux serait ainsi représenté le modèle « inverse », c'est-à-dire la représentation neurale nécessaire pour transformer la trajectoire de mouvement désirée en la commande motrice nécessaire pour l'exécuter (**Figure 5.B**). Dans le circuit cérébelleux, les potentiels d'action simples des cellules de Purkinje représentent la commande motrice en cours, et les fibres parallèles la trajectoire désirée tout comme le résultat sensoriel de l'état actuel de l'objet considéré (par exemple la main ou l'œil). Une microzone du cortex cérébelleux constitue donc ainsi un modèle inverse de cet objet spécifique. Dans ce modèle, une composante importante est l'entrée des fibres grimpantes qui est présumée porter une copie du rétrocontrôle moteur : les potentiels d'actions complexes qu'elles génèrent dans les cellules de Purkinje sont théorisés comme étant un signal d'erreur sensoriel déjà traduit en coordonnées de commande motrice. Ainsi, les théories de modèle interne du cervelet fournissent un substrat riche pour résoudre les problèmes inhérents au contrôle moteur.

### 1.3.3 La théorie du cervelet sensoriel

L'extension du rôle du cervelet au-delà du contrôle moteur pur a cependant remis en cause une explication simple des mécanismes cérébelleux, avec une computation sensorielle à seule fin motrice. Les données de traçage anatomique chez le singe rhésus (Middleton and

Strick, 2001) ainsi que les imageries fonctionnelles chez l'humain de connectivité fonctionnelle cérebello-corticale ont mis en évidence des associations fortes du cervelet avec d'autres aires corticales que les zones motrices. Une idée intéressante en regard du cervelet est la théorie de la fonction sensorielle du cervelet (Bower, 1997). Une hypothèse importante des descriptions cérébelleuses a longtemps été que cette structure n'a aucune influence sur la perception sensorielle, mais uniquement sur l'exécution motrice. Cependant, celle-ci repose sur la qualité des informations sensorielles acquises, et les auteurs de la théorie de la fonction sensorielle du cervelet prédisent qu'une dysfonction cérébelleuse pourrait avoir une conséquence sur cette qualité perceptive, une idée alimentée par des études chez l'humain montrant des déficits sensoriels primaires dans des tâches d'ordres élevées telles que le langage, la détection de mouvement ou l'analyse de séquences temporelles. Dans le système auditif chez l'humain par exemple, il a été montré que des patients présentant une dégénérescence cérébelleuse avaient une capacité à discriminer les tons (*pitch*) fortement diminuée par rapport aux patients contrôles. Les capacités de concentration, de restitution verbale ainsi que les niveaux de perception auditives étaient cependant similaires dans les deux groupes, suggérant un déficit dans l'acquisition sensorielle (Parsons *et al.*, 2009). Une autre étude phare a démontré chez l'humain une activité plus prononcée du cervelet lors d'une tâche de discrimination tactile utilisant les doigts que dans une tâche de motion simple des doigts (Gao *et al.*, 1996). Ils proposent donc que la conséquence des lésions cérébelleuses sur le mouvement serait le résultat d'une disruption d'acquisition des informations sensorielles sur lesquelles le contrôle moteur fin repose. De plus, ils suggèrent que l'implication cérébelleuse augmente à mesure qu'une acquisition sensorielle plus fine devient nécessaire, avec une augmentation de la difficulté de la tâche et du bruit sensoriel. Finalement, une implication particulière de leur théorie est que le cervelet est une structure de support, qui loin de participer directement à la perception sensorielle, permettrait de faciliter l'efficacité computationnelle du reste du cerveau, incluant le cortex cérébral. Dans leur théorie, sur la base du flot continu d'informations contextuelles en provenance du cortex, le cervelet combinerait les informations d'autres surfaces sensorielles impliquées dans l'acquisition de l'image complète de l'environnement – phénomène facilité par la somatotopie fracturée du cervelet (**Figure 4.B**). Cela permettrait ensuite des ajustements fins dans la position ou l'ajustement des organes sensoriels afin d'optimiser le contenu d'information. Il est intéressant de noter que dans le cas de l'expérimentation animale, c'est dans le système

des vibrisses du rongeur que les évidences expérimentales en faveur de cette théorie ont été le plus étayées.

# 2 : Les vibrisses : un système sensorimoteur complexe

Les rongeurs -rat et souris en particulier- sont les modèles animaux les plus utilisés en neurophysiologie du fait de leurs multiples avantages : petite taille, reproduction rapide et nombreuse, possibilité de créer des lignées génétiquement modifiées. Lorsqu'il s'agit d'étudier les systèmes sensori-moteurs, deux principales fonctions chez la souris viennent à l'esprit : les tâches de *reaching*, où l'animal utilise une patte avant afin d'atteindre un levier ou une récompense alimentaire, et les tâches d'exploration par les vibrisses, où l'animal utilise ses poils mystaciaux faciaux afin d'explorer un élément de son environnement. Cette seconde tâche présente un aspect de perception sensorielle plus prononcé que la première. Nous allons voir dans cette section l'anatomie et la physiologie bien décrite des vibrisses, puis comment la perception tactile s'effectue grâce à cet organe, et enfin quelles sont les inconnues subsistant dans ce système.

## 2.1 Un organe sensorimoteur essentiel pour les rongeurs d'une simplicité apparente

Les vibrisses composent un sens tactile important pour les rongeurs, autant que les mains peuvent l'être chez l'Humain ou d'autres primates. Les vibrisses sont des poils spécialisés en faisant un organe tactile, du fait de la présence de mécanorécepteurs situés dans leur follicule. Elles sont retrouvées chez une grande partie des mammifères, principalement sur la face, mais ne présentent pas la même fonctionnalité dans l'ensemble des espèces. Ainsi, si toutes les vibrisses peuvent à priori bouger, il y a une variabilité importante dans le panel de mouvements disponibles. Certaines vibrisses comme chez le hamster peuvent bouger grâce à une dynamique vasculaire et connective des tissus (Wineski, 1985), d'autres vibrisses peuvent êtres dressées grâce à des muscles responsables de l'érection des poils (Hyvärinen *et al.*, 2009). Enfin, les vibrisses mystaciales sont mues par un ensemble de muscles spécialisés (Brecht, Preilowski and Merzenich, 1997), et peuvent chez les rongeurs tels que le rat ou la souris être bougées rapidement et de façon rythmique afin d'explorer l'environnement immédiat (Woolsey, Dierker and Wann, 1975). Ce mouvement est

appelé *whisking* en anglais et sera utilisé dans la suite de ce manuscript pour décrire ce phénomène.

Les rats et les souris sont des animaux essentiellement nocturnes, il est donc probable que la perception tactile médiée par les vibrisses a évolué pour compenser la pauvreté des informations visuelles au cours de la vie du rongeur. Ainsi, pour explorer son environnement, le rat ou la souris va faire osciller ses vibrisses de manière rythmique autour d'un point spatial appelé le *setpoint*, d'abord avec des mouvements larges à une fréquence relativement peu élevée (5 à 15Hz), puis au cours d'une palpation tactile plus spécifique, avec des mouvements d'amplitude plus faible mais de fréquence plus élevée (15 à 25 Hz) pour identifier objets ou textures (Carvell and Simons, 1995). Grâce à cette exploration, l'animal peut de cette manière s'orienter ou identifier des éléments de son environnement. Par exemple, à l'aide du bout de leurs vibrisses, les rongeurs peuvent identifier la largeur d'une ouverture ou la distance d'un espace à franchir (Hutson and Masterton, 1986; Krupa *et al.*, 2001). En addition, de très fines variations dans la surface d'un objet vont provoquer l'arrêt du bout de la vibrisse pendant un temps court, suivi par une libération de cette vibrisse (Neimark *et al.*, 2003). Ce phénomène appelé *stick and slip* peut se répéter plusieurs fois au cours de l'exploration, et ainsi composer une carte de la texture de l'objet, dépendante de la vitesse d'oscillation des vibrisses notamment, ainsi que des évènements *stick and slip* sur les différentes vibrisses. Ces informations provoquent des réponses neuronales spécifiques au sein du système nerveux central, conférant une grande acuité de perception tactile au rongeur.

## 2.2 Anatomie du système vibrissal

### 2.2.1 Le bloc vibrissal

Au cours d'une exploration tactile, l'entrée des informations sensorielles vibrissales est initiée au niveau du museau du rongeur. Ce système chez la souris présente une architecture fixe où les vibrisses sont organisées en 5 rangées horizontales de 4 à 7 vibrisses sur le museau, avec notamment 4 vibrisses d'épaisseur plus importantes dans la partie caudale du bloc de vibrisses (**Figure 6, droite**). Il existe cependant plusieurs types de vibrisses, appelées respectivement macro-vibrisses et micro-vibrisses. Les 5 rangées principales composent les macro-vibrisses, mais dans la partie rostrale et ventrale du bloc vibrissal existent des vibrisses de plus petite taille. Celles-ci ne sont pas contrôlées aussi finement, et sous-tendent probablement des fonctions sensorielles différentes des macro-vibrisses. Dans

la suite de ce manuscrit, je désignerais par vibrisse uniquement les macrovibrisses. Des muscles intrinsèques permettent de mouvoir chacune des vibrisses, tandis que des muscles extrinsèques provoquent le mouvement de l'ensemble du bloc de vibrisse, une caractéristique utilisée notamment par les rongeurs afin d'ajuster l'épatement de l'éventail de vibrisses pour optimiser les contacts avec un objet (Towal *et al.*, 2011).

La transduction de l'information sensorielle apparaît au niveau des mécanorécepteurs situés à la base de chaque vibrisse, dans le complexe follicule-sinus. Ces mécanorécepteurs sont innervés par des neurones sensoriels localisés dans les ganglions trigéminaux. Chaque follicule vibrissal possède son nerf vibrissal profond (DVN) et son nerf vibrissal superficiel, (SVN) bien que la plupart de l'innervation soit médiée par le DVN. Ainsi, l'information sensorielle de chaque vibrisse est amenée séparément aux noyaux trigéminaux, avec entre 1 et 200 axones innervant chacun des larges follicules du bloc vibrissal (Lee and Woolsey, 1975). La déflection mécanique des vibrisses est ainsi traduite en impulsion électrique par les mécanorécepteurs et transportée via le nerf infraorbital jusqu'au tronc cérébral. Il rejoint dans le ganglion trigéminal le 5$^{ème}$ nerf crânien, avant d'arriver au tronc cérébral dans les noyaux trigéminaux.

### 2.2.2 Les noyaux trigéminaux

Le complexe trigéminal est composé de 4 noyaux : le noyau principal (PrV) et trois noyaux spinaux, l'oralis (SpVo), l'interpolaris (SpVi) et le caudalis (SpVc) **(Figure 6).** Au repos, les neurones du ganglion trigéminal sont silencieux. Ils présentent une large gamme d'activité en fonction de la vitesse, de l'amplitude mais aussi de l'orientation des vibrisses (Arabzadeh, Zorzin and Diamond, 2005). Ils relaient via une transmission glutamatergique des signaux depuis les ganglions trigéminaux, au sein de structures discrètes de neurones appelés tonnelets (ou *barrelettes*), qui reçoivent chacune des entrées sensorielles d'une vibrisse principale et qui peuvent être révélés par un marquage à la cytochrome oxidase (Veinante and Deschênes, 1999). Ces tonnelets ont une somatotopie inversée, où les vibrisses dorsales ont une représentation dorsale (et vice versa). Seuls l'oralis et la partie ventrale de l'interpolaris ne présentent pas de tonnelets. Il a été aussi observé que les neurones entre les tonnelets peuvent transmettre des signaux sensoriels multi-vibrissaux. Les neurones des barrelettes projettent ensuite contralatéralement vers le thalamus ventral, mais aussi vers les noyaux pontiques, l'olive inférieure, le colliculus supérieur et la zona incerta (ZI). Des

projections ipsilatérales parviennent aussi au cervelet et à la formation réticulaire. Il a longtemps été suggéré que ces noyaux permettaient le relais simple de l'information sensorielle, et que le traitement sensorimoteur des informations se faisaient plus loin dans la chaîne de transduction. Cependant, déjà à cette étape, l'état comportemental de la souris influence la transmission du signal sensoriel via des projections de wS1 qui activent les neurones GABAergiques de l'interpolaris, permettant une inhibition du noyau principal. Cela permet probablement aux noyaux trigéminaux de filtrer les informations parasites, nombreuses au cours du mouvement (Lee *et al.*, 2009).

Néanmoins, la majorité du traitement sensorimoteur se fait effectivement dans des structures d'ordres plus élevées, dont les plus étudiées sont le thalamus et le cortex.

### 2.2.3 Les voies lemniscale, paralemniscale, extralemniscale

Dans un premier temps, nous allons résumer les projections trigémino-thalamo-corticales, qui constituent les voies de transmission sensorielle vibrissales les mieux connues - nous aborderons dans le chapitre suivant les projections au cervelet. Puis, nous verrons les interactions entre les différents acteurs des boucles thalamo-corticales, et leur rôle dans l'intégration des informations tactiles vibrissales. Ainsi, il existe 3 voies trigemino-thalamo-corticales qui se différencient d'un point de vue anatomique, mais aussi fonctionnel.

La voie lemniscale (**Figure 6, en rouge**) relaye les signaux sensoriels depuis les tonnelets du PrV à la région dorsomédiale du noyau ventropostéromédian (VPM) du thalamus. Celui-ci présente aussi une somatotopie avec des barréloïdes qui prennent en charge les signaux d'une seule vibrisse. Une distinction supplémentaire existe aussi chez le rat, où il existe des projections depuis le PrV qui transmettent des informations de plusieurs vibrisses aux barreloides correspondants du VPM, qui en retour innervent les régions septales du cortex sensoriel vibrissal.

La voie extralemniscale (**Figure 6, en bleu**) reçoit des projections de la partie caudale de l'interpolaris, et projette à une portion ventrolatérale du VPM (VPMvl) où les barréloïdes sont moins bien définis. Cette zone cible ensuite le cortex somatosensoriel secondaire (S2) et les parties septales de la couche IV du cortex sensoriel primaire (Pierret, Lavallée and Deschênes, 2000). La distinction septa/tonneaux dans le cortex sensoriel primaire (wS1) n'existe que chez le rat : chez la souris les tonneaux sont apposés les uns aux autres sans

séparation visible. Mes expériences se basant uniquement chez la souris, je n'aborderai pas plus en détail les microcircuits internes à la distinction septa/tonneau.

Enfin, la voie paralemniscale (**Figure 6, en jaune**) est la cible de la partie rostrale de l'interpolaris, qui relaye des informations multi-vibrissales (Veinante, Lavall□e and Desch□nes, 2000) au noyau postero-médian du thalamus (POm). Les neurones du POm en retour innervent majoritairement les couches I et Va du cortex sensoriel primaire wS1. Des terminaisons en provenance du POm sont aussi trouvées dans wS2 et wM1 (Carvell and Simons, 1987).

Ainsi, les cibles principales des voies lemniscales et paralemniscales (la voie extralemniscale étant décrite uniquement chez le rat, elle ne sera pas abordée plus en détail ici), sont le cortex somatosensoriel primaire, secondaire, ainsi que le cortex moteur.

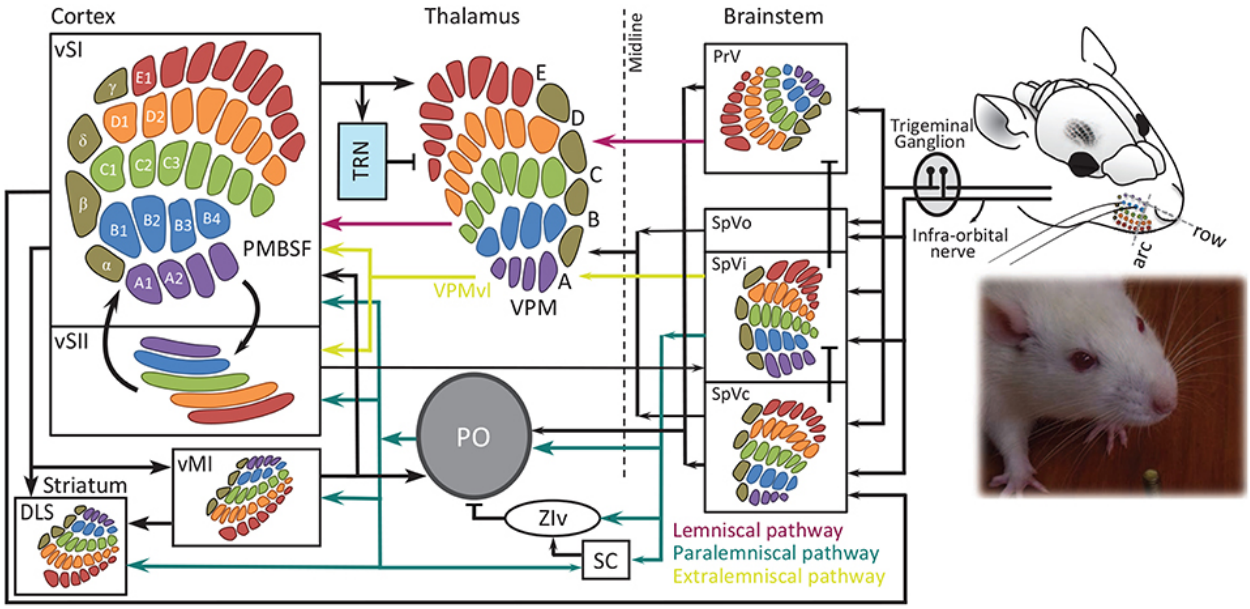


***Figure 6. Anatomie du système vibrissal***

*Représentation des voies anatomiques de transmission de l'information depuis le bloc vibrissal chez le rat.* ***À droite*** *sont représentées les vibrisses organisées en rangées, chacune des 5 rangées principales de macrovibrisses représentées dans une couleur et portant un nom correspondant à sa rangée (de A à E), et un numéro correspondant à son arc. Le nerf infra-orbital porte l'information née des méchanorécepteurs à la base de ces vibrisses jusqu'au ganglion trigéminal ipsilatéral, puis au tronc cérébral (brainstem), où chaque vibrisse est représentée dans une petite population de neurones appelée barrelettes. Depuis le tronc cérébral naissent les trois voies principales d'acheminement de l'information vibrissal :* ***la voie lemniscale, paralemniscale et extralemniscale*** *(absente chez la souris). En passant la ligne médiane du cerveau (midline), une décussation intervient et les projections se font alors dans la partie contralatérale du cerveau à la stimulation périphérique. Depuis le noyau principal (PrV) part* ***la voie lemniscale*** *(en rouge), qui projette au noyau ventro-postéromédian (VPM) du thalamus, om les vibrisses sont topographiquement représentées dans des structures appelées barréloides, puis au cortex sensoriel primaire où elles sont représentées dans des tonnelets. De là s'établissent des communication intercorticales avec le cortex moteur primaire et sensoriel secondaire****. La voie paralemniscale*** *(en bleu) projette principalement au noyau posteromédian du thalamus (PO), qui en retour contacte les cortex primaire moteur et sensoriel, et sensoriel secondaire. Cette voie projette aussi à la zona incerta ventrale qui*

*participe à l'inhibition du PO. Nous pouvons noter que le cervelet est absent dans cette représentation classique de transmission de l'information vibrissale.*
***From Adibi 2019***

### 2.2.4 Les acteurs corticaux du système vibrissal

#### 2.2.4.1 Organisation du néocortex

Le néocortex est une des divisions majeures du cerveau, réparti en deux hémisphères cérébraux plus ou moins foliés selon les espèces. Il est impliqué dans des fonctions cognitives d'ordre élevé incluant la perception sensorielle, la planification motrice, les prises de décisions. Il est divisé en trois régions fonctionnelles : les aires sensorielles, motrices et associatives. Dans les aires sensorielles primaires, une seule modalité sensorielle est traitée, telle que la vision ou l'audition, l'association entre les différents sens passant par des réseaux de neurones spécifiques cortico-corticaux ou thalamo-corticaux notamment. Le néocortex présente une architecture caractéristique en couches au sein desquelles les cellules sont organisées sous forme de colonnes interconnectées. La micro-circuiterie liée à cette organisation est une clé cruciale afin de comprendre le traitement des signaux arrivant au cortex. Ainsi, le néocortex est composé de six couches, qui contiennent chacune différents types cellulaires et différentes connectivités.

- La couche I (L1) contient les dendrites et les axones des neurones des couches plus profondes, avec la présence de petits neurones épars, principalement des interneurones GABAergiques. Des projectons *top-down* en provenance d'autres aires corticales (Vogt, 1991) ainsi que des axones thalamo-corticaux arrivent aussi en couche I (Jones and Diamond, 1995).
- La couche II (L2) est la couche granulaire externe, composé de petits neurones pyramidaux et de neurones en étoile. Les dendrites des cellules de L2 sont extensivement réparties dans la couche I (Feldmeyer, Lübke and Sakmann, 2006). Ces petits neurones projettent des axones vers la couche III et la couche V, avec des collatérales récurrentes vers la couche I. Les connections latérales de L2 sont assez extensives, pouvant couvrir une large surface au sein d'une aire corticale.
- La couche III (L3) est la couche pyramidale externe, composée de neurones pyramidaux de taille moyenne et d'interneurones, en particulier de type VIP+ (exprimant le *vasoactive intestinale peptide).* Les axones des neurones pyramidaux de L3 projettent aux couches infragranulaires au sein de la même colonne corticale, mais aussi vers les colonnes corticales adjacentes. Il existe aussi dans cette couche des

neurones de projection qui ciblent d'autres aires corticales du même hémisphère, ou de l'autre hémisphère cérébral.

- La couche IV (L4) est la couche granulaire interne, et contient principalement des neurones pyramidaux, des cellules en étoile et des interneurones parvalbumines (PV) et VIP+. Ces neurones projettent majoritairement verticalement et peu horizontalement, ciblant donc principalement leur colonne corticale, en particulier la couche II/III. Cette couche granulaire est la cible principale des entrées thalamiques, en particulier dans les aires somatosensorielles.
- La couche V (L5) est la couche interne pyramidale, elle fait partie du cortex infragranulaire, et peut être séparée en deux sous-couches Va et Vb, ayant des schémas de connectivité différenciés. Les neurones pyramidaux de cette couche reçoivent des synapses thalamocorticales, mais aussi des projections depuis L2/3 de la même colonne. La couche Va reçoit aussi des projections de L4, et envoie des projections vers les couches supragranulaires, mais aussi vers wS2 et wM1 (Mao *et al.*, 2011), ainsi que vers le striatum dorsal (Mercier, Legg and Glickstein, 1990). La couche Vb quant à elle, reçoit des projections plus importantes des noyaux thalamiques sensoriels primaires, et assez peu de L4. Elle cible en retour principalement les régions sous-corticales.
- La couche VI (L6) est la couche multiforme, et présente une grande hétérogénéité avec un mélange de grands et petits neurones pyramidaux et de neurones multiformes. Ces neurones projettent vers le thalamus et au sein de la colonne corticale dans les couches V, IV et III.

#### 2.2.4.2 Le cortex sensoriel primaire

Le cortex sensoriel primaire des vibrisses, aussi appelé *barrel field* cortex, est d'une importance primordiale pour percevoir et traiter les informations vibrissales. Son appellation, utilisée pour la première fois par Woolsey et Van der Loos en 1970, décrit une spécificité de ce cortex : les structures en tonneau observable dans sa couche IV. Ces formations en tonneau sont le résultat d'un agrégat de neurones en blocs d'environ 300µ de diamètre, recevant chacun des entrées sensorielles principalement d'une vibrisse contralatérale. Le cortex sensoriel vibrissal de la souris représente 13% de la surface corticale totale, et 69% de

l'ensemble du cortex somatosensoriel chez la souris (Lee, Lo and Erzurumlu, 2005), soulignant son importance dans le traitement des entrées vibrissales.

A travers wS1, les réponses sensorielles évoquées sont rares et presque simultanées, mais la probabilité de réponse diffère en fonction des couches corticales et de l'état comportemental de la souris. Ainsi, durant les périodes éveillées où l'animal ne bouge pas (*quiet wakefulness)*, une stimulation passive des vibrisses provoque des réponses fortes au niveau cortical, mais la même déflection lorsque l'animal *whiske* activement induit seulement une faible réponse (Crochet and Petersen, 2006; Ferezou, Bolea and Petersen, 2006; Hentschke, Haiss and Schwarz, 2006). Cela suggère l'existence d'un contrôle (*gating)* des informations sensorielles dans wS1 dépendant de l'état d'éveil ou d'attention de l'animal, d'autant plus que les informations sensorielles périphériques sont transmises de manière fiable à wS1 : des contacts de vibrisses sur un objet évoquent des réponses pendant une exploration tactile active. Ainsi au sein d'un barrel de la couche IV, la réponse neuronale dénote une préférence pour la vibrisse principale qui innerve ce barrel, encodant des propriétés spécifiques de la déflection de la vibrisse telles que la position, l'accélération ou la vitesse (Arabzadeh, Petersen and Diamond, 2003), la fréquence de l'oscillation et l'intervalle entre des stimulations répétées (Ahissar *et al.*, 2001). Des propriétés de réponse similaires sont observées pour les vibrisses adjacentes à la vibrisse principale, avec toutefois une amplitude réduite et des propriétés dynamiques différentes.

La principale source d'entrée thalamique à wS1 provient du VPM (**Figure 7**), qui innerve massivement la couche IV, un barréloïde innervant le barrel correspondant à la même vibrisse (Diamond, Armstrong-James and Ebner, 1992), et innerve aussi la couche V/VI (Constantinople and Bruno, 2013). L'information sensorielle est ensuite propagée à la couche II/III via les neurones étoilés de la couche IV (Petersen and Sakmann, 2001). Le signal se propage ensuite à la couche Va, Vb et VI superficielle (Feldmeyer, Roth and Sakmann, 2005) au sein de la colonne corticale. Le signal reçu est aussi transmis depuis la couche IV aux colonnes corticales adjacentes, afin de permettre l'intégration des informations multi-vibrissales (Bruno *et al.*, 2009). En sus de cette dynamique interne aux colonnes corticales au sein de l'aire somatosensorielle primaire, l'information sensorielle est aussi transmise à d'autres aires corticales.

#### 2.2.4.3 Le cortex moteur primaire

L'aire motrice primaire (wM1) et l'aire somatosensorielle secondaire (wS2) sont ainsi interconnectées avec wS1 (**Figure 7**). Les neurones pyramidaux de la couche II/III ainsi que de la couche Va de wS1 projettent en effet à wS2, wM1 et au wS1 contralatéral (Petreanu *et al.*, 2007). La projection de wS1 à wM1 est somatotopiquement organisée de façon à ce qu'une colonne de wS1 soit connectée à la colonne de wM1 correspondant à la même vibrisse (Ferezou *et al.*, 2007). La couche II/III de wS1 innerve préférentiellement la couche V/VI de wM1, tandis que la couche V/VI projette plutôt en couche I et II/III de wM1 (Miyashita, Keller and Asanuma, 1994). La connexion réciproque de wM1 projette en revanche préférentiellement depuis les couches II/III vers les couches V/VI de wS1, ainsi que la couche I. Regardant wS2, le cortex sensoriel primaire envoie des projections vers l'ensemble des couches de ce cortex secondaire.

Si wS1 encode de manière fiable l'information sensorielle, avec deux composantes en terme de latence de réponse, une courte à moins de 20ms, le résultat de l'entrée sensorielle primaire, et une longue, entre 50 et 200ms, supposée être le résultat de boucles de rétrocontrôles (Sachidhanandam *et al.*, 2013), wM1 présente un retard de 10-20ms par rapport à wS1. Le cortex moteur primaire possède une représentation topographique de tous les muscles du corps, et demande un seuil bas de stimulation pour évoquer des mouvements. Dans le système des vibrisses, à l'inverse de wS1, il ne reçoit pas de projections du VPM, étant un cortex agranulaire : les informations sensorielles périphériques lui parviennent depuis wS1 et le POm (Deschênes, Veinante and Zhang, 1998). Des microstimulations de wM1 permettent d'évoquer des mouvements vibrissaux rythmiques ressemblant à l'exploration normale (Matyas *et al.*, 2010), cependant une ablation complète de wM1 ne permet pas d'abolir complètement le whisking, en revanche cela perturbe les cinématiques du mouvement vibrissal, la coordination et la synchronisation des mouvements des vibrisses (Gao *et al.*, 2003). Globalement, la fonction précise du cortex moteur primaire des vibrisses n'est pas comprise actuellement. Deux études récentes se contredisent d'ailleurs sur ce sujet, l'une avançant que l'activité du cortex moteur permet de supprimer le mouvement (Ebbesen *et al.*, 2017), tandis que l'autre étude avance au contraire que l'activation de wM1 à travers l'excitation optogénétique de wS1 entraîne une exploration vibrissale (Sreenivasan *et al.*, 2016). Ce dernier point est intéressant, car il suggère que c'est les synapses du cortex sensoriel

sur le cortex moteur qui permettent d'initier et de guider le mouvement, tout du moins dans certains comportements.

#### 2.2.4.4 Le cortex sensoriel secondaire

Le cortex sensoriel secondaire (wS2) des vibrisses se situe latéralement par rapport à wS1 et possède aussi une représentation topographique des vibrisses. Cependant, à la différence de wS1, le champ récepteur des neurones de wS2 est très large et ne présente pas de réponse mono-vibrissale (Simons and Carvell, 1989). Les réponses dans wS2 à une stimulation vibrissale sont plus faibles que dans wS1, mais présentent une plus grande sensibilité directionnelle, avec des latences comparables à celles observées dans wS1 (Kwegyir-Afful *et al.*, 2005). wS2 reçoit en effet des projections directement depuis le VPM, mais aussi depuis le POm, et est réciproquement connecté à wS1 et wM1.

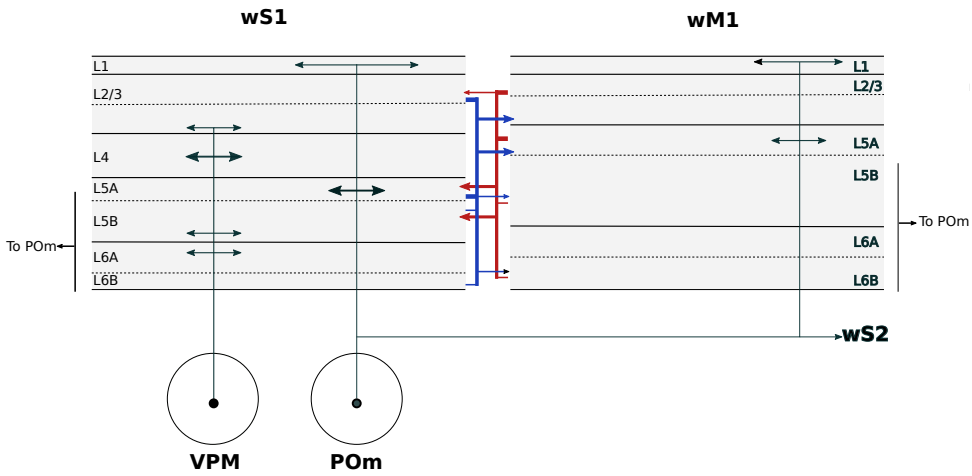


***Figure 7. Relations thalamo-corticales et cortico-corticales des cortex sensorimoteurs***
*Schéma simplifié des projections thalamiques depuis les noyaux thalamiques sensoriels aux cortex sensoriel et moteur primaires. En rouge sont symbolisées les projections de wM1 à wS1, et en bleu les projections inverses, montrant donc les relations corticocorticales directes entre ces cortex. VPM=noyau ventro postéro médian. POm = noyau postéromédian.*

## 2.3 Physiologie des voies thalamo-corticales pour le traitement de l'information sensorielle

### 2.3.1 Dynamiques intercorticales

Les rétro-projections entre ces aires corticales ont fait l'objet d'un nombre important d'études afin de comprendre comment les dynamiques inter-corticales influencent la perception, le traitement sensoriel ainsi que la sortie comportementale.

Ainsi, des enregistrements des neurones de projection wS1-wS2 et wS1-wM1, chez la souris éveillée qui exécute une tâche dirigée de conditionnement opérant ont fait émerger l'idée que wS2 et wM1 pourraient jouer des rôles distincts dans le traitement des informations sensorielles tactiles. Comme évoqué précédemment, les projections de wS1 à wM1 affectent le mouvement des vibrisses, suggérant que cette voie est impliquée dans l'initiation des plans moteurs après la détection d'un stimulus sensoriel (Sreenivasan *et al.*, 2016). La voie réciproque de wM1 à wS1 quant à elle convoie des informations mixtes regardant la cinématique des vibrisses, la localisation des objets et le contact aux objets (Petreanu *et al.*, 2012). L'imagerie calcique des dendrites des neurones pyramidaux de la couche V dans wS1, chez des souris effectuant une tâche de localisation d'objet a montré des signaux calciques de large amplitude dans les dendrites apicales lorsqu'un contact actif est effectué avec des objets ou des angles spécifiques de vibrisses. Ces signaux calciques nécessitent à la fois une entrée périphérique sensorielles et l'activité de wM1 (Xu *et al.*, 2012). Ces résultats suggèrent que la voie wM1-wS1 promeut la localisation spatiale d'objets par les vibrisses et potentiellement d'autres fonctions nécessitant une intégration sensorimotrice.

Les projections entre wS1 et wS2 en revanche semblent sous-tendre d'autres fonctions. Les enregistrements de cellules de S1 projetant à wS2 montrent une supralinéarité à des stimulations répétées des vibrisses, qui n'est pas observable dans wS1 (Yamashita *et al.*, 2013). Cela suggère que wS2 a la capacité d'intégrer des informations sensorielles sur une fenêtre de temps plus large, ce qui peut être essentiel pour la reconnaissance des caractéristiques d'objet. De surcroît, wS2 a été plus particulièrement impliqué dans l'encodage de la récompense dans le contexte d'une tâche de conditionnement opérant. En effet, au cours d'une tâche de discrimination de texture, les neurones de wS1 projetant à wS2 montrent une activité neuronale corrélée à la décision de l'animal par rapport à d'autres neurones de wS1 (Chen *et al.*, 2015). De plus, au sein de wS2, les neurones montrent une activité plus prononcée en lien avec la production comportementale résultant de l'apprentissage, notamment pour les neurones projetant en retour à wS1 (Kwon *et al.*, 2016). L'activité résultant du choix et du contact dans une tâche de détection vibrissale se propage ainsi en retour de wS2 à wS1, suggérant que le rétrocontrôle de wS2 peut renforcer l'entrée *feedforward*, 'en avant ' de wS1. Cette boucle intercorticale favoriserait l'intégration multi-vibrissale notamment dans le but d'obtenir une réponse adaptée au contexte général de l'entrée sensorielle.

Ainsi, il a été possible ces dix dernières années d'attribuer un corrélat physiologique spécifique de la perception sensorielle à ces dynamiques entre aires corticales sensorielles et motrice primaire et secondaire. En sus de ces interactions intercorticales médiées par les projections horizontales entre cortex, il existe des interactions entre cortex régulées par des boucles thalamo-corticales.

### 2.3.2 Dynamiques thalamo-corticales

Comme mentionné précédemment, le VPM (noyau ventro postéromédian du thalamus) et le POm (noyau posteromédian) constituent les cibles principales des noyaux trigéminaux, au sein respectivement des voies lemniscales et paralemniscales. Il est supposé que ces voies parallèles sous-tendent des fonctions différentes au cours de la perception sensorielle. Si les interactions thalamo-corticales depuis le VPM sont plutôt bien comprises, celles comprenant le POm restent nettement plus obscures.

#### 2.3.2.1 Activité feedforward de la voie lemniscale

Au sein de la voie lemniscale, le VPM est la cible du noyau principal du complexe trigéminal, et envoie des projections glutamatergiques dans les couches IV, Vb et VIa de wS1 (Petreanu *et al.*, 2009). Il existe dans le VPM des structures appelées barréloïdes, qui sont des agrégats de neurones recevant des projections focales depuis une vibrisse principale. Les neurones du VPM répondent avec des potentiels d'action temporellement précis à des déflections mono-vibrissales de la vibrisse principale, avec des latences courtes de 4 à 8ms (Diamond, Armstrong-James and Ebner, 1992). Ce noyau thalamique est donc classifié comme un noyau du premier ordre, recevant des informations depuis la périphérie et les relayant fidèlement et rapidement au cortex sensoriel primaire par le biais de synapses géantes qualifiées de *drivers* (directrices) produisant une très haute probabilité de décharge post-synaptique (Sherman and Guillery, 1998; Mo *et al.*, 2017). Ainsi, le VPM cible préférentiellement wS1, constituant la source majeure de projection à sa couche IV et ne reçoit pas de projections cortico-thalamiques en retour. Il a été suggéré qu'un contrôle de l'information thalamique pouvait être effectué au niveau du VPM du fait de l'existence d'une adaptation des réponses neuronales à des stimulations répétitives des vibrisses (Deschênes, Timofeeva and Lavallée, 2003). Cependant, des enregistrements extracellulaires au cours de protocoles de stimulations vibrissales de faibles et hautes intensités montrent que cette

adaptation est essentiellement le résultat d'une dépression synaptique, ne se retrouvant probablement pas en condition naturelle. Cette projection thalamo-corticale est ainsi théorisée comme sous-tendant une dynamique feed-forward dans le traitement de l'information sensorielle.

#### 2.3.2.2 Activité feedback de la voie paralemniscale

Le POm est la seconde source d'entrée sensorielle au cortex somatosensoriel. À l'inverse du VPM, les neurones du POm ont des champs récepteurs beaucoup plus larges, avec des réponses multivibrissales, et ne présentent pas d'organisation somatotopique (Diamond, Armstrong-James and Ebner, 1992). Il existe tout de même une organisation préférentielle des entrées sensorielles périphériques dans le POm, avec une organisation antéro-postérieures et médio-latérale en lamelles (similaire aux couches d'un oignon). Le centre du POm ne présente pas de réponses aux déflections vibrissales, les vibrisses principales favorisant une réponse dans la partie dorsale et périphérique du POm (Sumser *et al.*, 2017). Les déflections de vibrisses uniques ne provoquent ainsi pas ou de faibles réponses dans les neurones du POm, de même que le *whisking* en l'air en l'absence de contacts (Masri *et al.*, 2008). Une autre différence est la propriété du POm à répondre à des stimulations bilatérales des vibrisses, le VPM ne présentant de réponses qu'aux projections contralatérales (Castejon and Nuñez, 2020). De plus, les latences de réponse dans le POm sont très nettement supérieures à celles du VPM, variant entre 19 et 27ms, probablement du fait de projections inhibitrices depuis la zona incerta (ZI) (Trageser and Keller, 2004).

Dans cette voie paralemniscale, les interactions thalamo-cortico-thalamiques sont nettement plus complexes. Ainsi, le POm envoie des projections glutamatergiques à la fois à wS1, wS2, wM1, mais aussi au striatum (Alloway *et al.*, 2006), au cortex périrhinal et au cortex insulaire (Deschênes, Veinante and Zhang, 1998). En plus des projections depuis le complexe trigéminal, le POm est sous très fort contrôle cortical, recevant des projections cortico-thalamiques depuis les couches infra-granulaires de wS1 et wM1, une partie de ces projections provenant des neurones cortico-pontiques de la couche Vb. Environ un tiers des neurones du POm, dans sa partie rostrale, représentent des zones de convergence, recevant des entrées à la fois trigéminales et corticales (Groh *et al.*, 2014). Cependant une grande partie des neurones du POm ne dépend que de l'activité corticale, créant des synapses *drivers* sur ces neurones (Mease *et al.*, 2016). Cette puissante influence cortico-thalamique permet

d'ailleurs de favoriser la réponse dans une sous-population de neurones du POm aux entrées vibrissales. En particulier dans les zones de convergence, il semblerait que les projections glutamatergiques corticales au POm permettent de lever l'inhibition exercée par la formation réticulaire (RT) ainsi que la zona incerta (ZI) et l'aire prétectale antérieure (APT).

En effet, des boucles d'inhibition impliquant le POm sont probablement la cause de sa résistance au recrutement lors de stimulations vibrissales. Ainsi, le noyau thalamique réticulaire (NRT) reçoit des projections de la couche VI de wS1, ainsi que des collatérales des axones thalamo-corticaux depuis le VPM et le POm. En retour, le NRT envoie des projections GABAergiques sur les neurones du POm (Lam and Sherman, 2007). La ZI quant à elle, reçoit des entrées depuis wS1, wM1, mais aussi depuis les noyaux trigéminaux et les noyaux cérébelleux profonds (**Figure 8**), et envoie des projections GABAergiques aux neurones du POm, qui inhibent les réponses sensorielles évoquées dans ce noyau (Lavallée *et al.*, 2005). L'activité du cortex moteur vibrissal notamment supprime l'activité dans la ZI (Urbain and Deschênes, 2007), procurant une boucle de désinhibition pour le contrôle sensoriel dans le cadre d'une activité motrice exploratoire, en fonction de l'état comportemental de l'animal (Trageser and Keller, 2004; Mitrofanis, 2005).

Les axones du POm ciblent principalement la couche Va et I de wS1. In vitro, il semblerait que les neurones excitateurs dans toutes les couches de wS1 reçoivent des entrées synaptiques directes depuis le POm (Audette *et al.*, 2018), cependant les enregistrements in-vivo et les traçages anatomiques placent préférentiellement les projections paralemniscales en couche Va et I (Deschênes, Veinante and Zhang, 1998; Ohno *et al.*, 2012). Les projections en couche Va du POm ciblent particulièrement les neurones pyramidaux ainsi que les interneurones exprimant PV (parvalbumine) et 5HT3A (VIP) (Audette *et al.*, 2018). Ces projections du POm sont caractérisées par des synapses de classe II, avec des boutons de taille plus petite, et une activité principalement modulatrice, c'est-à-dire ne produisent pas systématiquement des potentiels d'action, mais plutôt des potentiels excitateurs post-synaptiques (Viaene, Petrof and Sherman, 2011). Les neurones de la couche V reçoivent aussi des projections du VPM, et sont théorisés comme pouvant intégrer le contenu de l'information sensorielle et le contexte (provenant notamment de l'activité de la couche I) pour former la perception sensorielle. En effet, lors d'une combinaison de la stimulation du POm avec une déflection des vibrisses, les réponses sensorielles en couche V sont exacerbées, et notamment prolongées sur une période de presque 800ms. Cela suggère l'intégration

temporelle des voies parallèles lemniscales et paralemniscales au niveau de la couche V (Mease *et al.*, 2016). De plus, il existe une dépendance de la décharge des neurones du POm en réponse à une entrée sensorielle : les signaux cortico-thalamiques de la couche V interagissent directement avec l'entrée sensorielle au niveau du POm, la stimulation conjointe corticale et périphérique entraînant des réponses plus importantes dans les neurones du POm (Groh *et al.*, 2014). Cela suggère un rôle d'intégrateur temporel du POm, non pas seulement relai comme le VPM, qui se répercute dans la boucle thalamocorticale notamment en favorisant la réponse sensorielle dans les couches infragranulaires.

Cependant, l'autre couche cible du POm, la couche I présente aussi une activité sur les dynamiques intracorticales et le traitement des informations sensorielles. Une des particularités des axones du POm dans la couche I est qu'ils couvrent de larges zones corticales, avec une distribution horizontale dans cette couche de très longs axones faisant de multiples synapses sur les dendrites apicales des neurones pyramidaux plus profonds, mais aussi que ces axones produisent des collatérales (Deschênes, Veinante and Zhang, 1998). Ainsi un axone du POm peut à la fois projeter dans wS1 et dans wM1, créant un substrat anatomique pour la création de cohérences inter-corticales s'ajoutant aux projections cortico-fugales entre cortex. En couche I, les axones du POm font notamment synapse avec des interneurones de type VIP (Audette *et al.*, 2018). Ces axones en couche I ont été corrélés avec une inhibition de la réponse vibrissale dans wS1 (Shlosberg, Amitai and Azouz, 2006). L'inhibition de ces projections empêche l'adaptation des neurones de la couche II/III en réponse aux stimulations vibrissales (Castejon, Barros-Zulaica and Nuñez, 2016). L'activation conjointe de la voie lemniscale et de la voie paralemniscale permet en réalité d'activer les interneurones PV et VIP, qui augmentent leur inhibition sur les interneurones à somatostatine (SST), permettant la désinhibition des neurones pyramidaux de la couche II/III (Williams and Holtmaat, 2019). L'activité du POm permet ainsi de contrôler le gain et la plasticité intra-corticale via ces projections en couche I. Cela a été prouvé pour wS1, mais pourrait aussi être le cas pour de multiples aires corticales du fait de l'étendue des axones en couche I.

En sus de cette modulation du gain intracortical, le POm est aussi un site de communication intercorticale trans-thalamique. Ainsi, l'activation de la couche V de wS1 provoque une diminution d'amplitude et de durée de la réponse des neurones à une entrée sensorielle périphérique dans wS2, adaptation qui est abolie lors de l'inactivation au muscimol du POm (Castejon, Barros-Zulaica and Nuñez, 2016). De plus, une autre voie de

communication transthalamique entre wS1 et wM1 existe aussi, avec des projections thalamo-corticales de classe I, *driver* sur wM1 (Mo and Sherman, 2019). Ainsi, le POm intervient aussi dans les communications inter-corticales, se surimposant aux projections corticofugales directes entre cortex. L'existence de cette voie supplémentaire n'est pas complètement expliquée, mais intervient très certainement dans le traitement sensorimoteur, notamment du fait que cette voie ne serait active que dans un contexte d'attention active, permettant la désinhibition du POm par la ZI.

En résumé, ce noyau thalamique d'ordre élevé qu'est le POm a une action multiple au niveau cortical sur l'intégration sensorimotrice. Cela va en faveur de l'activité complémentaire de la voie lemniscale et paralemniscale : l'une transmettant fidèlement les informations sensorielles périphériques au cortex, tandis que l'autre, via d'autres micro-circuits, module le gain intra et intercortical afin d'affiner à la fois le traitement sensoriel (via wS2 et wS1), et l'acquisition des informations sensorielles (via wM1).

Le système sensorimoteur des vibrisses, relativement bien détaillé tant physiologiquement qu'anatomiquement, se révèle ainsi déjà complexe, avec de multiples boucles cortico-corticales, thalamo-corticales et thalamo-thalamiques. De multiples lieux d'intégration, tant au niveau du POm, que des aires corticales existent, cependant, il reste un acteur qui n'a pas été présenté dans ce système : le cervelet. C'est pourtant un effecteur majeur des systèmes sensorimoteurs, souvent négligé par la communauté vibrissale, et qui pourrait avoir un rôle non pas moteur, mais aussi sensoriel dans le système des vibrisses.

# 3 : Les vibrisses – la clé du cervelet ?

Le cervelet, en tant qu'organe sensorimoteur, ajoute un degré de complexité à la compréhension du système vibrissal. Dans un premier temps, il reçoit des informations vibrissales de plusieurs sources, via les fibres grimpantes et les fibres moussues. Dans ses projections ascendantes, le cervelet permet d'influer sur le cortex moteur et l'activité motrice, mais comme nous allons le voir, potentiellement aussi dans l'intégration sensorimotrice.

### 3. 1. Fibres grimpantes

Les fibres grimpantes, comme évoqué précédemment, innervent fortement les cellules de Purkinje, évoquant des potentiels d'action dans ces dernières de manière fiable, appelés *complex spikes*. Elles ont pour origine l'olive inférieure contralatérale (**Figure 8**), qui dans le système des vibrisses, reçoit des entrées de la partie ventrale des noyaux trigéminaux mais pas du noyau principal (Yatim *et al.*, 1996), avec la plupart des neurones de l'olive inférieure qui répondent à des entrées sensorielles (Gibson, Horn and Pong, 2004). L'olive inférieure reçoit aussi des projections depuis de multiples aires : depuis la moelle épinière directement et indirectement, depuis le colliculus supérieur, le noyau raphé, la zona incerta, et le cortex ipsilatéral à la fois moteur et sensoriel (Bosman *et al.*, 2011). C'est pourquoi notamment la stimulation de wM1 provoque des *complex spikes* dans le cortex cérébelleux.

Les différents noyaux de l'olive inférieure projettent dans différentes bandes parasagitales du cortex cérébelleux, mais principalement dans les zones C3 et D (Apps and Hawkes, 2009) **(Figure 4)**. Les fibres grimpantes ne suivent pas, comme dans les noyaux trigéminaux, une organisation somatotopique reproduisant les rangées de vibrisses. Ainsi, le champ récepteur d'une cellule de Purkinje répondra à une seule vibrisse, tandis que les Purkinje adjacentes peuvent répondre à n'importe quelle autre entrée du bloc vibrissal (Bosman *et al.*, 2010).

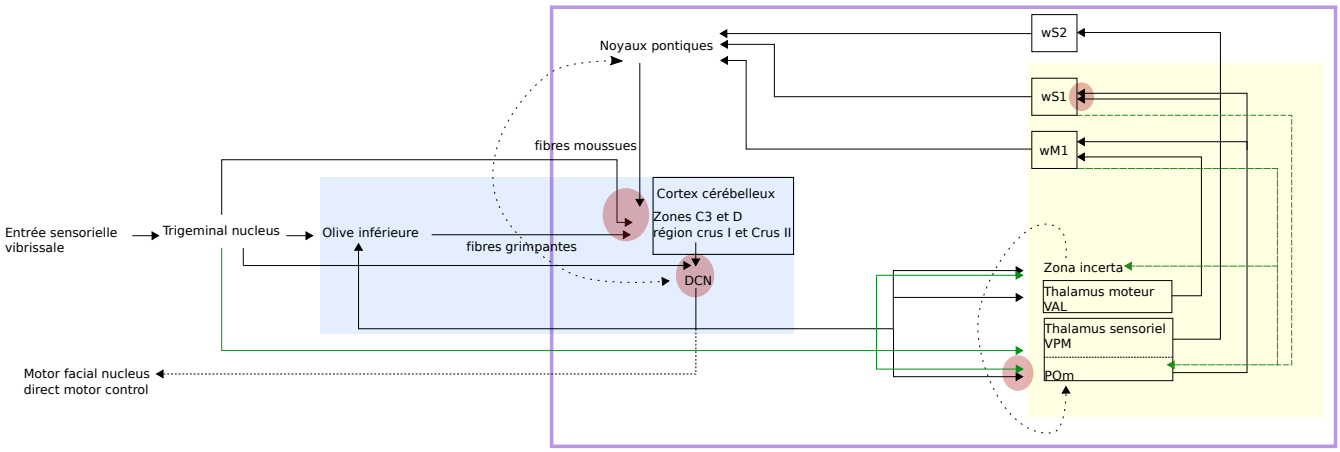


***Figure 8. Schéma résumé de la position du cervelet dans le système vibrissal***

*L'information sensorielle en provenance des vibrisses est propagée via les noyaux trigéminaux jusqu'au cervelet et au thalamus. Dans le cervelet, l'information brute de la périphérie est acheminée à la fois par les fibres moussues et les fibres grimpantes jusqu'au cortex cérébelleux, mais aussi aux noyaux cérébelleux profonds. Le cervelet projette ensuite au cortex moteur (VAL), mais aussi dans d'autres noyaux thalamiques tels que le POm (voir partie Résultats). De là, l'information est propagée aux cortex sensoriel et moteur primaires, avant de redescendre ver le cervelet via les noyaux pontiques. L'influence du cervelet sur le traitement des informations sensorielles se fait au niveau de plusieurs boucles imbriquées. Ainsi, il existe une première boucle olivo-cortico-nucléaire (en bleu), au sein de laquelle deux zones de convergence de l'information sensorielle « brute » et de l'information sensorielle pré-traitée se retrouvent (en rouge). Une deuxième boucle thalamo-cortico-thalamique*

*existe (en jaune), au sein de laquelle se trouvent des dynamiques thalamo-corticales et cortico-thalamiques modulées par le cervelet via le thalamus. Enfin, ces deux boucles s'imbriquent dans une grande boucle cérébello-cortico-thalamique, qui participe à plusieurs aspects des fonctions sensorimotrices des vibrisses, telles que la modulation du « setpoint ».*

### 3.2. Fibres moussues

Les fibres moussues sont donc l'autre source d'entrée au cortex cérébelleux, et synapsent sur les cellules en grain, qui en retour projettent des fibres parallèles contactant de nombreuses cellules de Purkinje, avec un gain assez faible (De Zeeuw *et al.*, 2011). Il existe deux sources de fibres moussues dans le système des vibrisses : l'une provient des noyaux trigéminaux et élicite des potentiels d'actions (*simple spike*) à courte latence dans les cellules de Purkinje des lobules Crus I et Crus II. La seconde source d'entrée provient des noyaux pontiques, qui reçoivent des projections depuis de nombreuses aires corticales, particulièrement wS1, wM1 et wS2. Ces fibres moussues évoquent des réponses à latence longue dans les Purkinkje, environ 17ms (Atkins and Apps, 1997).

Au sein des noyaux pontiques, les projections cérébropontines sont ségrégées et organisées en clusters (Panto *et al.*, 1995), avec peu de superpositions entre les aires de projections corticales (Leergaard *et al.*, 2004). Ainsi, le fait que la somatotopie continue observée dans wS1 ne soit pas retrouvée dans le cortex cérébelleux, qui a une somatotopie fracturée s'explique probablement par la divergence des fibres moussues qui forment des collatérales vers plusieurs zones du cervelet (**Figure 4**).

Les noyaux pontiques émettent des projections directes vers les noyaux cérébelleux profonds (DCN), en sus des projections principalement contralatérales vers le cortex cérébelleux. Ces afférents sont complétés par des projections retour des DCN vers les noyaux pontiques (Voogd and Ruigrok, 2012). La physiologie et le rôle de cette boucle dans le système des vibrisses ne sont pour l'instant pas clairs.

### 3.3. La sortie du cervelet

En résumé, de par les fibres grimpantes et les fibres moussues, de larges zones du cortex cérébelleux reçoivent des entrées vibrissales, directes ou indirectes. La sortie GABAergique du cortex cérébelleux est ensuite intégralement dirigée vers les DCN. Trois voies de sortie s'ouvrent ensuite :1- vers l'olive inférieure, afin de fermer la boucle olivo-cortico-nucléaires (Voogd and Glickstein, 1998) ; 2 - vers des aires qui projettent directement au

noyau facial, permettant potentiellement au cervelet de moduler directement le contrôle moteur ; 3- enfin, vers le thalamus, afin de moduler les aires corticales (Aumann *et al.*, 1994).

Les projections glutamatergiques des noyaux cérébelleux profonds projettent à des noyaux thalamiques relais primaires tels que le ventro-lateral thalamus (VAL), vers un noyau thalamique associé au fonctionnement moteur tel que le ventromédian (VM), mais aussi à des noyaux intralaminaires (Teune *et al.*, 2000). Ainsi, les DCN projettent dans des noyaux thalamiques qui assument à la fois un rôle de cœur comme le VAL (*core)* et de matrice (*matrix)* comme le VM, dénomination historique qui se chevauche avec les appellations de noyau thalamique primaire ou d'ordre élevé (Jones, 1998). Cette variété de fonctions et de projections thalamiques (Kuramoto *et al.*, 2009), notamment dans leurs projections corticales, suggère que le cervelet peut impacter un grand nombre de fonctions et de réseaux thalamo-corticaux.

### 3.4. Impact moteur du cervelet sur les vibrisses

Comme attendu du fait de la littérature extensive sur le rôle du cervelet dans le contrôle moteur, la décharge neuronale du cortex cérébelleux ainsi que sa sortie sont corrélées à des caractéristiques motrices des vibrisses.

Tout d'abord, dans le cervelet, les Purkinje de Crus I et Crus II répondent à des stimulations vibrissales (Bosman *et al.*, 2010), mais leur décharge en *complex spike* est aussi *phase-locked* (en verrouillage de phase) avec des mouvements induits des vibrisses (Lang, Sugihara and Llinás, 2006). Cette décharge en *complex spike* est aussi intrinsèquement liée à la direction du mouvement des vibrisses, à l'inverse de la décharge en *simple spike*. Ce second mode de décharge est lui plutôt lié à une autre caractéristique du whisking, qui est le *setpoint*, le point autour duquel les vibrisses oscillent, et qui est ajusté au cours d'une exploration tactile. La fréquence de décharge en *simple spike* dans les Purkinje de Crus I est ainsi liée à un encodage linéaire bilatéral du *setpoint* des vibrisses, créant une sorte de système de coordonnée de la position des vibrisses dans le cervelet (Chen, Augustine and Chadderton, 2016).

Dans un second temps, l'observation de la sortie du cervelet à l'aide d'enregistrements extracellulaires dans le noyau denté (DN), le VAL et wM1 combiné à des stimulations optogénétiques des Purkinje de Crus I a permis d'observer une activité propagée dans ces différentes structures (Proville *et al.*, 2014). Du fait de la sortie inhibitrice du cortex

cérébelleux, cette sortie est difficile à observer, et se fait principalement par l'analyse de l'activité rebond des structures en aval du cortex cérébelleux suite à l'inhibition conjointe d'un grand nombre de Purkinje. Cette voie cerebello-thalamo-corticale a été notamment impliqué dans la modification de l'encodage du *setpoint*, mais affecte aussi un paramètre plutôt lié aux fonctions sensorielles que sont le nombre et le temps de contact sur des objets.

Enfin, afin d'aborder une fonction motrice mais qui implique un degré d'intégration supérieure, il a été observé que dans le noyau fastigial du cervelet, une activité préparatoire similaire à celle observée dans le cortex frontal (ALM spécifiquement) quelques secondes avant l'exécution du mouvement (Gao *et al.*, 2018). De plus, l'inactivation du noyau fastigial a montré que cette activité est nécessaire au maintien de l'activité corticale préparatoire au mouvement.

Ainsi, le cervelet a été associé à plusieurs paramètres du mouvement, notamment au travers de la projection classiquement décrite de la littérature vers le cortex moteur, ou aires motrices associées. Cependant, un certain nombre d'études récentes pointent l'hypothèse de l'existence d'une voie directe vers les aires sensorielles.

### 3.5. Potentiel impact sensoriel du cervelet

Tout d'abord, si les projections cortico-pontiques depuis wS1 et wM1 sont ségrégées dans le pons avec peu d'overlap, elles convergent en revanche dans la partie latérale de Crus I au niveau cellulaire (Proville *et al.*, 2014). De plus, l'utilisation d'un traceur rétrograde transsynaptique, un pseudorabies, depuis différentes aires corticales chez le rat, a permis de mettre en évidence une infection au 3$^{ème}$ ordre de cellules de Purkinkje depuis plusieurs aires sensorielles primaires (Aoki, Coulon and Ruigrok, 2019). Si un seul des rats a été infecté dans le cortex sensoriel primaire vibrissal cependant, les cellules de Purkinje marquées correspondent à la partie latérale de Crus I où la convergence sensorimotrice a été observée chez la souris. Cela suggèrerait l'existence de boucles cérébello-corticales au moins en partie fermées, où une aire corticale projetant au cervelet reçoit en retour de cette aire cérébelleuse. Cette théorie avait été avancée chez le primate (Strick, Dum and Fiez, 2009) où l'utilisation de traceurs transsynatiques rétrogrades et antérogrades suggère que la sortie du cervelet cible de nombreuses aires corticales en sus des aires motrices. Ainsi, ces données suggèrent que le cervelet pourrait en effet posséder une voie de projection directe vers le cortex sensoriel primaire des vibrisses chez le rongeur.

Cette idée est renforcée par une évidence fonctionnelle de l'existence d'une telle voie. Ainsi, il a été observé qu'une inactivation pharmacologique des noyaux cérébelleux profonds chez le rat entraîne une disruption de la cohérence dans la bande gamma du potentiel de champ local entre les cortex moteur et sensoriel (Popa *et al.*, 2013). Cette perturbation n'était effective que lors d'un *whisking* actif, suggérant que le cervelet participe à la coordination des aires corticales sensorimotrices, et ainsi au traitement multirégional des informations sensorielles. Cette idée de cohérence entre le cervelet et de larges aires corticales est déjà retrouvée chez l'humain, où les études en *resting state* des activités cerebello-corticales montrent des covariations marquées en signal BOLD (Diedrichsen *et al.*, 2011) entre des aires spécifiques du cervelet et du cortex. Chez le rongeur, les projections des noyaux cérébelleux profonds vers le VM, mais potentiellement aussi dans le POm (Teune *et al.*, 2000), des noyaux thalamiques projetant notamment en couche I dans de vastes aires corticales va dans le sens d'un rôle du cervelet, non seulement dans les cohérences multi-corticales, mais aussi sur le contrôle des dynamiques intracorticales.

Mises en perspectives, l'ensemble de ces données donnent un potentiel substrat non seulement anatomique, mais aussi physiologique aux théories du contrôle sensoriel cérébelleux (CF chapitre 1), mais aussi de contrôle temporel des informations par le cervelet.

# 4 : Objectifs de la thèse

C'est pourquoi au cours de ma thèse, j'ai décidé de m'attacher à exploiter l'existence et la fonction d'une voie cérébello-thalamo-corticale liant le cervelet au cortex sensoriel primaire, dans le système des vibrisses. À cette fin, j'ai utilisé, notamment en collaboration avec d'autres membres de l'équipe ou d'équipes collaboratrices, une variété de techniques. Plusieurs questions ressortent notamment de ce travail :

1) **Quelles sont les interactions anatomiques et physiologiques du cervelet avec les aires sensorielles et motrices primaires vibrissales ?**
2) **Quel est l'impact de l'existence de voies de projections multiples du cervelet aux cortex sensorimoteurs, et quels sont les mécanismes d'actions de ces voies dans le traitement sensoriel ?**

Un des buts premiers au cours de cette thèse a donc été de cartographier la répartition des projections cérébelleuses dans les aires corticales motrices et primaires, en utilisant

notamment des techniques d'anatomie et d'histologie. A l'aide d'un traceur rétrograde trans-synaptique depuis les cortex moteur et sensoriel primaires, j'ai pu mettre en évidence l'existence d'une voie disynaptique des noyaux cérébelleux profonds à wS1, parallèle à celle existant pour wM1, avec cependant des zones de convergence. Je me suis notamment attaché à vérifier l'efficacité fonctionnelle de cette voie avec une combinaison d'enregistrements extracellulaires et de stimulations optogénétiques.

Dans la suite de ces efforts de cartographie, j'ai ensuite mis en évidence l'existence de plusieurs relais potentiels dans la projection cerebello-corticale à wS1. Combinée à mes observations dans les noyaux cérébelleux profonds, cela suggère l'existence de plusieurs voies cérébello-thalamo-corticales aux cortex sensorimoteurs, sous-tendant probablement différentes parties du traitement sensorimoteur.

Plus particulièrement, l'existence de colocalisation de terminaisons cérébelleuse et de cellules du POm rostral projetant à wS1 a attiré mon attention. Cette voie n'étant pas décrite dans la littérature, et semblant proéminente dans mes traçages anatomiques, j'ai décidé de focaliser mon attention dessus. Un contrôle cérébelleux du POm permettrait notamment de corroborer les théories précédemment exposées de discrimination tactile médiée par le cervelet, et de coordination d'aires multicorticales.

Nous avons donc tenté de comprendre quel corrélat comportemental pourrait être associé à cette voie spécifique, à l'aide d'un test de discrimination de texture et d'une analyse des caractéristiques d'exploration vibrissal lors d'une perturbation pharmacogénétique de cette voie. Enfin, afin de faire le lien avec les caractéristiques de traitement de l'information sensorielle dans wS1 et wM1, je me suis attachée à commencer à décrire l'impact de cette projection spécifique dans les couches thalamo-corticales, en particulier dans la couche I de wS1.

En sus de ce projet principal, regardant le couplage cérébello-cortical dans le système des vibrisses, j'ai eu le privilège au cours de ma thèse d'être impliqué dans plusieurs autres projets présentés en annexe. Le point commun de ces projets a toujours été d'étudier les voies de sortie du cervelet et leur impact sur d'autres structures cérébrales.

Ainsi, le premier projet auquel j'ai participé se concentrait sur les projections depuis le noyau fastigial du cervelet vers des structures impliquées dans la gestion de la peur, notamment la partie ventrale de la substance grise périaqueductale (vlPAG) **(Annexe 1)**. Nous

avons montré que cette projection pouvait contrôler bilatéralement l'intensité de la mémoire de peur, suggérant un rôle important de cette projection dans l'association entre le stimulus conditionnant et le stimulus non-conditionnant. La manipulation de cette projection permet aussi de moduler l'apprentissage de l'extinction de la peur. Ce premier projet m'a donc permis d'apercevoir le rôle du cervelet dans des processus, non plus purement sensorimoteurs, mais aussi émotionnels.

Le second projet auquel j'ai participé présentait quant à lui l'intérêt d'ouvrir vers des phénomènes pathologiques. Dans ce projet, nous avons étudié un modèle génétique de dystonie (GNAL ou DYT 25), pathologie fréquemment associée à des altérations fonctionnelles dans les projections cérebello-thalamiques. Ces souris exhibant des mouvements et des postures dystoniques à l'injection d'oxotremorine, nous avons étudié l'effet de stimulations optogénétiques des noyaux cérébelleux profonds avant et après l'injection d'oxotremorine. Nous avons ainsi pu observer une diminution de la sévérité des dystonies, via une potentiation des réponses dans le thalamus et le cortex moteur suite aux stimulations haute fréquence des noyaux cérébelleux profonds. **(Annexe 2).**

# Résultats

La première étape de ma thèse a été de déterminer quelles régions du cortex vibrissal recevaient des projections du cervelet et sous quelles modalités. Dans un premier temps j'ai utilisé une technique de traçage anatomo-fonctionnel utilisant un virus de la rage natif, injecté dans wS1 ou dans wM1, et qui permet une infection rétrograde des neurones avec des temps de cycle d'infection définis. Ainsi, une infection similaire entre les injections dans wS1 et wM1 a été observée dans les noyaux cérébelleux profonds, notamment le noyau denté, avec un temps d'infection cohérent avec le passage de deux synapses. Par la suite, j'ai procédé à des stimulations optogénétiques du noyau denté, et à des enregistrements extracellulaires de wS1 et wM1. wS1 présentait des latences de réponse courtes à la stimulation, de l'ordre de 7ms, tout comme wM1 qui est lui connu pour recevoir une projection disynaptique du cervelet. De plus, le potentiel de champ local de ces deux cortex présente des oscillations similaires au cours de la stimulation. Ces observations nous ont ainsi permis de déterminer qu'il existe une projection similaire du cervelet à wS1 et wM1, disynaptique, et semblant permettre une synchronisation relative de l'activité de ces deux cortex.

Le thalamus moteur est le relais thalamique connu dans la projection disynaptique du cervelet à wM1 ; la deuxième partie de ma thèse a été consacrée à la recherche du relais thalamique fonctionnel à la projection vers wS1. Des injections de traceur rétrogrades (CTb) dans wS1, wM1 combinées à un traceur antérograde dans le noyau denté nous a permis d'identifier plusieurs potentiels relais thalamiques. Le VAL, le VM et le POm rostral présentaient ainsi des cellules projetant vers wS1 dans des zones de terminaisons cérébelleuses, le POm présentant notamment de nombreuses cellules projetant à la fois vers wM1 et wS1. Nous avons alors procédé à des stimulations optogénétiques des terminaisons cérébelleuses in-vitro, provoquant de fortes réponses synaptiques dans les neurones du POm, de type driver-like. Cela nous a permis de montrer pour la première fois une connexion fonctionnelle cervelet-POm. Enfin, je me suis attachée à comprendre le corrélat comportemental associé à cette voie. Ainsi, une inactivation chémogénétique spécifique des neurones cervelet-POm, à l'aide de DREADDs inhibitrices, a été effectuée au cours d'une tâche de reconnaissance d'objets nouveaux. Dans ces conditions, les souris parvenaient toujours à reconnaître des objets différents par la forme, mais ne discriminaient (Voogd and De Zeeuw, 2020)pas ceux différents par la texture. Cette projection cervelet-POm semble donc impliquée dans des processus de discrimination tactile fine.

Or, nous savons que ces processus sensoriels sont dépendants de dynamiques cortico-corticales et corticothalamiques. La troisième partie de ma thèse a donc été consacrée à étudier l'impact cortical de la voie de projection DN-POm, particulièrement au niveau des axones longitudinaux se propageant en couche I. Pour ce faire, nous avons combiné des stimulations optogénétiques du noyau denté à l'imagerie biphotonique des axones de projection du POm en couche I de wS1. Nous avons donc observé l'activité calcique de ces axones exprimant la GCamp7f sous plusieurs conditions. Tout d'abord, nous avons observé qu'un petit nombre d'axones et boutons axonaux exprimaient une augmentation de l'activité calcique à courte latence après le début de la stimulation du DN, suggérant donc que le cervelet peut moduler l'activité corticale de wS1 via les projections en couche I du POm. Nous avons ensuite décidé de combiner des stimulations périphériques des vibrisses, sous la forme d'un puff d'air sur l'ensemble des vibrisses ipsilatérales à la stimulation cérébelleuse, avec les stimulations cérébelleuses.

Ainsi, au cours de ma thèse, j'ai pu mettre en évidence l'existence d'une voie de projection disynaptique depuis le cervelet vers le cortex sensoriel, passant notamment par un noyau thalamique d'ordre élevé, le POm. Cette projection est impliquée dans des processus de discrimination tactile fine, et nous émettons l'hypothèse que cette implication du cervelet passe par une modification du traitement de l'information sensorielle via un recrutement accru des projections en couche I du POm.

# Cerebellar modulation of sensory processing through a higher order thalamic nucleus

Baba Aïssa H., Varani A., Lourdiane A., Frontera J., Diana M., Coulon P., Leger J.F., Ruigrok T., Bourdieu L., Carcaud J., Veillard S., Popa D., Lena C.

## ABSTRACT

Accurate sensory acquisition and perception are key features to survival. Though many parameters underlying the processing of sensory information is known, several aspects are still poorly understood, such as the exact contribution of each cerebral structure. Here, we analyze the cerebellar contribution to sensory processing in the mouse whisker system. We identify an anatomical and physiological disynaptic projection from the cerebellar nuclei to the primary sensory cortex, involving notably by the posterior medial thalamus (POm). The modulation of this strong driver-like cerebello-thalamic projection induces an impairment in a fine sensory discrimination task, and its co-activation along with peripheral inputs induces the increased recruitment of POm projections to layer I of sensory cortex. Taken together, our results show that the cerebellum targets non-motor cortical areas and can directly modulate sensory processing through a higher order thalamic nucleus, the POm.

## INTRODUCTION

With more than two third of the central nervous system's neurons being located in the cerebellum, this structure long known for its somatic role in motor control and adaptation has been acknowledged in recent years as being involved in a wide spectrum of functions and dysfunctions in both animal models and human patients (Tsai *et al.*, 2012; Wang, Kloth and Badura, 2014; Stoodley *et al.*, 2017; Schmahmann and Sherman, 1998). Thus, the computational processing allowing sensory prediction and postulated to be executed by the cerebellum, traditionally used in models to modulate motor control, could also be used to modulate cognitive processing, sensory perception, spatial navigation (Manto *et al.*, 2012; Brooks, Carriot and Cullen, 2015; De Zeeuw and Ten Brinke, 2015). This view of the cerebellum has led to challenge the classical anatomical view of a closed loop between the cerebellum and the motor neocortex (Aumann *et al.*, 1994), and investigate the complexity of ascending projections from the cerebellum to other brain areas.

In the case of sensorimotor processes, the whisker system of the rodent has long involved the cerebellum in the control of the motor parameters of whisking (Bosman *et al.*, 2011). Hence, the patterns of whisker kinematics are reflected and controlled by the firing discharge of Purkinje Cells in the cerebellum (Proville *et al.*, 2014; Chen, Augustine and Chadderton, 2016; Brown and Raman, 2018); moreover, manipulating the cerebellar output can directly affect sensorimotor integration by somatosensory and motor cortices, thereby modulating direct movement (Popa *et al.*, 2013; Proville *et al.*, 2014). This large impact of cerebellar activity onto the cortex has mainly be explored through ascending anatomical projections involving the motor thalamus (VAL) and the primary motor cortex, though anatomical tracings have long suggested the existence of cerebellar projections onto various thalamic nuclei, and its influence on numerous cortical areas (Aumann *et al.*, 1994; Teune *et al.*, 2000; Kelly and Strick, 2003; Aoki, Coulon and Ruigrok, 2019).

In order to elucidate the involvement of the cerebellum onto sensorimotor integration, we decided to investigate the ascending projections of the cerebellum onto the somatosensory (wS1) and motor cortices (wM1) of the whiskers. Using transsynaptic retrograde tracing from the cortex, as well as optogenetic stimulation of the cerebellar ouput and extracellular recordings of the sensory cortex, we have identified a rapid disynaptic projection from the cerebellar nuclei onto the primary sensory cortex. Further anatomical tracings and in vitro recordings identified a higher order thalamic nucleus, the posterior thalamic nucleus (POm) as being a major relay from the cerebellum to the sensory cortex. We then proceeded to demonstrate that this cerebello-thalamo-cortical pathway contributes to fine sensory discrimination, and can influence the state of the sensory cortex via superficial layers.

**RESULTS**

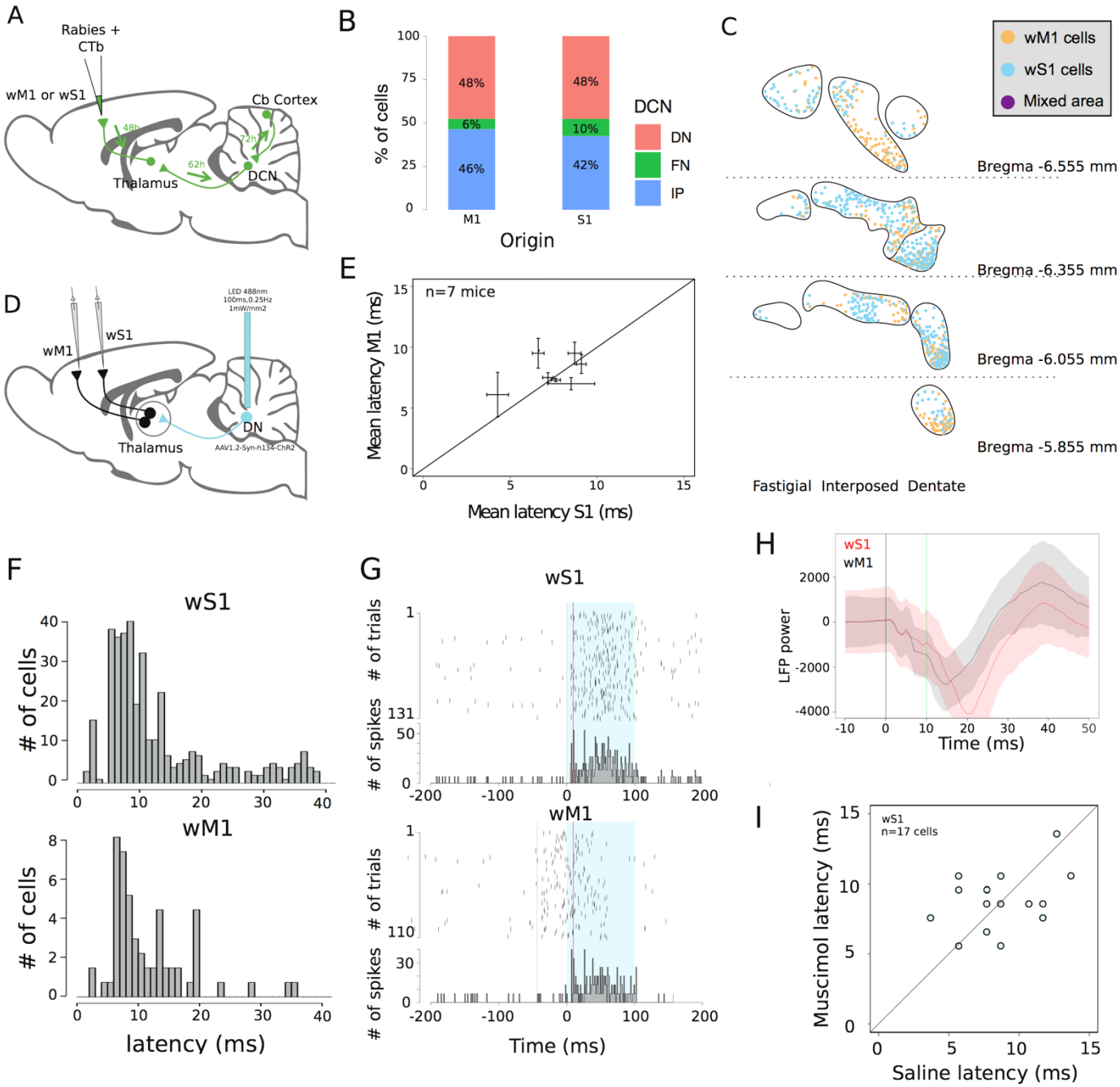


***Fig 1. Identification of a cerebello-cortical projections to wS1. A)*** *Scheme of retrograde injection from wS1 and wM1 using a trans-synaptic RABV virus, with the time needed to reach respectively the 1st, 2nd and 3rd order of infection.* ***B)*** *Proportion of cells found in the three DCN at the 2nd order of infections depending on the injection site. From wS1, for DN, IP and FN, cells found represented respectively 48, 42 and 10%. From wM1, respectively 48, 46 and 6%.* ***C)*** *Superposition of reconstitutions of the position of cells found in representative atlas slices from retrograde tracings from wM1(n=3 mice) and wS1 (n=3 mice).* ***D)*** *Scheme of extracellular recordings from awake freely-moving animals, electrodes were placed in wM1 and wS1, AAV-1.2-h134-Syn-ChR2 injected in the DN and an optic fiber positioned above DN.* ***E)*** *Comparative mean latencies under 15 ms between wM1 and wS1 recorded in the same mice (n=7 mice)* ***F)***

*Histogram representing for wM1(top) and wS1 (bottom) the latency for each cell to first respond above a threshold of Z=5 after the beginning of the optogenetic stimulation (n=6 mice).* ***G)*** *Rasterplot of representative responses for wM1 and wS1, where we can observe subsequent increases in the firing rate after the initial response, during DN stimulation.* ***H)*** *Superposed LFP responses example in wM1 and wS1 to the stimulation.* ***I)*** *Latencies of cells recorded in wS1 before and after muscimol inhibition of wM1 (pValue=0.2697).*

**wS1 to Cerebellum retrograde tracing**

In order to investigate the cerebello-cortical projections to the sensorimotor cortices, we performed a retrograde trans-synaptic anatomical exploration, as well as an electrophysiological assessment of those pathways.

First, we used a transneuronal RABV virus injected in either the primary whisker sensory cortex (wS1) or motor cortex (wM1) (Fig 1A). We first characterized the kinetics of transsynaptic infections. Injections in wM1 allowed us to investigate a well-described disynaptic pathway from the cerebellar nuclei to the motor cortex. At 48 hours post-injection in wM1, we found cells in the VAL, POm and VM thalamus consistent with known thalamo-cortical pattern of projection (Aumann *et al.*, 1994). At 62 hours post-injection in wM1, we found infected cells in the contralateral thalamus and the striatum, as well as the deep cerebellar nuclei. No cells were found at 62h post-infection in the cerebellar cortex, confirming that the 3$^{rd}$ order of infection was not reached yet. Cells were found in all three cerebellar nuclei, with the majority of cells evenly distributed between the interpositus and the dentate (Fig 1.B), though a denser proportion of cells were present in the ventro-anterior dentate and lateral anterior interpositus (Sup Fig 1.). Hence, we found cerebellar nuclei cells projecting to wM1 at a second order of infection, consistent with previous anatomical data from the literature (Allen and Tsukahara, 1974), reached 62h after infection.

Infections in wS1 produced cells infected at 48h post-injection in the VPM and POm thalamus (Sup fig 1.C), as well as in several areas of the neocortex including S2 and wM1. At 62h, the contralateral thalamus and deep cerebellar nuclei contained labeled cells, but not the cerebellar cortex. Similarly to infections in wM1, most cells were found in the dorso-lateral interpositus and ventro-anterior dentate nuclei (Sup Fig 1.E.). Interestingly, the distribution of cells between the three DCN was similar whether the infection was performed in wS1 and wM1 (Fig 1 C), with a notable area of super-imposition in the ventro-lateral portion of the dentate nucleus (Fig 1 C).

Hence, we have shown that with the same rate of infection, we were able to retrogradely infect DCN neurons from wS1 and wM1, suggesting the existence of a disynaptic pathway from DCN to the primary sensory cortex.

**Short sensory cortex responses to cerebellar stimulations**

We then performed optogenetic stimulations of the anterior dentate nucleus and extracellular recordings of wS1 and wM1 in freely moving awake animals (Fig 1D), in order to verify the existence of a physiological pathway from the cerebellum to these cortical areas.

We first looked at the motor cortex responses to the DN stimulation, and identified fast responses, with an average 7ms latency, consistent with a disynaptic pathway (Chen *et al.*, 2014). We identified the same early response in wS1 to the DN stimulation (Fig 1 F) for about 35% of all recorded cells. When comparing wS1 and wM1 fast-responding cells, no apparent lag was observed between the responses in the two cortices (Fig1.E). Interestingly LFP responses during the DN stimulations showed synchronous deflections in wS1 and wM1, beginning with a very early deflections in the first 5ms after the onset of the stimulation. This suggests the existence of a pathway influencing simultaneously wS1 and wM1, rather than influencing wS1 through wM1. To verify this hypothesis, we performed muscimol inhibition of wM1 and recorded wS1 using linear electrodes. We found that 71% of the cells responding at less than 15ms in control conditions presented the same profile of response under M1 muscimol inhibition. Interestingly, we observed a net effect on latencies for all cells responding with longer latencies in control conditions, which shifted to shorter latencies of responses (sup Fig 1G), possibly due to a relief of the inhibition mediated by the M1-ZI projections onto relay thalamic nuclei (Urbain and Deschênes, 2007).

Thus, we have shown the existence of a short latency response in the sensory cortex following cerebellar stimulations. This response was equivalent to the one produced in the motor cortex, which is presumed to be the result of a disynaptic pathway (Allen and Tsukahara, 1974), suggesting the existence of a disynaptic pathway from the DN to wS1.

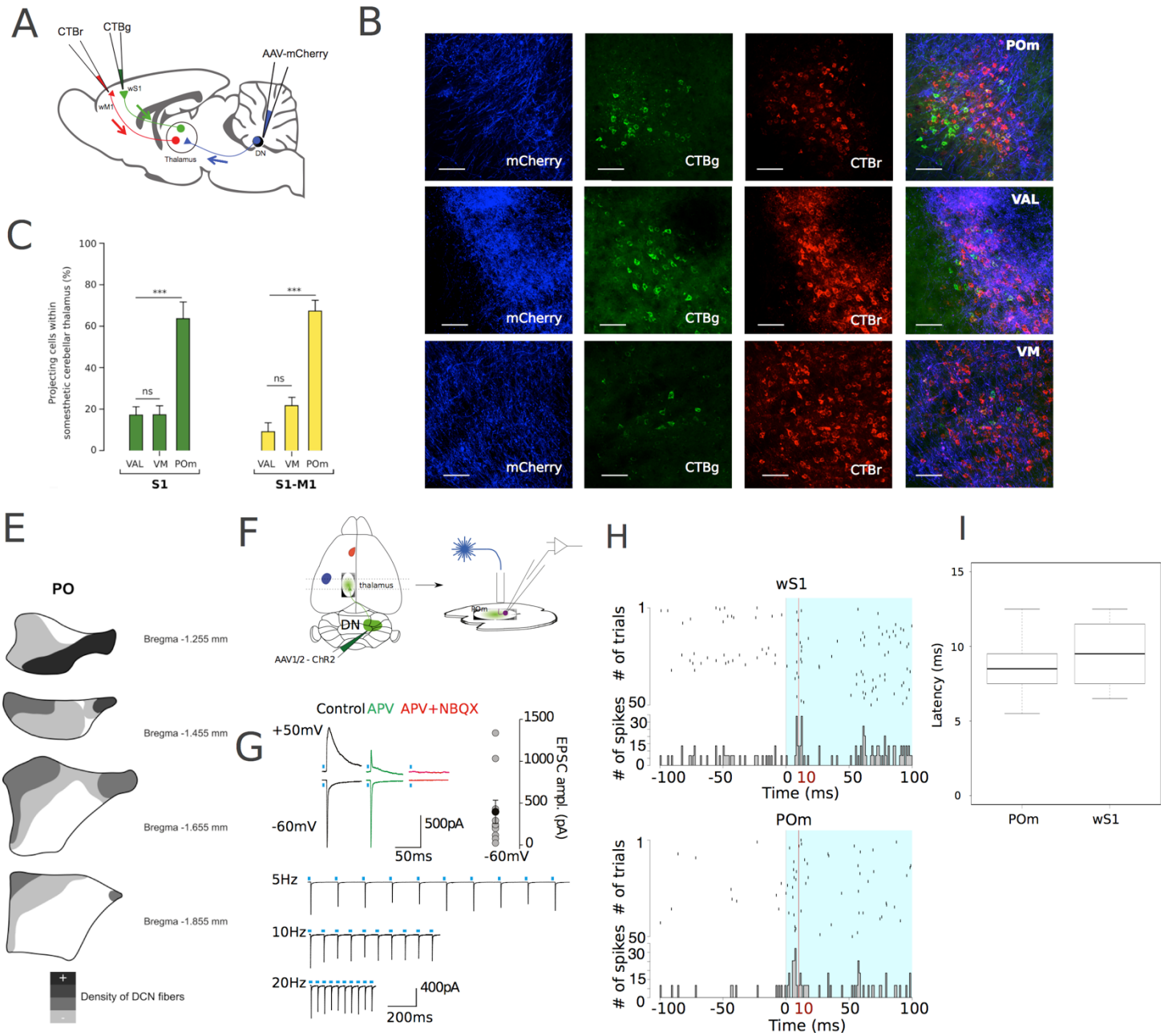


***Figure 2. Identification of thalamic relays in the DN-wS1 pathway****. A) Scheme representing the injections in wS1, wM1 and DN or respectively CTB-alexafluor 488, CTB-alexa fluor 555 and AAV-1.2-Syn-mCherry. B) Confocal images of colocalization in three thalamic nuclei : VAL, VM and POm (scale bar = 100microns). Cells projecting to wS1 (green) and to wM1 (red) colocalized in areas of cerebellar fiber terminals (blue). On the farther right images, yellow cells are cells projecting to both wS1 and wM1. C) Bar graph representing the proportion of S1 and colocalized S1-M1 projecting cells found in VM, VAL and POm receiving cerebellar fibers (***=p<0.001). D) Confocal microscopy image of synapses stained through synaptophysine from the DN (red). E) Reconstruction of the density of DN fibers found in the POm. F) Scheme of in-vitro recordings of POm neurons with optogenetic stimulation of DN fibers infected with AAV-1.2-Syn-h134-ChR2. G) Sample traces of in-vitro recording of POm neurons in response to DN fiber stimulation. H) Rasterplot of responses to DN stimulations in*

*wS1 and POm for representative cells. I) Boxplot comparing latencies of response to DN stimulations for POm(5 cells) and wS1 (11 cells) (N=2 mice). Median latency for POm is 8.5ms, median latency for wS1 is 9.5ms.*

**Identification of several thalamic nuclei as potential relays**

To identify the relay of a disynaptic projection from the DN to wS1, we used anatomical tracings to find an area of convergence in the thalamus.

We used anterograde tracing from the DN, and retrograde tracers injected in wS1 and wM1 (Fig 2A) in order to identify thalamic nuclei that could act as a relay in the cerebello-sensory cortex pathway. We identified several thalamic nuclei where S1-projecting cells colocalized with cerebellar fibers and terminals (Fig 2B): the ventro-antero lateral thalamus (VAL), the ventro-median thalamus (VM) and the posterior medial thalamus (POm). In these somesthetic cerebellar thalamic areas, we found that more than 60% of cells projecting to wS1 were located in the POm. Interestingly, we also found colocalization of wS1 and wM1 projecting cells. Most of them were located in the area of POm receiving cerebellar fibers (Fig 2C), but constituted only 7% of the S1-projecting cells in this area of the POm.

If the existence of cerebellar projections onto POm was suggested by the literature (Asanuma, Thach and Jones, 1983), it was never thoroughly investigated. To evaluate the influence of the cerebellum onto the POm, we first used anatomical tracings with synaptophysine to mark cerebellar synapses in the thalamus from the DN. We found cerebellar terminals in the very anterior portion of the POm (Fig 2 D), which was also the area where we found the highest density of cerebellar fibers (Supp. Fig 2. A). The tip of the POm, at the frontier with the VAL presented most of the cerebellar fibers, while the central and posterior portion of the POm presented few or no DN projections.

We performed extracellular recordings of the POm and wS1 simultaneously, and optogenetically stimulated the DN. We found short latency responses in both POm and wS1, with POm cells responded around 1ms before wS1 cells (Fig 1 H). Muscimol inhibition of POm failed to shunt the primary response in both POm and wS1 (Supp. Fig. 2B), probably due to the highly synchronizing optogenetic stimulation of DN providing strong inputs on POm cells sufficient to alleviate the gating.

In order to assert that these cerebellar terminals in the POm form functional synapses, we performed in vitro recordings of POm cells, combined with optogenetic stimulation of ChR2 infected projections from the DN (Fig 2F). We found strong AMPA-dependent responses

in POm neurons to the stimulation of cerebellar fibers (Fig 2G). The strength of these responses was not potentiated or depressed when applying increasing frequencies of stimulation. Altogether, these results attest to the existence of a strong drive exerted on anterior POm cells by cerebellar fibers from the DN.

Hence, we have found several potential thalamic relays in the ascending projection from the DN to wS1: the VAL, VM and POm. Interestingly, we showed that the POm presented the highest proportion of cells projecting to wS1 in areas where cerebellar fibers were found. We also showed a strong drive of the cerebellum onto the POm, where optogenetic stimulations of DN induced earlier responses in the POm than in wS1.

**Impairment of texture discrimination during DN-POm inhibition**

We next wanted to investigate the impact of cerebellar output on a specific whisker-related behavior. To this end, we used a novel-object recognition task combined with chemogenetic impairment of global or specific DCN output.

Novel object recognition is an ethologically relevant task using the natural curiosity of mice toward novelty. We used this task here using two conditions which depend on different discrimination mechanisms: identifying textures or objects (Fig 3 A). We first injected mice with inhibitory DREADDs in the three DCN to identify the effect of global cerebellar output on this behavior (Fig 3 B). Control mice injected with saline 30 min before the beginning of the experiment explored equally similar objects during the familiarization phase, and spent more time exploring the novel object in the test phase, whether the objects presented were textures or shapes (Fig 3 C and D). When injected with CNO, allowing the partial inhibition of cerebellar output (Varani *et al.*, 2020), mice spent the same time exploring the two objects in both the familiarization and habituation phases, showing that they were not able to recognize the novel object (Fig 3 C and D). On the opposite, mice in which the POm was inhibited with DREADDs were still able to recognize novel objects, but not novel textures (Supp. Fig. 3).

Inhibiting the three DCN has the disadvantage of impacting a lot of cerebral structures and functions. We thus decided to specifically target the pathway we previously identified, by injecting a retrograde CAV virus expressing the Cre recombinase in the anterior POm, while injecting a cre-dependent inhibitory DREADD in the DN. This allowed us to target specifically DN neurons projecting to POm (Fig 3 E). Under these conditions, control mice injected with

saline were still able to recognize the novel object, whether it was a novel shape or a novel texture (Fig 3 F). Mice in which we inhibited the DN-POm projections spent more time exploring the novel shape in the test phase, but surprisingly were not able to recognize the novel texture (Fig 3F). We had control mice with whiskers trimmed undergo the novel object recognition, and established that mice were able to recognize novel shapes without their whiskers (Fig 3 C and D), but not novel texture, showing that texture discrimination is a whisker-dependent fine sensory task. Not surprisingly, the DREADD inhibition of POm, a relay in the paralemniscal pathway, induced the same pattern of behavior, with an impairment on texture discrimination, but not shape recognition.

We then questioned whether the effect on novel object recognition of the impairment of DN-POm projections was the result of an impairment of motor control. During the familiarization phase, control mice, DN-POm inhibited mice and whisker-trimmed mice spent the same time exploring textures (Fig 3 G), showing that DN-POm inhibition did not impair global motor behavior nor interest in novelty.

Next, we used gap-crossing experiment, a motor task dependent on whiskers to evaluate different parameters of whisker movement (Fig 3 I). In this task, mice use their whiskers to evaluate the distance from one platform to the other to adapt their motor behavior in order to cross the gap (Fig 3 H). Both control and DN-POm inhibited mice performed similarly in the latency to cross the gap (Fig 3 J), showing that there was no lag in decision making, nor in performing a motor task dependent on global whisker control. Other parameters of sensorimotor whisker exploration in this task showed no difference between control and DN-POm impaired mice: cumulative touching per cross (Fig 3 K), number of contacts per cross (Fig 3 L) and touch duration (Fig 3 M) were not significantly different between the two groups. In our experiment, there seemed to be a significant decrease in the DN-POm inhibited group of the number of whiskers in contact simultaneously per touch (Fig 3 N).

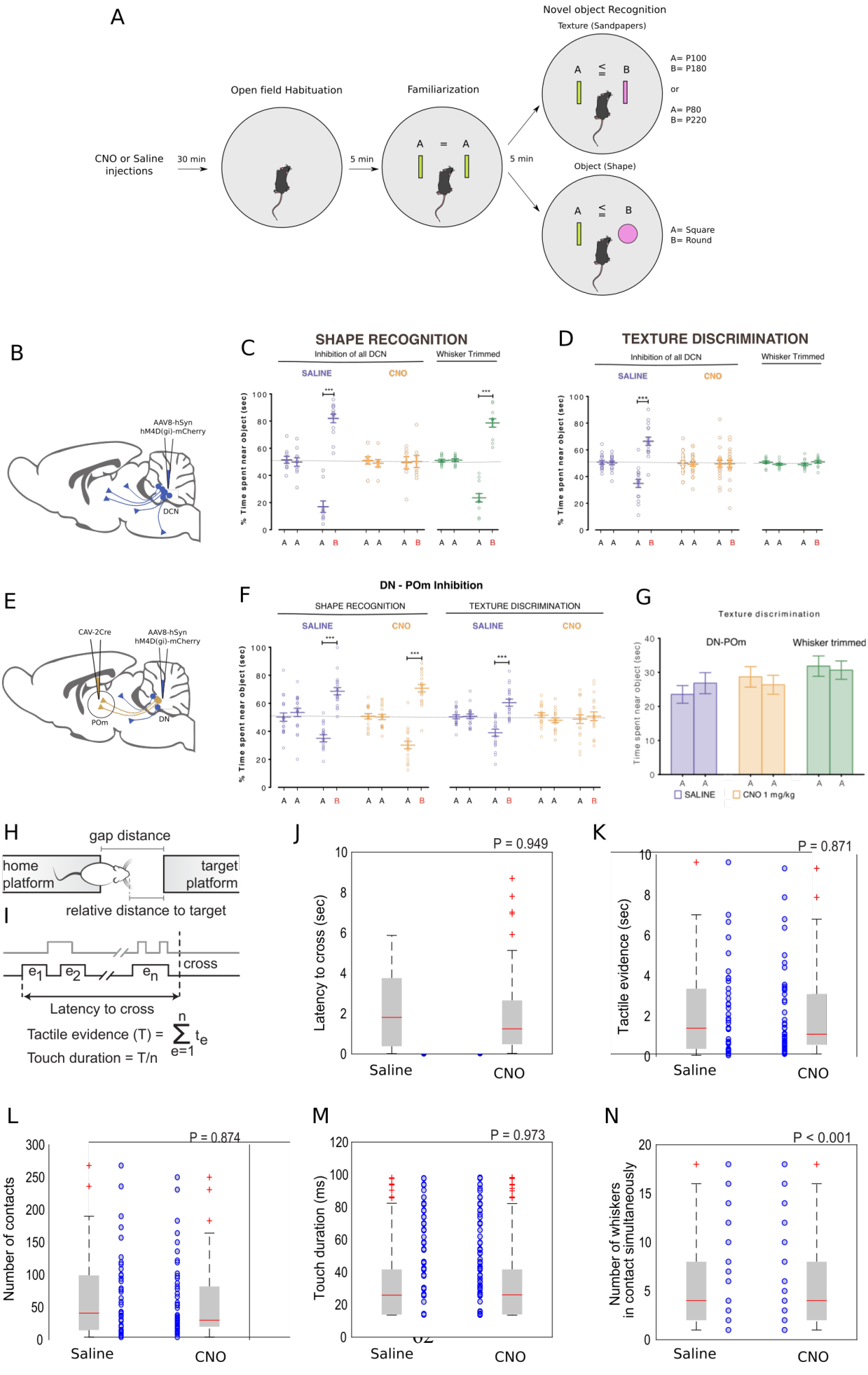
A
Novel object Recognition
Texture (Sandpapers)
A= P100
B= P180
or
A= P80
B= P220
Open field Habituation
Familiarization
CNO or Saline injections
30 min
5 min
5 min
Object (Shape)
A= Square
B= Round
B
AAV8-hSyn hM4D(gi)-mCherry
DCN
C
SHAPE RECOGNITION
Inhibition of all DCN
Whisker Trimmed
SALINE
CNO
% Time spent near object (sec)
D
TEXTURE DISCRIMINATION
E
CAV-2Cre
AAV8-hSyn hM4D(gi)-mCherry
POm
DN
F
DN - POm Inhibition
SHAPE RECOGNITION
TEXTURE DISCRIMINATION
G
Texture discrimination
DN-POm
Whisker trimmed
Time spent near object (sec)
SALINE
CNO 1 mg/kg
H
gap distance
home platform
target platform
I
relative distance to target
e1
e2
en
cross
Latency to cross
Tactile evidence (T) = $\sum_{e=1}^{n} t_e$
Touch duration = T/n
J
P = 0.949
Latency to cross (sec)
Saline
CNO
K
P = 0.871
Tactile evidence (sec)
L
P = 0.874
Number of contacts
M
P = 0.973
Touch duration (ms)
N
P < 0.001
Number of whiskers in contact simultaneously

***Figure 3. Evaluation of whisker behavior during global and specific cerebellar output inhibition. A)*** *Scheme representing the novel object recognition task, under two paradigms : exposition to similar shapes or similar textures.* ***B)*** *Scheme of injection of AAV8-hSyn-hM4D(gi)-mCherry in the fastigial, interposed and dentate nuclei (200nL/injection).* ***C)*** *Percentage of time spent exploring each shape objects in control mice (purple) and DCN inhibited mice (yellow), and whisker-trimmed mice for the familiarization phase (objects A-A) and test phase (objects A-B).* ***D)*** *Percentage of time spent exploring each textured objects in control mice (purple) and DCN inhibited mice (yellow), and whisker-trimmed mice for the familiarization phase (objects A-A) and test phase (objects A-B).****E)*** *Scheme of injection of AAV8-hSyn-DIO-hM4D(gi)-mCherry in the dentate nucleus (200nL) and CAV-Cre in the POm (100nL).* ***F)*** *Percentage of time spent exploring each object, for shape (left) and texture (right) objects for saline injected and cno injected mice.* ***G)*** *Total time spent exploring objects in second for the familiarization phase in saline injected and cno injected DN-POm mice, and whisker-trimmed mice.* ***H)*** *Scheme of gap-crossing experiment.* ***I)*** *Parameters used to assess several sensorimotor parameters in the behavior.* ***J,K,L,M,N)*** *Comparison for saline and CNO injected DN-POm mice for respectively: latency to cross the gap, cumulative touching per cross, number of contacts per cross, duration of touch and number of whiskers simultaneously in contact per touch. ***=pValue<0.001.*

Thus, we were able to illustrate the importance of the projection from the DN to the POm in a fine sensory discrimination task, in the absence of a global motor impairment or impairment of whisker behavior.

**Increased recruitment of POm-wS1 L1 boutons in concomitant peripheral and cerebellar stimulation**

This involvement of the cerebellar to posterior thalamic nucleus pathway in fine sensory discrimination suggests that cerebellar projections recruits thalamocortical loops involved in fine modulation of the somatosensory cortex. The posterior thalamic nucleus is described as a higher order thalamic nucleus (Casas-Torremocha *et al.*, 2019), and as such as having a modulatory input on cortical dynamics notably through its wide spreading projections in L1 (Audette *et al.*, 2018). We hypothesized that at least some of the inputs of the cerebellum on wS1 goes through POm-L1 projections.

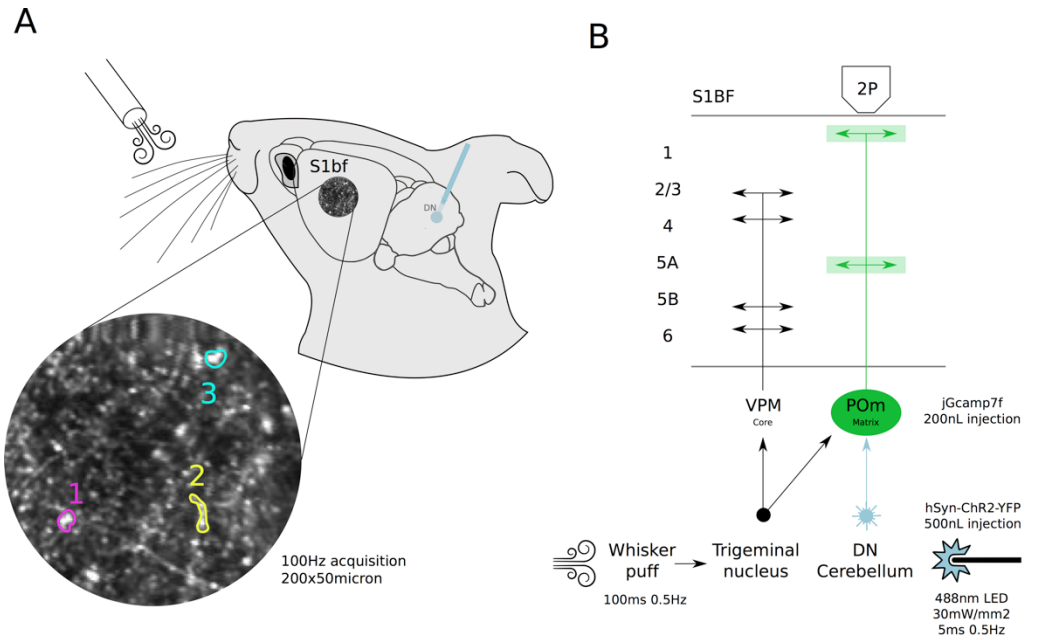
A
S1bf
DN
3
2
1
100Hz acquisition
200x50micron
B
S1BF
2P
1
2/3
4
5A
5B
6
VPM
Core
POm
Matrix
jGcamp7f
200nL injection
hSyn-ChR2-YFP
500nL injection
Whisker
puff
100ms 0.5Hz
Trigeminal
nucleus
DN
Cerebellum
488nm LED
30mW/mm2
5ms 0.5Hz

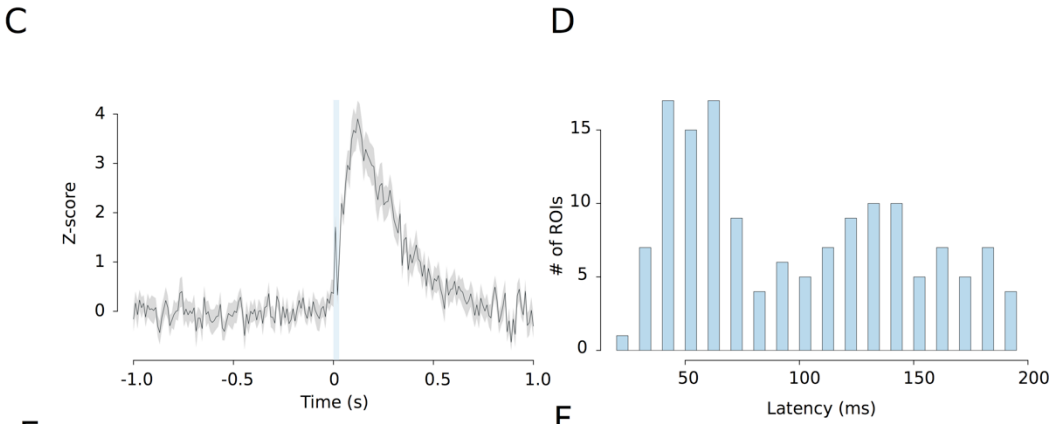
C
Z-score
Time (s)
D
# of ROIs
Latency (ms)

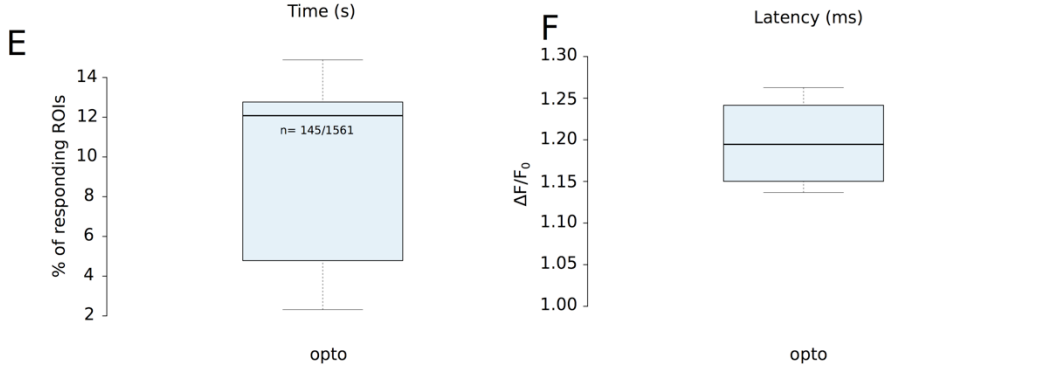
E
% of responding ROIs
n= 145/1561
opto
F
ΔF/F0
opto

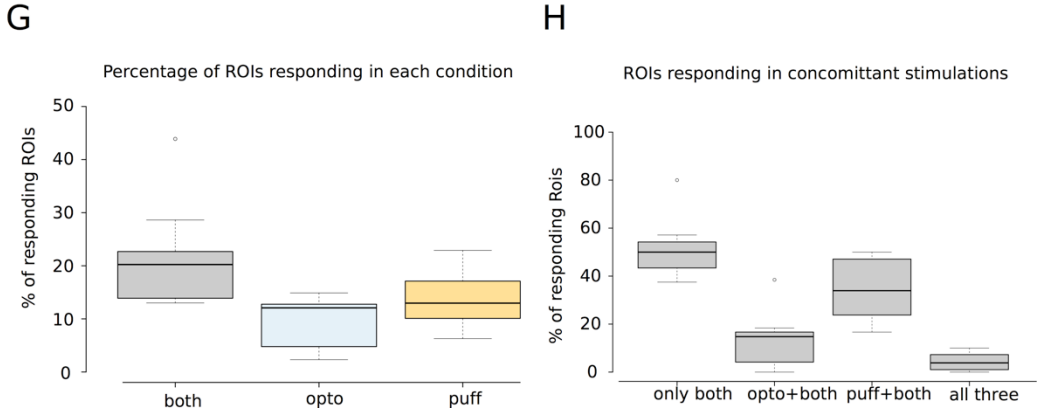
G
Percentage of ROIs responding in each condition
% of responding ROIs
both
opto
puff
H
ROIs responding in concomittant stimulations
% of responding Rois
only both
opto+both
puff+both
all three

***Figure 4. Biphoton calcium imaging of wS1 L1. A)*** *Schematic of acquisition paradigm with an example of a field of view and ROIs isolation of POm-L1 axons and buttons.* ***B)*** *Schematic of injections and expected projections in wS1.* ***C)*** *Representative example of fluorescence increase in layer 1 in response to DN optogenetic stimulations.* ***D)*** *Number of wS1-L1 rois crossing a threshold of Z=4 per bin of time in response to DN optogenetic stimulation.* ***E)*** *Percentage of putative axonal buttons in which a significant increase of fluorescence was observed in the 200ms following DN stimulations (N=3 mice, n=145 rois).* ***F)*** *dF/F at maximum peak during the 200ms following DN stimulations in responsive rois.* ***G)*** *Comparison of the percentage of responsive rois (over all the identified rois) in each stimulus conditions: both (concomitant DN stimulation and whisker puff), opto (optogenetic stimulation of DN) and puff (puff of air on the whisker pad).* ***H)*** *Comparison of the conditions in which responsive rois are recruited. 50% of responding rois are recruited only during concomitant stimulations (both) whereas around 30% of rois responds both during the air puff and the concomitant stimulations (puff+both).*

To investigate this effect, we performed two-photon calcium imaging of POm-L1 axons infected with GCamp7f, while optogenetically stimulating dentate nucleus projections (Fig 4.B). We found that a small percentage (2 to 14%) of all identified axons and buttons in L1 responded to DN stimulation. These ROIs responded reliably to DN stimulations, with a significant increase of fluorescence of about 18% (Fig 4.F) at the maximum peak of the response. The first significative bin of responses started at 20 ms, the artefact masking the first 10 ms, and spanned until 60ms (Fig. 4D), while the maximum peak of response is found around 140ms (Supp Fig 4C). Dentate nucleus stimulation thus induced a strong and reliable response, with a rather short onset in POm axons in L1 of wS1, although this response is found in a limited number of axons.

The posterior thalamic neurons have been described as being dependent on concomitant inputs from the periphery and primary sensory cortex to reliably fire (Mease *et al.*, 2016). We hypothesized that in the same way, a concomitant cerebellar and peripheric stimulation would produce an increased response of POm neurons. Thus, in a first time, we performed stimulations of the whole whisker pad using an air puff, and in a second time, we combined the optogenetic stimulation of the dentate nucleus with the whisker air puff. Whisker stimulations induced responses in 6 to 22% of POm-L1 axons (Fig 4 G), with an increase of fluorescence at maximum peak of 15% on average (Supp Fig 4. D). The first responses observed to the whisker stimulation from the onset of the stimulus were significantly longer than the responses to cerebellar stimulation, with most of the ROIs first responding between 50 and 100ms due to the delay in actually initiating whisker deflection

(see Material and Methods). This delay was taken into account to produce a concomitant cerebellar and peripheric stimulations onto the POm (Supp. fig.4 A). Interestingly, few ROIs (less than 20%, Supp Fig 4. F and G) presented a response in both the cerebellar and peripheric stimulations, suggesting that the responses in each case was mostly coming from different clusters of neurons in the POm. The concomitant whisker and cerebellar stimulations interestingly produced a significant increase in the percentage of responding ROIs, with 28 to 53% (Fig 4 G) of all identified rois presenting a neat increase in fluorescence (Supp. fig 4 D and E) in the first 200 ms. Notably, about 50% of the ROIs responding to the concomitant stimulations were only responsive in that case, and were not activated by either the whisker puff or the dentate stimulation (Fig 4H). This suggests that the increase in the percentage of L1-POm axons responding in the concomitant stimulation is not the result of the addition of the axons responding to either of the stimulations, but rather the result of the recruitment of a new pool of axons, so potentially a new pool of POm neurons. Interestingly, the maximum peak reached in response to the stimulation was higher in the concomitant stimulations, than in either optogenetic or whisker puff conditions for the same ROIs (Supp fig. 5). The intensity of maximum fluorescence in response to concomitant stimulations did not amount to the addition of maximum fluorescence for optogenetic or whisker puff stimulations, most likely due to the non-linearity of GCAMp7f, and saturation of the calcic signal.

Thus, we have shown, that dentate nucleus stimulation induces fast calcic responses in a significant portion of POm-L1 buttons in wS1, indicating a potential drive of the cerebellum on the surface of the cortex through a higher order thalamic nucleus the POm. In addition, we have seen the recruitment of specific thalamo-cortical projections from the POm to layer 1 dependent on the co-activation of POm neurons by the lemniscal and cerebellar inputs.

## DISCUSSION

Knowledge of cerebellar outputs has proven to still be very parcellar, with recent theories of parallel loops (Kelly and Strick, 2003) suggesting that motor and non-motor cerebrocerebellar interconnections make independent parallel loops. Here we show the existence of a short cerebellar output onto the primary sensory cortex, relayed by the POm, a higher-order thalamic nucleus allowing a modulation of cortical dynamics through superficial layers. We further demonstrate that this pathway is involved in fine sensory processing.

**Cerebellar projection to the sensory cortex**

Classical view of the cerebellum indicated that cerebellar output to cortical areas mainly converged onto the primary motor neocortex (Henneman, Cooke and Snider, 1952; Steriade, 1995) through the ventro-antero lateral (VAL) thalamus, with some projections from the fastigial nucleus targeting more widespread cortical areas through the ventro-median (VM) thalamus. Recent efforts in mapping cerebello-cortical loops have suggested that descending channels from the neocortex target specific regions of the cerebellar cortex, which in turn would project back to the same areas of neocortex (Kelly and Strick, 2003), a concept strongly supported by several anatomical, imaging and electrophysiological studies in both animal and humans (Kelly and Strick, 2003; Schmahmann, 2004; Allen, 2005). Although there has been a number of studies mapping new projections from the cerebellum onto various subcortical structures (Chen *et al.*, 2014), very few evidences are found in literature for distinct pathways from the cerebellum to non-motor areas of the neocortex (Aoki, Coulon and Ruigrok, 2019; Fujita, Kodama and Lac, 2020).

Here, taking advantage of efficient retrograde trans-synaptic tracing methods, we show that deep cerebellar nuclei neurons project in a disynaptic fashion to the primary sensory cortex, in a pathway parallel to the one going to the primary motor cortex. We also identify an area of convergence in the ventral part of the lateral cerebellar nuclei, wherein neurons project to wS1 as well as to wM1. Interestingly, this area has been previously demonstrated as being the recipient of lateral Crus I projections (Voogd, 2014), which in turn receive convergent inputs from the primary sensory and motor whisker cortices (Proville *et al.*, 2014). Using cerebellar optogenetic stimulations, we simultaneously recorded neurons in wS1 and wM1, showing a synchronous, short primary response to the DN activation in the two cortices, challenging the view of the cerebellum converging only onto the motor cortical areas, which then project to other neocortices. Combined with previous evidences (Kelly and Strick, 2003) (Proville *et al.*, 2014), our results reinforce the theory of existing functional parallel closed loop networks between the cerebellum and neocortical areas. Although we have focused on whisker cortices, other works in the literature (Aoki, Coulon and Ruigrok, 2019) suggest that cerebellar output targets various sensory cortices.

**Mapping polysynaptic pathways from cerebellum to sensory cortices**

In the rodent, few efforts have been made to unravel the cerebellar output to the neocortex, notably due to the complexity posed by the polysynaptic component of these pathways, though a new interest has emerged for these ascending cerebellar projections (Gornati *et al.*, 2018a; Fujita, Kodama and Lac, 2020)(Chabrol *et al.*, 2015). Deciphering the specificities of the circuits going out of the cerebellum seems to hold the key to furthering our understanding of the influence of the cerebellum on non-motor behavior, as well as its implication in multiple diseases ranging from autism to neurodegenerative diseases such as Parkinson. Through the use of several anatomical approaches, we have shown that the three cerebellar nuclei indeed send putative disynaptic projections toward the whisker sensory cortex. We have particularly focused onto the dentate nucleus since it provided the potential to make a comparison of electrophysiological data between the previously detailed projection onto wM1 through the VAL (Proville *et al.*, 2014) and our newly described projection onto wS1. In addition to previously explored DN projections onto VM and VAL (Gornati *et al.*, 2018a), we show the presence of cerebellar fibers and terminals onto the POm thalamus. Though data had long suggested that this nucleus might receive cerebellar inputs (Asanuma, Thach and Jones, 1983; Teune *et al.*, 2000), these projections to our knowledge have been mostly overlooked until now. Here, we have demonstrated driver-like inputs from the DN onto the anterior portion of POm, similar to inputs provided by paralemniscal projections and cortico-thalamic layer V projections onto this nucleus (Sherman and Guillery, 1998; Mease *et al.*, 2016). Through the POm, the cerebellum can target both deep and superficial layers of the sensory cortex (Castejon, Barros-Zulaica and Nuñez, 2016), accessing notably simultaneously several cortical areas through long-range projections in layer I.

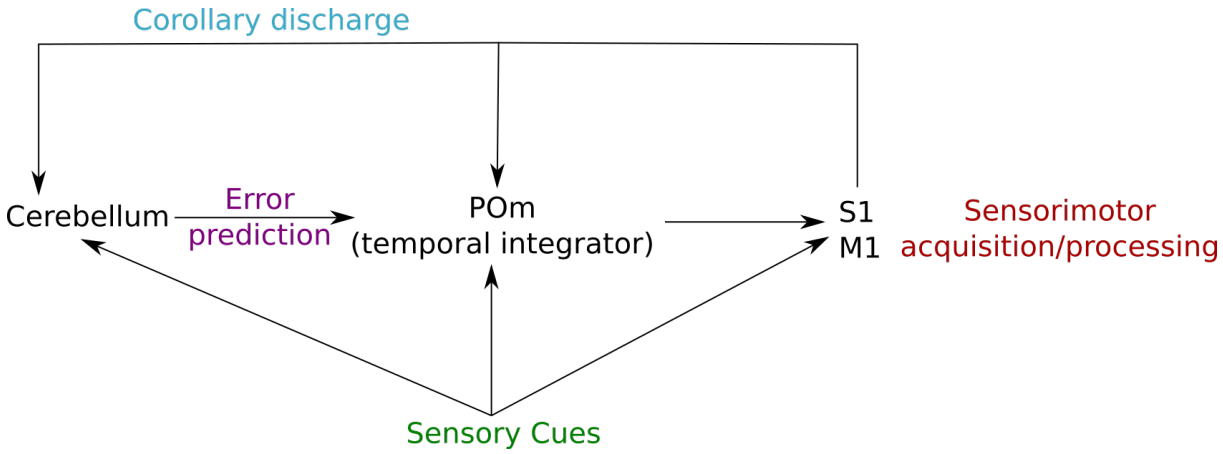


***Figure 5. Cerebellar influence on sensory processing.*** *Schematic diagram summarizing ascending the ascending cerebello-thalamo-cortical projection onto sensorimotor cortices.*

*Peripheral sensory cues are fed to the cerebellum, the POm, and faithfully to S1 through the VPM. The cortical block of S1 and M1 process the sensory inputs and control sensorimotor acquisition, sending these informations through the corollary discharge to the cerebellum. In turn, the cerebellum, according to internal model theories, putatively computes an error prediction which is sent to the POm. Integrating inputs from sensory cues, cortex and cerebellum, the POm is freed of subcortical gating and modulates the sensorimotor cortical areas to adjust sensory acquisition and processing.*

**A role of cerebellum in specific sensory acquisition**

We managed to show that this newly described DN-POm pathway was specifically involved in a fine sensory discrimination task, without noticeable changes in motor behavior or exploration strategy. Interestingly, several studies had previously questioned the role of the cerebellum onto sensory acquisition, and called into question the weight of sensory versus motor goals mediated by the cerebellum (Bower, 1997). Specifically, the lateral cerebellar hemisphere and dentate nucleus have been suggested to come into play in pure sensory discrimination, independently of motor activity (Gao *et al.*, 1996; Parsons *et al.*, 1997). In the whisker system, it has been demonstrated that the primary sensory cortex was essential for mice to perform efficiently in texture discrimination tasks (Park *et al.*, 2020), here we show that the cerebellum also reduces performance to chance levels in this fine sensory task.

We also show that an additional convergence between the paralemniscal pathway and cerebellum happens at the level of the POm, a higher order thalamic nucleus. The function of this higher order thalamus has not yet been elucidated, though many papers have placed the POm as an important modulator of the sensory and motor cortices (Chen *et al.*, 2015; Williams and Holtmaat, 2019). In the paralemniscal pathway, this nucleus does not faithfully relay sensory inputs to the cortices, being under a strong gating from the zona incerta (Lavallée *et al.*, 2005), and presents a higher firing probability under joined stimulations from sensory periphery and cortico-thalamic glutamatergic driver inputs (Groh *et al.*, 2014). Hence, the POm has been postulated as being a temporal integrator allowing the modulation of sensory acquisition through its projections to S1, S2 and M1, especially its widespread projections to superficial layers which are involved in changes in cortical excitability in various whisker-related behaviors (Helmchen, Gilad and Chen, 2018). Taken together, our results reinforce the view of the POm as a temporal integrator, this time integrating cerebellar inputs together with peripheral entries to recruit more LI projections in the primary sensory cortex (Fig 5). This feature could explain the impairment of fine sensory discrimination when we inhibit

projections from DN to the POm, preventing adaptability of the sensory cortex to detect fine changes in pattern of stimulation during active whisking, though we do not yet know under which precise circumstances the dentate nucleus feeds back to the POm. Further experiments would be needed to decipher the modalities under which the POm is modulated by the cerebellum during active behavior. Though such experiences will be compelx due to the invasivity of multi-site recordings in small animal models such as mice, which are hard to reconcile with ethnologically relevant behaviors.

## MATERIAL AND METHODS

### Animals

All animal procedures were performed in accordance with the recommendations contained in the European Community Council Directives (authorization number APAFIS#1334-2015070818367911 v3).

Experimental subjects were adult C57BL/6 N mice, 8–12-week-old, wild-type (Charles River Laboratories). Equal number of male and female mice were used. All mice were housed in groups of four litter-mate mice per cage, room temperature controlled at 21–22 °C, humidity between 40 and 50%, in a 12 h light/dark cycle. Implanted mice were isolated prior to surgery and post-surgery to preserve the integrity of the implant. Food and water were available ad libitum.

### Surgeries and stereotaxic injections

Mice were placed in a stereotaxic apparatus, anesthetized with isofluorane (1.75%) and their body temperature was monitored and kept at 37.2°C through a rectal thermometer. Buprenorphine was injected 15min prior to surgery for pain relief and 1 ml of 0.02% of lidocaïne was locally injected before skin incision. A scalp incision was made along the midline, and the skull was cleaned by scraping and by application of hydrogen peroxide.

### Rabies tracing

Before surgery, animals were anesthetized with ketamine (80 mg/ kg; Imalgene, France) and xylazine (10mg/kg; Bayer, Germany). Appropriate levels of anesthesia were monitored by the absence of whisker movements and pinch withdrawal reflex. The viral stock

was kept at −80°C until use. Under visual guidance, viral solution containing the "French" subtype of CVS-11 strain of RABV (titrating $4 \times 10^7$ plaque-forming units/ml) in conjunction with cholera toxin β-subunit (CTb, low salt; List Biological Laboratories, 1% w/v in 0.2 M phosphate buffer (PB) at pH 7.4: the injection solution consisted of 4 parts RABV and 1 part CTb) was injected with a 1-µl Hamilton syringe attached to a microsyringe pump. This RABV strain is confirmed to be transported trans-synaptically in a retrograde direction. No neighboring neurons are infected unless they maintain synaptic contacts to the already infected cells (Ugolini, 1995; Ruigrok *et al.*, 2008). Adding CTb to the injectate enabled accurate determination of the injection site. Mice were injected with 200nL of virus in wS1 and 100nL in wM1, in order to target a maximum of the area without spilling out of it, wM1 being significantly smaller, at depths of 0.2 to 0.9µm from the surface of the brain. The injection needle was placed for another 5 min to allow the virus to spread. After surgery, animals were monitored for signs of stress or discomfort after the surgery but all cases recovered uneventfully and behaved normally during their allotted survival time. During this time, injected animals were housed in the same BSL2 lab. Mice were sacrificed at different times after injection: 48h, 62h, 72h, times which are expected to infect respectively 1st order, 2nd order and 3rd order neurons, according to previous test injections.

**Anatomical tracings**

For the identification of relay thalamic nuclei, two consecutive surgeries were performed on the mice at 10 days interval. For the first surgery, a craniotomy was performed above the dentate nucleus. An anterograde virus (AAV2.1.CB7.CI.mCherry.WPRE.rBG) was pressure-injected at a depth of 2.4mm from the surface of the brain at a rate of 70nL/min. 10 days after, the second surgery was performed, craniotomies were done over wS1 cortex and wM1 cortex. An Alexa fluor 488 - conjugated cholera toxin B was injected in wS1 with 200nL per site at 70nL/min, at 6 injection points. An Alexa fluor 555 - conjugated cholera toxin B was injected in wM1, at 4 injection points, with 200 nL per injection site.

For the CTBs infusions, mice were perfused the fourth day after the injections. For the AAVs infusions, mice were perfused 21 days after the injections. Mice were anesthetized with ketamine 80 mg $kg^{-1}$ and xylazine 10 mg $kg^{-1}$, i.p., and the perfusions were performed with formalin (Sigma). Dissected brains were kept in formalin solution overnight at 4 °C, and the

brains were then stored in PBS solution at 4 °C. Brains were sliced entirely at 90 µm using a vibratome (Leica VT 1000 S), and mounted on gelatin-coated slides, dried, and then coverslipped with Mowiol (Sigma). Slices were analyzed and imaged using a confocal microscope (Leica TCS Sp8), and images were edited and analyzed using Image J. In the same way, the placement of the optic fiber, electrodes, and injections sites for all the experiments were assessed when the experiment was completed. Mice with no viral expression, or misplacement of the optic fiber or electrode were excluded from the analysis.

To identify thalamic relays, one out of two 90µm brain slices were imaged using a SP8 confocal microscope. We defined the sensory cerebellar thalamic areas as zones in the thalamic nuclei which presented a superposition of wS1-projecting cells and cerebellar fibers or terminals. The number of wM1 and ws1 projecting cells were manually quantified only in these areas using the ImageJ "cell counting" widget.

**Immunohistochemistry**

In the case of rabies injected brains, a double immunohistochemistry was performed to reveal CTb and Rabies particles. Brains were sliced at 50µm to allow a better penetrance of antibodies. Slices were rinsed with PBS, and sections were floated for 20 min in 3% hydrogen peroxydase (H2O2) in PBS for 20 mins to block reaction against endogenous peroxidase. Slices were incubated overnight with anti-rabies phosphoprotein mouse monoclonal antibody (Iseni *et al.*, 1997) diluted at 1:5000 in PBS+, that is, PBS containing 2% normal donkey serum and 0.5% Triton X-100. They were then rinsed and incubated overnight with a Rabbit polyclonal to beta subunit Cholera Toxin (1:5000 in PBS+, abcam). Slices were rinsed and then incubated for 2h with secondary antibodies: Donkey Anti-Mouse IgG H&L (Alexa Fluor® 488) (1:1000 in PBS+, abcam) and Donkey polyclonal Secondary Antibody to Rabbit IgG - H&L (Alexa Fluor® 555) (1:1000 in PBS+, abcam). Slices were analyzed and imaged using a confocal microscope (Leica TCS Sp8).

For the reconstruction of the position of neurons in the cerebellar nuclei following wS1 and wM1 injections, representative slices of the DCN in mice sacrificed 62h post injection were selected with 200 microns between each slice. Mice where the infection seemed to have spread to a 3$^{rd}$ order in other parts of the brain were excluded. Slices selected ranged from -5.855mm to -6.555mm from Bregma in the anterio-posterior axis, so from the most anterior

part of the DN to the middle of the DCN, more posterior slices presented few to no stained cells.

**Chemogenetics**

To see the effect of a global DCN or POm neurons inactivation, we expressed inhibitory DREADDs by bilaterally injecting pAAV-hSyn-hM3Dq-mCherry in those structures. To specifically modulate the activity of DN neurons projecting to POm, VAL or VM, a cre-dependent inhibitory DREADD was injected bilaterally in the DN, in combination of 200nL CAV2-cre-GFP in either of these thalamic nuclei. Surgeries and injections were performed 2 weeks before mice underwent the behavioral tests. For neuronal modulation of neurons expressing DREADDs, Clozapine N-oxide (CNO) (Tocris Bioscience, 1.24mg.kg$^{-1}$) was diluted in saline and injected i.p. 30 min before the start of the experimental session. Control group was injected with saline.

**Object discrimination**

The object discrimination test took place under two conditions: mice were presented either with textures or object shapes. Mice were acclimated to the experimental room for 1 hour before undergoing the test. In both conditions, the test followed three phases. Mice were placed for 5 minutes in the bare open field for the habituation period. In the control phase, they were exposed to the same objects, placed in the middle of the open field, at equidistance from the borders and each other. In the test phase, mice were presented with one object similar to the control phase, and one new object. Each phase lasted 5 minutes, and mice were placed back in their home cage for 5 minutes in between each period, while objects were changed and the open field cleaned. For this experiment, the open field (38cm diameter, Noldus) was under an infrared light, to prevent mice from using vision to distinguish the objects. For the shape discrimination, two sets of rectangular versus round objects were used. For the texture discrimination, two sets of textures with different roughness were used: P100 vs P180 or P80 vs P220. Each mouse underwent the shape and discrimination tests twice, using different sets of objects and different conditions, saline injections or CNO-injections. The position of the new object during the test phase, either left or right was randomly generated. Analysis for statistical significance was done on the percentage of time spent near each object using a one-way Anova followed by Tukey Posthoc test for each phase. To control

the need of whiskers to perform these tasks, a group of mice performed the tests after having their whiskers trimmed bilaterally, at the base of the whiskers, 5 days before undergoing the behavioral experiment.

**Gap-crossing experiment**

In order to evaluate the parameters of whisking during DN-POm inhibition, we performed a gap-crossing experiment on a custom-made setup, consisting of two elevated platforms separated by a gap of variable distances. Mice first performed the task under saline conditions, and the next day under CNO injections. The distance between the platform was randomly generated between 2.5 and 7cm wide, with the constraints of the first 5 crossings limited between 2.5 and 4cm to habituate the mouse. To cross. Food and water were available ad libitum before and after the experiment, and no food reward was used during the test. Mice performed between 10 and 20 crosses per session in a span of 30 min. The gap area was filmed from above at 70Hz, and the platform was lit from below using an infrared panel. A custom-written software quantified the duration and frequency of sensory exploration through the tracking of each whisker separately and the estimation of the whisker tip position from the whisker curvature on each frame.

**In vivo electrophysiology**

For optical manipulation combined with electrophysiological recordings, electrodes were implanted in mice injected with 350 nl of AAV-ChR2-GFP in the wS1, wM1, POm, and implanted unilaterally with an optic fiber in the DN (0.22 numerical aperture, Thor labs) housed in a stainless steel ferula (Thor Labs). The DN preferentially sends projections to the contralateral thalamus, therefore we recorded thalamus and cortex contralaterally to the fiber implantation. To record cell activity in the thalamus and cortex, we used bundle of electrodes consisting of nickel/Chrome wire (0.004 inches diameter, Coating 1/4 Hard PAC) folded and twisted into bundles of six electrodes. Pairs of bundles were inserted in metal cannulas (stainless steel, 29 G, 8 mm length, Phymep), in order to protect them and to guarantee a correct placement into the brain. Cannulas and bundles were also attached to an electrode interface board (EIB-16; Neuralynx, Bozeman) by Loctite universal glue in a configuration allowing us to record structures of interest. The microwires of each bundle were connected to the EIB with gold pins (Neuralynx). The entire EIB and its connections were fixed

in place by dental cement (Super Bond). The impedance of each electrode was measured and the 1 kHz impedance was set to 200–500 kΩ, using gold-plating (cyanure-free gold solution, Sifco). During the surgery, the electrode bundles were inserted into the brain and the ground was placed over the cerebellum, between the dura and the skull. The viral injection, optical fiber and electrodes implantation were performed in the same surgery, and the optical manipulation and recordings were performed 3 weeks after surgery to ensure ChR2 expression.

The recordings were performed on freely moving mice in an open field, spontaneous unit and LFP activity were recorded with a sampling rate of 25 kHz (Tucker-Davis Technologies System 3) while the animal freely explored the recording arena. Three to five salient objects were present in the arena to maintain the animal's interest for the environment. The animal was filmed with a monochrome video camera (50 Hz, AVT Marlin F033). Several blocks of 10 min of recordings were performed per session, alternating blocks with or without optogenetic stimulations, of 100ms at 0.25 Hz.

**Muscimol inhibition**

For muscimol inhibition of wM1, a 29G canula was implanted over the surface of the motor cortex, and a linear electrode with 16 channels (Neuralynx) was implanted with a 20° angle in wS1, in addition to the injection of an AAV-ChR2 and implantation of an optic fiber in the DN. Muscimol (4 µmol in 1 µl of saline) was administrated via the cerebellar guide cannula in awake, freely moving animals, during exploration. For this purpose, a hollow silica fiber (150 µm outer diameter) connected to a Hamilton syringe containing muscimol was inserted in a guide cannula (29G). At the end of the injection, the silica fiber was removed from the cannula and was stocked until the next session. Session with muscimol inhibitions started with 3 blocks of explorations alternating with or without optogenetic stimulations, followed by muscimol injections. The analysis of the response to optogenetic stimulations during muscimol inhibitions of DN projections was done on the recording blocks between 20 and 40 min after injections, to observe the peak of the inhibition. At the end of behavioral experiments, a dose of muscimol coupled with a fluorescent molecule was injected to evaluate the area affected by the muscimol injections.

**In-vitro electrophysiology**

To assess the existence and characteristics of cerebellar DN projections on thalamic POm neurons, mice were injected in the DN using an AAV-hSyn-ChR2. After 3 weeks to allow time for AAV expression, mice were sacrificed and the brains were sliced in 300 microns and kept at 34°C. The extracellular solution was composed of 1.6mM Ca2+, 1.5mm Mg2+, and the intracellular solution consisted of CsMeSO4. POm neurons were patched and cerebellar-ChR2 infected fibers were stimulated using 2ms pulses at 5, 10 and 20Hz. To evaluate the component of the response, a selective NMDA-antagonist DL-2-amino-5-phosphonovaleric acid (APV; 10 microM) was added. In a second time, in addition to NPV, the AMPA-antagonist 2,3-dioxo-6-nitro-7-sulfamoyl-benzo[f]quinoxaline was added to the solution.

**Calcium imaging**

In order to evaluate the activity of POm axons projecting to L1, calcium imaging was performed on WT C57bL6/J mice (n=3). During the surgery, mice were injected with 150nL of an AAV expressing the genetically encoded calcium indicator GCamp7f in the POm. As for optogenetic experiments, 350nL of AAV-hSyn-ChR2 was injected in the DN and an optical fiber was implanted above the DN. A transparent glass window (3mm wide) was placed above wS1 and fixed using dental cement. A home-made steel implant was also cemented to the skull to allow for head-fixed experiment. To make sure the optogenetic stimulation did not induce a light artefact, black cement covered the fiber, and black tape was wrapped around the stimulating patchcord.

After 3 weeks, to allow for viral expression, mice were habituated to the head-fixed apparatus for short sessions increasing from 1 to 30 min over a couple of days prior to the test session. The day of the test, mice were fixed on the apparatus, and were monitored using an infrared camera recording at 30Hz and an infrared light panel. A biphoton microscope was placed over the window in wS1, and the laser was calibrated at 350mW. First, windows of 250 by 300µm at a depth between 5 and 20µm below the glass window were used at a scanning frequency of 40Hz, and short 5ms optogenetic stimulations were applied over the DN. The response to the optogenetic stimulation was then evaluated by roughly summing the calcic activity in the imaging field divided in 6 rectangles. Once an area presenting responses was identified, we reduced the imaging window to 100µm by 50µm and increased the scanning frequency to 100Hz. A protocol in 3 phases was then conducted. First, optogenetic stimulations of 5ms at 0.50Hz were applied for 3 min. In the next phase, air puff stimulations

were performed using a picospritzer and aimed at the middle of the contralateral whisker pad to wS1. 100ms air puff were applied at 0.50Hz for 3 min. Using the video, we estimated that between the TTL launching the air puff and the actual whisker deflection, there was a latency of 40ms. The third phase consisted of combining the optogenetic stimulations and whisker deflections. In order to have whisker and cerebellar input arrive in the same time window to the POm thalamic nucleus, the air puff was first triggered, and after 50ms the optogenetic stimulation was launched. These combined stimuli were applied at 0.50Hz for 3 min (Figure Sup. 4A). A resting period of 10 min was observed in between each phase to allow the axons to recover from any potential bleaching due to the high-speed frequency imaging. At the end of the behavioral tests, mice were sacrificed and optical fiber placement as well as viral expressions were verified. Using a custom software, images were corrected for movement. Regions of interest (ROIs) defined as axonal bodies or buttons were isolated automatically using ImageJ.

| Experiment | Injection site | Virus | Quantity | AP (µm) | ML (µm) | Z (µm) |
|---|---|---|---|---|---|---|
| **Triple colocalisation** | DN | AAV2.1.CB7.CI.mCherry.WPRE.rBG (UPenn) | 250nL | (-)6.0 | (+)2.3 | (-)2.4 |
| | wS1 | Alexa fluor 488 - conjugated cholera toxin B (ThermoFisher) | 800nL | (-)1.1 to (-)1.5 | (-)2.8 to (-)3.2 | (-)0.8 and (-)0.4 |
| | wM1 | Alexa fluor 555 - conjugated cholera toxin B (Thermofisher) | 600nL | (-)0.9 to (-)0.1 | (-)0.9 to (-)1.1 | (-)0.7 and (-)0.3 |
| **Optogenetic** | DN | pAAV8-Syn-ChR2(H134R)-GFP (Addgene) | 250nL | (-)6.0 | (+)2.3 | (-)2.4 |
| **Behavior** | DN | pAAV-hSyn-hM4Di-mCherry or pAAV-hsyn-DIO-hM4Di-mCherry (Addgene) | 200nL | (-)6.0 | (+/-)2.3 | (-)2.4 |
| | IP | pAAV-hsyn-DIO-hM4Di-mCherry (Addgene) | 200nL | (-)6.0 | (+/-)1.5 | (-)2.1 |
| | FG | pAAV-hsyn-DIO-hM4Di-mCherry (Addgene) | 200nL | (-)6.37 | (+/-)0.7 | (-)2.12 |
| | POm | CAV2-cre-GFP (Plateforme de Vectorologie de Montpellier) | 100nL | (-)1.3 | (+/-)1.27 | (-)3.1 |
| | VAL | CAV2-cre-GFP (Plateforme de Vectorologie de Montpellier) | 100nL | (-)1.4 | (+/-)1.0 | (-)3.5 |
| **Calcium Imaging** | DN | pAAV8-Syn-ChR2(H134R)-GFP (Addgene) | 250nL | (-)6.0 | (+)2.3 | (-)2.4 |
| | POm | pGP-AAV8-syn-jGCaMP7f-WPRE | 150nL | (-)1.3 | (+/-)1.27 | (-)3.1 |

***Table 1. List of viruses used per experiments and their injection coordinates.***

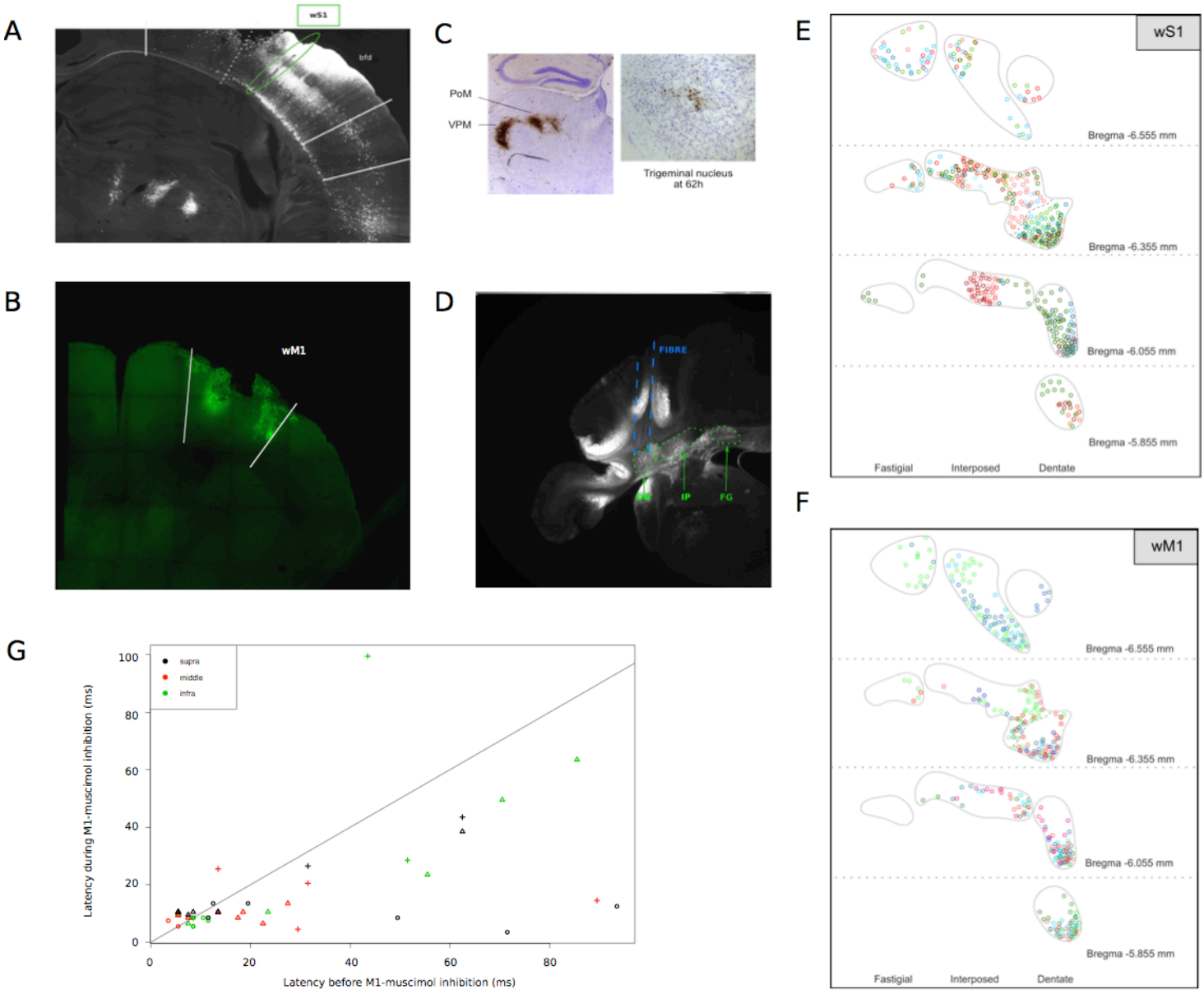


***Supplementary Figure 1. Characteristics of the cerebellum-wS1 pathway. A)*** *Injection site in wS1, showing the CTb injection performed along with the RABv virus. We can see POm, intralaminar and VPM thalamic nuclei stained as well as wS2 on the bottom right of the image.* ***B)*** *Injection site in wM1 showing the CTb injected along with the RABV virus. We clearly see the 2 sites of injection performed to infect a larger portion of wM1.* ***C)*** *Rabies-stained neurons revealed through a non-fluorescent immunohistochemistry in brains injected in wS1. We observe stained neurons in the POm and VPM 48h after injections, and in the trigeminal nucleus 62h post-injection.* ***D)*** *Histologicy of a representative example of optic fiber lesion over the DN in a mouse responding with short latencies in wS1 to DN stimulations. We can also see the fluorescence of the ChR2 coupled with the GFP.* ***E and F)*** *Reconstruction of rabies-infected neurons from injections in wS1 (E) and wM1 (F). Each color represents a different mouse.* ***G)*** *Comparative latencies to respond to DN optogenetic stimulations in wS1, before and after wM1-muscimol inhibition. The different shapes represent the different mice, while the different colors represent the position on the linear electrode where the cell was recorded. supra= putative supragranular layers, infra= putative infragranular layers, middle=putative granular layer.*

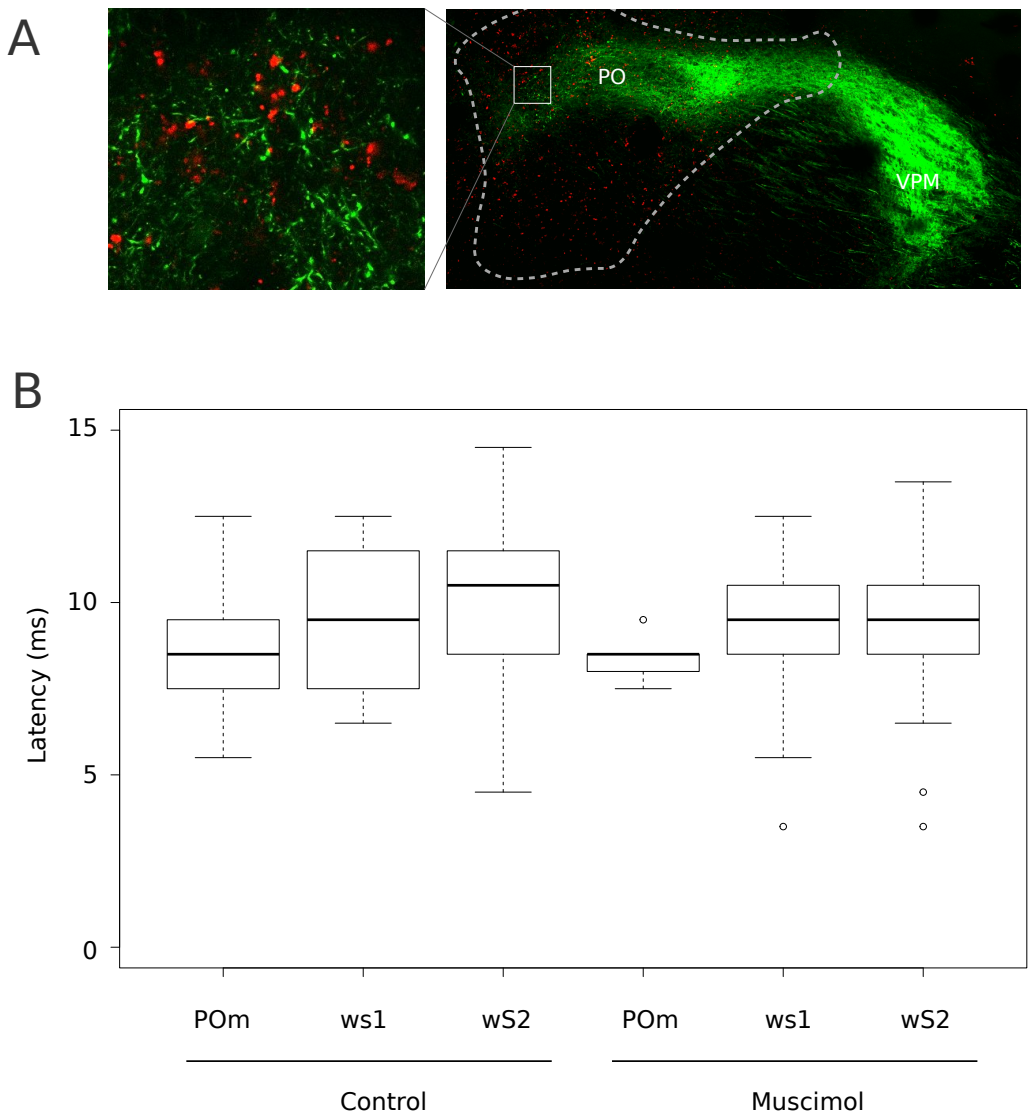


***Supplementary Figure 2. Cerebellum forms functional synapses onto POm. A)*** *Confocal images of synaptophysine expressing cerebellar projections. Mice were injected with a retrograde Cre-dependent AAV-synaptophysine-mCherry in the POm (150nL), an anterograde Cre AAV in the dentate nucleus of the cerebellum (250nL) as well as an AAV-retrograde-GFP in wS1. The AAVr (Addgene) did not seem to be functioning in a retrograde fashion on thalamo-cortical projections, but presented an anterograde staining instead (Green varicosities and fibers). Synaptophysine was expressed through all the anterior POm, as well as intralaminar, VM and VAL thalamic nuclei (not shown here), showing the existence of functional synapses in those structures from the DN. No synaptophysine was found in the sensory thalamus (VPM) as expected from the literature and previous experiments.* ***B)*** *Boxplots comparing latencies in POm, wS1 as well as wS2 recorded in the same mice, in control conditions and PO-inhibited with muscimol conditions. We can see that muscimol failed to inhibit short latency responses in PO and wS1, suggesting that the high synchrony of our DN stimulation provoked currents strong enough to overcome the inhibition. Interestingly, we also see short latency responses to DN stimulations (less than 10 ms) in wS2. N=2 mice (POm.ctrl=5 cells, S1.ctrl=11 cells, S2.ctrl=17 cells, POm.musc=7 cells, S1.musc=13 cells, S2.musc=17 cells).*

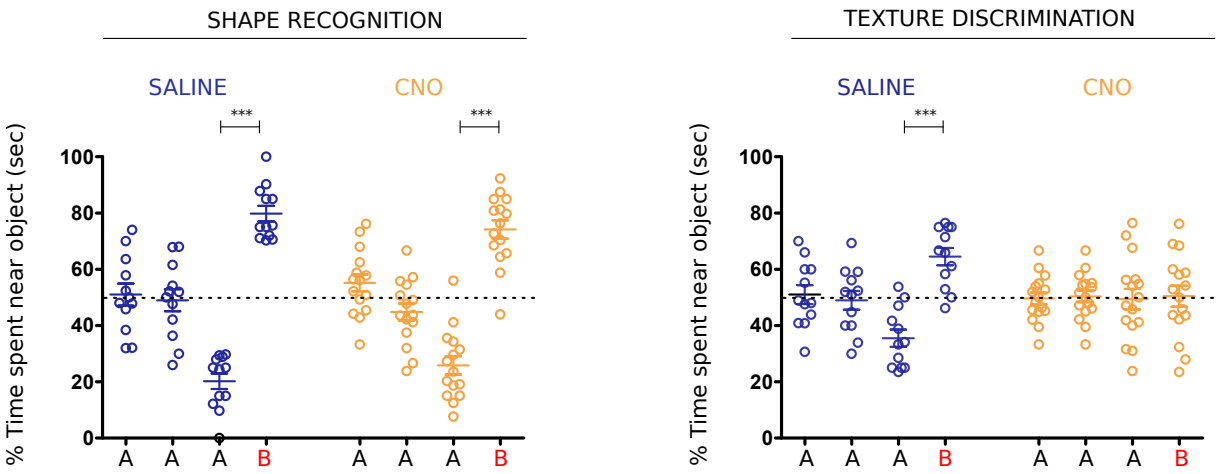


***Supplementary Figure 3. Global PO inhibtion during shape and texture discrimination.***

*On the left, during shape recognition, we see that mice are still spending more time exploring the novel object (B), whether the POm is inhibited (CNO, pValue<0.0001) or not (SALINE pValue<0.0001). On the right, during texture discrimination, mice are spending more time exploring the novel texture in control conditions (SALINE pValue<0.0001), but not when the PO is inhibited (CNO, pValue=0.0611).*

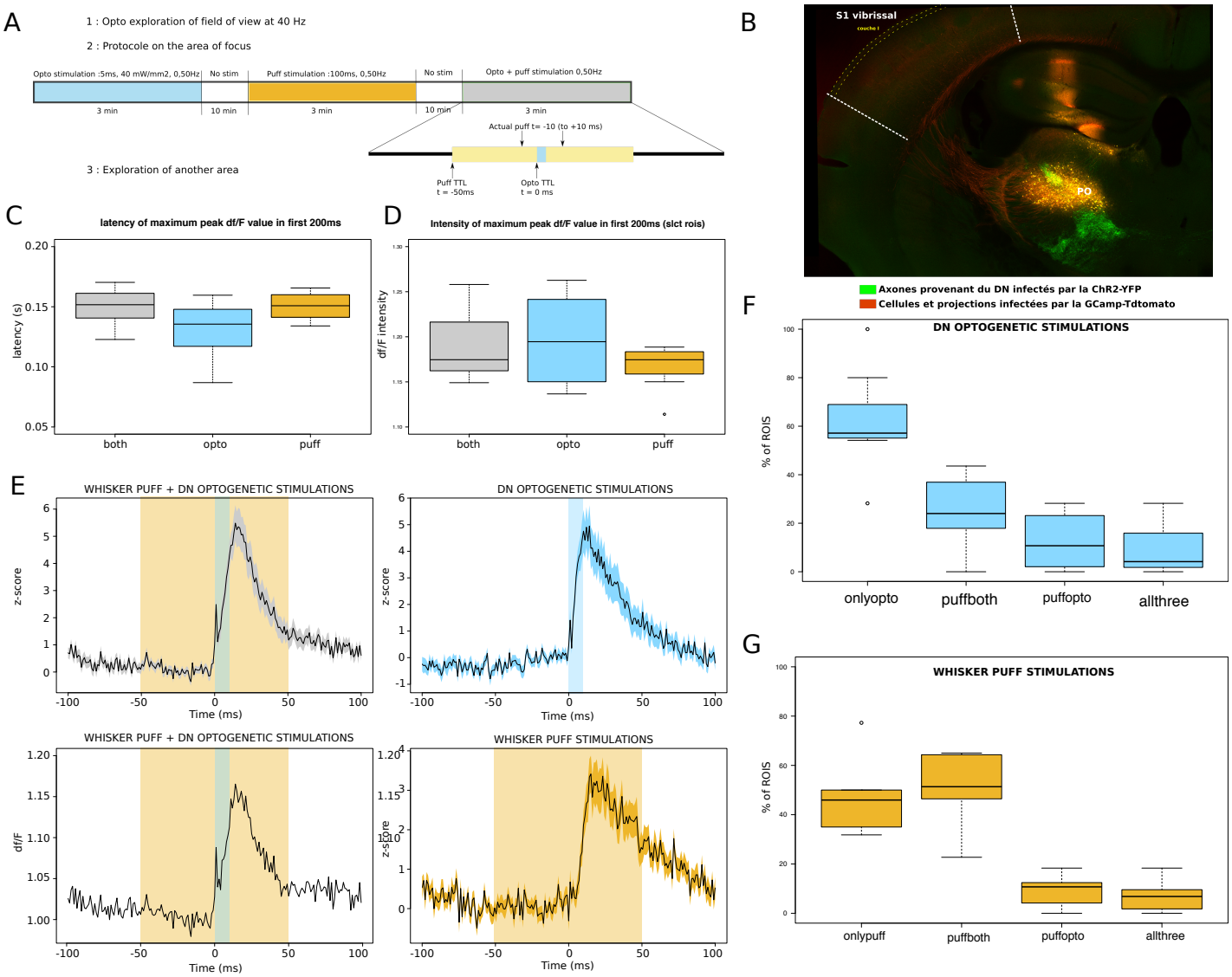


***Supplementary Figure 4. Calcium imaging of wS1-L1.*** ***A)*** *Scheme detailing phases of the experiment, starting with the exploration of field of view at 40Hz. The protocol in the second step is performed at 100Hz on a smaller field of view, starting with the optogenetic stimulation (in blue), followed by air puffs on the whisker pad, and finishing with the simultaneous DN optogenetic stimulation and whisker air puff.* ***B)*** *Representative histology of thalamus with GCamp injections in the POm (in red) and cerebellar terminals infected with ChR2 (in green).* ***C)*** *Boxplot of comparative latencies to reach the maximum peak of responses (df/F) in the first 200ms following the start of the stimulation for simultaneous stimulations (both), DN optogenetic stimulations (opto) and whisker air puff stimulation (puff).* ***D)*** *Boxplot of df/F maximum intensity reached for each condition of stimulation.* ***E)*** *Averaged responses for responsive ROIs in a representative block of each stimuli condition.* ***F)*** *Boxplot comparing, for ROIs responsive to DN optogenetic stimulations, in which conditions they are also responsive. Here, 60% of ROIs responding to DN stimulations only respond in this case (onlyopto), while 15% respond also to whisker stimulations (puffopto).* ***G)*** *Boxplot comparing, for ROIs responsive to whisker puff stimulations, in which conditions they are also responsive. Nearly all ROIs were either responsive only to whisker stimulations or to simultaneous DN and optogenetic stimulations. Overall very few ROIs responded to both whisker and cerebellar stimulations independently, and even less responded in each phases of the protocol.*

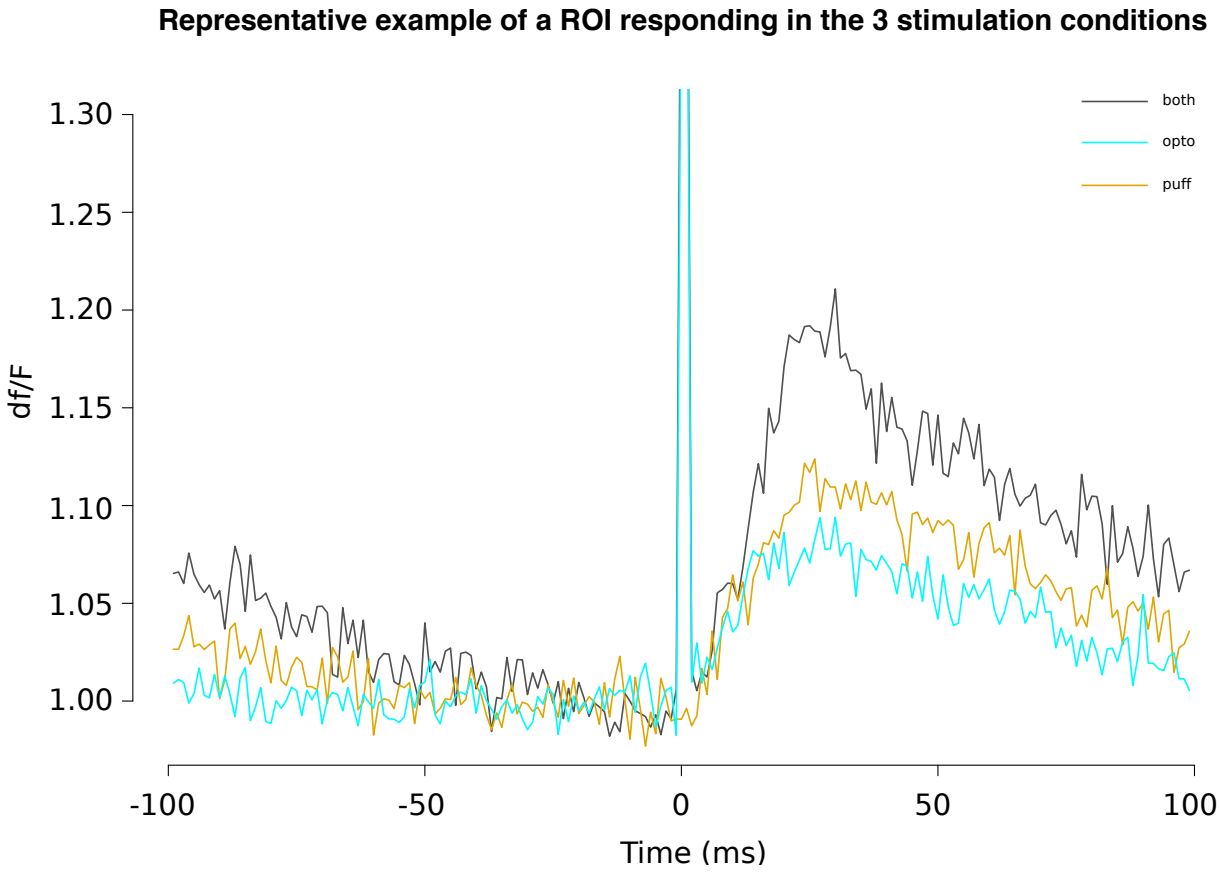


***Supplementary Figure 5. Representative example of a ROI responding in the three phases of the experiment.*** *Although few putative buttons from POm responded in the three conditions, among those who do, we can observe a supralinearity of the response in these ROIs when both peripheral and cerebellar stimuli are simultaneously presented.*

## REFERENCES


Ahissar, E. *et al.* (2001) 'Temporal frequency of whisker movement. II. Laminar organization of cortical representations', *Journal of Neurophysiology*, 86(1), pp. 354–367. doi: 10.1152/jn.2001.86.1.354.

Allen, G. (2005) 'The Cerebellum in Autism', *Clinical Neuropsychiatry: Journal of Treatment Evaluation*, 2(6), pp. 321–337.

Allen, G. I. and Tsukahara, N. (1974) 'Cerebrocerebellar communication systems.', *Physiological Reviews*, 54(4), pp. 957–1006. doi: 10.1152/physrev.1974.54.4.957.

Alloway, K. D. *et al.* (2006) 'Topography of cortical projections to the dorsolateral neostriatum in rats: Multiple overlapping sensorimotor pathways', *Journal of Comparative Neurology*, 499(1), pp. 33–48. doi: https://doi.org/10.1002/cne.21039.

Aoki, S., Coulon, P. and Ruigrok, T. J. H. (2019) 'Multizonal Cerebellar Influence Over Sensorimotor Areas of the Rat Cerebral Cortex', *Cerebral Cortex*, 29(2), pp. 598–614. doi: 10.1093/cercor/bhx343.

Apps, R. and Hawkes, R. (2009) 'Cerebellar cortical organization: a one-map hypothesis', *Nature Reviews. Neuroscience*, 10(9), pp. 670–681. doi: 10.1038/nrn2698.

Arabzadeh, E., Petersen, R. S. and Diamond, M. E. (2003) 'Encoding of Whisker Vibration by Rat Barrel Cortex Neurons: Implications for Texture Discrimination', *Journal of Neuroscience*, 23(27), pp. 9146–9154. doi: 10.1523/JNEUROSCI.23-27-09146.2003.

Arabzadeh, E., Zorzin, E. and Diamond, M. E. (2005) 'Neuronal encoding of texture in the whisker sensory pathway', *PLoS biology*, 3(1), p. e17. doi: 10.1371/journal.pbio.0030017.

Asanuma, C., Thach, W. T. and Jones, E. G. (1983) 'Distribution of cerebellar terminations and their relation to other afferent terminations in the ventral lateral thalamic region of the monkey', *Brain Research Reviews*, 5(3), pp. 237–265. doi: 10.1016/0165-0173(83)90015-2.

Ashizawa, T. and Xia, G. (2016) 'Ataxia', *Continuum : Lifelong Learning in Neurology*, 22(4 Movement Disorders), pp. 1208–1226. doi: 10.1212/CON.0000000000000362.

Atkins, M. J. and Apps, R. (1997) 'Somatotopical organisation within the climbing fibre projection to the paramedian lobule and copula pyramidis of the rat cerebellum', *The Journal of Comparative Neurology*, 389(2), pp. 249–263.

Audette, N. J. *et al.* (2018) 'POm Thalamocortical Input Drives Layer-Specific Microcircuits in Somatosensory Cortex', *Cerebral Cortex*, 28(4), pp. 1312–1328. doi: 10.1093/cercor/bhx044.

Aumann, T. D. *et al.* (1994) 'Projections from the lateral and interposed cerebellar nuclei to the thalamus of the rat: a light and electron microscopic study using single and double anterograde labelling', *The Journal of Comparative Neurology*, 349(2), pp. 165–181. doi: 10.1002/cne.903490202.

Bastian, A. J. (2006) 'Learning to predict the future: the cerebellum adapts feedforward movement control', *Current Opinion in Neurobiology*, 16(6), pp. 645–649. doi: 10.1016/j.conb.2006.08.016.

Beitzel, C. S. *et al.* (2017) 'Rubrocerebellar Feedback Loop Isolates the Interposed Nucleus as an Independent Processor of Corollary Discharge Information in Mice', *The Journal of Neuroscience: The Official Journal of the Society for Neuroscience*, 37(42), pp. 10085–10096. doi: 10.1523/JNEUROSCI.1093-17.2017.

Bickford, M. E. (2016) 'Thalamic Circuit Diversity: Modulation of the Driver/Modulator Framework', *Frontiers in Neural Circuits*, 9. doi: 10.3389/fncir.2015.00086.

Bohne, P. *et al.* (2019) 'A New Projection From the Deep Cerebellar Nuclei to the Hippocampus via the Ventrolateral and Laterodorsal Thalamus in Mice', *Frontiers in Neural Circuits*, 13. doi: 10.3389/fncir.2019.00051.

Bosman, L. W. J. *et al.* (2010) 'Encoding of whisker input by cerebellar Purkinje cells', *The Journal of Physiology*, 588(Pt 19), pp. 3757–3783. doi: 10.1113/jphysiol.2010.195180.

Bosman, L. W. J. *et al.* (2011) 'Anatomical Pathways Involved in Generating and Sensing Rhythmic Whisker Movements', *Frontiers in Integrative Neuroscience*, 5. doi: 10.3389/fnint.2011.00053.

Bower, J. M. (1997) 'Is the cerebellum sensory for motor's sake, or motor for sensory's sake: the view from the whiskers of a rat?', *Progress in Brain Research*, 114, pp. 463–496. doi: 10.1016/s0079-6123(08)63381-6.

Brecht, M., Preilowski, B. and Merzenich, M. M. (1997) 'Functional architecture of the mystacial vibrissae', *Behavioural Brain Research*, 84(1–2), pp. 81–97. doi: 10.1016/s0166-4328(97)83328-1.

Brooks, J. X., Carriot, J. and Cullen, K. E. (2015) 'Learning to expect the unexpected: rapid updating in primate cerebellum during voluntary self-motion', *Nature Neuroscience*, 18(9), pp. 1310–1317. doi: 10.1038/nn.4077.

Brown, I. E. and Bower, J. M. (2001) 'Congruence of mossy fiber and climbing fiber tactile projections in the lateral hemispheres of the rat cerebellum', *The Journal of Comparative Neurology*, 429(1), pp. 59–70. doi: 10.1002/1096-9861(20000101)429:1<59::aid-cne5>3.0.co;2-3.

Brown, S. T. and Raman, I. M. (2018) 'Sensorimotor Integration and Amplification of Reflexive Whisking by Well-Timed Spiking in the Cerebellar Corticonuclear Circuit', *Neuron*, 99(3), pp. 564-575.e2. doi: 10.1016/j.neuron.2018.06.028.

Bruno, R. M. *et al.* (2009) 'Sensory experience alters specific branches of individual corticocortical axons during development', *The Journal of Neuroscience: The Official Journal of the Society for Neuroscience*, 29(10), pp. 3172–3181. doi: 10.1523/JNEUROSCI.5911-08.2009.

Calderon, D. P. *et al.* (2011) 'The neural substrates of Rapid-Onset Dystonia-Parkinsonism', *Nature neuroscience*, 14(3), pp. 357–365. doi: 10.1038/nn.2753.

Carvell, G. E. and Simons, D. J. (1987) 'Thalamic and corticocortical connections of the second somatic sensory area of the mouse', *The Journal of Comparative Neurology*, 265(3), pp. 409–427. doi: 10.1002/cne.902650309.

Carvell, G. E. and Simons, D. J. (1995) 'Task- and subject-related differences in sensorimotor behavior during active touch', *Somatosensory & Motor Research*, 12(1), pp. 1–9. doi: 10.3109/08990229509063138.

Casas-Torremocha, D. *et al.* (2019) 'Posterior thalamic nucleus axon terminals have different structure and functional impact in the motor and somatosensory vibrissal cortices', *Brain Structure and Function*. doi: 10.1007/s00429-019-01862-4.

Castejon, C., Barros-Zulaica, N. and Nuñez, A. (2016) 'Control of Somatosensory Cortical Processing by Thalamic Posterior Medial Nucleus: A New Role of Thalamus in Cortical Function', *PLOS ONE*. Edited by M. Maravall, 11(1), p. e0148169. doi: 10.1371/journal.pone.0148169.

Castejon, C. and Nuñez, A. (2020) 'Higher-order thalamic implication in the codification of bilateral sensory events', *bioRxiv*, p. 2020.05.01.073098. doi: 10.1101/2020.05.01.073098.

Çavdar, S. *et al.* (2014) 'Motor afferents from the cerebellum, zona incerta and substantia nigra to the mediodorsal thalamic nucleus in the rat', *Journal of Integrative Neuroscience*, 13(4), pp. 565–578. doi: 10.1142/S0219635214500198.

Cerminara, N. L. *et al.* (2015) 'Redefining the cerebellar cortex as an assembly of non-uniform Purkinje cell microcircuits', *Nature Reviews. Neuroscience*, 16(2), pp. 79–93. doi: 10.1038/nrn3886.

Chabrol, F. P. *et al.* (2015) 'Synaptic diversity enables temporal coding of coincident multisensory inputs in single neurons', *Nature Neuroscience*, 18(5), pp. 718–727. doi: 10.1038/nn.3974.

Chen, C. H. *et al.* (2014) 'Short latency cerebellar modulation of the basal ganglia', *Nature Neuroscience*, 17(12), pp. 1767–1775. doi: 10.1038/nn.3868.

Chen, J. L. *et al.* (2015) 'Pathway-specific reorganization of projection neurons in somatosensory cortex during learning', *Nature Neuroscience*, 18(8), pp. 1101–1108. doi: 10.1038/nn.4046.

Chen, S., Augustine, G. J. and Chadderton, P. (2016) *The cerebellum linearly encodes whisker position during voluntary movement*, *eLife*. eLife Sciences Publications Limited. doi: 10.7554/eLife.10509.

Coco, M. and Perciavalle, V. (2015) 'Where did the motor function of the cerebellum come from?', *Cerebellum & Ataxias*, 2, p. 10. doi: 10.1186/s40673-015-0029-8.

Constantinople, C. M. and Bruno, R. M. (2013) 'Deep cortical layers are activated directly by thalamus', *Science (New York, N.Y.)*, 340(6140), pp. 1591–1594. doi: 10.1126/science.1236425.

Crochet, S. and Petersen, C. C. H. (2006) 'Correlating whisker behavior with membrane potential in barrel cortex of awake mice', *Nature Neuroscience*, 9(5), pp. 608–610. doi: 10.1038/nn1690.

De Zeeuw, C. I. *et al.* (2011) 'Spatiotemporal firing patterns in the cerebellum', *Nature Reviews. Neuroscience*, 12(6), pp. 327–344. doi: 10.1038/nrn3011.

De Zeeuw, C. I. and Ten Brinke, M. M. (2015) 'Motor Learning and the Cerebellum', *Cold Spring Harbor Perspectives in Biology*, 7(9), p. a021683. doi: 10.1101/cshperspect.a021683.

Deschênes, M., Timofeeva, E. and Lavallée, P. (2003) 'The Relay of High-Frequency Sensory Signals in the Whisker-to-Barreloid Pathway', *Journal of Neuroscience*, 23(17), pp. 6778–6787. doi: 10.1523/JNEUROSCI.23-17-06778.2003.

Deschênes, M., Veinante, P. and Zhang, Z. W. (1998) 'The organization of corticothalamic projections: reciprocity versus parity', *Brain Research. Brain Research Reviews*, 28(3), pp. 286–308. doi: 10.1016/s0165-0173(98)00017-4.

Diamond, M. E., Armstrong-James, M. and Ebner, F. F. (1992) 'Somatic sensory responses in the rostral sector of the posterior group (POm) and in the ventral posterior medial nucleus (VPM) of the rat thalamus', *Journal of Comparative Neurology*, 318(4), pp. 462–476. doi: https://doi.org/10.1002/cne.903180410.

Diedrichsen, J. *et al.* (2011) 'Imaging the deep cerebellar nuclei: a probabilistic atlas and normalization procedure', *NeuroImage*, 54(3), pp. 1786–1794. doi: 10.1016/j.neuroimage.2010.10.035.

Doya, K. (1999) 'What are the computations of the cerebellum, the basal ganglia and the cerebral cortex?', *Neural Networks*, 12(7), pp. 961–974. doi: 10.1016/S0893-6080(99)00046-5.

Ebbesen, C. L. *et al.* (2017) 'Vibrissa motor cortex activity suppresses contralateral whisking behavior', *Nature Neuroscience*, 20(1), pp. 82–89. doi: 10.1038/nn.4437.

Feldmeyer, D., Lübke, J. and Sakmann, B. (2006) 'Efficacy and connectivity of intracolumnar pairs of layer 2/3 pyramidal cells in the barrel cortex of juvenile rats', *The Journal of Physiology*, 575(Pt 2), pp. 583–602. doi: 10.1113/jphysiol.2006.105106.

Feldmeyer, D., Roth, A. and Sakmann, B. (2005) 'Monosynaptic Connections between Pairs of Spiny Stellate Cells in Layer 4 and Pyramidal Cells in Layer 5A Indicate That Lemniscal and Paralemniscal Afferent Pathways Converge in the Infragranular Somatosensory Cortex', *The Journal of Neuroscience*, 25(13), pp. 3423–3431. doi: 10.1523/JNEUROSCI.5227-04.2005.

Ferezou, I. *et al.* (2007) 'Spatiotemporal Dynamics of Cortical Sensorimotor Integration in Behaving Mice', *Neuron*, 56(5), pp. 907–923. doi: 10.1016/j.neuron.2007.10.007.

Ferezou, I., Bolea, S. and Petersen, C. C. H. (2006) 'Visualizing the cortical representation of whisker touch: voltage-sensitive dye imaging in freely moving mice', *Neuron*, 50(4), pp. 617–629. doi: 10.1016/j.neuron.2006.03.043.

Fujita, H., Kodama, T. and Lac, S. du (2020) 'Modular output circuits of the fastigial nucleus mediate diverse motor and nonmotor functions of the cerebellar vermis', *bioRxiv*, p. 2020.04.23.047100. doi: 10.1101/2020.04.23.047100.

Gambino, F. *et al.* (2014) 'Sensory-evoked LTP driven by dendritic plateau potentials in vivo', *Nature*, 515(7525), pp. 116–119. doi: 10.1038/nature13664.

Gao, J. H. *et al.* (1996) ‘Cerebellum implicated in sensory acquisition and discrimination rather than motor control’, *Science (New York, N.Y.)*, 272(5261), pp. 545–547. doi: 10.1126/science.272.5261.545.

Gao, P. *et al.* (2003) ‘Whisker motor cortex ablation and whisker movement patterns’, *Somatosensory & Motor Research*, 20(3–4), pp. 191–198. doi: 10.1080/08990220310001622924.

Gao, Z. *et al.* (2018) ‘A cortico-cerebellar loop for motor planning’, *Nature*, 563(7729), pp. 113–116. doi: 10.1038/s41586-018-0633-x.

Gibson, A. R., Horn, K. M. and Pong, M. (2004) ‘Activation of climbing fibers’, *Cerebellum (London, England)*, 3(4), pp. 212–221. doi: 10.1080/14734220410018995.

Glickstein, M., Strata, P. and Voogd, J. (2009) ‘Cerebellum: history’, *Neuroscience*, 162(3), pp. 549–559. doi: 10.1016/j.neuroscience.2009.02.054.

Gornati, S. V. *et al.* (2018a) ‘Differentiating Cerebellar Impact on Thalamic Nuclei’, *Cell Reports*, 23(9), pp. 2690–2704. doi: 10.1016/j.celrep.2018.04.098.

Gornati, S. V. *et al.* (2018b) ‘Differentiating Cerebellar Impact on Thalamic Nuclei’, *Cell Reports*, 23(9), pp. 2690–2704. doi: 10.1016/j.celrep.2018.04.098.

Groh, A. *et al.* (2014) ‘Convergence of Cortical and Sensory Driver Inputs on Single Thalamocortical Cells’, *Cerebral Cortex (New York, NY)*, 24(12), pp. 3167–3179. doi: 10.1093/cercor/bht173.

Guo, K. *et al.* (2018) ‘Anterolateral Motor Cortex Connects with a Medial Subdivision of Ventromedial Thalamus through Cell Type-Specific Circuits, Forming an Excitatory Thalamo-Cortico-Thalamic Loop via Layer 1 Apical Tuft Dendrites of Layer 5B Pyramidal Tract Type Neurons’, *The Journal of Neuroscience*, 38(41), pp. 8787–8797. doi: 10.1523/JNEUROSCI.1333-18.2018.

Helmchen, F., Gilad, A. and Chen, J. L. (2018) ‘Neocortical dynamics during whisker-based sensory discrimination in head-restrained mice’, *Neuroscience*, 368, pp. 57–69. doi: 10.1016/j.neuroscience.2017.09.003.

Henneman, E., Cooke, P. M. and Snider, R. S. (1952) ‘Cerebellar projections to the cerebral cortex’, *Research Publications - Association for Research in Nervous and Mental Disease*, 30, pp. 317–333.

Hentschke, H., Haiss, F. and Schwarz, C. (2006) ‘Central Signals Rapidly Switch Tactile Processing in Rat Barrel Cortex during Whisker Movements’, *Cerebral Cortex*, 16(8), pp. 1142–1156. doi: 10.1093/cercor/bhj056.

Herculano-Houzel, S. (2010) ‘Coordinated scaling of cortical and cerebellar numbers of neurons’, *Frontiers in Neuroanatomy*, 4. doi: 10.3389/fnana.2010.00012.

Hodos, W. (2009) ‘Evolution of Cerebellum’, in Binder, M. D., Hirokawa, N., and Windhorst, U. (eds) *Encyclopedia of Neuroscience*. Berlin, Heidelberg: Springer, pp. 1240–1243. doi: 10.1007/978-3-540-29678-2_3124.

Hutson, K. A. and Masterton, R. B. (1986) 'The sensory contribution of a single vibrissa's cortical barrel', *Journal of Neurophysiology*, 56(4), pp. 1196–1223. doi: 10.1152/jn.1986.56.4.1196.

Hyvärinen, H. *et al.* (2009) 'Aquatic environment and differentiation of vibrissae: comparison of sinus hair systems of ringed seal, otter and pole cat', *Brain, Behavior and Evolution*, 74(4), pp. 268–279. doi: 10.1159/000264662.

Iseni, F. *et al.* (1997) 'Mapping of monoclonal antibody epitopes of the rabies virus P protein.', *Journal of General Virology*, 78(1), pp. 119–124. doi: 10.1099/0022-1317-78-1-119.

Ito, M. (1984) 'The modifiable neuronal network of the cerebellum', *The Japanese Journal of Physiology*, 34(5), pp. 781–792. doi: 10.2170/jjphysiol.34.781.

Jones, E. G. (1998) 'Viewpoint: the core and matrix of thalamic organization', *Neuroscience*, 85(2), pp. 331–345. doi: 10.1016/s0306-4522(97)00581-2.

Jones, E. G. and Diamond, I. T. (1995) *The Barrel Cortex of Rodents: Volume 11: The Barrel Cortex of Rodents*. Springer Science & Business Media.

Kelly, R. M. and Strick, P. L. (2003) 'Cerebellar loops with motor cortex and prefrontal cortex of a nonhuman primate', *The Journal of Neuroscience: The Official Journal of the Society for Neuroscience*, 23(23), pp. 8432–8444.

Krupa, D. J. *et al.* (2001) 'Behavioral Properties of the Trigeminal Somatosensory System in Rats Performing Whisker-Dependent Tactile Discriminations', *Journal of Neuroscience*, 21(15), pp. 5752–5763. doi: 10.1523/JNEUROSCI.21-15-05752.2001.

Küper, M. *et al.* (2011) 'Lesions of the dentate and interposed nuclei are associated with impaired prehension in cerebellar patients', *Neuroscience Letters*, 499(2), pp. 132–136. doi: 10.1016/j.neulet.2011.05.055.

Kuramoto, E. *et al.* (2009) 'Two types of thalamocortical projections from the motor thalamic nuclei of the rat: a single neuron-tracing study using viral vectors', *Cerebral Cortex (New York, N.Y.: 1991)*, 19(9), pp. 2065–2077. doi: 10.1093/cercor/bhn231.

Kwegyir-Afful, E. E. *et al.* (2005) 'The Role of Thalamic Inputs in Surround Receptive Fields of Barrel Neurons', *Journal of Neuroscience*, 25(25), pp. 5926–5934. doi: 10.1523/JNEUROSCI.1360-05.2005.

Kwon, S. E. *et al.* (2016) 'Sensory and decision-related activity propagate in a cortical feedback loop during touch perception', *Nature Neuroscience*, 19(9), pp. 1243–1249. doi: 10.1038/nn.4356.

Lam, Y.-W. and Sherman, S. M. (2007) 'Different Topography of the Reticulothalmic Inputs to First- and Higher-Order Somatosensory Thalamic Relays Revealed Using Photostimulation', *Journal of Neurophysiology*, 98(5), pp. 2903–2909. doi: 10.1152/jn.00782.2007.

Lang, E. J., Sugihara, I. and Llinás, R. (2006) 'Olivocerebellar modulation of motor cortex ability to generate vibrissal movements in rat', *The Journal of Physiology*, 571(Pt 1), pp. 101–120. doi: 10.1113/jphysiol.2005.102764.

Lavallée, P. *et al.* (2005) 'Feedforward Inhibitory Control of Sensory Information in Higher-Order Thalamic Nuclei', *The Journal of Neuroscience*, 25(33), pp. 7489–7498. doi: 10.1523/JNEUROSCI.2301-05.2005.

Lee, K. J. and Woolsey, T. A. (1975) 'A proportional relationship between peripheral innervation density and cortical neuron number in the somatosensory system of the mouse', *Brain Research*, 99(2), pp. 349–353. doi: 10.1016/0006-8993(75)90035-9.

Lee, L.-J. *et al.* (2009) 'Neonatal whisker trimming causes long-lasting changes in structure and function of the somatosensory system', *Experimental Neurology*, 219(2), pp. 524–532. doi: 10.1016/j.expneurol.2009.07.012.

Lee, L.-J., Lo, F.-S. and Erzurumlu, R. S. (2005) 'NMDA Receptor-Dependent Regulation of Axonal and Dendritic Branching', *The Journal of Neuroscience*, 25(9), pp. 2304–2311. doi: 10.1523/JNEUROSCI.4902-04.2005.

Leergaard, T. B. *et al.* (2004) 'Three-dimensional topography of corticopontine projections from rat sensorimotor cortex: comparisons with corticostriatal projections reveal diverse integrative organization', *The Journal of Comparative Neurology*, 478(3), pp. 306–322. doi: 10.1002/cne.20289.

Manto, M. *et al.* (2012) 'Consensus paper: roles of the cerebellum in motor control--the diversity of ideas on cerebellar involvement in movement', *Cerebellum (London, England)*, 11(2), pp. 457–487. doi: 10.1007/s12311-011-0331-9.

Mao, T. *et al.* (2011) 'Long-range neuronal circuits underlying the interaction between sensory and motor cortex', *Neuron*, 72(1), pp. 111–123. doi: 10.1016/j.neuron.2011.07.029.

Masri, R. *et al.* (2006) 'Cholinergic Regulation of the Posterior Medial Thalamic Nucleus', *Journal of Neurophysiology*, 96(5), pp. 2265–2273. doi: 10.1152/jn.00476.2006.

Masri, R. *et al.* (2008) 'Encoding of stimulus frequency and sensor motion in the posterior medial thalamic nucleus', *Journal of Neurophysiology*, 100(2), pp. 681–689. doi: 10.1152/jn.01322.2007.

Matyas, F. *et al.* (2010) 'Motor control by sensory cortex', *Science (New York, N.Y.)*, 330(6008), pp. 1240–1243. doi: 10.1126/science.1195797.

Mease, R. A. *et al.* (2016) 'Cortical Dependence of Whisker Responses in Posterior Medial Thalamus In Vivo', *Cerebral Cortex*, 26(8), pp. 3534–3543. doi: 10.1093/cercor/bhw144.

Mercier, B. E., Legg, C. R. and Glickstein, M. (1990) 'Basal ganglia and cerebellum receive different somatosensory information in rats', *Proceedings of the National Academy of Sciences of the United States of America*, 87(11), pp. 4388–4392. doi: 10.1073/pnas.87.11.4388.

Middleton, F. A. and Strick, P. L. (2001) 'Cerebellar Projections to the Prefrontal Cortex of the Primate', *Journal of Neuroscience*, 21(2), pp. 700–712. doi: 10.1523/JNEUROSCI.21-02-00700.2001.

Mitrofanis, J. (2005) 'Some certainty for the "zone of uncertainty"? Exploring the function of the zona incerta', *Neuroscience*, 130(1), pp. 1–15. doi: 10.1016/j.neuroscience.2004.08.017.

Miyashita, E., Keller, A. and Asanuma, H. (1994) 'Input-output organization of the rat vibrissal motor cortex', *Experimental brain research. Experimentelle Hirnforschung. Expérimentation cérébrale*, 99, pp. 223–32. doi: 10.1007/BF00239589.

Mo, C. *et al.* (2017) 'Synaptic properties of the lemniscal and paralemniscal pathways to the mouse somatosensory thalamus', *Proceedings of the National Academy of Sciences*, 114(30), pp. E6212–E6221. doi: 10.1073/pnas.1703222114.

Mo, C. and Sherman, S. M. (2019) 'A Sensorimotor Pathway via Higher-Order Thalamus', *The Journal of Neuroscience*, 39(4), pp. 692–704. doi: 10.1523/JNEUROSCI.1467-18.2018.

Moberget, T. and Ivry, R. B. (2016) 'Cerebellar contributions to motor control and language comprehension: searching for common computational principles', *Annals of the New York Academy of Sciences*, 1369(1), pp. 154–171. doi: 10.1111/nyas.13094.

Neimark, M. A. *et al.* (2003) 'Vibrissa Resonance as a Transduction Mechanism for Tactile Encoding', *The Journal of Neuroscience*, 23(16), pp. 6499–6509. doi: 10.1523/JNEUROSCI.23-16-06499.2003.

Nikolov, P. *et al.* (2019) 'Cerebellar Involvement in DYT-THAP1 Dystonia', *The Cerebellum*, 18(5), pp. 969–971. doi: 10.1007/s12311-019-01062-0.

Odeh, F. *et al.* (2005) 'Pontine Maps Linking Somatosensory and Cerebellar Cortices Are in Register with Climbing Fiber Somatotopy', *The Journal of Neuroscience*, 25(24), pp. 5680–5690. doi: 10.1523/JNEUROSCI.0558-05.2005.

Ohno, S. *et al.* (2012) 'A morphological analysis of thalamocortical axon fibers of rat posterior thalamic nuclei: a single neuron tracing study with viral vectors', *Cerebral Cortex (New York, N.Y.: 1991)*, 22(12), pp. 2840–2857. doi: 10.1093/cercor/bhr356.

Palkovits, M. *et al.* (1977) 'Quantitative histological analysis of the cerebellar nuclei in the cat. I. Numerical data on cells and on synapses', *Experimental Brain Research*, 28(1–2), pp. 189–209. doi: 10.1007/BF00237096.

Panto, M. R. *et al.* (1995) 'The projection from the primary motor and somatic sensory cortex to the basilar pontine nuclei. A detailed electrophysiological and anatomical study in the rat', *Journal Fur Hirnforschung*, 36(1), pp. 7–19.

Park, J. M. *et al.* (2020) *Deep and superficial layers of the primary somatosensory cortex are critical for whisker-based texture discrimination in mice*. preprint. Neuroscience. doi: 10.1101/2020.08.12.245381.

Parsons, L. M. *et al.* (1997) 'Lateral cerebellar hemispheres actively support sensory acquisition and discrimination rather than motor control', *Learning & Memory (Cold Spring Harbor, N.Y.)*, 4(1), pp. 49–62. doi: 10.1101/lm.4.1.49.

Parsons, L. M. *et al.* (2009) ‘Pitch discrimination in cerebellar patients: evidence for a sensory deficit’, *Brain Research*, 1303, pp. 84–96. doi: 10.1016/j.brainres.2009.09.052.

Patel, V. R. and Zee, D. S. (2015) *The cerebellum in eye movement control: nystagmus, coordinate frames and disconjugacy*. Report 2. Nature Publishing Group, pp. 191–195. Available at: https://www.nature.com/articles/eye2014271 (Accessed: 1 March 2021).

Person, A. L. and Raman, I. M. (2011) ‘Purkinje neuron synchrony elicits time-locked spiking in the cerebellar nuclei’, *Nature*, 481(7382), pp. 502–505. doi: 10.1038/nature10732.

Petersen, C. C. and Sakmann, B. (2001) ‘Functionally independent columns of rat somatosensory barrel cortex revealed with voltage-sensitive dye imaging’, *The Journal of Neuroscience: The Official Journal of the Society for Neuroscience*, 21(21), pp. 8435–8446.

Petreanu, L. *et al.* (2007) ‘Channelrhodopsin-2-assisted circuit mapping of long-range callosal projections’, *Nature Neuroscience*, 10(5), pp. 663–668. doi: 10.1038/nn1891.

Petreanu, L. *et al.* (2009) ‘The subcellular organization of neocortical excitatory connections’, *Nature*, 457(7233), pp. 1142–1145. doi: 10.1038/nature07709.

Petreanu, L. *et al.* (2012) ‘Activity in motor-sensory projections reveals distributed coding in somatosensation’, *Nature*, 489(7415), pp. 299–303. doi: 10.1038/nature11321.

Pierret, T., Lavallée, P. and Deschênes, M. (2000) ‘Parallel Streams for the Relay of Vibrissal Information through Thalamic Barreloids’, *The Journal of Neuroscience*, 20(19), pp. 7455–7462. doi: 10.1523/JNEUROSCI.20-19-07455.2000.

Pijpers, A. *et al.* (2006) ‘Precise Spatial Relationships between Mossy Fibers and Climbing Fibers in Rat Cerebellar Cortical Zones’, *Journal of Neuroscience*, 26(46), pp. 12067–12080. doi: 10.1523/JNEUROSCI.2905-06.2006.

Popa, D. *et al.* (2013) ‘Functional role of the cerebellum in gamma-band synchronization of the sensory and motor cortices’, *The Journal of Neuroscience: The Official Journal of the Society for Neuroscience*, 33(15), pp. 6552–6556. doi: 10.1523/JNEUROSCI.5521-12.2013.

Proville, R. D. *et al.* (2014) ‘Cerebellum involvement in cortical sensorimotor circuits for the control of voluntary movements’, *Nature Neuroscience*, 17(9), pp. 1233–1239. doi: 10.1038/nn.3773.

Roger, M. and Cadusseau, J. (1985) ‘Afferents to the zona incerta in the rat: a combined retrograde and anterograde study’, *The Journal of Comparative Neurology*, 241(4), pp. 480–492. doi: 10.1002/cne.902410407.

Ruigrok, T. J. H. *et al.* (2008) ‘Multiple cerebellar zones are involved in the control of individual muscles: a retrograde transneuronal tracing study with rabies virus in the rat’, *European Journal of Neuroscience*, 28(1), pp. 181–200. doi: https://doi.org/10.1111/j.1460-9568.2008.06294.x.

Sachidhanandam, S. *et al.* (2013) ‘Membrane potential correlates of sensory perception in mouse barrel cortex’, *Nature Neuroscience*, 16(11), pp. 1671–1677. doi: 10.1038/nn.3532.

Schmahmann, J. D. (1991) ‘An emerging concept. The cerebellar contribution to higher function’, *Archives of Neurology*, 48(11), pp. 1178–1187. doi: 10.1001/archneur.1991.00530230086029.

Schmahmann, J. D. (2004) ‘Disorders of the Cerebellum: Ataxia, Dysmetria of Thought, and the Cerebellar Cognitive Affective Syndrome’, *The Journal of Neuropsychiatry and Clinical Neurosciences*, 16(3), pp. 367–378. doi: 10.1176/jnp.16.3.367.

Schmahmann, J. D. (2016) ‘A Brief History of the Cerebellum’, in Gruol, D. L. et al. (eds) *Essentials of Cerebellum and Cerebellar Disorders: A Primer For Graduate Students*. Cham: Springer International Publishing, pp. 5–20. doi: 10.1007/978-3-319-24551-5_2.

Schmahmann, J. D. and Sherman, J. C. (no date) ‘The cerebellar cognitive affective syndrome’, p. 19.

Serapide, M. F. *et al.* (2001) ‘Multiple zonal projections of the basilar pontine nuclei to the cerebellar cortex of the rat’, *Journal of Comparative Neurology*, 430(4), pp. 471–484. doi: https://doi.org/10.1002/1096-9861(20010219)430:4<471::AID-CNE1044>3.0.CO;2-G.

Sherman, S. M. and Guillery, R. W. (1998) ‘On the actions that one nerve cell can have on another: distinguishing “drivers” from “modulators”’, *Proceedings of the National Academy of Sciences of the United States of America*, 95(12), pp. 7121–7126. doi: 10.1073/pnas.95.12.7121.

Shidara, M. *et al.* (1993) ‘Inverse-dynamics model eye movement control by Purkinje cells in the cerebellum’, *Nature*, 365(6441), pp. 50–52. doi: 10.1038/365050a0.

Shlosberg, D., Amitai, Y. and Azouz, R. (2006) ‘Time-Dependent, Layer-Specific Modulation of Sensory Responses Mediated by Neocortical Layer 1’, *Journal of Neurophysiology*, 96(6), pp. 3170–3182. doi: 10.1152/jn.00520.2006.

Simons, D. J. and Carvell, G. E. (1989) ‘Thalamocortical response transformation in the rat vibrissa/barrel system’, *Journal of Neurophysiology*, 61(2), pp. 311–330. doi: 10.1152/jn.1989.61.2.311.

Sobolewski, A. *et al.* (2015) ‘Alertness opens the effective flow of sensory information through rat thalamic posterior nucleus’, *European Journal of Neuroscience*, 41(10), pp. 1321–1331. doi: 10.1111/ejn.12901.

Sreenivasan, V. *et al.* (2016) ‘Movement Initiation Signals in Mouse Whisker Motor Cortex’, *Neuron*, 92(6), pp. 1368–1382. doi: 10.1016/j.neuron.2016.12.001.

Steriade, M. (1995) ‘Two channels in the cerebellothalamocortical system’, *The Journal of Comparative Neurology*, 354(1), pp. 57–70. doi: 10.1002/cne.903540106.

Stoodley, C. J. *et al.* (2016) ‘Location of lesion determines motor vs. cognitive consequences in patients with cerebellar stroke’, *NeuroImage: Clinical*, 12, pp. 765–775. doi: 10.1016/j.nicl.2016.10.013.

Stoodley, C. J. *et al.* (2017) ‘Altered cerebellar connectivity in autism spectrum disorders and rescue of autism-related behaviors in mice’, *Nature neuroscience*, 20(12), pp. 1744–1751. doi: 10.1038/s41593-017-0004-1.

Strick, P. L., Dum, R. P. and Fiez, J. A. (2009) 'Cerebellum and nonmotor function', *Annual Review of Neuroscience*, 32, pp. 413–434. doi: 10.1146/annurev.neuro.31.060407.125606.

Sugihara, I. and Shinoda, Y. (2004) 'Molecular, topographic, and functional organization of the cerebellar cortex: a study with combined aldolase C and olivocerebellar labeling', *The Journal of Neuroscience: The Official Journal of the Society for Neuroscience*, 24(40), pp. 8771–8785. doi: 10.1523/JNEUROSCI.1961-04.2004.

Sumser, A. *et al.* (2017) 'Organization and somatotopy of corticothalamic projections from L5B in mouse barrel cortex', *Proceedings of the National Academy of Sciences of the United States of America*, 114(33), pp. 8853–8858. doi: 10.1073/pnas.1704302114.

Teune, T. M. *et al.* (2000) 'Topography of cerebellar nuclear projections to the brain stem in the rat', *Progress in Brain Research*, 124, pp. 141–172. doi: 10.1016/S0079-6123(00)24014-4.

Thach, W. T., Goodkin, H. P. and Keating, J. G. (1992) 'The cerebellum and the adaptive coordination of movement', *Annual Review of Neuroscience*, 15, pp. 403–442. doi: 10.1146/annurev.ne.15.030192.002155.

*The Mouse Nervous System* (2012). Elsevier. doi: 10.1016/C2009-0-00185-8.

Timmann, D. and Daum, I. (2007) 'Cerebellar contributions to cognitive functions: A progress report after two decades of research', *The Cerebellum*, 6(3), p. 159. doi: 10.1080/14734220701496448.

Towal, R. B. *et al.* (2011) 'The Morphology of the Rat Vibrissal Array: A Model for Quantifying Spatiotemporal Patterns of Whisker-Object Contact', *PLOS Computational Biology*, 7(4), p. e1001120. doi: 10.1371/journal.pcbi.1001120.

Trageser, J. C. *et al.* (2006) 'State-Dependent Gating of Sensory Inputs by Zona Incerta', *Journal of neurophysiology*, 96(3), pp. 1456–1463. doi: 10.1152/jn.00423.2006.

Trageser, J. C. and Keller, A. (2004) 'Reducing the uncertainty: gating of peripheral inputs by zona incerta', *The Journal of Neuroscience: The Official Journal of the Society for Neuroscience*, 24(40), pp. 8911–8915. doi: 10.1523/JNEUROSCI.3218-04.2004.

Tsai, P. T. *et al.* (2012) 'Autistic-like behaviour and cerebellar dysfunction in Purkinje cell Tsc1 mutant mice', *Nature*, 488(7413), pp. 647–651. doi: 10.1038/nature11310.

Ugolini, G. (1995) 'Specificity of rabies virus as a transneuronal tracer of motor networks: Transfer from hypoglossal motoneurons to connected second-order and higher order central nervous system cell groups', *Journal of Comparative Neurology*, 356(3), pp. 457–480. doi: https://doi.org/10.1002/cne.903560312.

Urbain, N. and Deschênes, M. (2007) 'A New Thalamic Pathway of Vibrissal Information Modulated by the Motor Cortex', *Journal of Neuroscience*, 27(45), pp. 12407–12412. doi: 10.1523/JNEUROSCI.2914-07.2007.

Uusisaari, M., Obata, K. and Knöpfel, T. (2007) 'Morphological and electrophysiological properties of GABAergic and non-GABAergic cells in the deep cerebellar nuclei', *Journal of Neurophysiology*, 97(1), pp. 901–911. doi: 10.1152/jn.00974.2006.

Varani, A. P. *et al.* (2020) ‘Dual contributions of cerebellar-thalamic networks to learning and offline consolidation of a complex motor task’, *bioRxiv*, p. 2020.08.27.270330. doi: 10.1101/2020.08.27.270330.

Veinante, P. and Deschênes, M. (1999) ‘Single- and multi-whisker channels in the ascending projections from the principal trigeminal nucleus in the rat’, *The Journal of Neuroscience: The Official Journal of the Society for Neuroscience*, 19(12), pp. 5085–5095.

Veinante, P., Lavall□e, P. and Desch□nes, M. (2000) ‘Corticothalamic projections from layer 5 of the vibrissal barrel cortex in the rat’, *The Journal of Comparative Neurology*, 424(2), pp. 197–204. doi: 10.1002/1096-9861(20000821)424:2<197::AID-CNE1>3.0.CO;2-6.

Viaene, A. N., Petrof, I. and Sherman, S. M. (2011) ‘Synaptic properties of thalamic input to the subgranular layers of primary somatosensory and auditory cortices in the mouse’, *The Journal of Neuroscience: The Official Journal of the Society for Neuroscience*, 31(36), pp. 12738–12747. doi: 10.1523/JNEUROSCI.1565-11.2011.

Vogt, B. A. (1991) ‘The Role of Layer I in Cortical Function’, in Peters, A. and Jones, E. G. (eds) *Normal and Altered States of Function*. Boston, MA: Springer US (Cerebral Cortex), pp. 49–80. doi: 10.1007/978-1-4615-6622-9_2.

Voogd, J. (2011) ‘Cerebellar Zones: A Personal History’, *Cerebellum (London, England)*, 10(3), pp. 334–350. doi: 10.1007/s12311-010-0221-6.

Voogd, J. (2014) ‘What we do not know about cerebellar systems neuroscience’, *Frontiers in Systems Neuroscience*, 8. doi: 10.3389/fnsys.2014.00227.

Voogd, J. and De Zeeuw, C. I. (2020) ‘Cerebellum: What is in a Name? Historical Origins and First Use of This Anatomical Term’, *Cerebellum (London, England)*, 19(4), pp. 550–561. doi: 10.1007/s12311-020-01133-7.

Voogd, J. and Glickstein, M. (1998) ‘The anatomy of the cerebellum’, *Trends in Neurosciences*, 21(9), pp. 370–375. doi: 10.1016/s0166-2236(98)01318-6.

Voogd, J. and Ruigrok, T. (2012) ‘Cerebellum and Precerebellar Nuclei’, in *The Human Nervous System*, pp. 471–545. doi: 10.1016/B978-0-12-374236-0.10015-X.

Wang, S. S.-H., Kloth, A. D. and Badura, A. (2014) ‘The Cerebellum, Sensitive Periods, and Autism’, *Neuron*, 83(3), pp. 518–532. doi: 10.1016/j.neuron.2014.07.016.

Williams, L. E. and Holtmaat, A. (2019) ‘Higher-Order Thalamocortical Inputs Gate Synaptic Long-Term Potentiation via Disinhibition’, *Neuron*, 101(1), pp. 91-102.e4. doi: 10.1016/j.neuron.2018.10.049.

Wineski, L. E. (1985) ‘Facial morphology and vibrissal movement in the golden hamster’, *Journal of Morphology*, 183(2), pp. 199–217. doi: https://doi.org/10.1002/jmor.1051830208.

Wolpert, D. M., Miall, R. C. and Kawato, M. (1998) ‘Internal models in the cerebellum’, *Trends in Cognitive Sciences*, 2(9), pp. 338–347. doi: 10.1016/s1364-6613(98)01221-2.

Woolsey, T. A., Dierker, M. L. and Wann, D. F. (1975) ‘Mouse SmI cortex: qualitative and quantitative classification of golgi-impregnated barrel neurons’, *Proceedings of the National Academy of Sciences of the United States of America*, 72(6), pp. 2165–2169. doi: 10.1073/pnas.72.6.2165.

Xu, N. *et al.* (2012) ‘Nonlinear dendritic integration of sensory and motor input during an active sensing task’, *Nature*, 492(7428), pp. 247–251. doi: 10.1038/nature11601.

Yamashita, T. *et al.* (2013) ‘Membrane potential dynamics of neocortical projection neurons driving target-specific signals’, *Neuron*, 80(6), pp. 1477–1490. doi: 10.1016/j.neuron.2013.10.059.

Yatim, N. *et al.* (1996) ‘Trigeminocerebellar and trigemino-olivary projections in rats’, *Neuroscience Research*, 25(3), pp. 267–283. doi: 10.1016/0168-0102(96)01061-9.

# Discussion générale

Au cours de cette thèse, j'ai analysé plusieurs aspects des voies de projection ascendantes cérébelleuses vers les cortex sensorimoteurs, utilisant pour ce faire des techniques allant des traçages trans-synaptiques, des stimulations optogénétiques et des enregistrements multisites extracellulaires à l'imagerie calcique en biphoton, ainsi que des tests comportementaux.

## 1 - Le cervelet cible le cortex sensoriel primaire

Le premier point que nous avons abordé est l'idée de l'existence d'une voie de projection « directe », disynaptique vers le cortex sensoriel primaire. La combinaison des traçages rabiques rétrogrades, des stimulations optogénétiques du cervelet et l'enregistrement simultané des cortex sensoriels et moteurs primaires donnent un substrat convaincant de l'existence d'une projection disynaptique ciblant parallèlement wS1 et wM1 depuis les noyaux cérébelleux profonds. Les réponses électrophysiologiques de très courte latence dans wS1, simultanées avec celles trouvées dans wM1, ainsi que leur persistance après l'inhibition pharmacologique de wM1 suggère que l'influence du cervelet sur wS1 ne passe pas par wM1 mais potentiellement par des structures sous-corticales.

## 2 - Plusieurs voies ascendantes parallèles ?

Cependant, il est à noter que la stimulation optogénétique du noyau denté, peu physiologique et massivement synchronisante provoque des réponses pendant la stimulation dans l'ensemble des couches corticales de wS1 avec plusieurs phases de réponses s'échelonnant sur la durée de la stimulation. Plusieurs facteurs peuvent venir expliquer la multiplicité de cette réponse. L'une des composantes de la réponse peut résulter de communications intercorticales, notamment dans les latences les plus longues. Cela peut aussi s'expliquer par l'existence de projections depuis le DN sur plusieurs noyaux thalamiques. En effet, les traçages anatomiques ont montré une localisation des fibres cérébelleuses au voisinage du soma de neurones projetant vers wS1 dans plusieurs noyaux thalamiques : le VAL, le VM et le POm. La quantification du nombre de cellules dans ces zones de projections cérébelleuses nous a conduit à nous focaliser sur la projection DN-POm, cependant il est possible que plusieurs voies ascendantes fonctionnelles existent vers wS1 depuis le DN,

passant aussi par le VAL et le VM. En effet, l'entraînement du DN sur ces deux noyaux thalamiques est bien décrit (Gornati *et al.*, 2018b), et présente une caractéristique intéressante pour notre compréhension de ces projections: pour des courants similaires, les courants post-synaptiques évoqués dans le VAL sont plus importants que ceux évoqués dans le VM. Cette différence est intéressante notamment du fait de l'appartenance du VM aux noyaux thalamiques d'ordre élevé, et du VAL comme noyau thalamique primaire.

Cette découverte suggère un mode d'action différent de la sortie cérébelleuse sur les différents noyaux thalamiques, provoquant en aval une modulation différente du cortex cérébral. Ainsi par exemple, le résultat d'une pause dans la décharge des noyaux profonds aura un effet bien plus important sur la réponse post-synaptique dans le VAL(Gornati *et al.*, 2018b), et donc ensuite sur les couches intermédiaires du cortex moteur. En revanche, la modulation du VM par les noyaux cérébelleux elle sera dépendante aussi de l'activité des autres entrées sur ce noyau, et permettra une modulation subséquente de vastes aires corticales via les projections en couche I de ce noyau. Si ces observations ont été faites en regard du caractère moteur du VAL et du VM, il est possible que l'activité du DN influence aussi wS1 via le VAL et le VM. La présence plus éparse des cellules projetant vers wS1 dans ces noyaux suggère cependant qu'un impact cérébelleux en condition normale, hors d'une stimulation artificielle très synchronisante via ces noyaux est probablement minime. Si une telle influence existe cependant, elle ne semble pas influencer le mécanisme de discrimination de texture étudié ici, puisque la modulation de ces voies ne modifie pas l'exploration de l'animal sur la nouvelle texture.

Un autre aspect de notre étude suggère que le cervelet pourrait moduler l'activité de wS1 via un autre noyau cérébelleux profond que le DN. Lors de nos traçages rétrogrades via wS1, au 2$^{ème}$ temps d'infection, nous avons observé des cellules non seulement dans le DN, mais aussi massivement dans le noyau interposé dorsal. Le nombre de cellules trouvées en moyenne dans le DN et l'IP était similaire, suggérant que l'interposé projette aussi assez massivement, de manière disynaptique, vers le cortex sensoriel primaire. La fonction d'une telle projection reste à élucider, avec notamment les noyaux intermédiaires de cette projection, très probablement des noyaux thalamiques. L'interposé présentant des rétro-connections très importantes avec le noyau rouge (Beitzel *et al.*, 2017), une structure prémotrice du tronc cérébral, il a principalement été impliqué dans les processus de locomotion, d'activation des paires de muscles agonistes-antagonistes et dans la fluidité

d'exécution des mouvements dirigés. Notamment, l'interposé est impliqué dans les mouvements de préhension dans le cadre de mouvements demandant une dextérité élevée chez l'humain (Küper *et al.*, 2011).

### 3 - Zones de convergence pour l'intégration sensorielle

Le rôle global du fonctionnement cérébelleux et de la sortie cérébelleuse est encore à ce stade un puzzle dont beaucoup de pièces manquent. Si l'architecture des connexions au sein du cervelet est bien connue, l'organisation des modules, leurs interactions, ainsi que la divergence des entrées provenant de la périphérie et du cortex soulèvent de nombreuses questions. Au sein du système vibrissal, l'implication du cervelet intervient à plusieurs niveaux et présente plusieurs zones de convergence avec les entrées périphériques et corticales. Or ces zones de convergence présentent un intérêt puisqu'elles constituent des zones potentielles d'intégration du contexte sensoriel immédiat avec le traitement et/ou les prédictions effectués au sein du cerveau. Ainsi, une première zone de convergence avait été montrée dans le cortex cérébelleux entre les entrées tactiles directes provenant de la face via les fibres grimpantes, et par la voie indirecte via les fibres moussues depuis le cortex sensoriel primaire et les noyaux pontiques (Odeh *et al.*, 2005; Pijpers *et al.*, 2006). Cette convergence semble être temporelle autant qu'anatomique puisque les deux voies ont une latence estimée d'environ 17ms pour arriver au cortex cérébelleux. Cette convergence temporelle à quelques millisecondes d'écart pourrait ainsi avoir une forte influence sur l'activité corticale du cervelet, cependant l'impact physiologique de cette convergence reste à élucider.

Nous avons quant à nous mis en évidence une seconde zone probable de convergence des informations corticales, cérébelleuses, et probablement périphériques au niveau du thalamus. Ainsi, notre étude montre pour la première fois de manière fonctionnelle et anatomique la projection cérébelleuse sur le POm, précédemment suggérée dans la littérature (Teune *et al.*, 2000). Plus précisément, nous trouvons une projection cérébelleuse plus importante dans la partie très antérieure du POm, avec une densification des fibres en provenance du noyau denté dans cette zone et des agrégats de cellules projetant aux cortex moteur et sensoriel. Il est intéressant de noter que cette zone antérieure du POm est aussi l'aire où la densité de terminaisons vGluT2 subcorticaux, en provenance donc de la voie paralemniscale, sont principalement situés chez le rat (Ohno *et al.*, 2012; Groh *et al.*, 2014) en agrégats de gros boutons synaptiques situés au niveau des dendrites proximales des neurones

thalamiques. De surcroît, ce POm très antérieur reçoit aussi des terminaisons corticales en provenance de la couche Vb de wS1 (Sumser *et al.*, 2017), formant des boutons synaptiques géants de type « driver ». Le degré de convergence, qu'il soit au niveau de la conjonction trigémino-corticale ou au niveau cérébello-cortical ou trigémino-cébérelleux dans le POm reste à déterminer plus précisément. Dans le POm, il a été estimé que deux tiers des neurones reçoivent uniquement une influence corticale, tandis que le tiers restant subit une influence conjointe de la périphérie et du cortex (Groh *et al.*, 2014). Ce tiers de neurones se situe pour une bonne partie dans la zone antérieure du POm, dénommée POa par A. Groh et collègues.

Les enregistrements in vitro de neurones du POm chez le rat tendent à montrer que la plupart sinon tous les neurones du POm reçoivent des projections corticales en provenance de la couche Vb (Groh *et al.*, 2014). En dépit du faible nombre de neurones enregistrés étant à l'origine de cette conclusion, si cette observation s'avère être généralisable, les projections cérébelleuses dans le POm devraient converger au niveau cellulaire avec des afférences corticales. Il serait cependant intéressant de poursuivre notre étude avec des expériences évaluant la possibilité d'une triple convergence. Ainsi, en utilisant des opsines aux longueurs d'ondes différentes injectées respectivement dans les noyaux cérébelleux profonds et dans le SpVi, combinées à un marquage rétrograde depuis wS1, des enregistrements in vitro des neurones du POm projetant à wS1 combinées à des stimulations des fibres en provenance du cervelet et de la voie paralemniscale nous renseigneraient quant à l'existence d'une convergence au niveau cellulaire des informations sensorielles cérébelleuses et périphériques directes. De plus, nous pourrions comparer les propriétés de décharges post-synaptiques de ces projections, et ainsi tenter de situer le rôle probable de chacune de ces entrées au sein du POm.

Il a été proposé que les zones de convergence thalamiques, caractérisées notamment par la présence de projections de type « driver » sur les neurones thalamiques servent à créer des fenêtres d'intégration temporelle dans le traitement des informations sensorielles. Ceci a été particulièrement théorisé par Sherman et Guillery qui dénotent ainsi l'existence de noyaux thalamiques d'ordre élevé en sus des plus classiques noyaux thalamiques de premier ordre. Les noyaux d'ordre élevé sont caractérisés par un fort contrôle cortical de leurs neurones, combiné ou non à des entrées périphériques fortes (Bickford, 2016). Les synapses de type « driver » ont pour propriété d'être formées par des boutons géants au niveau des dendrites proximales, dont l'activation provoque un fort potentiel excitateur post-synaptique,

et qui se dépriment rapidement. La décharge conjuguée de deux types de synapses driver permet ainsi une sommation de la réponse assurant une décharge en aval du neurone, dans une fenêtre temporelle assez courte. C'est ce qui a été observé dans le POm avec les projections wS1-Vb et SpVi : leur stimulation appairée permettant une augmentation de la probabilité de décharge supra linéaire lorsqu'effectuée dans une fenêtre de temps de l'ordre de 100ms (Mease *et al.*, 2016). Cependant ces deux projections présentent un profil de type « driver », tandis que nos enregistrements in vitro de neurones du POm répondant aux stimulations des fibres en provenance du DN ont un profil de réponse « driver-like », avec une absence de potentiation en réponse des trains de stimulation. Ceci suggère que la projection cérebelleuse dans le POm pourrait avoir un rôle différent des autres entrées dans l'intégration sensorielle au sein du thalamus. Cette projection provenant d'une zone cérebelleuse présentant une convergence cellulaire sensorielle et motrice, il est envisageable que la projection cérébelleuse au POm puisse servir à affiner l'intégration sensorimotrice, tandis que la convergence cortico-trigéminale servirait préférentiellement la mise en exergue d'entrées sensorielles dans une fenêtre temporelle spécifique, correspondant notamment à des changements attentionnels de l'animal (Sobolewski *et al.*, 2015).

### 4 - Inhibition dans le POm

En effet, au sein du système sensoriel des vibrisses, une composante majeure du traitement des informations est l'inhibition des noyaux thalamiques d'ordre élevés. Cette inhibition au niveau du POm est principalement assurée par trois noyaux : la Zona Incerta ventrale (ZIv), le noyau prétectal antérieur (APT) et le noyau réticulaire (RT). L'activité de ces noyaux est modulée à la fois par le cortex, la voie paralemniscale et le cervelet (Lavallée *et al.*, 2005). La relation se complexifie d'autant plus que l'APT émet aussi des projections inhibitrices et excitatrices à la ZI. Nous n'avons pas au sein de ce travail examiné la composante inhibitrice dans la voie ascendante du cervelet au cortex sensoriel, du fait de la complexité des relations entre les différents noyaux, mais il est certain qu'elle devra être explorée à l'avenir. Il sera d'autant plus important de comprendre comment le cervelet peut agir aussi au niveau de l'inhibition thalamique, puisque le noyau denté, en sus de projeter au POm, envoie aussi des projections excitatrices au niveau de la ZI (Roger and Cadusseau, 1985). Cette double projection permet probablement de limiter temporellement le relais sensoriel au sein du POm. Ainsi, la projection cérébelleuse dans le POm permettrait de faciliter la

transmission des informations en provenance de la voie paralemniscale vers les cortex sensorimoteurs, tandis que la projection vers la ZI permettrait dans une seconde volée d'augmenter l'inhibition au sein du POm. Toutefois, cette hypothèse est à nuancer par notre méconnaissance des interactions tant au niveau anatomique et physiologique entre la ZI et le POm. Il reste à déterminer le degré de convergence des projections inhibitrices incertales et excitatrices cérébelleuses au sein du PO notamment. De plus, la plupart des études effectuées sur la ZI ont été faites in vitro ou chez l'animal anesthésié, or il est probable que l'activité de la ZI soit modulée d'une part par des changements attentionnels médiés par des neurones cholinergiques du tronc cérébral (Masri *et al.*, 2006; Trageser *et al.*, 2006), mais aussi par l'établissement via une activité motrice d'une désinhibition thalamique (Urbain and Deschênes, 2007).

### 5 - Le cervelet : modulateur de l'activité intracorticale

Si dans ce travail nous n'avons pas évalué plus avant les dynamiques intra-thalamiques, nous nous sommes en revanche intéressés à l'impact du recrutement du cervelet au niveau du cortex. Ainsi, nous avons pu observer que le recrutement optogénétique du noyau denté provoquait dans wS1 et wM1 une augmentation de la décharge dans les couches infra-granulaires, avec un décours temporel similaire au sein des deux cortex. Les enregistrements multi-couches à l'aide d'électrodes linéaires ont cependant montré qu'il était difficile d'identifier précisément l'origine et les séquences d'activation en réponse aux stimulations du noyau denté. En effet, si nous avons pu observer une réponse primaire très rapide dans les couches profondes, l'inhibition au muscimol du POm ne nous a pas permis d'abolir cette réponse, sans pour autant affirmer qu'elle n'est pas due à la projection DN-POm-wS1. En effet, nos stimulations optogénétiques du noyau denté sont hautement synchronisantes et permettent probablement de compenser en partie l'effet inhibiteur de l'agoniste GABAergique qu'est le muscimol. En revanche, cette inhibition provoquait des changements notables dans les dynamiques de réponse corticales subséquents, notamment dans les réponses secondaires que nous avions théorisé comme résultant des projections cortico-corticales. La position centrale du POm au sein des dynamiques cortico-thalamo-corticales et son rôle dans la modulation de l'état cortical rend compliqué l'interprétation de résultats via son inhibition globale, et il sera plus intéressant à l'avenir d'utiliser des

techniques plus spécifiques afin d'activer ou d'inhiber des projections spécifiques telles que le DN-POm.

C'est donc une approche plus spécifique que nous avons utilisée dans un second temps et qui nous a permis d'observer un phénomène intéressant. Le POm a été montré comme projetant majoritairement en couche Va et I du cortex sensoriel primaire et moteur. La couche I du cortex étant très superficielle, mince, et peu peuplée en corps cellulaires, il est complexe de l'enregistrer à l'aide d'électrodes. Nous avons donc opté pour l'enregistrement de l'activité calcique au sein des axones du POm en couche I de wS1. Nous avons alors observé qu'un faible nombre d'axones et boutons en couche I présente une augmentation de l'activité calcique en réponse aux stimulations optogénétiques du DN dans un délai court. De manière plus intéressante, nous avons observé que la stimulation conjointe du cervelet et des vibrisses permettait de recruter en couche I du cortex sensoriel des axones et boutons axonaux qui ne présentaient pas d'activité calcique en présence de l'une ou l'autre de ces stimulations. Ces observations suggèrent plusieurs éléments.

Tout d'abord, peu d'axones en couche I répondaient à la fois aux stimulations uniques du cervelet ou des vibrisses, suggérant que ces projections au sein du PO pourraient être ségrégées et contacter des populations cellulaires différentes. La combinaison des stimulations périphériques et cérébelleuses en revanche provoque le recrutement d'axones supplémentaires, suggérant qu'il existe une population au sein du POm où ces deux types de projections convergent, et dont l'activation simultanée est nécessaire afin de moduler l'activité en couche I du POm. Cette dernière observation va dans le sens du rôle du POm comme un détecteur temporel d'activité. Il n'est cependant pas clair à ce stade dans quel contexte cette activation simultanée est recrutée et nécessaire. Il serait de plus intéressant de vérifier si ces observations faites dans wS1 sont vérifiables aussi dans wM1 puisque les axones du POm en couche I couvrent de vastes surfaces corticales.

La question de l'intérêt du recrutement d'axones du POm en couche I dans le traitement des informations sensorielles se pose alors. Les axones du POm en couche I contactent principalement les dendrites distales de neurones dont le corps cellulaire se trouve en couche II/III. L'activation du POm est nécessaire et suffisante à évoque dans les neurones de la couche II/III des plateaux dépendants des récepteurs NMDA, similaires à ceux provoqués par des stimulations rythmiques des vibrisses observées notamment au cours de l'exploration d'objets par un animal (Gambino *et al.*, 2014). Cette potentiation post-synaptique à long

terme est un élément important puisqu'elle permet notamment de rapprocher du seuil de dépolarisation les neurones des couches II/III et ainsi augmenter leur sensibilité aux informations sensorielles périphériques arrivant via la voie lemniscale. Ainsi un papier subséquent de la même équipe a montré que la convergence des entrées lemniscales via la voie VPM-LIV et paralemniscales via la voie POm-LI permet la désinhibition neurones de la couche II/III de wS1. Cette désinhibition s'effectue via l'activation des interneurones VIP, qui inhibent les interneurones SST exerçant une forte activité inhibitrice sur l'activité dendritiques des neurones de la couche II/III (Williams and Holtmaat, 2019). Cela permet ainsi une potentiation des synapses du premier ordre, probablement au cours d'un apprentissage sensoriel ou de la discrimination sensorielle.

Nos données d'imageries calciques suggèrent que le cervelet joue un rôle dans la facilitation de ce processus, en permettant l'activation d'un plus grand nombre de projections POm-LI que la seule stimulation des vibrisses. Le recrutement de cette projection ascendante cervelet-POm-wS1LI est probablement nécessaire dans le cadre d'une exploration tactile fine, où l'intégration multi-vibrissale est nécessaire, l'engagement du cervelet permettant de renforcer la modulation de l'activité en couche II/III et ainsi d'augmenter la perception sensorielle dans une fenêtre temporelle donnée. Cette hypothèse est renforcée par l'expérience de discrimination tactile que nous avons effectuée, où l'engagement spécifique de la voie DN-POm est nécessaire afin de discriminer deux objets aux textures différentes au cours d'une exploration naturelle de l'animal.

# Conclusion

Ainsi au cours de ma thèse, je me suis intéressée particulièrement aux voies ascendantes du cervelet vers le cortex, plus particulièrement dans le système sensori-moteur des vibrisses. Si j'ai pu mettre au jour quelques caractéristiques intéressantes de cette voie ascendante, telles que l'implication du POm, ce noyau thalamique d'ordre élevé, et le recrutement de ses projections en couche I de manière préférentielle en cas d'entrées cérébelleuses et périphériques conjointes, j'ai aussi beaucoup été confrontée à la complexité de ce système. En effet, la multiplicité des zones de convergence et des structures impliquées dans le relais des informations présente un défi non négligeable dans l'interprétation des données et invite à la prudence.

Une des caractéristiques majeures qui émane de mes travaux de thèse, ainsi que de la littérature très récente du cervelet, est la multiplicité des canaux par lesquels cette structure communique avec le reste du diencéphale. Il convient alors de se demander comment réconcilier les théories computationnelles du cervelet, notamment le concept de modèle interne et de prédiction sensorielle avec ces canaux multiples. Le cortex cérébelleux est présumé effectuer des comparaisons entre le contexte immédiat, la commande motrice, et les entrées sensorielles attendues, afin notamment de soustraire la réafférence sensorielle née d'un mouvement volontaire, et ainsi mettre en exergue les évènements inattendus. Il est possible que différentes zones du cortex cérébelleux soient recrutées afin d'effectuer cette computation selon l'état attentionnel de l'animal, la complexité du mouvement en cours ou encore la prédictibilité sensorielle dans un contexte donné. Ainsi, en fonction de l'engagement de l'animal, que ce soit dans une tâche d'apprentissage moteur, dans l'exécution d'un mouvement pour obtenir une récompense, dans un contexte d'exploration simple, différentes voies de sortie du cervelet seraient recrutées, permettant la modulation de l'activité ou le recrutement de diverses zones du diencéphalon.

Ainsi, selon le degré de prédictibilité sensorielle liée au mouvement, le degré d'incertitude sensorielle (*discrimination)*, ou la valence accordée à l'acquisition sensorielle, différentes voies cérebello-thalamo-corticales seraient recrutées. Regardant les projections des noyaux cérébelleux vers le thalamus, et particulièrement vers les noyaux qui nous ont intéressés au cours du projet, nous pouvons ainsi spéculer quant à leurs modalités de recrutement. Tout d'abord, le VM est connu pour sa capacité à moduler de vastes zones corticales via la couche I, notamment dans la bande gamma du potentiel de champ local (Steriade, 1995). La zone VM recevant des projections cérébelleuses a aussi été montrée comme étant réciproquement connectée avec l'ALM, une aire corticale prémotrice. Cette zone du VM joue un rôle dans la préparation motrice en réponse à un stimulus sensoriel, dans un canal parallèle à celui liant le VM à M1 (Guo *et al.*, 2018). Ainsi, nous pouvons imaginer un recrutement préférentiel de la voie DCN-VM dans le cadre d'actions sensori-motrices associées à des processus cognitifs et/ou attentionnels, requérant la coordination de multiples aires corticales. La voie DCN-VAL quant à elle correspondrait plutôt à la voie classique de modulation motrice : les projections du VAL vers les couches intermédiaires et de sortie du cortex moteur, mais aussi du cortex sensoriel (impliqué lui aussi dans la génération de mouvement dans le système des vibrisses, (Sreenivasan *et al.*, 2016)). Cette

projection permettrait donc une correction rapide à l'initiation du mouvement dans le cadre de comportements moteurs simples d'exploration. En ce qui concerne la voie DN-PO qui nous a intéressé plus précisément dans ce travail, il est probable qu'elle soit particulièrement recrutée dans le cadre d'une exploration tactile nécessitant une précision sensorielle importante. En permettant la modulation de l'état cortical de wS1 et wM1 via le POm, le cervelet permettrait donc, via cette voie, de favoriser la perception sensorielle. Il est aussi possible qu'elle soit recrutée préférentiellement lorsque la souris est exposée à un contexte sensoriel nouveau, comme ici dans notre paradigme expérimental, où les animaux n'avaient jamais été en contact avec des textures complexes comme celles du papier de verre, et n'ont donc pas d'attente sensorielle particulière.

Ainsi au cours de ma thèse, dans mon projet principal comme dans les autres projets sur lesquels j'ai collaboré, je me suis penchée sur la diversité et la richesse des voies de sortie du cervelet, et leur implication dans des processus variés : conditionnement de peur, pathologies motrices et exploration tactile. Le raffinement de nouvelles approches spécifiques de contrôle de ces voies et le développement de tâches comportementales permettant de différencier leurs impacts respectifs devraient faciliter à l'avenir leur étude. La connaissance de cette sortie du cervelet est cruciale, tant pour la compréhension des différents processus qui y sont liés, mais aussi pour mieux comprendre le rôle du cervelet et étayer les théories computationnelles qui lui sont liées.

# Références


Ahissar, E. *et al.* (2001) 'Temporal frequency of whisker movement. II. Laminar organization of cortical representations', *Journal of Neurophysiology*, 86(1), pp. 354–367. doi: 10.1152/jn.2001.86.1.354.

Allen, G. (2005) 'The Cerebellum in Autism', *Clinical Neuropsychiatry: Journal of Treatment Evaluation*, 2(6), pp. 321–337.

Allen, G. I. and Tsukahara, N. (1974) 'Cerebrocerebellar communication systems.', *Physiological Reviews*, 54(4), pp. 957–1006. doi: 10.1152/physrev.1974.54.4.957.

Alloway, K. D. *et al.* (2006) 'Topography of cortical projections to the dorsolateral neostriatum in rats: Multiple overlapping sensorimotor pathways', *Journal of Comparative Neurology*, 499(1), pp. 33–48. doi: https://doi.org/10.1002/cne.21039.

Aoki, S., Coulon, P. and Ruigrok, T. J. H. (2019) 'Multizonal Cerebellar Influence Over Sensorimotor Areas of the Rat Cerebral Cortex', *Cerebral Cortex*, 29(2), pp. 598–614. doi: 10.1093/cercor/bhx343.

Apps, R. and Hawkes, R. (2009) 'Cerebellar cortical organization: a one-map hypothesis', *Nature Reviews. Neuroscience*, 10(9), pp. 670–681. doi: 10.1038/nrn2698.

Arabzadeh, E., Petersen, R. S. and Diamond, M. E. (2003) 'Encoding of Whisker Vibration by Rat Barrel Cortex Neurons: Implications for Texture Discrimination', *Journal of Neuroscience*, 23(27), pp. 9146–9154. doi: 10.1523/JNEUROSCI.23-27-09146.2003.

Arabzadeh, E., Zorzin, E. and Diamond, M. E. (2005) 'Neuronal encoding of texture in the whisker sensory pathway', *PLoS biology*, 3(1), p. e17. doi: 10.1371/journal.pbio.0030017.

Asanuma, C., Thach, W. T. and Jones, E. G. (1983) 'Distribution of cerebellar terminations and their relation to other afferent terminations in the ventral lateral thalamic region of the monkey', *Brain Research Reviews*, 5(3), pp. 237–265. doi: 10.1016/0165-0173(83)90015-2.

Ashizawa, T. and Xia, G. (2016) 'Ataxia', *Continuum : Lifelong Learning in Neurology*, 22(4 Movement Disorders), pp. 1208–1226. doi: 10.1212/CON.0000000000000362.

Atkins, M. J. and Apps, R. (1997) 'Somatotopical organisation within the climbing fibre projection to the paramedian lobule and copula pyramidis of the rat cerebellum', *The Journal of Comparative Neurology*, 389(2), pp. 249–263.

Audette, N. J. *et al.* (2018) 'POm Thalamocortical Input Drives Layer-Specific Microcircuits in Somatosensory Cortex', *Cerebral Cortex*, 28(4), pp. 1312–1328. doi: 10.1093/cercor/bhx044.

Aumann, T. D. *et al.* (1994) 'Projections from the lateral and interposed cerebellar nuclei to the thalamus of the rat: a light and electron microscopic study using single and double anterograde labelling', *The Journal of Comparative Neurology*, 349(2), pp. 165–181. doi: 10.1002/cne.903490202.

Bastian, A. J. (2006) ‘Learning to predict the future: the cerebellum adapts feedforward movement control’, *Current Opinion in Neurobiology*, 16(6), pp. 645–649. doi: 10.1016/j.conb.2006.08.016.

Beitzel, C. S. *et al.* (2017) ‘Rubrocerebellar Feedback Loop Isolates the Interposed Nucleus as an Independent Processor of Corollary Discharge Information in Mice’, *The Journal of Neuroscience: The Official Journal of the Society for Neuroscience*, 37(42), pp. 10085–10096. doi: 10.1523/JNEUROSCI.1093-17.2017.

Bickford, M. E. (2016) ‘Thalamic Circuit Diversity: Modulation of the Driver/Modulator Framework’, *Frontiers in Neural Circuits*, 9. doi: 10.3389/fncir.2015.00086.

Bohne, P. *et al.* (2019) ‘A New Projection From the Deep Cerebellar Nuclei to the Hippocampus via the Ventrolateral and Laterodorsal Thalamus in Mice’, *Frontiers in Neural Circuits*, 13. doi: 10.3389/fncir.2019.00051.

Bosman, L. W. J. *et al.* (2010) ‘Encoding of whisker input by cerebellar Purkinje cells’, *The Journal of Physiology*, 588(Pt 19), pp. 3757–3783. doi: 10.1113/jphysiol.2010.195180.

Bosman, L. W. J. *et al.* (2011) ‘Anatomical Pathways Involved in Generating and Sensing Rhythmic Whisker Movements’, *Frontiers in Integrative Neuroscience*, 5. doi: 10.3389/fnint.2011.00053.

Bower, J. M. (1997) ‘Is the cerebellum sensory for motor’s sake, or motor for sensory’s sake: the view from the whiskers of a rat?’, *Progress in Brain Research*, 114, pp. 463–496. doi: 10.1016/s0079-6123(08)63381-6.

Brecht, M., Preilowski, B. and Merzenich, M. M. (1997) ‘Functional architecture of the mystacial vibrissae’, *Behavioural Brain Research*, 84(1–2), pp. 81–97. doi: 10.1016/s0166-4328(97)83328-1.

Brooks, J. X., Carriot, J. and Cullen, K. E. (2015) ‘Learning to expect the unexpected: rapid updating in primate cerebellum during voluntary self-motion’, *Nature Neuroscience*, 18(9), pp. 1310–1317. doi: 10.1038/nn.4077.

Brown, I. E. and Bower, J. M. (2001) ‘Congruence of mossy fiber and climbing fiber tactile projections in the lateral hemispheres of the rat cerebellum’, *The Journal of Comparative Neurology*, 429(1), pp. 59–70. doi: 10.1002/1096-9861(20000101)429:1<59::aid-cne5>3.0.co;2-3.

Brown, S. T. and Raman, I. M. (2018) ‘Sensorimotor Integration and Amplification of Reflexive Whisking by Well-Timed Spiking in the Cerebellar Corticonuclear Circuit’, *Neuron*, 99(3), pp. 564-575.e2. doi: 10.1016/j.neuron.2018.06.028.

Bruno, R. M. *et al.* (2009) ‘Sensory experience alters specific branches of individual corticocortical axons during development’, *The Journal of Neuroscience: The Official Journal of the Society for Neuroscience*, 29(10), pp. 3172–3181. doi: 10.1523/JNEUROSCI.5911-08.2009.

Calderon, D. P. *et al.* (2011) ‘The neural substrates of Rapid-Onset Dystonia-Parkinsonism’, *Nature neuroscience*, 14(3), pp. 357–365. doi: 10.1038/nn.2753.

Carvell, G. E. and Simons, D. J. (1987) ‘Thalamic and corticocortical connections of the second somatic sensory area of the mouse’, *The Journal of Comparative Neurology*, 265(3), pp. 409–427. doi: 10.1002/cne.902650309.

Carvell, G. E. and Simons, D. J. (1995) ‘Task- and subject-related differences in sensorimotor behavior during active touch’, *Somatosensory & Motor Research*, 12(1), pp. 1–9. doi: 10.3109/08990229509063138.

Casas-Torremocha, D. *et al.* (2019) ‘Posterior thalamic nucleus axon terminals have different structure and functional impact in the motor and somatosensory vibrissal cortices’, *Brain Structure and Function*. doi: 10.1007/s00429-019-01862-4.

Castejon, C., Barros-Zulaica, N. and Nuñez, A. (2016) ‘Control of Somatosensory Cortical Processing by Thalamic Posterior Medial Nucleus: A New Role of Thalamus in Cortical Function’, *PLOS ONE*. Edited by M. Maravall, 11(1), p. e0148169. doi: 10.1371/journal.pone.0148169.

Castejon, C. and Nuñez, A. (2020) ‘Higher-order thalamic implication in the codification of bilateral sensory events’, *bioRxiv*, p. 2020.05.01.073098. doi: 10.1101/2020.05.01.073098.

Çavdar, S. *et al.* (2014) ‘Motor afferents from the cerebellum, zona incerta and substantia nigra to the mediodorsal thalamic nucleus in the rat’, *Journal of Integrative Neuroscience*, 13(4), pp. 565–578. doi: 10.1142/S0219635214500198.

Cerminara, N. L. *et al.* (2015) ‘Redefining the cerebellar cortex as an assembly of non-uniform Purkinje cell microcircuits’, *Nature Reviews. Neuroscience*, 16(2), pp. 79–93. doi: 10.1038/nrn3886.

Chabrol, F. P. *et al.* (2015) ‘Synaptic diversity enables temporal coding of coincident multisensory inputs in single neurons’, *Nature Neuroscience*, 18(5), pp. 718–727. doi: 10.1038/nn.3974.

Chen, C. H. *et al.* (2014) ‘Short latency cerebellar modulation of the basal ganglia’, *Nature Neuroscience*, 17(12), pp. 1767–1775. doi: 10.1038/nn.3868.

Chen, J. L. *et al.* (2015) ‘Pathway-specific reorganization of projection neurons in somatosensory cortex during learning’, *Nature Neuroscience*, 18(8), pp. 1101–1108. doi: 10.1038/nn.4046.

Chen, S., Augustine, G. J. and Chadderton, P. (2016) *The cerebellum linearly encodes whisker position during voluntary movement*, *eLife*. eLife Sciences Publications Limited. doi: 10.7554/eLife.10509.

Coco, M. and Perciavalle, V. (2015) ‘Where did the motor function of the cerebellum come from?’, *Cerebellum & Ataxias*, 2, p. 10. doi: 10.1186/s40673-015-0029-8.

Constantinople, C. M. and Bruno, R. M. (2013) ‘Deep cortical layers are activated directly by thalamus’, *Science (New York, N.Y.)*, 340(6140), pp. 1591–1594. doi: 10.1126/science.1236425.

Crochet, S. and Petersen, C. C. H. (2006) ‘Correlating whisker behavior with membrane potential in barrel cortex of awake mice’, *Nature Neuroscience*, 9(5), pp. 608–610. doi: 10.1038/nn1690.

De Zeeuw, C. I. *et al.* (2011) ‘Spatiotemporal firing patterns in the cerebellum’, *Nature Reviews. Neuroscience*, 12(6), pp. 327–344. doi: 10.1038/nrn3011.

De Zeeuw, C. I. and Ten Brinke, M. M. (2015) ‘Motor Learning and the Cerebellum’, *Cold Spring Harbor Perspectives in Biology*, 7(9), p. a021683. doi: 10.1101/cshperspect.a021683.

Deschênes, M., Timofeeva, E. and Lavallée, P. (2003) ‘The Relay of High-Frequency Sensory Signals in the Whisker-to-Barreloid Pathway’, *Journal of Neuroscience*, 23(17), pp. 6778–6787. doi: 10.1523/JNEUROSCI.23-17-06778.2003.

Deschênes, M., Veinante, P. and Zhang, Z. W. (1998) ‘The organization of corticothalamic projections: reciprocity versus parity’, *Brain Research. Brain Research Reviews*, 28(3), pp. 286–308. doi: 10.1016/s0165-0173(98)00017-4.

Diamond, M. E., Armstrong-James, M. and Ebner, F. F. (1992) ‘Somatic sensory responses in the rostral sector of the posterior group (POm) and in the ventral posterior medial nucleus (VPM) of the rat thalamus’, *Journal of Comparative Neurology*, 318(4), pp. 462–476. doi: https://doi.org/10.1002/cne.903180410.

Diedrichsen, J. *et al.* (2011) ‘Imaging the deep cerebellar nuclei: a probabilistic atlas and normalization procedure’, *NeuroImage*, 54(3), pp. 1786–1794. doi: 10.1016/j.neuroimage.2010.10.035.

Doya, K. (1999) ‘What are the computations of the cerebellum, the basal ganglia and the cerebral cortex?’, *Neural Networks*, 12(7), pp. 961–974. doi: 10.1016/S0893-6080(99)00046-5.

Ebbesen, C. L. *et al.* (2017) ‘Vibrissa motor cortex activity suppresses contralateral whisking behavior’, *Nature Neuroscience*, 20(1), pp. 82–89. doi: 10.1038/nn.4437.

Feldmeyer, D., Lübke, J. and Sakmann, B. (2006) ‘Efficacy and connectivity of intracolumnar pairs of layer 2/3 pyramidal cells in the barrel cortex of juvenile rats’, *The Journal of Physiology*, 575(Pt 2), pp. 583–602. doi: 10.1113/jphysiol.2006.105106.

Feldmeyer, D., Roth, A. and Sakmann, B. (2005) ‘Monosynaptic Connections between Pairs of Spiny Stellate Cells in Layer 4 and Pyramidal Cells in Layer 5A Indicate That Lemniscal and Paralemniscal Afferent Pathways Converge in the Infragranular Somatosensory Cortex’, *The Journal of Neuroscience*, 25(13), pp. 3423–3431. doi: 10.1523/JNEUROSCI.5227-04.2005.

Ferezou, I. *et al.* (2007) ‘Spatiotemporal Dynamics of Cortical Sensorimotor Integration in Behaving Mice’, *Neuron*, 56(5), pp. 907–923. doi: 10.1016/j.neuron.2007.10.007.

Ferezou, I., Bolea, S. and Petersen, C. C. H. (2006) ‘Visualizing the cortical representation of whisker touch: voltage-sensitive dye imaging in freely moving mice’, *Neuron*, 50(4), pp. 617–629. doi: 10.1016/j.neuron.2006.03.043.

Fujita, H., Kodama, T. and Lac, S. du (2020) 'Modular output circuits of the fastigial nucleus mediate diverse motor and nonmotor functions of the cerebellar vermis', *bioRxiv*, p. 2020.04.23.047100. doi: 10.1101/2020.04.23.047100.

Gambino, F. *et al.* (2014) 'Sensory-evoked LTP driven by dendritic plateau potentials in vivo', *Nature*, 515(7525), pp. 116–119. doi: 10.1038/nature13664.

Gao, J. H. *et al.* (1996) 'Cerebellum implicated in sensory acquisition and discrimination rather than motor control', *Science (New York, N.Y.)*, 272(5261), pp. 545–547. doi: 10.1126/science.272.5261.545.

Gao, P. *et al.* (2003) 'Whisker motor cortex ablation and whisker movement patterns', *Somatosensory & Motor Research*, 20(3–4), pp. 191–198. doi: 10.1080/08990220310001622924.

Gao, Z. *et al.* (2018) 'A cortico-cerebellar loop for motor planning', *Nature*, 563(7729), pp. 113–116. doi: 10.1038/s41586-018-0633-x.

Gibson, A. R., Horn, K. M. and Pong, M. (2004) 'Activation of climbing fibers', *Cerebellum (London, England)*, 3(4), pp. 212–221. doi: 10.1080/14734220410018995.

Glickstein, M., Strata, P. and Voogd, J. (2009) 'Cerebellum: history', *Neuroscience*, 162(3), pp. 549–559. doi: 10.1016/j.neuroscience.2009.02.054.

Gornati, S. V. *et al.* (2018a) 'Differentiating Cerebellar Impact on Thalamic Nuclei', *Cell Reports*, 23(9), pp. 2690–2704. doi: 10.1016/j.celrep.2018.04.098.

Gornati, S. V. *et al.* (2018b) 'Differentiating Cerebellar Impact on Thalamic Nuclei', *Cell Reports*, 23(9), pp. 2690–2704. doi: 10.1016/j.celrep.2018.04.098.

Groh, A. *et al.* (2014) 'Convergence of Cortical and Sensory Driver Inputs on Single Thalamocortical Cells', *Cerebral Cortex (New York, NY)*, 24(12), pp. 3167–3179. doi: 10.1093/cercor/bht173.

Guo, K. *et al.* (2018) 'Anterolateral Motor Cortex Connects with a Medial Subdivision of Ventromedial Thalamus through Cell Type-Specific Circuits, Forming an Excitatory Thalamo-Cortico-Thalamic Loop via Layer 1 Apical Tuft Dendrites of Layer 5B Pyramidal Tract Type Neurons', *The Journal of Neuroscience*, 38(41), pp. 8787–8797. doi: 10.1523/JNEUROSCI.1333-18.2018.

Helmchen, F., Gilad, A. and Chen, J. L. (2018) 'Neocortical dynamics during whisker-based sensory discrimination in head-restrained mice', *Neuroscience*, 368, pp. 57–69. doi: 10.1016/j.neuroscience.2017.09.003.

Henneman, E., Cooke, P. M. and Snider, R. S. (1952) 'Cerebellar projections to the cerebral cortex', *Research Publications - Association for Research in Nervous and Mental Disease*, 30, pp. 317–333.

Hentschke, H., Haiss, F. and Schwarz, C. (2006) 'Central Signals Rapidly Switch Tactile Processing in Rat Barrel Cortex during Whisker Movements', *Cerebral Cortex*, 16(8), pp. 1142–1156. doi: 10.1093/cercor/bhj056.

Herculano-Houzel, S. (2010) ‘Coordinated scaling of cortical and cerebellar numbers of neurons’, *Frontiers in Neuroanatomy*, 4. doi: 10.3389/fnana.2010.00012.

Hodos, W. (2009) ‘Evolution of Cerebellum’, in Binder, M. D., Hirokawa, N., and Windhorst, U. (eds) *Encyclopedia of Neuroscience*. Berlin, Heidelberg: Springer, pp. 1240–1243. doi: 10.1007/978-3-540-29678-2_3124.

Hutson, K. A. and Masterton, R. B. (1986) ‘The sensory contribution of a single vibrissa’s cortical barrel’, *Journal of Neurophysiology*, 56(4), pp. 1196–1223. doi: 10.1152/jn.1986.56.4.1196.

Hyvärinen, H. *et al.* (2009) ‘Aquatic environment and differentiation of vibrissae: comparison of sinus hair systems of ringed seal, otter and pole cat’, *Brain, Behavior and Evolution*, 74(4), pp. 268–279. doi: 10.1159/000264662.

Iseni, F. *et al.* (1997) ‘Mapping of monoclonal antibody epitopes of the rabies virus P protein.’, *Journal of General Virology*, 78(1), pp. 119–124. doi: 10.1099/0022-1317-78-1-119.

Ito, M. (1984) ‘The modifiable neuronal network of the cerebellum’, *The Japanese Journal of Physiology*, 34(5), pp. 781–792. doi: 10.2170/jjphysiol.34.781.

Jones, E. G. (1998) ‘Viewpoint: the core and matrix of thalamic organization’, *Neuroscience*, 85(2), pp. 331–345. doi: 10.1016/s0306-4522(97)00581-2.

Jones, E. G. and Diamond, I. T. (1995) *The Barrel Cortex of Rodents: Volume 11: The Barrel Cortex of Rodents*. Springer Science & Business Media.

Kelly, R. M. and Strick, P. L. (2003) ‘Cerebellar loops with motor cortex and prefrontal cortex of a nonhuman primate’, *The Journal of Neuroscience: The Official Journal of the Society for Neuroscience*, 23(23), pp. 8432–8444.

Krupa, D. J. *et al.* (2001) ‘Behavioral Properties of the Trigeminal Somatosensory System in Rats Performing Whisker-Dependent Tactile Discriminations’, *Journal of Neuroscience*, 21(15), pp. 5752–5763. doi: 10.1523/JNEUROSCI.21-15-05752.2001.

Küper, M. *et al.* (2011) ‘Lesions of the dentate and interposed nuclei are associated with impaired prehension in cerebellar patients’, *Neuroscience Letters*, 499(2), pp. 132–136. doi: 10.1016/j.neulet.2011.05.055.

Kuramoto, E. *et al.* (2009) ‘Two types of thalamocortical projections from the motor thalamic nuclei of the rat: a single neuron-tracing study using viral vectors’, *Cerebral Cortex (New York, N.Y.: 1991)*, 19(9), pp. 2065–2077. doi: 10.1093/cercor/bhn231.

Kwegyir-Afful, E. E. *et al.* (2005) ‘The Role of Thalamic Inputs in Surround Receptive Fields of Barrel Neurons’, *Journal of Neuroscience*, 25(25), pp. 5926–5934. doi: 10.1523/JNEUROSCI.1360-05.2005.

Kwon, S. E. *et al.* (2016) ‘Sensory and decision-related activity propagate in a cortical feedback loop during touch perception’, *Nature Neuroscience*, 19(9), pp. 1243–1249. doi: 10.1038/nn.4356.

Lam, Y.-W. and Sherman, S. M. (2007) 'Different Topography of the Reticulothalmic Inputs to First- and Higher-Order Somatosensory Thalamic Relays Revealed Using Photostimulation', *Journal of Neurophysiology*, 98(5), pp. 2903–2909. doi: 10.1152/jn.00782.2007.

Lang, E. J., Sugihara, I. and Llinás, R. (2006) 'Olivocerebellar modulation of motor cortex ability to generate vibrissal movements in rat', *The Journal of Physiology*, 571(Pt 1), pp. 101–120. doi: 10.1113/jphysiol.2005.102764.

Lavallée, P. *et al.* (2005) 'Feedforward Inhibitory Control of Sensory Information in Higher-Order Thalamic Nuclei', *The Journal of Neuroscience*, 25(33), pp. 7489–7498. doi: 10.1523/JNEUROSCI.2301-05.2005.

Lee, K. J. and Woolsey, T. A. (1975) 'A proportional relationship between peripheral innervation density and cortical neuron number in the somatosensory system of the mouse', *Brain Research*, 99(2), pp. 349–353. doi: 10.1016/0006-8993(75)90035-9.

Lee, L.-J. *et al.* (2009) 'Neonatal whisker trimming causes long-lasting changes in structure and function of the somatosensory system', *Experimental Neurology*, 219(2), pp. 524–532. doi: 10.1016/j.expneurol.2009.07.012.

Lee, L.-J., Lo, F.-S. and Erzurumlu, R. S. (2005) 'NMDA Receptor-Dependent Regulation of Axonal and Dendritic Branching', *The Journal of Neuroscience*, 25(9), pp. 2304–2311. doi: 10.1523/JNEUROSCI.4902-04.2005.

Leergaard, T. B. *et al.* (2004) 'Three-dimensional topography of corticopontine projections from rat sensorimotor cortex: comparisons with corticostriatal projections reveal diverse integrative organization', *The Journal of Comparative Neurology*, 478(3), pp. 306–322. doi: 10.1002/cne.20289.

Manto, M. *et al.* (2012) 'Consensus paper: roles of the cerebellum in motor control--the diversity of ideas on cerebellar involvement in movement', *Cerebellum (London, England)*, 11(2), pp. 457–487. doi: 10.1007/s12311-011-0331-9.

Mao, T. *et al.* (2011) 'Long-range neuronal circuits underlying the interaction between sensory and motor cortex', *Neuron*, 72(1), pp. 111–123. doi: 10.1016/j.neuron.2011.07.029.

Masri, R. *et al.* (2006) 'Cholinergic Regulation of the Posterior Medial Thalamic Nucleus', *Journal of Neurophysiology*, 96(5), pp. 2265–2273. doi: 10.1152/jn.00476.2006.

Masri, R. *et al.* (2008) 'Encoding of stimulus frequency and sensor motion in the posterior medial thalamic nucleus', *Journal of Neurophysiology*, 100(2), pp. 681–689. doi: 10.1152/jn.01322.2007.

Matyas, F. *et al.* (2010) 'Motor control by sensory cortex', *Science (New York, N.Y.)*, 330(6008), pp. 1240–1243. doi: 10.1126/science.1195797.

Mease, R. A. *et al.* (2016) 'Cortical Dependence of Whisker Responses in Posterior Medial Thalamus In Vivo', *Cerebral Cortex*, 26(8), pp. 3534–3543. doi: 10.1093/cercor/bhw144.

Mercier, B. E., Legg, C. R. and Glickstein, M. (1990) 'Basal ganglia and cerebellum receive different somatosensory information in rats', *Proceedings of the National Academy of*

*Sciences of the United States of America*, 87(11), pp. 4388–4392. doi: 10.1073/pnas.87.11.4388.

Middleton, F. A. and Strick, P. L. (2001) 'Cerebellar Projections to the Prefrontal Cortex of the Primate', *Journal of Neuroscience*, 21(2), pp. 700–712. doi: 10.1523/JNEUROSCI.21-02-00700.2001.

Mitrofanis, J. (2005) 'Some certainty for the "zone of uncertainty"? Exploring the function of the zona incerta', *Neuroscience*, 130(1), pp. 1–15. doi: 10.1016/j.neuroscience.2004.08.017.

Miyashita, E., Keller, A. and Asanuma, H. (1994) 'Input-output organization of the rat vibrissal motor cortex', *Experimental brain research. Experimentelle Hirnforschung. Expérimentation cérébrale*, 99, pp. 223–32. doi: 10.1007/BF00239589.

Mo, C. *et al.* (2017) 'Synaptic properties of the lemniscal and paralemniscal pathways to the mouse somatosensory thalamus', *Proceedings of the National Academy of Sciences*, 114(30), pp. E6212–E6221. doi: 10.1073/pnas.1703222114.

Mo, C. and Sherman, S. M. (2019) 'A Sensorimotor Pathway via Higher-Order Thalamus', *The Journal of Neuroscience*, 39(4), pp. 692–704. doi: 10.1523/JNEUROSCI.1467-18.2018.

Moberget, T. and Ivry, R. B. (2016) 'Cerebellar contributions to motor control and language comprehension: searching for common computational principles', *Annals of the New York Academy of Sciences*, 1369(1), pp. 154–171. doi: 10.1111/nyas.13094.

Neimark, M. A. *et al.* (2003) 'Vibrissa Resonance as a Transduction Mechanism for Tactile Encoding', *The Journal of Neuroscience*, 23(16), pp. 6499–6509. doi: 10.1523/JNEUROSCI.23-16-06499.2003.

Nikolov, P. *et al.* (2019) 'Cerebellar Involvement in DYT-THAP1 Dystonia', *The Cerebellum*, 18(5), pp. 969–971. doi: 10.1007/s12311-019-01062-0.

Odeh, F. *et al.* (2005) 'Pontine Maps Linking Somatosensory and Cerebellar Cortices Are in Register with Climbing Fiber Somatotopy', *The Journal of Neuroscience*, 25(24), pp. 5680–5690. doi: 10.1523/JNEUROSCI.0558-05.2005.

Ohno, S. *et al.* (2012) 'A morphological analysis of thalamocortical axon fibers of rat posterior thalamic nuclei: a single neuron tracing study with viral vectors', *Cerebral Cortex (New York, N.Y.: 1991)*, 22(12), pp. 2840–2857. doi: 10.1093/cercor/bhr356.

Palkovits, M. *et al.* (1977) 'Quantitative histological analysis of the cerebellar nuclei in the cat. I. Numerical data on cells and on synapses', *Experimental Brain Research*, 28(1–2), pp. 189–209. doi: 10.1007/BF00237096.

Panto, M. R. *et al.* (1995) 'The projection from the primary motor and somatic sensory cortex to the basilar pontine nuclei. A detailed electrophysiological and anatomical study in the rat', *Journal Fur Hirnforschung*, 36(1), pp. 7–19.

Park, J. M. *et al.* (2020) *Deep and superficial layers of the primary somatosensory cortex are critical for whisker-based texture discrimination in mice*. preprint. Neuroscience. doi: 10.1101/2020.08.12.245381.

Parsons, L. M. *et al.* (1997) 'Lateral cerebellar hemispheres actively support sensory acquisition and discrimination rather than motor control', *Learning & Memory (Cold Spring Harbor, N.Y.)*, 4(1), pp. 49–62. doi: 10.1101/lm.4.1.49.

Parsons, L. M. *et al.* (2009) 'Pitch discrimination in cerebellar patients: evidence for a sensory deficit', *Brain Research*, 1303, pp. 84–96. doi: 10.1016/j.brainres.2009.09.052.

Patel, V. R. and Zee, D. S. (2015) *The cerebellum in eye movement control: nystagmus, coordinate frames and disconjugacy*. Report 2. Nature Publishing Group, pp. 191–195. Available at: https://www.nature.com/articles/eye2014271 (Accessed: 1 March 2021).

Person, A. L. and Raman, I. M. (2011) 'Purkinje neuron synchrony elicits time-locked spiking in the cerebellar nuclei', *Nature*, 481(7382), pp. 502–505. doi: 10.1038/nature10732.

Petersen, C. C. and Sakmann, B. (2001) 'Functionally independent columns of rat somatosensory barrel cortex revealed with voltage-sensitive dye imaging', *The Journal of Neuroscience: The Official Journal of the Society for Neuroscience*, 21(21), pp. 8435–8446.

Petreanu, L. *et al.* (2007) 'Channelrhodopsin-2-assisted circuit mapping of long-range callosal projections', *Nature Neuroscience*, 10(5), pp. 663–668. doi: 10.1038/nn1891.

Petreanu, L. *et al.* (2009) 'The subcellular organization of neocortical excitatory connections', *Nature*, 457(7233), pp. 1142–1145. doi: 10.1038/nature07709.

Petreanu, L. *et al.* (2012) 'Activity in motor-sensory projections reveals distributed coding in somatosensation', *Nature*, 489(7415), pp. 299–303. doi: 10.1038/nature11321.

Pierret, T., Lavallée, P. and Deschênes, M. (2000) 'Parallel Streams for the Relay of Vibrissal Information through Thalamic Barreloids', *The Journal of Neuroscience*, 20(19), pp. 7455–7462. doi: 10.1523/JNEUROSCI.20-19-07455.2000.

Pijpers, A. *et al.* (2006) 'Precise Spatial Relationships between Mossy Fibers and Climbing Fibers in Rat Cerebellar Cortical Zones', *Journal of Neuroscience*, 26(46), pp. 12067–12080. doi: 10.1523/JNEUROSCI.2905-06.2006.

Popa, D. *et al.* (2013) 'Functional role of the cerebellum in gamma-band synchronization of the sensory and motor cortices', *The Journal of Neuroscience: The Official Journal of the Society for Neuroscience*, 33(15), pp. 6552–6556. doi: 10.1523/JNEUROSCI.5521-12.2013.

Proville, R. D. *et al.* (2014) 'Cerebellum involvement in cortical sensorimotor circuits for the control of voluntary movements', *Nature Neuroscience*, 17(9), pp. 1233–1239. doi: 10.1038/nn.3773.

Roger, M. and Cadusseau, J. (1985) 'Afferents to the zona incerta in the rat: a combined retrograde and anterograde study', *The Journal of Comparative Neurology*, 241(4), pp. 480–492. doi: 10.1002/cne.902410407.

Ruigrok, T. J. H. *et al.* (2008) 'Multiple cerebellar zones are involved in the control of individual muscles: a retrograde transneuronal tracing study with rabies virus in the rat', *European Journal of Neuroscience*, 28(1), pp. 181–200. doi: https://doi.org/10.1111/j.1460-9568.2008.06294.x.

Sachidhanandam, S. *et al.* (2013) 'Membrane potential correlates of sensory perception in mouse barrel cortex', *Nature Neuroscience*, 16(11), pp. 1671–1677. doi: 10.1038/nn.3532.

Schmahmann, J. D. (1991) 'An emerging concept. The cerebellar contribution to higher function', *Archives of Neurology*, 48(11), pp. 1178–1187. doi: 10.1001/archneur.1991.00530230086029.

Schmahmann, J. D. (2004) 'Disorders of the Cerebellum: Ataxia, Dysmetria of Thought, and the Cerebellar Cognitive Affective Syndrome', *The Journal of Neuropsychiatry and Clinical Neurosciences*, 16(3), pp. 367–378. doi: 10.1176/jnp.16.3.367.

Schmahmann, J. D. (2016) 'A Brief History of the Cerebellum', in Gruol, D. L. et al. (eds) *Essentials of Cerebellum and Cerebellar Disorders: A Primer For Graduate Students*. Cham: Springer International Publishing, pp. 5–20. doi: 10.1007/978-3-319-24551-5_2.

Schmahmann, J. D. and Sherman, J. C. (no date) 'The cerebellar cognitive affective syndrome', p. 19.

Serapide, M. F. *et al.* (2001) 'Multiple zonal projections of the basilar pontine nuclei to the cerebellar cortex of the rat', *Journal of Comparative Neurology*, 430(4), pp. 471–484. doi: https://doi.org/10.1002/1096-9861(20010219)430:4<471::AID-CNE1044>3.0.CO;2-G.

Sherman, S. M. and Guillery, R. W. (1998) 'On the actions that one nerve cell can have on another: distinguishing "drivers" from "modulators"', *Proceedings of the National Academy of Sciences of the United States of America*, 95(12), pp. 7121–7126. doi: 10.1073/pnas.95.12.7121.

Shidara, M. *et al.* (1993) 'Inverse-dynamics model eye movement control by Purkinje cells in the cerebellum', *Nature*, 365(6441), pp. 50–52. doi: 10.1038/365050a0.

Shlosberg, D., Amitai, Y. and Azouz, R. (2006) 'Time-Dependent, Layer-Specific Modulation of Sensory Responses Mediated by Neocortical Layer 1', *Journal of Neurophysiology*, 96(6), pp. 3170–3182. doi: 10.1152/jn.00520.2006.

Simons, D. J. and Carvell, G. E. (1989) 'Thalamocortical response transformation in the rat vibrissa/barrel system', *Journal of Neurophysiology*, 61(2), pp. 311–330. doi: 10.1152/jn.1989.61.2.311.

Sobolewski, A. *et al.* (2015) 'Alertness opens the effective flow of sensory information through rat thalamic posterior nucleus', *European Journal of Neuroscience*, 41(10), pp. 1321–1331. doi: 10.1111/ejn.12901.

Sreenivasan, V. *et al.* (2016) 'Movement Initiation Signals in Mouse Whisker Motor Cortex', *Neuron*, 92(6), pp. 1368–1382. doi: 10.1016/j.neuron.2016.12.001.

Steriade, M. (1995) 'Two channels in the cerebellothalamocortical system', *The Journal of Comparative Neurology*, 354(1), pp. 57–70. doi: 10.1002/cne.903540106.

Stoodley, C. J. *et al.* (2016) 'Location of lesion determines motor vs. cognitive consequences in patients with cerebellar stroke', *NeuroImage: Clinical*, 12, pp. 765–775. doi: 10.1016/j.nicl.2016.10.013.

Stoodley, C. J. *et al.* (2017) 'Altered cerebellar connectivity in autism spectrum disorders and rescue of autism-related behaviors in mice', *Nature neuroscience*, 20(12), pp. 1744–1751. doi: 10.1038/s41593-017-0004-1.

Strick, P. L., Dum, R. P. and Fiez, J. A. (2009) 'Cerebellum and nonmotor function', *Annual Review of Neuroscience*, 32, pp. 413–434. doi: 10.1146/annurev.neuro.31.060407.125606.

Sugihara, I. and Shinoda, Y. (2004) 'Molecular, topographic, and functional organization of the cerebellar cortex: a study with combined aldolase C and olivocerebellar labeling', *The Journal of Neuroscience: The Official Journal of the Society for Neuroscience*, 24(40), pp. 8771–8785. doi: 10.1523/JNEUROSCI.1961-04.2004.

Sumser, A. *et al.* (2017) 'Organization and somatotopy of corticothalamic projections from L5B in mouse barrel cortex', *Proceedings of the National Academy of Sciences of the United States of America*, 114(33), pp. 8853–8858. doi: 10.1073/pnas.1704302114.

Teune, T. M. *et al.* (2000) 'Topography of cerebellar nuclear projections to the brain stem in the rat', *Progress in Brain Research*, 124, pp. 141–172. doi: 10.1016/S0079-6123(00)24014-4.

Thach, W. T., Goodkin, H. P. and Keating, J. G. (1992) 'The cerebellum and the adaptive coordination of movement', *Annual Review of Neuroscience*, 15, pp. 403–442. doi: 10.1146/annurev.ne.15.030192.002155.

*The Mouse Nervous System* (2012). Elsevier. doi: 10.1016/C2009-0-00185-8.

Timmann, D. and Daum, I. (2007) 'Cerebellar contributions to cognitive functions: A progress report after two decades of research', *The Cerebellum*, 6(3), p. 159. doi: 10.1080/14734220701496448.

Towal, R. B. *et al.* (2011) 'The Morphology of the Rat Vibrissal Array: A Model for Quantifying Spatiotemporal Patterns of Whisker-Object Contact', *PLOS Computational Biology*, 7(4), p. e1001120. doi: 10.1371/journal.pcbi.1001120.

Trageser, J. C. *et al.* (2006) 'State-Dependent Gating of Sensory Inputs by Zona Incerta', *Journal of neurophysiology*, 96(3), pp. 1456–1463. doi: 10.1152/jn.00423.2006.

Trageser, J. C. and Keller, A. (2004) 'Reducing the uncertainty: gating of peripheral inputs by zona incerta', *The Journal of Neuroscience: The Official Journal of the Society for Neuroscience*, 24(40), pp. 8911–8915. doi: 10.1523/JNEUROSCI.3218-04.2004.

Tsai, P. T. *et al.* (2012) 'Autistic-like behaviour and cerebellar dysfunction in Purkinje cell Tsc1 mutant mice', *Nature*, 488(7413), pp. 647–651. doi: 10.1038/nature11310.

Ugolini, G. (1995) 'Specificity of rabies virus as a transneuronal tracer of motor networks: Transfer from hypoglossal motoneurons to connected second-order and higher order central nervous system cell groups', *Journal of Comparative Neurology*, 356(3), pp. 457–480. doi: https://doi.org/10.1002/cne.903560312.

Urbain, N. and Deschênes, M. (2007) 'A New Thalamic Pathway of Vibrissal Information Modulated by the Motor Cortex', *Journal of Neuroscience*, 27(45), pp. 12407–12412. doi: 10.1523/JNEUROSCI.2914-07.2007.

Uusisaari, M., Obata, K. and Knöpfel, T. (2007) ‘Morphological and electrophysiological properties of GABAergic and non-GABAergic cells in the deep cerebellar nuclei’, *Journal of Neurophysiology*, 97(1), pp. 901–911. doi: 10.1152/jn.00974.2006.

Varani, A. P. *et al.* (2020) ‘Dual contributions of cerebellar-thalamic networks to learning and offline consolidation of a complex motor task’, *bioRxiv*, p. 2020.08.27.270330. doi: 10.1101/2020.08.27.270330.

Veinante, P. and Deschênes, M. (1999) ‘Single- and multi-whisker channels in the ascending projections from the principal trigeminal nucleus in the rat’, *The Journal of Neuroscience: The Official Journal of the Society for Neuroscience*, 19(12), pp. 5085–5095.

Veinante, P., Lavall□e, P. and Desch□nes, M. (2000) ‘Corticothalamic projections from layer 5 of the vibrissal barrel cortex in the rat’, *The Journal of Comparative Neurology*, 424(2), pp. 197–204. doi: 10.1002/1096-9861(20000821)424:2<197::AID-CNE1>3.0.CO;2-6.

Viaene, A. N., Petrof, I. and Sherman, S. M. (2011) ‘Synaptic properties of thalamic input to the subgranular layers of primary somatosensory and auditory cortices in the mouse’, *The Journal of Neuroscience: The Official Journal of the Society for Neuroscience*, 31(36), pp. 12738–12747. doi: 10.1523/JNEUROSCI.1565-11.2011.

Vogt, B. A. (1991) ‘The Role of Layer I in Cortical Function’, in Peters, A. and Jones, E. G. (eds) *Normal and Altered States of Function*. Boston, MA: Springer US (Cerebral Cortex), pp. 49–80. doi: 10.1007/978-1-4615-6622-9_2.

Voogd, J. (2011) ‘Cerebellar Zones: A Personal History’, *Cerebellum (London, England)*, 10(3), pp. 334–350. doi: 10.1007/s12311-010-0221-6.

Voogd, J. (2014) ‘What we do not know about cerebellar systems neuroscience’, *Frontiers in Systems Neuroscience*, 8. doi: 10.3389/fnsys.2014.00227.

Voogd, J. and De Zeeuw, C. I. (2020) ‘Cerebellum: What is in a Name? Historical Origins and First Use of This Anatomical Term’, *Cerebellum (London, England)*, 19(4), pp. 550–561. doi: 10.1007/s12311-020-01133-7.

Voogd, J. and Glickstein, M. (1998) ‘The anatomy of the cerebellum’, *Trends in Neurosciences*, 21(9), pp. 370–375. doi: 10.1016/s0166-2236(98)01318-6.

Voogd, J. and Ruigrok, T. (2012) ‘Cerebellum and Precerebellar Nuclei’, in *The Human Nervous System*, pp. 471–545. doi: 10.1016/B978-0-12-374236-0.10015-X.

Wang, S. S.-H., Kloth, A. D. and Badura, A. (2014) ‘The Cerebellum, Sensitive Periods, and Autism’, *Neuron*, 83(3), pp. 518–532. doi: 10.1016/j.neuron.2014.07.016.

Williams, L. E. and Holtmaat, A. (2019) ‘Higher-Order Thalamocortical Inputs Gate Synaptic Long-Term Potentiation via Disinhibition’, *Neuron*, 101(1), pp. 91-102.e4. doi: 10.1016/j.neuron.2018.10.049.

Wineski, L. E. (1985) ‘Facial morphology and vibrissal movement in the golden hamster’, *Journal of Morphology*, 183(2), pp. 199–217. doi: https://doi.org/10.1002/jmor.1051830208.

Wolpert, D. M., Miall, R. C. and Kawato, M. (1998) ‘Internal models in the cerebellum’, *Trends in Cognitive Sciences*, 2(9), pp. 338–347. doi: 10.1016/s1364-6613(98)01221-2.

Woolsey, T. A., Dierker, M. L. and Wann, D. F. (1975) ‘Mouse SmI cortex: qualitative and quantitative classification of golgi-impregnated barrel neurons’, *Proceedings of the National Academy of Sciences of the United States of America*, 72(6), pp. 2165–2169. doi: 10.1073/pnas.72.6.2165.

Xu, N. *et al.* (2012) ‘Nonlinear dendritic integration of sensory and motor input during an active sensing task’, *Nature*, 492(7428), pp. 247–251. doi: 10.1038/nature11601.

Yamashita, T. *et al.* (2013) ‘Membrane potential dynamics of neocortical projection neurons driving target-specific signals’, *Neuron*, 80(6), pp. 1477–1490. doi: 10.1016/j.neuron.2013.10.059.

Yatim, N. *et al.* (1996) ‘Trigeminocerebellar and trigemino-olivary projections in rats’, *Neuroscience Research*, 25(3), pp. 267–283. doi: 10.1016/0168-0102(96)01061-9.

# ANNEXE 1

nature COMMUNICATIONS

ARTICLE

https://doi.org/10.1038/s41467-020-18953-0 OPEN

# Bidirectional control of fear memories by cerebellar neurons projecting to the ventrolateral periaqueductal grey

Jimena Laura Frontera[1], Hind Baba Aissa[1], Romain William Sala[1], Caroline Mailhes-Hamon[1], Ioana Antoaneta Georgescu[1], Clément Léna[1] & Daniela Popa[1✉]

Fear conditioning is a form of associative learning that is known to involve different brain areas, notably the amygdala, the prefrontal cortex and the periaqueductal grey (PAG). Here, we describe the functional role of pathways that link the cerebellum with the fear network. We found that the cerebellar fastigial nucleus (FN) sends glutamatergic projections to vlPAG that synapse onto glutamatergic and GABAergic vlPAG neurons. Chemogenetic and optogenetic manipulations revealed that the FN-vlPAG pathway controls bi-directionally the strength of the fear memories, indicating an important role in the association of the conditioned and unconditioned stimuli, a function consistent with vlPAG encoding of fear prediction error. Moreover, FN-vlPAG projections also modulate extinction learning. We also found a FN-parafascicular thalamus pathway, which may relay cerebellar influence to the amygdala and modulates anxiety behaviors. Overall, our results reveal multiple contributions of the cerebellum to the emotional system.

[1] Neurophysiology of Brain Circuits Team, Institut de Biologie de l'Ecole normale supérieure (IBENS), Ecole normale supérieure, CNRS, INSERM, PSL Research University, 75005 Paris, France. ✉email: daniela.popa@bio.ens.psl.eu

Fear conditioning is a form of associative learning in which an animal learns to associate the presence of a neutral stimulus (conditioned stimulus, CS), with the presence of an aversive fear eliciting stimulus (unconditioned stimulus, US). The amygdala complex, comprised of the basolateral complex (BLA), the central nucleus (CEA), and the intercalated cell masses, is one of the key brain regions for the fear memory acquisition and storage[1–4]. Fear conditioning induces changes not only into the amygdala, but also in auditory and multimodal nuclei of the thalamus, auditory cortex, medial prefrontal cortex (mPFC), and hippocampus[2,5–8]. In addition, fear extinction involves the formation of a new memory trace that attenuates fear responses to a conditioned aversive memory. The distributed network that controls fear extinction involves many of the brain areas that are important for fear conditioning[2,7,9].

The midbrain periaqueductal gray (PAG) is known to mediate both learned and innate freezing behavior via excitatory projections to the magnocellular medulla from the ventrolateral PAG (vlPAG)[10]. In learned freezing, the recruitment of these neurons is produced by a disinhibition triggered by GABAergic inputs from the amygdala in cued fear[10], and glutamatergic inputs from the mPFC in contextual fear[6]. Some vlPAG projection neurons also participates to pain processing[11–13]. However, vlPAG is not a simple regulator of sensory and motor functions, it is also involved in fear learning by generating a "fear prediction error" assessing how unexpected is an incoming US[14]; this step is essential in implementing the Rescorla–Wagner rule which states that learning is driven by departure from expectation[15].

Despite the well-described role of the cerebellum in motor coordination and sensorimotor integration, it is now well established that the cerebellum is also involved in a number of non-motor functions, e.g., refs. [16–19]. Notably, the cerebellum is strongly recruited in aversive emotional states: in humans, neuroimaging studies have revealed changes in cerebellar activation, also mainly in the vermis, in relation to negative emotions (e.g., during recall of self-generated emotional episodes[20]). Consistent with this, localized cerebellar lesions, principally in the midline vermis, account in large part for the emotional disturbances, inappropriate behavior and changes in affect, which are collectively termed the "cerebellar cognitive affective syndrome"[21] and reported in cerebellar patients. Several studies have shown that the cerebellum has functional connections with fear-related areas, including the PAG, the amygdala, and the PFC[22–26]. In accordance with the existence of such connections, Pavlovian fear conditioning affects cerebellar plasticity[27], post-conditioning cerebellar inactivation affects memory consolidation[28], and cerebellar lesions—or inactivation—modulate freezing[24,29].

The cerebellar vermis, which is most consistently associated with emotional pathologies and fear expression[20,24,30], but see ref. [31], projects to the fastigial nucleus (FN), one of the deep cerebellar nuclei that projects to many targets from the spinal cord to the diencephalon[22,32]. The purpose of the present work is to study the contribution of specific FN output pathways to fear learning. Using neuroanatomical tracings, chemogenetic modulation of the cerebellar input to the vlPAG during fear conditioning and extinction, optogenetics and extracellular electrophysiological recordings in awake freely moving animals, we demonstrate the contribution of the cerebellum to fear learning through its inputs to the vlPAG.

## Results

**Neuroanatomical link between the cerebellum and vlPAG.** In order to examine cerebellar projections to areas involved in the fear circuitry, we used anterograde viral tracing and we have identified fear-related target areas of the projections from the FN. We stereotaxically infused AAV-mCherry in the FN and we found projections exhibiting varicosities into the vlPAG (Fig. 1a–f), which receives inputs from the CEA driving the freezing behavior[10]. Retrograde tracing from vlPAG also indicated the existence of monosynaptic projections from the FN, as well as from the CEA, from the PL and IL areas of the mPFC (Supplementary Fig. 1a–e). Quantification of retrograde labeling from the vlPAG showed that at least 11.2 ± 0.8% of neurons in the FN projects to vlPAG ($n = 4$; Fig. 1g–i), suggesting that this pathway plays an important contribution to cerebellar control of the emotional system[22]. Moreover, combining a *vglut2-cre* mice line with the infusion of AAV-DIO-tdTom in FN, and retrograde AAV-GFP in vlPAG allowed us to determine that the FN–vlPAG-projecting neurons correspond to vesicular glutamate transporter 2 expressing (vGluT2+) neurons (85.4 ± 4.0% of GFP-expressing cells co-localized with vGluT2+ neurons, $n = 4$; Fig. 1j–l). On the other hand, the retrograde tracing in *glyt2-gfp* mice failed to reveal the FN–vlPAG glycinergic-projecting neurons (none of retrograde stained cell co-localized with GlyT2+ neurons in the FN, $n = 3$; Supplementary Fig. 1f, g). Moreover, FN GABAergic neurons are known to only project to the inferior olive[33]. Overall, these results indicate that the vlPAG receives glutamatergic monosynaptic inputs from the FN of the cerebellum.

**FN input onto glutamatergic and GABAergic vlPAG neurons.** To determine whether the inputs from the FN synapse either onto excitatory or inhibitory neurons in the vlPAG, we analyzed the axonal projections and synaptic boutons of FN vGluT2+ neurons. We localized glutamatergic FN terminals by cre-dependent viral expression of the presynaptic marker synaptophysin-GFP in adult *vglut2-cre* mice (Fig. 2a, e). In addition, we identified glutamatergic neurons in the vlPAG by infusion of AAV-DIO-tdTomato, or the GABAergic neurons by immunostaining of GAD67. Glutamatergic FN terminals were found to contact both vGlut2+ and GAD67+ neurons in vlPAG (Fig. 2a–d, e–h, respectively). In fields of vlPAG with dense cerebellar inputs, we found synaptophysin+ boutons on 70.1 ± 3.0% of GAD67+ cells ($n = 9$ slices from three mice, counted on fields of 8.1e4 $\mu m^2$) and on 90.1 ± 1.1% of vGluT2+ cells ($n = 10$ slices from three mice, Fig. 2i, same field size), from a similar GAD67+ and vGluT2+ cell density area in vlPAG (419 ± 54 GAD67+Syn+ cells $mm^{-2}$, from 613 ± 86 GAD67+ cells $mm^{-2}$; and 604 ± 57 vGluT2+ Syn+ cells $mm^{-2}$, from 675 ± 64 vGluT2+ cells $mm^{-2}$; Fig. 2j). Therefore, these results indicate that FN glutamatergic projections target high proportion of both glutamatergic and GABAergic vlPAG neurons in regions of the vlPAG.

**Fastigial stimulation induces short-latency response in vlPAG.** To study the impact of optogenetic FN stimulation in the vlPAG, we expressed channel-rhodopsin-2 (ChR2) specifically in FN–vlPAG-projecting neurons by local injection of cre-dependent AAV-DIO-ChR2-GFP in the FN, combined with local injection of retrograde AAV-cre-EBFP into the vlPAG (Supplementary Fig. 2a, b). Then, we stimulated FN–vlPAG neurons via FN illumination and we recorded vlPAG activity in awake freely moving animals (Fig. 3a–f). Under FN stimulation, we found LFP negative deflection (Fig. 3a) and cells exhibiting an increase of firing in vlPAG contra-lateral to the FN stimulation (Fig. 3b, c), where the FN is preferentially sending projections. The ramp of stimulation produced a range of vlPAG responses, which increased as a function of light intensity (Fig. 3d). Responses at low intensities were found in the vlPAG contra-lateral to the stimulated FN, while increasing intensities recruited cells on the ipsi-lateral vlPAG (Fig. 3e). The latencies

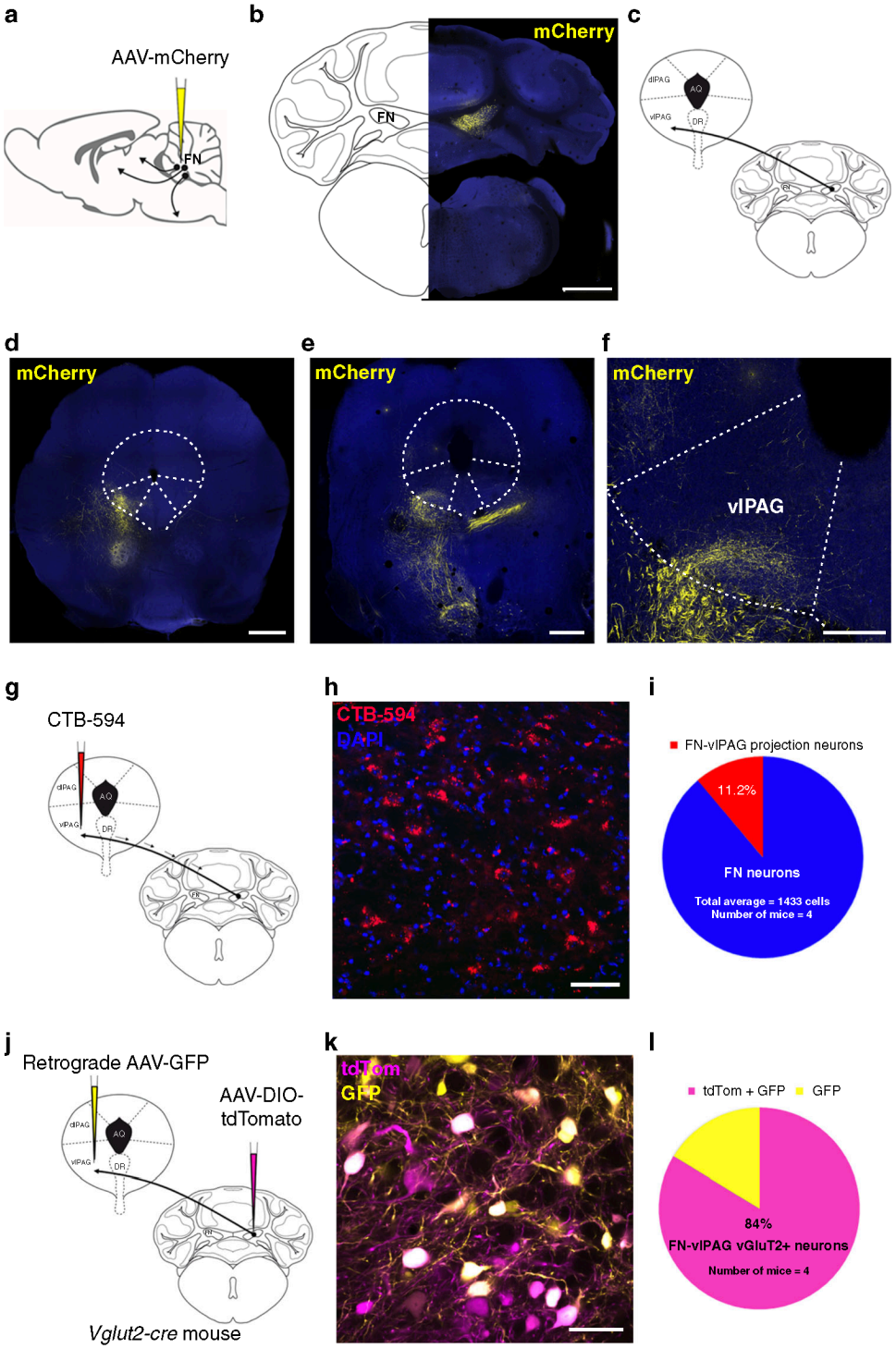


**Fig. 1 Cerebellum sends excitatory monosynaptic projections to vlPAG. a** Anterograde tracing strategy by AAV-mCherry injection in the FN. **b** Expression of anterograde AAV-mCherry in the FN of the cerebellum (scale bar, 1 mm). **c** Schematic representation of anterograde tracing of AAV-mCherry from the FN into vlPAG. **d**, **e** Anterograde expression of mCherry in FN neuronal projections exhibiting varicosities in the vlPAG (scale bar, 500 μm), anterior (**d**) and medial (**e**) PAG sections. **f** Zoom-in from **d** (scale bar, 250 μm). **g** Retrograde labeling approach by injecting CTB-594 in the vlPAG. **h** Retrograde labeling of FN-vlPAG-projecting neurons with CTB-594, co-staining with DAPI (scale bar, 50 μm). **i** Quantification of retrograde labeled FN neurons projecting to the vlPAG ($n = 4$ mice, total average = 1433 cells). **j** Viral injection of retrograde AAV-GFP and anterograde AAV-DIO-tdTom into *vglut2-cre* mice strategy. **k** Co-expression of anterograde AAV-DIO-tdTom and retrograde AAV-GFP in vGluT2+ FN neurons projecting to vlPAG (scale bar, 50 μm). **l** Quantification of co-localizing retrograde AAV-GFP and AAV-DIO-tdTomato vGluT2+ neurons in the FN ($n = 4$ mice). Source data are provided as Source data file.

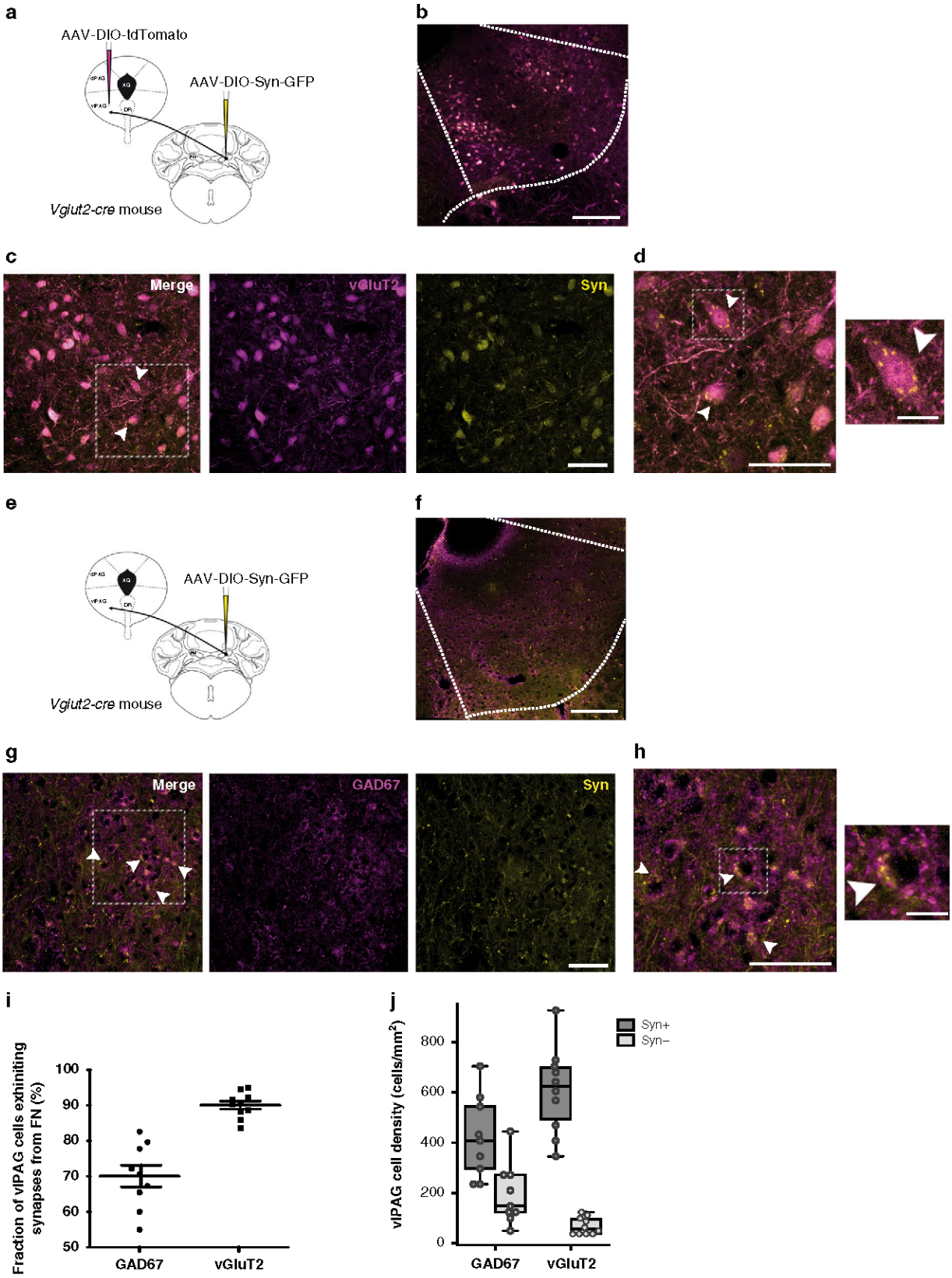


of response at the highest intensity range from 7 to 50 ms (Fig. 3f), suggesting the existence of direct and indirect excitation of the recorded vlPAG cells by FN input[26]. These results demonstrate the existence of a functional connectivity between the FN and the vlPAG.

**Cerebellar output to vlPAG controls fear memory formation.** To determine whether the FN–vlPAG plays a role in Pavlovian fear conditioning, we examined the effect of activating or inhibiting transiently these projections. First, we expressed excitatory or inhibitory DREADD receptors activated by CNO in FN

**Fig. 2 Glutamatergic FN input onto excitatory and inhibitory neurons in the vlPAG. a** Injection of cre-dependent AAV-DIO-Syn-GFP and AAV-DIO-tdTomato in vglut2-cre mice line strategy. **b** Expression of tdTomato in vGluT2+ neurons and Syn-GFP in FN terminals in the vlPAG (scale bar, 250 µm). **c** FN glutamatergic synapses contacting vGlut2+ neurons in vlPAG identified by expression of Syn-GFP (arrowheads, scale bar, 50 µm). Some of the somatic labeling likely reflects the high somatic tdTomato expression and cross talk detection with the GFP; intense synaptophysin labeling is best visualized in high-magnification panel. **d** High magnification from **c** (left panel, scale bar, 50 µm) and zoom-in of box area (right panel, scale bar, 12.5 µm). **e** Injection of cre-dependent AAV-DIO-Syn-GFP in vglut2-cre mice line strategy. **f** Immunostaining of GAD67 and Syn-GFP expression in FN terminals in the vlPAG (scale bar, 250 µm). **g** FN glutamatergic projections synapsing on vlPAG GABAergic neurons identified by co-staining of Syn-GFP and GAD67 in vlPAG (arrowheads, scale bar, 50 µm). **h** High-magnification from **g** (left panel, scale bar, 50 µm) and zoom-in of box area (right panel, scale bar, 12.5 µm). **i** quantification of GAD67 ($n = 9$ PAG slices) and vGluT2 ($n = 10$ PAG slices) cell fraction (%) exhibiting synaptophysin boutons on their cell bodies in the vlPAG. Data are presented as mean values ± SEM. **j** quantification of GAD67 ($n = 9$ PAG slices) and vGluT2 ($n = 10$ PAG slices) cell density (cells/mm$^2$) in the vlPAG showing synaptophysin boutons (Syn+) or not (Syn−). Data are presented as boxplots with dots representing data points, center line corresponds to the median of the distribution, the lower and the upper bounds of the box correspond to the 25th and 75th percentiles, respectively, and the whiskers correspond to 1.5 of the IQR (inter quartile ratio). Source data are provided as Source data file.

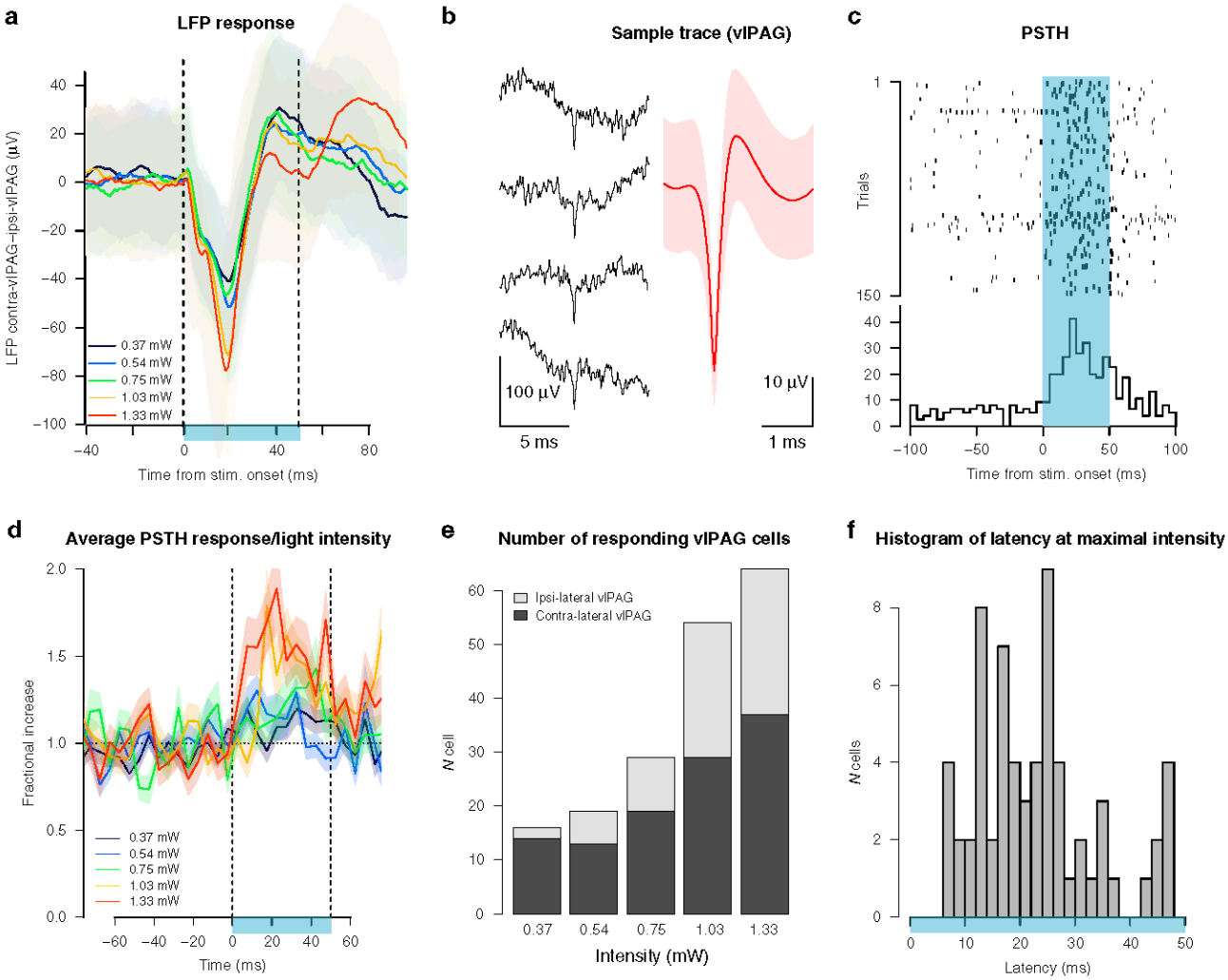


**Fig. 3 Optogenetic FN stimulation induces short-latency responses in vlPAG. a** LFP response in vlPAG to FN stimulation for five different light intensity showed with different colors. Error bands represent SEM. **b** Excerpt of unfiltered traces and spikes from a vlPAG unit; right: average filtered waveform for the neuron sorted on the channel; red line represent the mean value and shaded area represent the SD of the trace. **c** Raster plot for a cell recorded in vlPAG around the 50 ms period of FN stimulation. Blue area indicates periods with cerebellar optogenetic stimulation. **d** Light-dependent effect for the cells in the vlPAG that increased their firing during 50 ms light stimuli at each intensity bin = 5 ms ($n = 61$ out of 222 neurons from four mice with significant response at the highest intensity; significance is established with 2 ms bin, threshold used to identify significance in PSTHs is: 4.1 × SD). Error bands represent SEM. **e** Number of responding vlPAG cells (ipsi and contra-lateral) to FN stimulation ($n = 222$ neurons from four mice). **f** Latencies of responses in cells in vlPAG at highest intensity during the 50 ms of FN stimulation. Source data are provided as Source data file.

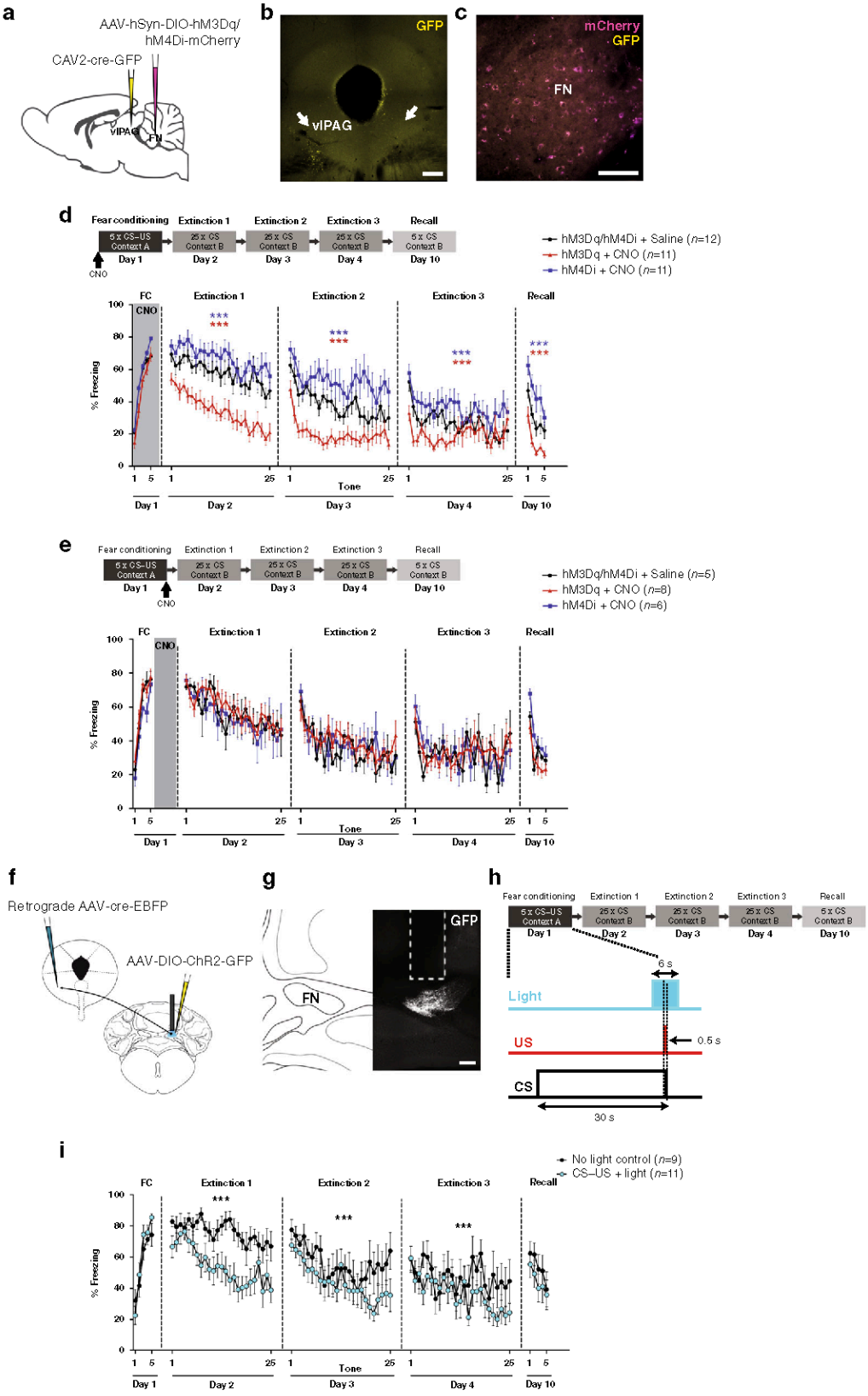


neurons that target the vlPAG, by infusing cre-dependent anterograde AAV-hM3Dq or -hM4Di in FN in combination with the infusion of retrograde CAV2-cre in the vlPAG (Fig. 4a–c). We performed a classical Pavlovian fear conditioning protocol, which consisted in five CS–US presentations, followed by three extinctions sessions of 25 CS, and a final recall test of five CS presentations 1 week after to evaluate long-term maintenance of fear and extinction memories (Fig. 4d). Mice injected with saline and expressing the excitatory or the inhibitory DREADDs had similar freezing levels (Supplementary Fig. 3a), thus they were

**Fig. 4 FN–vlPAG projections control CS–US association and fear memory formation. a** Chemogenetic modulation of FN–vlPAG pathway, bilateral cre-dependent expression of excitatory or inhibitory DREADDs (hM3Dq or hM4Di, respectively) in the FN by retrograde CAV2-cre-GFP injection in the vlPAG. **b** Injection site of CAV2-cre-GFP in the vlPAG (arrows, scale bar, 200 µm). **c** Cre-dependent expression of DREADDs in the FN (scale bar, 100 µm). **d** Classical fear conditioning and extinction protocol (upper panel). FN–vlPAG pathway stimulation (hM3Dq + CNO, $n = 11$) or inhibition (hM4Di + CNO, $n = 11$) during fear conditioning (FC) exhibited similar freezing levels than the control group (hM3Dq/hM4Di + saline, $n = 12$; respectively, FC: $F(1,54) = 0.0767$, $P = 0.285$; FC: $F(1,130) = 1.15$, $P = 0.285$, two-way ANOVA). Stimulation of FN–vlPAG pathway during FC provoked a decrease in freezing levels during the extinction sessions (extinction 1: $F(1,546) = 251.5$, extinction 2: $F(1,546) = 159.3$, extinction 3: $F(1,546) = 25.9$, $P < 0.0001$, two-way ANOVA), while inhibition induced an increase of freezing levels along the extinctions (extinction 1: $F(1,546) = 27.5$; extinction 2: $F(1,520) = 46.5$, extinction 3: $F(1,546) = 25.3$, $P < 0.0001$, two-way ANOVA), compared to the control group. During the recall, stimulated mice expressed less fear than the control group (recall: $F(1,120) = 0.36$, $P < 0.0001$, two-way ANOVA), while inhibited mice expressed higher levels of freezing (recall: $F(1,102) = 16.1$, $P < 0.0001$, two-way ANOVA). **e** Stimulation (hM3Dq + CNO, $n = 8$) and inhibition (hM4Di + CNO, $n = 6$) of FN–vlPAG pathway during consolidation phase post-FC had not effect on freezing behavior (hM3Dq/hM4Di + saline, $n = 5$; stimulation: extinction 1: $F(1,275) = 0.57$, $P = 0.347$, extinction 2: $F(1,250) = 3.50$, $P = 0.624$, extinction 3: $F(1,250) = 0.37$, $P = 0.543$; inhibition: extinction 1: $F(1,200) = 0.98$, $P = 0.324$, extinction 2: $F(1,200) = 1.38$, $P = 0.241$, extinction 3: $F(1,200) = 0.09$, $P = 0.770$; two-way ANOVA). **f** Optogenetic stimulation of FN–vlPAG inputs by cre-dependent expression of ChR2-GFP in FN and retrograde cre in vlPAG. **g** ChR2 expression in FN–vlPAG-projecting neurons (scale bar, 200 µm). **h** Optogenetic stimulation protocol of FN–vlPAG pathway during CS–US presentation in fear conditioning. Light pulses were delivered every CS–US presentation. **i** Mice under light stimulation during CS–US pairing (CS–US + light, $n = 11$) exhibited an enhanced extinction of fear response compared to the control mice (no light control, $n = 9$; extinction 1: $F(1,450) = 104.1$, extinction 2: $F(1,422) = 18.8$, extinction 3: $F(1,455) = 13.4$, $P < 0.0001$, two-way ANOVA). Lines represent means ± SEM. ***$P < 0.001$. Source data are provided as Source data file.

grouped together in the control (injected with saline) group. In addition, we checked that CNO had no effect per se on the freezing behavior by performing the fear and extinction protocols on control sham mice. Mice exposed to CNO indeed exhibited the same freezing levels than the control mice, which received saline (Supplementary Fig. 3b). Moreover, chemogenetic activation or inhibition of FN–vlPAG pathway had not effect on the immobility state of the mice in an open field compared to the saline group (Supplementary Fig. 3c), neither on the freezing levels in the context A before fear conditioning (Supplementary Fig. 3d) or in the context B before extinction training (Supplementary Fig. 3e). These results indicate that FN–vlPAG pathway does not affect the immobility or freezing behavior.

We then analyzed the impact of the modulation of the FN–vlPAG pathway on fear conditioning. For this purpose, we activated or inhibited DREADD-expressing FN–vlPAG-projecting neurons with CNO during the acquisition phase. Under these conditions, mice exhibited similar fear response than the control group. Strikingly, during the first extinction training the following day, mice in which the FN–vlPAG pathway had been activated during fear conditioning, exhibited a drastic drop in freezing behavior along the CS presentations, reaching basal freezing levels already at the end of the first extinction session (Fig. 4d). During the second extinction training, this group of mice succeeded to retrieve the fear memory at the first CS presentation, but they reached basal levels of freezing at the third CS presentation, indicating a faster extinction than in the control mice. In contrast, mice in which the FN–vlPAG pathway had been inhibited presented a stronger freezing behavior throughout the first extinction training, as well as for the second and third extinction sessions, compared to the control mice (Fig. 4d). Moreover, when we evaluated the long-term maintenance of the fear and extinction memories by a recall session of five CS presentations 1 week after, mice that underwent FN–vlPAG activation during fear conditioning exhibited a lower recall of fear memory than the control mice, while mice that underwent FN–vlPAG inhibition exhibited an increased fear memory compared to the control mice. These results indicate that FN–vlPAG projections contribute to the formation of conditioned fear memories, in which the activation of this pathway during the fear conditioning decreases the strength of the fear memory formation, while the inhibition of this pathway increases it. Consequently, the extinction of fear response during the extinction session is faster or slower, respectively.

In addition, we found an increase of c-Fos+ vlPAG neurons following fear conditioning when FN–vlPAG pathway was chemogenetically activated, compared to the control (Supplementary Fig. 4a, b), confirming that FN–vlPAG glutamatergic projections induce an increase in neuronal recruitment when it is stimulated during fear conditioning.

Since the systemic CNO administration exerts an effect on neuronal activity for hours[34–36], we wondered whether the bidirectional control of FN–vlPAG pathway on fear memory occurs specifically during the acquisition or during the consolidation phase that immediately followed[37,38]. To answer this question, we compared the effect of activating and inhibiting the FN–vlPAG pathway starting from the acquisition phase or from the consolidation phase. Then, we evaluated the fear response during the following recall and extinction sessions. We surprisingly found that activating and inhibiting the FN–vlPAG pathway only during the consolidation phase of fear memory had no effect on the strength of the fear memory (Fig. 4e). Mice with FN–vlPAG activation or inhibition exhibited similar levels of fear response than the control group, during the recall and along the extinctions sessions. Taken together, these results indicate that the bidirectional control of the FN–vlPAG pathway of the fear memory occurs during the acquisition phase of the fear memory, in which the association of the CS–US is taking place.

**FN–vlPAG pathway activation at CS–US reduces fear learning.** Furthermore, to evaluate whether the state of the FN–vlPAG projections regulates the fear learning at the time of the CS–US association[39,40], we optogenetically stimulated the FN during the CS–US presentation (from the last 3 s of the CS until 3 s post CS–US, Fig. 4f–h). We found that light stimulation during CS–US association is sufficient to induce a significant enhanced extinction of the fear response, during the extinction sessions compared to the control group (Fig. 4i). Moreover, the light stimulation had not effect on the immobility state in an open field (Supplementary Fig. 5b) or on the freezing behavior, during the fear acquisition phase (Fig. 4i). Therefore, these results indicate that the cerebellum exerts a control over the fear memory formation through the FN–vlPAG pathway during the association between the CS and US, without affecting the fear behavior during conditioning.

Interestingly, mice optogenetically stimulated randomly within the intertrial interval (ITI) exhibited a reduced freezing during fear conditioning, suggesting a weaker fear during learning (Supplementary Fig. 5c, d), followed by a lower fear response

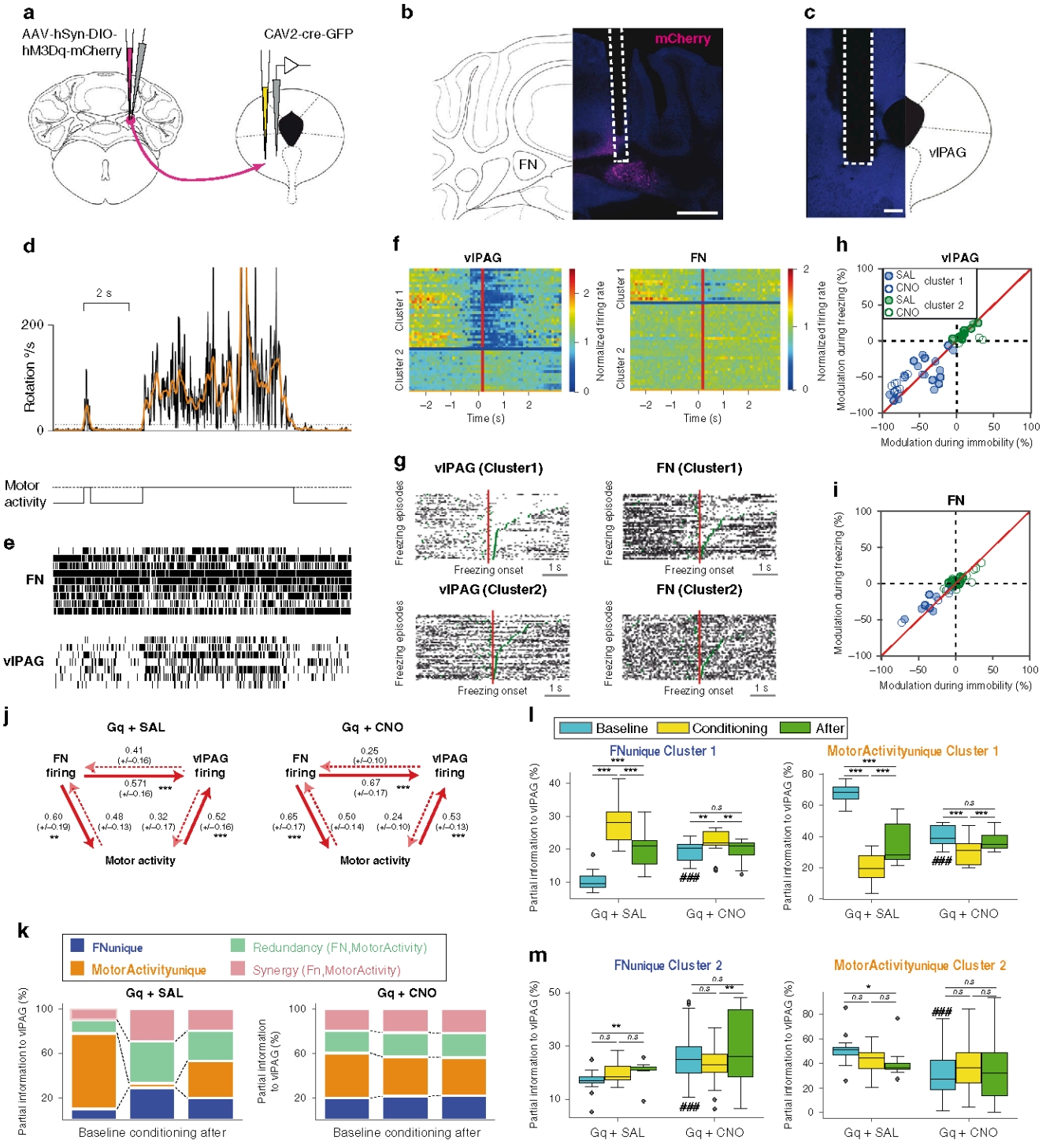


during retrieval of fear memory, and along the first and second extinction sessions, compared to the mice that were not stimulated. Thus, this suggests that FN–vlPAG projections could also contribute to US-induced fear extrinsically from the CS–US association coding.

**Cellular FN–vlPAG interaction during fear learning**. Therefore, to assess the neuronal correlates of fear learning in FN and vlPAG, we recorded extracellular activity during the conditioning. In order to relate the firing activity in the FN and vlPAG to the mouse immobility, we combined the cellular recordings with measurements of the mouse movements, using an inertial sensor attached to the head of mice expressing an excitatory DREADD in the FN–PAG neurons receiving saline (Gq + SAL group) or CNO (Gq + CNO group; Fig. 5a–e).

To examine the link between cellular activity and freezing/immobility, we examined the modulation of firing around the onset of immobility in vlPAG and FN neurons (Fig. 5f). Two classes of association with immobility were observed in the vlPAG and in the FN: a set of cells ("cluster 1") exhibited a strong reduction of firing at the onset of immobility (Gq + SAL group, PAG: 17 cells, FN: 7 cells from 4 mice; Gq + CNO group, PAG: 13, FN: 5 cells from 3 mice), while a second set ("cluster 2")

**Fig. 5 Firing of FN and vlPAG neurons exhibit strong modulations as a function of motor activity and increased directional FN to vlPAG interactions during conditioning. a** Schematic of the experiment. **b** Histology of electrode position in the vlPAG (scale bar, 200 µm). **c** hM3Dq expression in FN–vlPAG-projecting neurons and electrode position (scale bar, 500 µm). **d** Top: instantaneous head rotation (black line) and smoothed rotations (orange line). Dashed line: threshold of immobility (12 deg $s^{-1}$). Bottom: binarized motor activity. **e** Raster of units recorded simultaneously in the FN and vlPAG, same time period as **c**. **f–j** Modulation of cell firing in the vlPAG and FN in relation with immobility **f**, PSTH of the vlPAG (left) and FN (right) neurons around the onset of immobility events; each line correspond to a different cell. Cells are grouped in cluster 1 and cluster 2 determined by using a *K*-means algorithm on the PSTHs. **g** Example rasters of clusters 1 and 2 cells in vlPAG and FN. Each plot corresponds to a single cell and each line to a different immobility episode. The rasters are aligned around the onset of immobility episodes and ordered by decreasing duration of the immobility episodes. The end of the immobility episode (and its preceding episode) is indicated in green. **h** Comparison of the change of vlPAG firing between mobility and immobility during baseline and conditioning (when immobility largely reflects freezing). The red line indicates an identical modulation in immobility and in freezing. **i** Same as **h** for FN neurons. **j** Pairwise information transfer between the vlPAG, FN firing, and binarized motor activity ("motor activity"); bin: 10 ms, lag: 1 bin. The information transfer is averaged over all FN–vlPAG pairs, and all FN and vlPAG unit and motor activity. Left: unit pairs Gq + SAL group. Right: units from the Gq + CNO group. Values correspond to mean ± SEM of the entropy transfer (in bits), $^{**}P < 0.01$, $^{***}P < 0.001$, Mann–Whitney. **k–m** Partial information decomposition using FN firing and motor activity as sources, and vlPAG firing as target (bin: 10 ms, lag: 1 bin). **k** Example of evolution of the proportion of information transfer components from motor activity, and one FN neuron to a vlPAG neuron during the 5 min before (baseline), during (conditioning), and after (after) conditioning. The information transfer is computed at a 10 ms latency. **l** Evolution of the proportion of unique contribution from cluster one FN (left) and motor activity (right) to vlPAG firing. Tukey's post hoc comparisons: $^{*}P < 0.05$, $^{**}P < 0.01$, $^{***}P < 0.001$. Comparison between Gq + SAL and Gq + CNO, Mann–Whitney: $\#\#\#P < 0.001$, $\#\#P < 0.01$. **m** Same as **l** for cluster 2. **l**, **m** Boxplots the center line corresponds to the median of the distribution, the lower and the upper bounds of the box correspond to the 25th and 75th percentiles, respectively, and the whiskers correspond to 1.5 of the IQR (inter quartile ratio), the dots correspond to outliers. **j**, **l**, **m** statistics are detailed in Supplementary Table 1. Source data are provided as Source data file.

only exhibited mild modulations (Gq + SAL group: PAG: 8, FN: 11 cells from 4 mice; Gq + CNO group: PAG: 8, FN: 20 cells from 3 mice). We then examined the modulation of the cells in response to the CS and US (Supplementary Fig. 6). A number of cells exhibited responses after the onset of to the CS and after the US; however, these cells were observed in the cluster 1 group, and are thus strongly modulated by motor state, which switches to active both at the CS and US onsets. Although the change in firing at CS/US onset may correspond to fear prediction errors[41,42], we cannot exclude that the change motor state is responsible for the changes of firing at CS and US onset. The reduction of firing was usually observed throughout the period of immobility (Fig. 5g). To test whether the reduction of firing was correlated to immobility or to freezing, we compared the firing modulation between immobility and active state during the 5 min preceding conditioning and during conditioning, when immobility reflects freezing. We found a strong correspondence between the modulation observed in relation to immobility before and after conditioning, no cell exhibiting a clear modulation unique to freezing neither in the vlPAG nor in the FN (Fig. 5h, i); thus, although this result does not rule out the presence of freezing-related modulations of firing in the FN and vlPAG, the modulations observed seem primarily to reflect a motor activity.

To look at the interdependencies between FN and vlPAG firing, and take into account immobility, we turned to information theory approaches[43], which provide unbiased estimates of the relationship, whether linear or nonlinear, between time series. We first used the transfer of entropy, a specific case of conditional mutual information, to examine pairwise, temporally ordered, transmission of information between FN and PAG firing (Fig. 5j). Consistent with the observation of direct connections from the FN to the vlPAG reported above, we observed stronger transfer of entropy from the FN to vlPAG than the reverse. However, as suggested by the modulations reported in the Fig. 5f–i, there was also transfer of entropy between the motor activity and the FN and vlPAG firing, with a stronger transfer from the FN toward the motor state and motor state toward the vlPAG firing than the reverse (Fig. 5j). Therefore, the vlPAG units recorded in our study seem more strongly influenced by the FN and the motor activity than the reverse.

To disentangle the contributions of FN and motor state on the vlPAG firing, we used a partial information decomposition (PID) which breaks down the interdependency between two sources and one target into four components: the unique contribution of each source, and two terms of interactions ("redundancy" and "synergy", respectively, corresponding to the transfer on the target of the linear and nonlinear interactions of the sources). We then determined these components during 5 min before ("baseline"), during ("conditioning"), and 5 min after ("after") conditioning using the (binarized) mobility signal ("motor activity"), and the firing from single FN neurons as sources and the firing of single PAG neurons as targets. The amplitude of information transfer is dependent on the variability of the signals, and thus can hardly be compared between conditions; however, the proportion of the components of information transfer can be compared across conditions (Fig. 5k).

In the baseline condition, the unique contribution of the FN to vlPAG firing is only a small fraction of the total contribution of FN and motor activity, but is significantly lower in the control group than in the Gq + CNO group (Fig. 5l, m); this indicates that the excitation of the FN by the CNO increases its relative contribution to PAG firing.

For cluster 1 units, the proportion of unique contribution of FN neurons to vlPAG firing increases relative to baseline during conditioning in the Gq + SAL group (Fig. 5l, m), while the proportion of information transfer carried by the motor state alone ($MotorActivity_{unique}$) exhibited the reciprocal evolution; cluster 1 units from the Gq + CNO group exhibited similar, but smaller modulation (significant ANOVA interaction stage × treatment; Supplementary Table 1). Cluster 2 units exhibited less significant modulations between the conditions in the Gq + SAL group, suggesting a weaker contribution of these units. This indicates that a transmission of information from the FN to the vlPAG increases during conditioning when learning is taking place, but exhibit weaker evolutions when the FN is excited by the DREADD.

**Fastigial inputs to the vlPAG modulate extinction learning**. We also examined whether the cerebellum plays a role in fear extinction. For this purpose, mice expressing hM3Dq or hM4Di in the vlPAG-projecting FN neurons were exposed to CNO, during the first and second extinction sessions (Fig. 6a, b). Fear-conditioned mice were subjected to the first recall and extinction training the following day under CNO effect. During the first CS presentations, the different groups of mice exhibited the same levels of freezing, suggesting that FN–vlPAG neurons do not

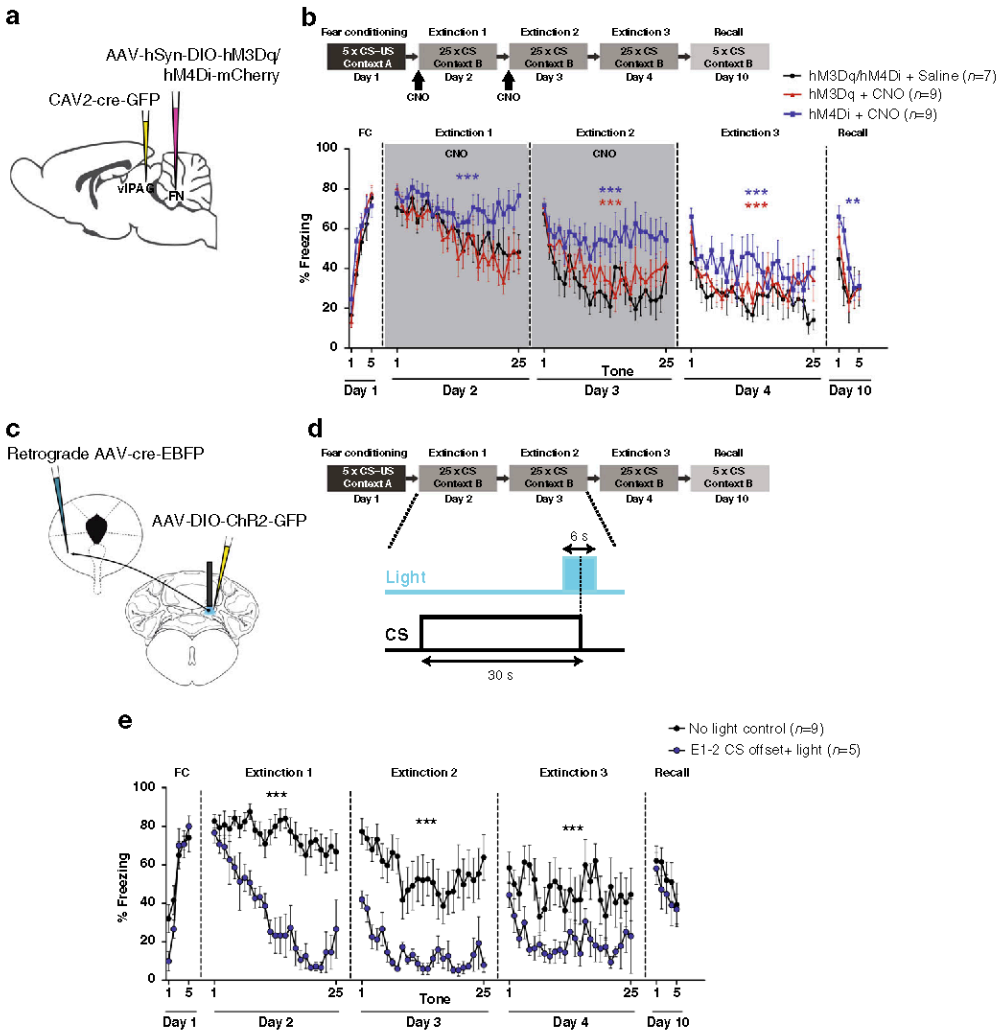


**Fig. 6 Involvement of FN–vlPAG pathway in fear extinction learning. a** Chemogenetic strategy to stimulate or inhibit the activity of FN–vlPAG-projecting neurons by bilateral cre-dependent expression of excitatory or inhibitory DREADDs (hM3Dq or hM4Di, respectively) in the FN in combination, with retrograde CAV2-cre-GFP injection in the vlPAG. **b** Stimulation and inhibition of FN–vlPAG pathway during first and second extinction sessions. Inhibition of FN–vlPAG pathway induced higher levels of freezing behavior during the extinction sessions under effect of CNO, and along the third extinction session and recall test without CNO, compared to the control group (hM3Dq/hM4Di + saline, $n = 7$; hM4Di + CNO, $n = 9$; extinction 1: $F(1,364) = 37.9$, extinction 2: $F(1,364) = 96.9$, extinction 3: $F(1,364) = 44.2$, $P < 0.0001$; recall: $F(1,78) = 10.5$, $P = 0.0017$, two-way ANOVA). Stimulation of this pathway during the extinctions also induced an increase of freezing behavior during the second and third extinction sessions (hM3Dq/hM4Di + saline, $n = 7$; hM3Dq + CNO, $n = 9$; extinction 2: $F(1,364) = 12.7$, extinction 3: $F(1,364) = 12.0$, $P < 0.0001$, two-way ANOVA), but not during the recall (recall: $F(1,78) = 0.87$, $P = 0.353$, two-way ANOVA). **c** Optogenetic stimulation of FN–vlPAG projections expressing cre-dependent ChR2-GFP strategy. **d** Optogenetic stimulation protocol of FN–vlPAG-projecting neurons during CS offset in extinction sessions 1 and 2 (E1–2). **e** Freezing levels during fear conditioning and extinction sessions in control (no light control, $n = 9$) and FN–vlPAG stimulated mice (E1–2 CS offset + light, $n = 5$). Mice that received light stimulation during CS offset exhibited a enhanced curve of extinction learning during the first and second extinctions, and lower fear response during third extinction in absence of light stimulation, compared to the mice that were not stimulated (extinction 1: $F(1,306) = 372.3$, extinction 2: $F(1,281) = 212.7$, extinction 3: $F(1,306) = 65.04$, $P < 0.0001$, two-way ANOVA), but there was not significant difference during the recall (recall: $F(1,61) = 1.32$, $P = 0.254$, two-way ANOVA). Lines represent means ± SEM. $^{**}P < 0.01$, $^{***}P < 0.001$, two-way ANOVA. Lines represent means ± SEM. Source data are provided as Source data file.

affect the fear memory retrieval (Fig. 6b). In addition, control sham mice exposed to CNO during the first and second extinction showed similar freezing levels compared to the control group (Supplementary Fig. 3b), indicating that CNO has not effect on fear extinction in absence of DREADD receptors. During the first extinction session, mice under FN–vlPAG activation did not exhibit differences in the freezing levels compared to the control group. However, mice under FN–vlPAG inhibition exhibited impairment in the extinction of the fear response during the first and second extinction training (Fig. 6b). Moreover, at the third extinction session, without exposure to CNO, these mice still exhibited higher levels of freezing compared to the control group, suggesting that FN–vlPAG neurons could also control the extinction learning.

Moreover, to evaluate whether similar to the role on the CS–US association in fear conditioning, this FN inputs to vlPAG might also have a contribution to the negative fear prediction error ("false alarm") or new association learning in extinction, we performed the optogenetic stimulation of FN–vlPAG projections during the CS offset along the first two extinction sessions (Fig. 6c, d). Interestingly, we found that the light stimulation of FN–vlPAG ChR2-expressing neurons at CS offset enhanced significantly the extinction learning from the first extinction session; this was not due just to the decrease on fear expression

but to learning, which is evidenced by the lower fear levels in the recall during the second extinction (Fig. 6e). This effect was also sustained in the absence of light stimulation during the third extinction. Interestingly, contrarily to fear learning, the sign of the effects on fear extinction of excitatory DREADD and of the optogenetic stimulation are different. This suggests that the effect on extinction depends on the temporal pattern of activation of the FN–vlPAG neurons. Overall, these results indicate that stimulation of the FN–vlPAG pathway may considerably accelerate the fear extinction learning.

Taken together, our results indicate that FN inputs to the vlPAG are able to control in a bidirectional way the strength of fear memory encoding, reinforcing the CS–US association when this pathway is inhibited or diminishing the CS–US association when it is activated. In addition, FN–vlPAG neurons may also exert a robust modulation of extinction learning.

**FN–vlPAG projections send collaterals to other areas**. We analyzed whether FN projections to vlPAG have axon collaterals targeting other areas in the brain, through the expression of retrograde AAV-cre-EBFP in vlPAG neurons in combination with cre-dependent Syn-GFP in FN, to evaluate the presence of synaptic boutons, together with cre-dependent tdTomato, to trace the axonal projections (Supplementary Fig. 7a). We were able to determine few axon collaterals from the FN–vlPAG-projecting neurons (Supplementary Fig. 7b, c) to different nuclei in the thalamus, such as the thalamic parafascicular nucleus (PF, Supplementary Fig. 7d), the mediodorsal nucleus (Supplementary Fig. 7e), the ventromedial nucleus (Supplementary Fig. 7e), and the ventral-anterior lateral nucleus (Supplementary Fig. 7f). Thus, as FN–vlPAG pathway, these axon collaterals could also impact on fear memory.

**Neuroanatomical link between the cerebellum and the amygdala**. Since FN–vlPAG neurons have also some axon collaterals to thalamic nuclei, we studied whether any of these nuclei have a link with the BLA, which is a key brain structure for fear memory acquisition and consolidation. Therefore, in order to evaluate a possible neuroanatomical connection between the cerebellum and the BLA, we combined anterograde tracing from the FN with retrograde tracing from the BLA (Fig. 7a–c). This analysis revealed BLA-projecting neurons in the area of the thalamic PF receiving neuronal projections from FN (Fig. 7d, e), suggesting that PF could be a relay area between the cerebellum and the BLA.

**FN projections to PF does not modulate fear memories**. To test if these FN projections to the PF play a role on fear learning, we examined the effect of activating or inhibiting this pathway during fear conditioning in mice expressing cre-dependent anterograde AAV-hM3Dq or -hH4MD injected in FN neurons, and retrograde CAV2-cre injected in the PF (Fig. 8a–c). Chemogenetic modulation of FN–PF projections did not induce significant differences in freezing behavior during fear conditioning or during extinction compared to the control mice (Fig. 8d). In addition, either activation or inhibition had not effect on the basal freezing levels in the context A before fear conditioning (Fig. 8e). Therefore, these results indicate that the FN–PF neurons do not contribute to fear memory formation, despite the proximity of their terminals with neurons projecting to the BLA.

**FN–PF projections contribute to anxiety-like behavior**. The neuronal circuits for fear and anxiety are overlapping and closely related[7,44]. Therefore, we evaluated if the FN–vlPAG or the FN–PF pathways contribute to anxiety behavior in three different anxiety tasks: open field, elevated plus maze and dark–light box. We found no difference in anxiety parameters that indicate generalized anxiety-like behavior, neither when FN–vlPAG pathway was activated or inhibited (Supplementary Fig. 8a), nor in the sham group exposed to CNO (Supplementary Fig. 8c). On the other hand, mice under activation of FN–PF neurons exhibited a decrease in the frequency of entries in the open arms in the EPM, and decreased frequency of entries into the light zone in the light–dark box test, indicating an anxiogenic effect induced by the activation of these neurons (Supplementary Fig. 8b). Therefore, these results suggest that FN–PF projections modulate anxiety levels, while FN–vlPAG does not affect anxiety, but has a specific role on fear conditioning.

Therefore, despite the existence of collaterals of FN–vlPAG in the PF, the chemogenetic manipulations of FN–vlPAG and FN–PF neurons produce distinct, nonoverlapping effects, the former impacting fear learning and the latter anxiety.

**FN inputs to vlPAG and PF do not affect pain sensitivity**. PAG is involved in processing pain information from the periphery[13]. Since the activation or inhibition of FN–vlPAG neurons during CS–US presentations respectively diminished or reinforced fear memory, we tested if that could result from an alteration on the sensitivity to painful stimuli by hot plate and tail-immersion tests. No differences were found in the hot plate or the tail-immersion sensitivities for FN–vlPAG (Supplementary Fig. 8d, e) or FN–PF projections (Supplementary Fig. 8f, g), indicating that those inputs do not modulate the sensitivity to painful stimuli. Therefore, alteration in sensitivity is not responsible for the effect of FN–vlPAG inputs on fear memories formation and expression.

## Discussion

Despite many clinical and anatomical evidence indicating an involvement of the cerebellum in emotional functions[19], the nature of its contribution remains unclear. Here, we describe a link between the cerebellum and one element of the fear circuitry, the vlPAG, through which it exerts a bidirectional control over fear learning during the association of a cue and aversive events. Our experiments reveal that glutamatergic neurons in the FN send projections to the vlPAG where they form synapses onto glutamatergic and GABAergic neurons. The chemogenetic or optogenetic activation of this pathway during fear conditioning increases the activity of vlPAG neurons, but yields reduced fear expression during the recall and extinction. In contrast, the inhibition of this pathway during fear conditioning results in a higher expression of conditioned fear and a slower extinction learning. Thus, our experiments are consistent with a participation of the cerebellum to the function of the vlPAG in fear learning and memory (Fig. 9).

The PAG has long been implicated as the organizer of behavioral components of the response to threat. The most characterized function of the vlPAG is its direct control of freezing via glutamatergic projections to premotor targets in the magnocellular nucleus of the medulla; this pathway is recruited in innate freezing, and in cued- or context-driven freezing respectively by GABAergic afferents from CEA[10], and glutamatergic afferents from the mPFC[6]. The cerebellum may also participate to freezing expression. Indeed, the vlPAG has been shown to entrain (via an unknown pathway) the climbing fiber in the lobule 8 of the rat cerebellum, a region found to reduce both innate and cued-freezing expression if lesioned[24], and recent in vitro work indicate functional connections to freezing-related neurons[26]. This modulation on freezing expression is unlikely supported by the cerebellum–vlPAG projections targeted in our experiments, since the chemogenetic or optogenetic stimulation of the FN–vlPAG

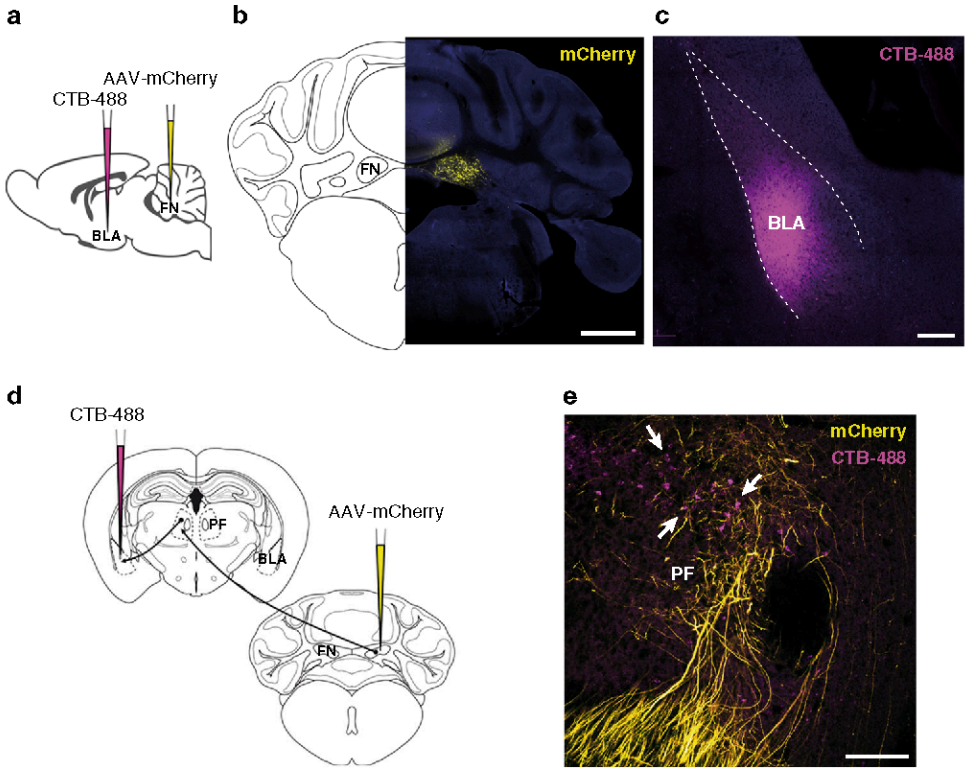


**Fig. 7 Cerebellar link to the BLA through thalamic PF. a** BLA injection of retrograde CTB-488 in combination with anterograde AAV-mCherry in the FN strategy. **b** Expression of anterograde AAV-mCherry in the FN (scale bar, 1 mm). **c** Infusion of CTB-488 in the BLA (scale bar, 200 µm). **d** Retrograde tracing from BLA combined with anterograde tracing from the FN converged at the thalamic PF nucleus. **e** PF neurons projecting to the BLA (arrows) surrounded by fibers from FN (scale bar, 200 µm).

did not affect the freezing evoked by the aversive stimulus during the presentation of the US, and failed to modify the cued-freezing at the time of recall (i.e., beginning of the extinction training). However, we found a small reduction of freezing when the FN–vlPAG neurons were stimulated between the CS–US pairing during the fear acquisition. Therefore, our results unlikely result from an entrainment by FN–vlPAG of the vlPAG neurons projecting to the magnocellular medulla responsible for freezing, or to their afferent inhibitory neurons. Thus, the effects revealed in our work would not result from the regulation of the motor control of freezing behavior, but from a modulation of fear memories.

The changes in the conditioned fear response observed during extinction following the modulation of FN–vlPAG neurons during fear conditioning, shall indeed result from a change in the learning of the CS–US association. A trivial explanation could be that the FN–vlPAG pathway modulates the sensory perception of the US at the time of fear encoding. Although excitatory and inhibitory neurons in the vlPAG exert an antinociceptive effect[10,11], we found that chemogenetic manipulations failed to change the responses to pain in the tail-immersion and hot plate tests. This indicates that the changes in fear learning were not due to an effect of the FN–vlPAG directly on the antinociceptive circuit of the vlPAG, also consistent with the similar fear levels (freezing) exhibited by the animals induced by the US. An alternative hypothesis to explain the changes in fear learning observed during the extinction is an alteration of fear consolidation[28]; however, the modulation of the FN–vlPAG pathway during consolidation phase after fear conditioning had not effect on the retrieval of the conditioned fear response in the following days. Moreover, the optogenetic stimulation of the pathway only at the time of the CS–US presentation was sufficient to induce a robust decrease in the conditioned fear expression in the following days, consistent with a modulation on the encoding of the CS–US association and a limited contribution of the FN–vlPAG pathway to the consolidation process.

At odds with the classical view of the PAG as a relay mediating emotional responses, increasing evidence points toward a bidirectional contribution of vlPAG neurons to fear learning: the chemogenetic activation of vlPAG during learning subsequently reduces the cued feeding suppression indicating a reduced cued fear[45] (consistent with the chemogenetic and optogenetic findings of the present work), while the pharmacological inhibition of vlPAG before CS–US presentation may prevent learning of freezing responses[46]. Some of the effect of the vlPAG on fear learning may involve a cued-antinociception triggered by an amygdala–vlPAG pathway[12], although we have not observed a change in sensitivity to aversive stimuli in our chemogenetic experiments. However, the optogenetic inhibition of vlPAG has been found to inhibit the acquisition of conditioned fear response not only using aversive shocks, but also using threatening visual stimuli[39]; thus, pointing to a broad role of the vlPAG in fear learning.

Several electrophysiological and optogenetic studies indicate that vlPAG neurons encode positive fear prediction errors, determining the intensity of fear learning[40,42,46,47]. Since the optogenetic stimulation of the FN–vlPAG pathway specifically during CS–US pairing was sufficient to enhance the extinction of the fear response, indicating a decrease in the intensity of fear learning, this could be explained by an alteration of the positive prediction error signal during conditioning (Fig. 9). In our recordings, we found neurons in the vlPAG and FN that exhibited a strong reduction of firing during immobility and freezing, and an increase in the transfer of information between these FN and vlPAG neurons during, but also

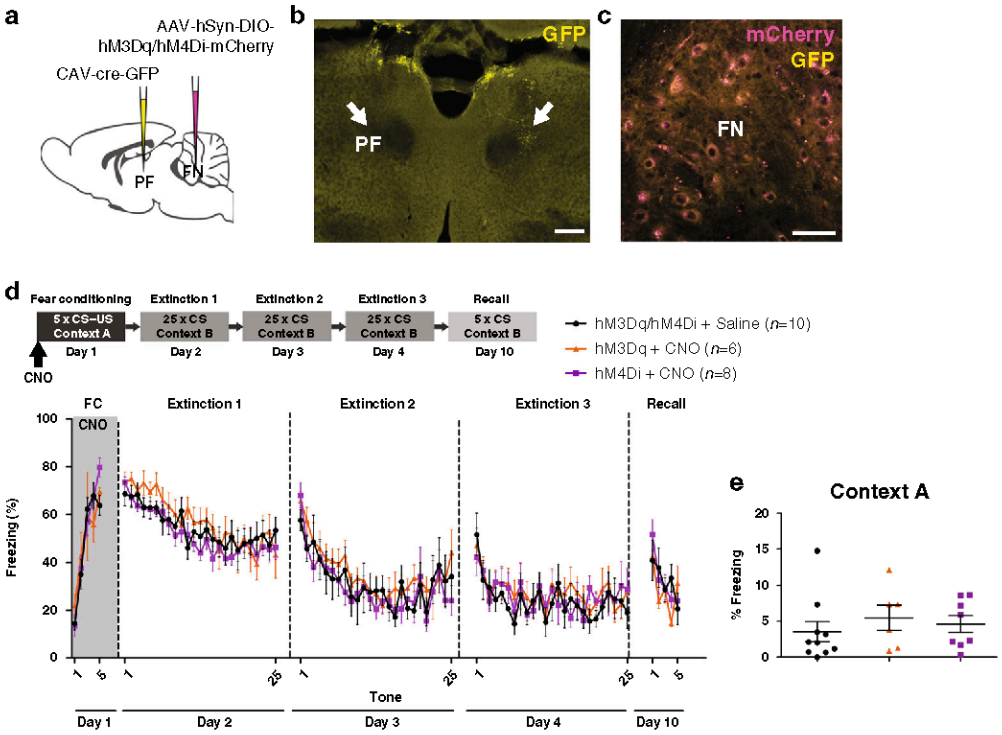


**Fig. 8 FN-PF pathway does not contribute to fear memory formation. a** Chemogenetic modulation of FN-PF-projecting neurons by bilateral cre-dependent expression of excitatory or inhibitory DREADDs (hM3Dq or hM4Di, respectively) in the FN in combination of CAV2-cre-GFP injection in the PF. **b** Injection site of CAV2-cre-GFP in PF (arrows, scale bar, 200 µm). **c** Cre-dependent expression of DREADDs in the FN (scale bar, 50 µm). **d** FN-PF pathway stimulation (hM3Dq + CNO, $n = 6$ mice) or inhibition (hM4Di + CNO, $n = 8$ mice) during fear conditioning had not significant effect on freezing behavior during the sessions (for stimulation: FC: $F(1,55) = 0.07$, $P = 0.795$; extinction 1: $F(1,323) = 3.03$, $P = 0.0826$, extinction 2: $F(1,267) = 3.87$, $P = 0.0503$, extinction 3: $F(1,279) = 3.65$, $P = 0.0571$; recall: $F(1,65) = 1.49$, $P = 0.226$; for inhibition: FC: $F(1,100) = 0.53$, $P = 0.468$; extinction 1: $F(1,405) = 3.86$, $P = 0.0502$, extinction 2: $F(1,247) = 0.76$, $P = 0.386$, extinction 3: $F(1,232) = 1.18$, $P = 0.279$; recall: $F(1,65) = 0.00$, $P = 0.956$; two-way ANOVA) compared to the control group (hM3Dq/hM4Di + saline, $n = 10$ mice). Data are presented as mean values ± SEM. **e** Percentage of freezing in context A before fear conditioning. Mice under inhibition (hM4Di + CNO, $n = 8$ mice) or activation (hM3Dq + CNO, $n = 6$ mice) of the FN-vlPAG pathway exhibit similar basal levels of freezing to the context A compared to the control group (hM3Dq/hM4Di + saline, $n = 10$ mice, $df = 2$, $F = 0.435$, $P = 0.653$, one-way ANOVA). Scatter dot plot with mean ± SEM. Source data are provided as Source data file.

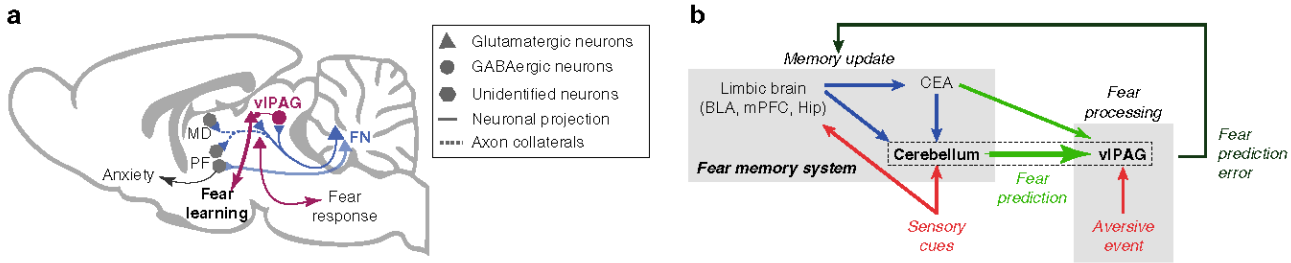


**Fig. 9 Summary of results and putative insertion of the FN-vlPAG pathway in fear learning process. a** Glutamatergic FN inputs form synaptic contacts on glutamatergic and GABAergic vlPAG neurons (see Figs. 1 and 2) that excite the vlPAG neurons (Fig. 3). FN-vlPAG axon collaterals (dotted lines) also target several thalamic nuclei involved in limbic circuits (PF parafasciclular, MD mediodorsal; Supplementary Fig. 7). vlPAG-projecting FN neurons control fear learning rather than fear responses (Figs. 4 and 5, and Supplementary Figs. 4 and 5)—this is consistent with the observation that vlPAG does not contact freezing-inducing vlPAG neurons[26]. PF-projecting FN neurons rather control anxiety (Fig. 8 and Supplementary Fig. 8). **b** Schematics of the putative insertion of the cerebellum–vlPAG pathway studied here (dotted rectangle) in the fear prediction circuits: the cerebellum receives inputs from the sensory and emotional system[56]. The central amygdala, CEA, which carries fear predictions to the vlPAG[12], also projects to the cerebellum[25]. Departure from the predictions yields a fear prediction error[15], which drives the update of the fear memory. The cerebellum could thus participate to the propagation of fear predictions to the vlPAG: potentiated cerebellar output yields stronger prediction of US following CS, thus lower error at the occurrence of US, hence weaker learning of CS–US association during conditioning. Conversely, inhibited cerebellar output yields weaker prediction following CS, stronger error at the occurrence of US, and stronger CS–US association. N.B.: the aversive effect of US and the fear response to US are preserved by cerebellar manipulations.

after, conditioning. However, it remains unclear whether these neurons encode fear prediction error[41,42], notably since the CS and US usually induced motor responses which may also explain the increased firing. The elaboration of a fear prediction error signal in the cerebellum shall recruit a large network, possibly involving the amygdala (Fig. 9). Indeed, the amygdala and the vlPAG have reciprocal connections that are essential for fear prediction error treatment[12,42]. However, the amygdala also projects heavily to the

ponto-cerebellar system and is essential for cerebellar CS activity in reflex conditioning[25], suggesting that a fear prediction signal could be provided by the amygdala both to the vlPAG and cerebellum. In addition, a recent imaging study has shown in a cued fear learning experiment that large portions of the cerebellar cortex are activated by fear prediction error[48]. Moreover, the participation of the cerebellum to shock prediction is illustrated in aversive eyeblink conditioning, where climbing fibers respond to the onset of the CS after learning[49]. Nevertheless, the nature of cerebellar computations in fear prediction is still unknown, but the cerebellum provides an extensive representation of the context thanks to the massive mossy fiber system and fine temporal learning, which may help tuning the fear prediction (Fig. 9).

Our study also indicates a modulatory role of the FN–vlPAG pathway in fear extinction. Optogenetic stimulation of FN–vlPAG inputs at the CS offset in extinction training was sufficient to enhance the extinction learning. Consistent with our results, evidence for negative fear prediction error, needed to drive extinction learning, was found in vlPAG[45], as well as in the ventral tegmental area and dorsal raphe[50,51], which also receive inputs from the vlPAG.

A striking finding of our work was that FN–vlPAG projections send collaterals to different thalamic nuclei, such as regions of the PF thalamus that projects to the BLA (Fig. 9). Nevertheless, FN–PF projections did not exert the modulation on fear learning found in FN–vlPAG neurons. In contrast, FN–PF activation increased anxiety in multiple anxiety tests, pointing toward an involvement of FN–PF in the modulation of anxiety states, which could be related to the reported contribution of PF to observational social fear[52].

Understanding how cerebellar circuits engage with processing and associative learning of emotions in other areas of the central nervous system is an important avenue for future research[17,25]. Indeed, the cerebellar involvement in reward processing is engaging a pathway between the cerebellum and the ventral tegmental area[17]. Our work shows that another pathway linking the cerebellum to vlPAG is controlling fear learning (Fig. 9). The study of this pathway could be particularly relevant for the deeper understanding of emotional control and maladaptive threat processing.

## Methods

**Animals**. Experimental subjects were adult C57BL/6 N male mice, 8–12-week-old, wild-type (Charles River Laboratories) or mutant male mice *Vglut2-cre* and *Glyt2-GFP* from an in-house colony (IBENS, Paris, France).

All mice were housed in groups of four mice per cage, room temperature controlled at 21–22 °C, humidity between 40 and 50%, in a 12 h light/dark cycle (light from 7:a.m. to 7:p.m.), and all the experiments were performed in awake freely moving mice during the light cycle. Food and water were available ad libitum. All animal procedures were performed in accordance with the recommendations contained in the European Community Council Directives (authorization number APAFIS#1334-2015070818367911 v3).

**Surgeries and stereotaxic injections**. Male mice 7–8-weeks old received a dose of buprenorphine and 15 min later they were deeply anesthetized with isoflurane 3%, and placed in a stereotaxic frame (Kopf Instruments). Anesthesia was kept constant with 1.5–2% isoflurane supplied via an anesthesia nosepiece, and body temperature maintained at 36 °C with a heating pad controlled by rectal thermometer. A local analgesia with 1 ml of 0.02% of lidocaine was injected subcutaneously above the skull, and then the skull was exposed and perforated with a stereotaxic drill at the desired coordinates relative to Bregma. For viral delivery, a capillary was lowered to coordinates just above the target area and 100–250 nl of virus solution was infused. After infusion, capillary was kept at the injection site for five more minutes before being slowly withdrawn. For viral injections and implants, the stereotaxic coordinates used were: FN: AP: −6.37, ML: ±0.70, DV: −2.12; vlPAG: AP: −4.45; ML: ± 0.55; DV: −2.50 to −2.40; PF: AP: −2.10; ML: ±0.70; DV: −3.42 to −3.00; BLA: AP: −1.35; ML: ±3.43; DV: −4.0; depths were taken relative to the dura.

**Neuroanatomical tracing**. For neuroanatomical tracing, mice were injected with 100 nl of anterograde AAV1-CB7-Cl-mCherry-WPRE-rBG (Upenn Vector) in the FN ($n = 14$), 100 nl CTB-alexa 488 or -alexa 555 (Invitrogen) in the BLA ($n = 6$), and 250 nl CTB-CF594 (Biotium) or retrograde AAV-Syn-eGFP (Addgene) were injected in the vlPAG ($n = 6$). For synaptophysin labeling, 200 nl of AAV8.2-hEF1a-DIO-synaptophysin-GFP (Massachusetts General Hospital) was injected in FN of *vglut2-cre* mice ($n = 7$), and a group of these mice were injected with 300 nl of AAV1.CAG.Flex.tdTomato.WPRE.bGH (Upenn Vector) in vlPAG ($n = 4$), while the rest were used for gad67 immunostaining.

To study FN–vlPAG axon collaterals, mice were injected with 200 nl of retrograde AAV-cre-EBFP (Addgene) in the vlPAG, AAV1.CAG.Flex.tdTomato.WPRE.Bgh, and 200 nl of AAV8.2-hEF1a-DIO-synaptophysin-GFP in FN.

For the CTBs infusions, mice were perfused the fourth day after the injections. For the AAVs infusions, mice were perfused 21 days after the injections. Mice were anesthetized with ketamine 80 mg kg $^{-1}$ and xylazine 10 mg kg $^{-1}$, i.p., and the perfusions were performed with formalin (Sigma). Dissected brains were kept in formalin solution overnight at 4 °C, and the brains were then stored in PBS solution at 4 °C. Brains were sliced entirely at 90 µm using a vibratome (Leica VT 1000 S), and mounted on gelatin-coated slides, dried, and then coverslipped with Mowiol (Sigma). For counterstaining, sections were coverslipped with a mounting medium with DAPI (Fluoroshield, Sigma). Slices were analyzed and imaged using a confocal microscope (Leica TCS Sp8), and images were edited and analyzed using Image J. In the same way, the placement of the optic fiber, electrodes, and injections sites for all the experiments were assessed when the experiment was completed. Mice with no viral expression, or misplacement of the optic fiber or electrode were excluded from the analysis.

**Immunohistochemistry**. For the identification of GABAergic neurons in the vlPAG, mice were perfused with PFA 4%, stored overnight in PFA 4% at 4 °C, and then stored in 25% sucrose solution in PBS. Brains were sliced coronally at 50 µm using a vibratome and slices were stored at −20 °C in a cryoprotective solution until the moment of the immunostaining.

In order to analyze neuronal activity, immunostaining of the immediate early gene c-Fos was performed. Mice underwent fear conditioning protocol and 50 min after the end of the protocol each mice was perfused as has been described above.

For the immunostaining, selected slices were washed with PBS-0.3% Triton X-100, blockage of nonspecific sites was assessed by 2 h of incubation with 3% normal donkey serum (NDS) for GAD67-immunostaining ($n = 3$) or with normal goat serum (NGS) for c-Fos-immunostaining ($n = 10$). Sections were then incubated in a solution containing mouse anti-GAD67 (1:500, Milipore #MAB5406) in PBS-0.3% Triton X-100 with 1.5% NDS at 4 °C for 72 h; or rabbit polyclonal anti-c-fos (1:800, Milipore #ABE457) in PBS-0.3% Triton X-100 with 1.5% NGS at 4 °C for 24 h. After first antibody incubation, slices were rinsed and sections were 2 h incubated at room temperature with secondary antibody, donkey anti-mouse IgG conjugated to Alexa Fluor 488 or to Alexa 555 (1:400, Invitrogen), or goat anti-rabbit IgG-FITC (1:300, Jackson Immunoresearch). Slices were mounted on gelatin-coated slides with Mowiol and analyzed with the confocal microscope.

**Chemogenetics**. To specifically modulate the activity of FN neurons projecting to vlPAG, excitatory or inhibitory DREADDs were expressed by bilaterally injection (200 nl per injection site) of pAAV-hSyn-DIO-hM3Dq-mCherry (cre-dependent expression of excitatory DREADD, Addgene) or pAAV-hSyn-DIO-hM4Di-mCherry (cre-dependent expression of inhibitory DREADD, Addgene) in the FN in combination of 300 nl CAV2-cre-GFP (Plateforme de Vectorologie de Montpellier) viral infusion in vlPAG. Surgeries and injections were performed 2 weeks before mice performed the behavioral tests. For neuronal modulation of animals expressing DREADDs, Clozapine N-oxide (Tocris Bioscience, 1.25 mg kg $^{-1}$) was diluted in saline and injected i.p. 30 min before the start of the experimental session. Control group was injected with saline. Animals that received this treatment in experiments were habituated by saline injections during handling sessions.

Another group of mice called sham, underwent the same surgery procedures included the insertion of the cannula without withdrawal of virus. To evaluate whether CNO had an effect in absence of DREADD expression, these mice were injected with saline or CNO before performing the behavioral tests.

**Pavlovian fear conditioning and extinction**. Pavlovian fear conditioning and extinction took place in two different contexts (A and B), located inside of a sound attenuating box (Ugo Basile). Pavlovian fear conditioning was conducted in a context A: 17 × 17 × 25 cm square chamber with black/white-checkered walls and a grid floor, with peppermint-soup odor. The chamber was cleaned with a 70% ethanol within mice. Following a 180 s acclimation period, mice received five pairings between a 30 s, 80 dB, 2.7 kHz tone (CS) and a 0.5 s, 0.4 mA electrical footshock (US), in which the US was presented during the last 0.5 s of the CS, and with an ITI of 120 s after each CS–US pairing. Stimuli presentation were controlled by the Ethovision XT 14 (Noldus).

Twenty-four hours later, recall of the response to the CS and the first extinction training were performed. Mice were placed in a novel context B: cylindrical chamber with yellow semitransparent wall, an opaque solid-Plexiglas floor, and vanilla-extract solution to provide a distinctive olfactory cue. The chamber was cleaned with the disinfectant detergent solution Surfa'safe premium (Anios) between different run. Following an initial 180 s acclimation period, the mouse received 25 × 30 s presentations of the CS alone (30 s no-stimulus interval). The

second and third extinction sessions took place in the next 2 days under the same conditions. Finally, on day 10, recall test was performed in context B, by 5 × 30 s presentations of the CS (30 s no-stimulus interval).

Mice were videotracked using Ethovision XT 14 during all the trial. Freezing (no visible movement except that required for respiration) was assessed by the inactive periods, defined as periods of time during which the average pixel change of the entire video image was <0.5 % (from one video frame to another one), and the threshold was fixed avoiding the detection of the breathing movements. Freezing behavior was analyzed during each CS presentation, and during the habituation period to the context A and B.

**Anxiety tests**. *Open field test*. To evaluate anxiety-like behavior and locomotor activity, mice were placed in a circular arena (38 cm diameter, Noldus) and videotracked from above. The position of the center point of the mice was tracked with Ethovision XT 14 and the distance moved, time in the center area, frequency of entries in the center area, were analyzed for a 20 min period.

*Elevated plus maze*. Mice were placed in the center zone (6 × 6 cm), facing an open arm of an elevated plus maze (Noldus, elevated 52 cm above the floor) with two open arms (36 cm length, 6 cm width) and two wall-enclosed arms (closed arms, 36 cm length, 6 cm width, walls 25 cm high), and let explore freely for 5 min. Their path was videotracked using Ethovision XT 14, and the amount of time spent and distance moved in the open arms, closed arms, and center zone were analyzed.

*Light–dark box*. Mice were placed in the light zone and let to explore the light–dark arena (Noldus) freely for 5 min. Light zone was 40 cm × 20 cm in size, 150 lux, while dark zone was 20 × 20 cm and ~0 lux. Their path was videotracked in the light and dark zones using Ethovision XT 14, the amount of time spent in the light versus dark zones and distance traveled in the light zone were evaluated, as well as the latency until they escaped to the dark zone.

**Hot plate and tail-immersion tests**. Effect on sensitivity was tested 1 week after recall test using a hot plate analgesia meter (Harvard apparatus) and tail-immersion test. Mice received a CNO or saline i.p. injection and 30 min after were put on the hot plate at 55 °C. The experiment was stopped as soon as the mice performed the first licking or jump. Mice were videotracked and the latency to the first reaction (hindpaw shaking or licking, or jump) was recorded.

Tail-immersion test was performed after hot plate test. Mice tale tips were immersed in hot water with a temperature of 50 °C, and tail withdrawal latency was recorded.

**Optogenetic stimulation**. For optical manipulation, mice were injected bilaterally with 200 nl of cre-dependent AAV-ChR2-GFP (Addgene) in the FN combined with local injection of 200 nl of retrograde AAV-cre-EBFP into the vlPAG. To perform optical stimulation, mice were implanted bilaterally with an optic fiber (0.22 numerical aperture, Thor labs) housed in a stainless steel ferula (Thor Labs) just dorsal to the FN. Ferrules were adhered to the skull with adhesive, and then a protective head cap was constructed using dental cement. The viral injections and optic fiber implantations were performed in the same surgery, and the optical manipulation and fear conditioning were performed 3 weeks after surgery to ensure ChR2 expression. At the end of the experiments, optic fiber positions were verified.

For the optogenetic activation of the FN during fear conditioning or extinction, mice were randomly designated to non-stimulated or stimulated groups. The stimulated groups received 20 ms blue light pulses, at 10 Hz, 1 mW during a total of 6 s. The CS–US group received the light stimulation on each of the five CS–US presentations, from the last 3 s of the CS until 3 s posterior to the end of CS–US presentation; the ITI group received the light stimulation randomly within the ITI, 30 s after and before the CS, during fear conditioning. For CS offset group, mice received light stimulation from the last 3 s of the CS until 3 s posterior to the end of CS presentation during extinction sessions 1 and 2.

**Optogenetics and electrophysiological recordings**. For optical manipulation combined with electrophysiological recordings, electrodes were implanted in mice injected bilaterally with 200 nl of cre-dependent AAV-ChR2-GFP in the FN, and with 200 nl of retrograde AAV-cre-EBFP into the vlPAG, and implanted unilaterally with an optic fiber in the FN (see "Optogenetic stimulation" section). The cerebellar FN preferentially sends projections to the contra-lateral vlPAG regions (Fig. 1a, b). Therefore, in order to compare responses, we recorded neuronal activity in both contra- and ipsi-lateral vlPAGs when we unilaterally stimulated the FN. To record cell activity in the vlPAG, we used bundle of electrodes consisting of nickel/Chrome wire (0.004 inches diameter, Coating 1/4 Hard PAC) folded and twisted into bundles of six electrodes. Pairs of bundles were inserted in metal cannulas (stainless steel, 29 G, 8 mm length, Phymep), in order to protect them and to guarantee a correct placement into the brain. Cannulas and bundles were also attached to an electrode interface board (EIB-16; Neuralynx, Bozeman) by Loctite universal glue in a configuration allowing us to record vlPAG. The microwires of each bundle were connected to the EIB with gold pins (Neuralynx). The entire EIB and its connections were fixed in place by dental cement (Super Bond). The impedance of each electrode was measured and the 1 kHz impedance was set to 200–500 kΩ, using gold-plating (cyanure-free gold solution, Sifco). During the surgery, the electrode bundles were inserted into the brain and the ground was placed over the cerebellum, between the dura and the skull. The viral injections, optical fiber and electrodes implantation were performed in the same surgery, and the optical manipulation and recordings were performed 3 weeks after surgery to ensure ChR2 expression.

For the ramp of optical activations, electrophysiological recordings in the vlPAG were performed in freely moving mice placed in an open field. Recordings were performed using an acquisition system with 16 channels (sampling rate 25 kHz; Tucker-Davis Technology System 3, Tucker-Davis Technologies) as described[53,54]. Mice received a stimulation at 0.5 Hz, 50 ms, and the light intensities used were 0.37, 0.54, 0.75, 1.03, and 1.33 mW (at the fiber tip). The signal was acquired by a headstage and amplifier from TDT (RZ2, RV2, Tucker-Davis Technologies). The spike sorting was performed with Matlab (Mathworks) scripts based on *K*-means clustering on PCA of the spike waveforms (Paz et al. 2006). At the end of the experiments, the position of the electrodes was verified by electrolytic lesions and comparison to a brain atlas after brain slicing was performed.

**Chemogenetics and electrophysiological recordings**. Mice were injected bilaterally with 300 nl CAV2-cre-GFP in the vlPAG, and with 200 nl of pAAV-hSyn-DIO-hM3Dq-mCherry or pAAV-hSyn-DIO-hM4Di-mCherry in the FN, as has been detailed above (see "Chemogenetics" section). After viral infusions, electrodes were placed in FN and vlPAG as was described above (see "Optogenetics and electrophysiological recordings" section). Fear conditioning was performed 2–3 weeks after the surgeries, and electrophysiological and inertial recordings during fear conditioning were analyzed. Gyroscopic data were acquired using the MultiChannelSystems wireless headstage W2100-HS16 embedded gyroscope. The motor activity signal was computed as the norm of the rotation vector, smoothed by convoluting it with a Gaussian kernel (s.d. = 64 ms). The smoothed signal was then binarized by applying a threshold of 12 degree $s^{-1}$ between active and immobile states.

**Statistical analysis**. The effect of activation or inhibition of FN–vlPAG projections was analyzed using analysis of variance (ANOVA) and Newman–Keuls or Bonferroni post hoc comparisons, or paired *t* test, where appropriate. All statistics were performed in Graph Pad Prism® (Version 5) and RStudio® (R version 3.6.3 and RStudio version 1.2.5), unless otherwise indicated, and all statistical tests used are indicated in the figures legends. The effect of trial on freezing during fear conditioning and extinction was analyzed using two-way ANOVA. Experimental designs with two categorical independent variables were assumed to be normal and analyzed by two-way ANOVA without formally testing normality. All significance levels are given as two-sided and were corrected for multiple comparisons, wherever applicable. Statistical significance was set at $P < 0.05$.

To analyze the response to the optogenetic stimulations, we constructed the PSTH (bin 2 ms) and converted these PSTH to a *z*-score using the pre-PSTH period (subtracting by baseline mean and dividing by the baseline standard deviation), the latency was determined by the time of the first bin with strongly significant *z*-score (>4).

Classification of cells in two sets based on the link between firing and immobility was performed by computing the PSTH (bin 100 ms) around the onset of immobility episodes, irrespective of their duration. The PSTH were normalized by their average and clustered in two groups using *K*-mean algorithm. The average firing rate during immobility and active behavior was simply computing by dividing the number of spikes in each of these states by the total duration spent in each of these states.

Information theory methods were used to examine the relation between cell firing and binarized motor activity. Spiketrains of neuronal activities were binned using bins of 10 ms. To obtain a matching motor signal, the binarized motor activity was interpolated and resampled at every time point corresponding to the bin timestamp (left edge of the bin). To study directional influences, we related the source signal to the target signal one time bin (10 ms) later. The transfer entropy[43] was calculated using the PyIF Python package (v0.1), allowing the computation of bivariate transfer entropy between two binned spiketrains, or between a binned spiketrain and the corresponding motor signal. The PID was used to decompose the influence of the neuronal activity in FN and locomotion on the neuronal activity in vlPAG. The PID was computed using the iDTxl Python package (v1.0)[55], as a decomposition of the multivariate mutual information at lag −10 ms between the two sources signals and the target signal, using the Goettingen estimator.

**Statistics and reproducibility**. For anatomical tracing in Fig. 1b, d–f, analysis was repeated independently in eight mice showing similar results. For Fig. 2b–d, f–h, independent analysis of three mice exhibited similar results. For fear conditioning and extinction experiments in DREADD mice, each experiment was repeated independently at least four times, and pooled together (Figs. 4d, e, 6b and 8, and Supplementary Figs. 3 and 8). Viral injection site and expression were checked in each mouse included in the results, showing similar results (Figs. 4b, c, 5b, c and 8b, c). For electrophysiological recordings, experiments were repeated independently two times, and viral expression and electrode positions were checked showing similar results (Fig. 5b, c). For optogenetics (Figs. 4g, i and 6e, and

Supplementary Fig. 5), each experiment was repeated independently two times, obtaining similar results; thus, the results were pooled together. Viral expression and optic fiber position were checked in each mouse included in the results, showing similar results (Fig. 4g). For anatomical tracing in Fig. 7b, c, e, analysis was repeated independently in four mice showing similar results. For anatomical tracing in Supplementary Fig. 1b–e, the experiment was carried out three independently times, for Supplementary Fig. 1g, two independently times, and for Supplementary Fig. 7b-f was repeated four independently times, all showing similar results.

**Reporting summary**. Further information on experimental design is available in the Nature Research Reporting Summary linked to this paper.

## Data availability

The data that support the findings of this study (Figs. 1–9, Supplementary Figs. 1–8) are available from the corresponding author upon reasonable request. For additional information, please refer to the corresponding Life Sciences Reporting Summary. Source data are provided with this paper.

## Code availability

The code for analysis is available from the corresponding author upon reasonable request.

Received: 13 December 2019; Accepted: 17 September 2020;
Published online: 15 October 2020

## References

1. Ehrlich, I. et al. Amygdala inhibitory circuits and the control of fear memory. *Neuron* **62**, 757–771 (2009).
2. Pape, H. C. & Pare, D. Plastic synaptic networks of the amygdala for the acquisition, expression, and extinction of conditioned fear. *Physiol. Rev.* **90**, 419–463 (2010).
3. Pare, D., Quirk, G. J. & Ledoux, J. E. New vistas on amygdala networks in conditioned fear. *J. Neurophysiol.* **92**, 1–9 (2004).
4. Duvarci, S. & Pare, D. Amygdala microcircuits controlling learned fear. *Neuron* **82**, 966–980 (2014).
5. Herry, C. & Johansen, J. P. Encoding of fear learning and memory in distributed neuronal circuits. *Nat. Neurosci.* **17**, 1644–1654 (2014).
6. Rozeske, R. R. et al. Prefrontal-periaqueductal gray-projecting neurons mediate context fear discrimination. *Neuron* **97**, 898–910 e896 (2018).
7. Tovote, P., Fadok, J. P. & Luthi, A. Neuronal circuits for fear and anxiety. *Nat. Rev. Neurosci.* **16**, 317–331 (2015).
8. Klavir, O., Prigge, M., Sarel, A., Paz, R. & Yizhar, O. Manipulating fear associations via optogenetic modulation of amygdala inputs to prefrontal cortex. *Nat. Neurosci.* **20**, 836–844 (2017).
9. Herry, C. et al. Neuronal circuits of fear extinction. *Eur. J. Neurosci.* **31**, 599–612 (2010).
10. Tovote, P. et al. Midbrain circuits for defensive behaviour. *Nature* **534**, 206–212 (2016).
11. Behbehani, M. M. Functional characteristics of the midbrain periaqueductal gray. *Prog. Neurobiol.* **46**, 575–605 (1995).
12. Ozawa, T. et al. A feedback neural circuit for calibrating aversive memory strength. *Nat. Neurosci.* **20**, 90–97 (2017).
13. Ossipov, M. H., Morimura, K. & Porreca, F. Descending pain modulation and chronification of pain. *Curr. Opin. Support. Palliat. Care* **8**, 143–151 (2014).
14. McNally, G. P., Johansen, J. P. & Blair, H. T. Placing prediction into the fear circuit. *Trends Neurosci.* **34**, 283–292 (2011).
15. Rescorla, R . A. & Wanger, A. R. In *Classical Conditioning II: Current Research and Theory* (eds Black A. H. & Prokasy W. F.) (Appleton Century Crofts, 1972).
16. Koziol, L. F. et al. Consensus paper: the cerebellum's role in movement and cognition. *Cerebellum* **13**, 151–177 (2014).
17. Carta, I., Chen, C. H., Schott, A. L., Dorizan, S. & Khodakhah, K. Cerebellar modulation of the reward circuitry and social behavior. *Science* **363**, eaav0581 (2019).
18. Stoodley, C. J. et al. Altered cerebellar connectivity in autism and cerebellar-mediated rescue of autism-related behaviors in mice. *Nat. Neurosci.* **20**, 1744–1751 (2017).
19. Stoodley, C. J. & Schmahmann, J. D. Functional topography in the human cerebellum: a meta-analysis of neuroimaging studies. *Neuroimage* **44**, 489–501 (2009).
20. Damasio, A. R. et al. Subcortical and cortical brain activity during the feeling of self-generated emotions. *Nat. Neurosci.* **3**, 1049–1056 (2000).
21. Schmahmann, J. D. & Sherman, J. C. The cerebellar cognitive affective syndrome. *Brain* **121**, 561–579 (1998).
22. Teune, T. M., van der Burg, J., van der Moer, J., Voogd, J. & Ruigrok, T. J. Topography of cerebellar nuclear projections to the brain stem in the rat. *Prog. Brain Res.* **124**, 141–172 (2000).
23. Watson, T. C., Jones, M. W. & Apps, R. Electrophysiological mapping of novel prefrontal - cerebellar pathways. *Front. Integr. Neurosci.* **3**, 18 (2009).
24. Koutsikou, S. et al. Neural substrates underlying fear-evoked freezing: the periaqueductal grey-cerebellar link. *J. Physiol.* **592**, 2197–2213 (2014).
25. Farley, S. J., Radley, J. J. & Freeman, J. H. Amygdala modulation of cerebellar learning. *J. Neurosci.* **36**, 2190–2201 (2016).
26. Vaaga, C. E., Brown, S. T. & Raman, I. M. Cerebellar modulation of synaptic input to freezing-related neurons in the periaqueductal gray. *eLife* **9**, e54302 (2020).
27. Sacchetti, B., Scelfo, B., Tempia, F. & Strata, P. Long-term synaptic changes induced in the cerebellar cortex by fear conditioning. *Neuron* **42**, 973–982 (2004).
28. Sacchetti, B., Baldi, E., Lorenzini, C. A. & Bucherelli, C. Cerebellar role in fear-conditioning consolidation. *Proc. Natl Acad. Sci. USA* **99**, 8406–8411 (2002).
29. Supple, W. F. Jr, Leaton, R. N. & Fanselow, M. S. Effects of cerebellar vermal lesions on species-specific fear responses, neophobia, and taste-aversion learning in rats. *Physiol. Behav.* **39**, 579–586 (1987).
30. Sacchetti, B., Scelfo, B. & Strata, P. Cerebellum and emotional behavior. *Neuroscience* **162**, 756–762 (2009).
31. Jackman, S. L. et al. Cerebellar Purkinje cell activity modulates aggressive behavior. *eLife* **9**, e53229 (2020).
32. Fujita, H., Kodama, T. & du Lac, S. Modular output circuits of the fastigial nucleus for diverse motor and nonmotor functions of the cerebellar vermis. *eLife* **9**, e58613 (2020).
33. Uusisaari, M. Y. & Knopfel, T. Diversity of neuronal elements and circuitry in the cerebellar nuclei. *Cerebellum* **11**, 420–421 (2012).
34. Alexander, G. M. et al. Remote control of neuronal activity in transgenic mice expressing evolved G protein-coupled receptors. *Neuron* **63**, 27–39 (2009).
35. Roth, B. L. DREADDs for neuroscientists. *Neuron* **89**, 683–694 (2016).
36. Vlasov, K., Van Dort, C. J. & Solt, K. Optogenetics and chemogenetics. *Methods Enzymol.* **603**, 181–196 (2018).
37. McGaugh, J. L. Memory–a century of consolidation. *Science* **287**, 248–251 (2000).
38. Popa, D., Duvarci, S., Popescu, A. T., Lena, C. & Pare, D. Coherent amygdalocortical theta promotes fear memory consolidation during paradoxical sleep. *Proc. Natl Acad. Sci. USA* **107**, 6516–6519 (2010).
39. Assareh, N., Bagley, E. E., Carrive, P. & McNally, G. P. Brief optogenetic inhibition of rat lateral or ventrolateral periaqueductal gray augments the acquisition of Pavlovian fear conditioning. *Behav. Neurosci.* **131**, 454–459 (2017).
40. Walker, R. A., Wright, K. M., Jhou, T. C. & McDannald, M. A. The ventrolateral periaqueductal grey updates fear via positive prediction error. *Eur. J. Neurosci.* **51**, 866–880 (2019).
41. Wright, K. M. & McDannald, M. A. Ventrolateral periaqueductal gray neurons prioritize threat probability over fear output. *eLife* **8**, e45013 (2019).
42. Groessl, F. et al. Dorsal tegmental dopamine neurons gate associative learning of fear. *Nat. Neurosci.* **21**, 952–962 (2018).
43. Timme, N. M. & Lapish C. A. Tutorial for information theory in neuroscience. *eNeuro* **5**, 12–16 (2018).
44. Likhtik, E., Stujenske, J. M., Topiwala, M. A., Harris, A. Z. & Gordon, J. A. Prefrontal entrainment of amygdala activity signals safety in learned fear and innate anxiety. *Nat. Neurosci.* **17**, 106–113 (2014).
45. Arico, C., Bagley, E. E., Carrive, P., Assareh, N. & McNally, G. P. Effects of chemogenetic excitation or inhibition of the ventrolateral periaqueductal gray on the acquisition and extinction of Pavlovian fear conditioning. *Neurobiol. Learn Mem.* **144**, 186–197 (2017).
46. Johansen, J. P., Tarpley, J. W., LeDoux, J. E. & Blair, H. T. Neural substrates for expectation-modulated fear learning in the amygdala and periaqueductal gray. *Nat. Neurosci.* **13**, 979–986 (2010).
47. Roy, M. et al. Representation of aversive prediction errors in the human periaqueductal gray. *Nat. Neurosci.* **17**, 1607–1612 (2014).
48. Ernst, T. M. et al. The cerebellum is involved in processing of predictions and prediction errors in a fear conditioning paradigm. *eLife* **8**, e46831 (2019).
49. Ohmae, S. & Medina, J. F. Climbing fibers encode a temporal-difference prediction error during cerebellar learning in mice. *Nat. Neurosci.* **18**, 1798–1803 (2015).
50. Berg, B. A., Schoenbaum, G. & McDannald, M. A. The dorsal raphe nucleus is integral to negative prediction errors in Pavlovian fear. *Eur. J. Neurosci.* **40**, 3096–3101 (2014).
51. Salinas-Hernandez, X. I. et al. Dopamine neurons drive fear extinction learning by signaling the omission of expected aversive outcomes. *eLife* **7**, e38818 (2018).
52. Jeon, D. et al. Observational fear learning involves affective pain system and Cav1.2 Ca2+ channels in ACC. *Nat. Neurosci.* **13**, 482–488 (2010).

53. Popa, D. et al. Functional role of the cerebellum in gamma-band synchronization of the sensory and motor cortices. *J. Neurosci.* **33**, 6552–6556 (2013).
54. Proville, R. D. et al. Cerebellum involvement in cortical sensorimotor circuits for the control of voluntary movements. *Nat. Neurosci.* **17**, 1233–1239 (2014).
55. Wollstadt, P. et al. IDTxl: The Information Dynamics Toolkit xl: a Python package for the efficient analysis of multivariate information dynamics in networks. *J. Open Source Softw.* **4**, 1081 (2018).
56. Apps, R. & Strata, P. Neuronal circuits for fear and anxiety - the missing link. *Nat. Rev. Neurosci.* **16**, 642 (2015).

## Acknowledgements

This work was supported by Fondation pour la Recherche Medicale (FRM, DPP20151033983) to D.P., and Agence Nationale de Recherche to D.P. (ANR-16-CE37-0003-02 Amedyst, ANR-19-CE37-0007-01 Multimod, Labex Memolife) and to C.L. (ANR-17-CE37-0009 Mopla, ANR-17-CE16-0019 Synpredict) and by the Institut National de la Santé et de la Recherche Médicale (France). I.A.G. was supported by the project 819/11.01.2019 by UMF Carol Davila, Bucharest. We thank the Imaging Facility at IBENS (IMACHEM-IBiSA, France-BioImaging ANR-10-INBS-04, FRC Rotary International France, Investments for the future, ANR-10-LABX-54 MEMOLIFE).

## Author contributions

J.L.F. and D.P. designed the experiments; J.L.F., C.L., and D.P. wrote the manuscript; J.L.F., R.W.S., and C.L. analyzed the data; and J.L.F., H.B.A., I.A.G., R.W.S., and C.M.H. performed the experiments.

## Competing interests

The authors declare no competing interests.

## Additional information

**Supplementary information** is available for this paper at https://doi.org/10.1038/s41467-020-18953-0.

**Correspondence** and requests for materials should be addressed to D.P.

**Peer review information** *Nature Communications* thanks the anonymous reviewer(s) for their contribution to the peer review of this work. Peer reviewer reports are available.

**Reprints and permission information** is available at http://www.nature.com/reprints

**Publisher's note** Springer Nature remains neutral with regard to jurisdictional claims in published maps and institutional affiliations.

# ANNEXE 2

# Functional abnormalities in the cerebello-thalamic pathways in an animal model of dystonia

Elena Laura Margarint[1,#], Hind Baba Aïssa[1,#], Andrés Pablo Varani[1], Romain Sala[1], Fabien Menardy[1], Assunta Pelosi[2,3,4], Denis Hervé[2,3,4], Clément Léna[1], Daniela Popa[1]

[1] Neurophysiology of Brain Circuits Team, Institut de biologie de l'Ecole normale supérieure (IBENS), Ecole normale supérieure, CNRS, INSERM, PSL Research University, 75005 Paris, France

[2] Inserm UMR-S 1270, 75005 Paris, France,

[3] *Sorbonne Université*, Sciences and Technology Faculty, Paris, France,

[4] *Institut du Fer à Moulin*, 75005 Paris, France

[#] These authors contributed equally to this work.

Correspondence should be addressed to D.P (daniela.popa@ens.fr).

One sentence summary: A mouse model of DYT25 dystonia, carrying a *Gnal* mutation disrupting striatal neurotransmission, exhibits anomalous cerebello-thalamic plasticity in the non-manifesting state, but theta-burst cerebellar stimulations during cholinergic-induced dystonia depress the cerebello-thalamic transmission and reduce the severity of the motor symptoms.

Author contributions: DP, CL and DH acquired funding; ELM, APV and DP conceived and designed the experiments; ELM, HBA, CL and DP wrote the initial manuscript; ELM, HBA, APV, RS, CL analyzed the data; ELM, HBA, APV, RS, FM, AP, DH generated the mouse model and/or performed the experiments. All authors interpreted results, revised the final manuscript, and approved the final manuscript.

Data, code and materials availability: The data and the code for electrophysiological analysis will be made available on the team website upon acceptance:
https://www.ibens.ens.fr/spip.php?rubrique53&lang=en

Acknowledgments: This work was supported by Agence Nationale de Recherche to D.P. and D.H. (ANR-16-CE37-0003 Amedyst) and to C.L. (ANR-17-CE37-0009 Mopla) and by the Labex Memolife and the Institut National de la Santé et de la Recherche Médicale (France). The authors declare no competing financial interests.

***ABSTRACT***

Dystonia is often associated with functional alterations in the cerebello-thalamic pathways, which have been proposed to contribute to the disorder by propagating pathological firing patterns to the forebrain. Here, we examined the function of the cerebello-thalamic pathways in a model of DYT25 dystonia, mice carrying a heterozygous invalidation of *Gnal* gene which notably disrupts striatal function, exhibiting dystonic movements and postures following systemic or striatal administration of oxotremorine. Theta-burst optogenetic stimulations of the cerebellar nuclei evoked a potentiation of the responses to cerebellar stimulations in the thalamus and motor cortex in WT mice, without evident motor function disruption. In contrast, theta burst stimulations evoked a depression of these responses only in dystonia-manifesting *Gnal*+/- mice after oxotremorine administration, decreased the disabling dystonia attacks, and increased normal active wake behaviour in *Gnal*+/- mice. The cerebellum could thus offer a gateway for a corrective treatment of motor impairments in dystonia including striatal dysfunction.

Keywords: cerebellum; electrophysiology; optogenetics, *Gnal*; thalamus, motor cortex; dystonia.

## *Introduction*

The purposeful motion of our body is central in the human activity, and neurological diseases altering motor function represent major clinical issues. Dystonias are characterized by involuntary muscle contractions that induce abnormal twisted positions and postures, or cause patterned or stereotyped movements (Albanese et al., 2013). Many primary dystonias have a hereditary component (Breakefield et al., 2008), but the penetrance of genetic forms of dystonia is variable and even in patients carrying identical mutation, symptoms vary in severity, age of onset, focal or generalized localization or progression (Fuchs and Ozelius, 2013; Dufke et al., 2014). This intrinsic variability in dystonia suggests the existence of interacting mechanisms that synergize or cancel out at different levels of the motor centres to determine symptom onset (Hendrix and Vitek, 2012; Prudente et al., 2014; Kaji et al., 2017).

Dysfunctions of the cerebellum and cerebello-cortical pathways have been implicated in dystonia (Neychev et al., 2011; Lehéricy et al., 2013). Patients with various forms of dystonia exhibit structural and functional alterations of the cerebellum as well as abnormalities in the cerebello-thalamic connections (Lehéricy et al., 2013). The relevance of the cerebellum in dystonia has also been demonstrated in animal models (Neychev et al., 2011). In three genetic models of dystonia *(dt* rat, tottering mouse and mouse with invalidation of type 1 inositol triphosphate receptor in the cerebellum/brainstem), the removal of the cerebellum, or only of the cerebellar Purkinje neurons or deep cerebellar nuclei (DCN), abolishes dystonic movements (LeDoux et al., 1993; LeDoux et al., 1995; Campbell et al., 1999; Neychev et al., 2008; Hensch et al., 2013). The down-regulation of the DYT1 gene, Torsin A, in the cerebellum is sufficient to trigger dystonia (Fremont et al., 2017). Neurons of the cerebellar nuclei can rapidly excite the dorsolateral striatum through a di-synaptic pathway with a relay in the centro-lateral (CL) nucleus of the thalamus (Chen et al., 2014). Aberrant cerebellar activity can

cause dystonia by dynamically forcing a pathological state via the cerebello-thalamo-striatal pathway (Calderon et al., 2011). Structural defects in the cerebello-thalamo-cortical pathway have been identified in a mouse model of DYT1 dystonia (Ulug et al., 2011), but they have been proposed to provide a protective effect and limit the penetrance of the disease in patients (Argyelan et al., 2009), consistent with the view that dystonias are brain motor network disorders, where dysfunction of one node results in dysfunctions/adaptations in the others.

Dystonia also derive from basal ganglia dysfunction. One example is the adult-onset DYT25 dystonia (Fuchs et al., 2013; Vemula et al., 2013; Pelosi et al., 2017), caused by loss-of-function mutations of the *GNAL* gene encoding $G\alpha_{olf}$, a G protein stimulating adenylate cyclase activity in the striatum. *Gnal* haplo-deficiency in mice mimics the genetic alterations discovered in DYT25 dystonic patients (Pelosi et al., 2017). *Gnal* haplo-deficiency reduces striatal cAMP production and disrupts striatal functions but the mice are asymptomatic in terms of dystonia. Dystonic symptoms were generated by injections of a muscarinic cholinergic agonist (oxotremorine M) systemically or in the striatum, but not in the cerebellum, indicating that an increase in striatal cholinergic tone is critical to the onset of disorder (Pelosi et al., 2017). The present study is aimed at examining the role of cerebello-thalamic tract and its plasticity in this model.

To study the functional connectivity in the cerebello-thalamic tract, we combined optogenetic stimulations in the cerebellar dentate nucleus with recordings in the thalamus and motor cortex, and with behavioural measures. Moreover, we probed the plasticity induced by cerebellar stimulations using theta-burst stimulation protocols. Indeed, transcranial theta-burst stimulations are used to treat various motor and non-motor disorders (Suppa et al., 2016; Jannati et al., 2017). When administered on the cerebellar cortex, they induce lasting changes of motor cortex excitability (Popa et al., 2010; Gallea et

al., 2013). Here, we investigated the behavioural and neurophysiological impacts of dentate nucleus (DN) low frequency or theta-burst frequency optogenetic stimulation on the centro-lateral (CL), ventro-anterior-lateral (VAL) thalamus, and motor (M1) cortex in both the pre-symptomatic (saline injection), and symptomatic states (oxotremorine injection), of *Gnal*+/- animal model of dystonia.

## Results:

### *Gnal*+/- mice do not have a constitutive locomotor impairment

Young 3 to 7-month-old mice *Gnal*+/- mice are asymptomatic (Pelosi et al., 2017) and to further verify that they do not exhibit constitutive motor deficit we performed a set of locomotor experiments including vertical pole, horizontal bar, grid test, fixed speed rotarod, gait test and an open-field test (Figure 1). Overall, we did not observe major motor deficits; however, mild effects were noted when the analysis was performed separately on males and females as reported below. A total of 16 *Gnal*+/- mice were studied, 12 males and 4 females. Regarding the wild-type (WT) mice, 19 mice were studied, 11 males and 8 females.

We observed that the motor performance of *Gnal*+/- mice was not impaired in the vertical pole test (Mann-Whitney test; $p = 0.176$ for males; $p = 0.246$ for females), horizontal bar test (Mann-Whitney test; $p = 0.487$ for males; $p = 0.134$ for females) and grid test (Mann-Whitney test; $p = 0.164$ for males; $p = 0.298$ for females).

We also performed a fixed speed rotarod test to test the motor coordination. We did not find significant differences between *Gnal*+/- and WT mice (Repeated measure ANOVA $F(1,4)=7.348$ $p = 0.053$), nor when comparing males and females for each speed steps (Student's T test Welsch corrected, with a Bonferroni correction for multitests, $p= 0.171$ for both males and females).

We performed the gait test and different parameters were computed. We were not able to find significant differences in gait width (Mann-Whitney test; p = 0.154 for males; p = 0.074 for females), alternation coefficient (Mann-Whitney test; p = 0.391 for males; p = 0.175 for females), linear movement (Mann-Whitney test; p = 0.221 for males; p = 0.101 for females) or sigma (Mann-Whitney test; p = 0.488 for males; p = 0.134 for females). However, the length of stride was significantly longer in *Gnal*+/- females compared to female WT mice (Mann-Whitney test; p = 0.007 for females; p = 0.322 for males).

We also studied both the average locomotor speed and the total distance travelled during an open-field session. We observed no significant differences when comparing *Gnal*+/- and WT males (Mann-Whitney test; p = 0.141 for the average speed; p = 0.203 for the distance travelled). However, we observed that both average speed and distance travelled were lower in females *Gnal*+/- compared to females WT (Mann-Whitney test; p = 0.037 for the average speed; p = 0.037 for the distance). In conclusion, motor activity and motor coordination are not dramatically impaired in young 3 to 7-month-old mice *Gnal*+/- mice as previously described (Pelosi et al., 2017); however, mild differences were observed in females only, raising the possibility of higher susceptibility in female mice.

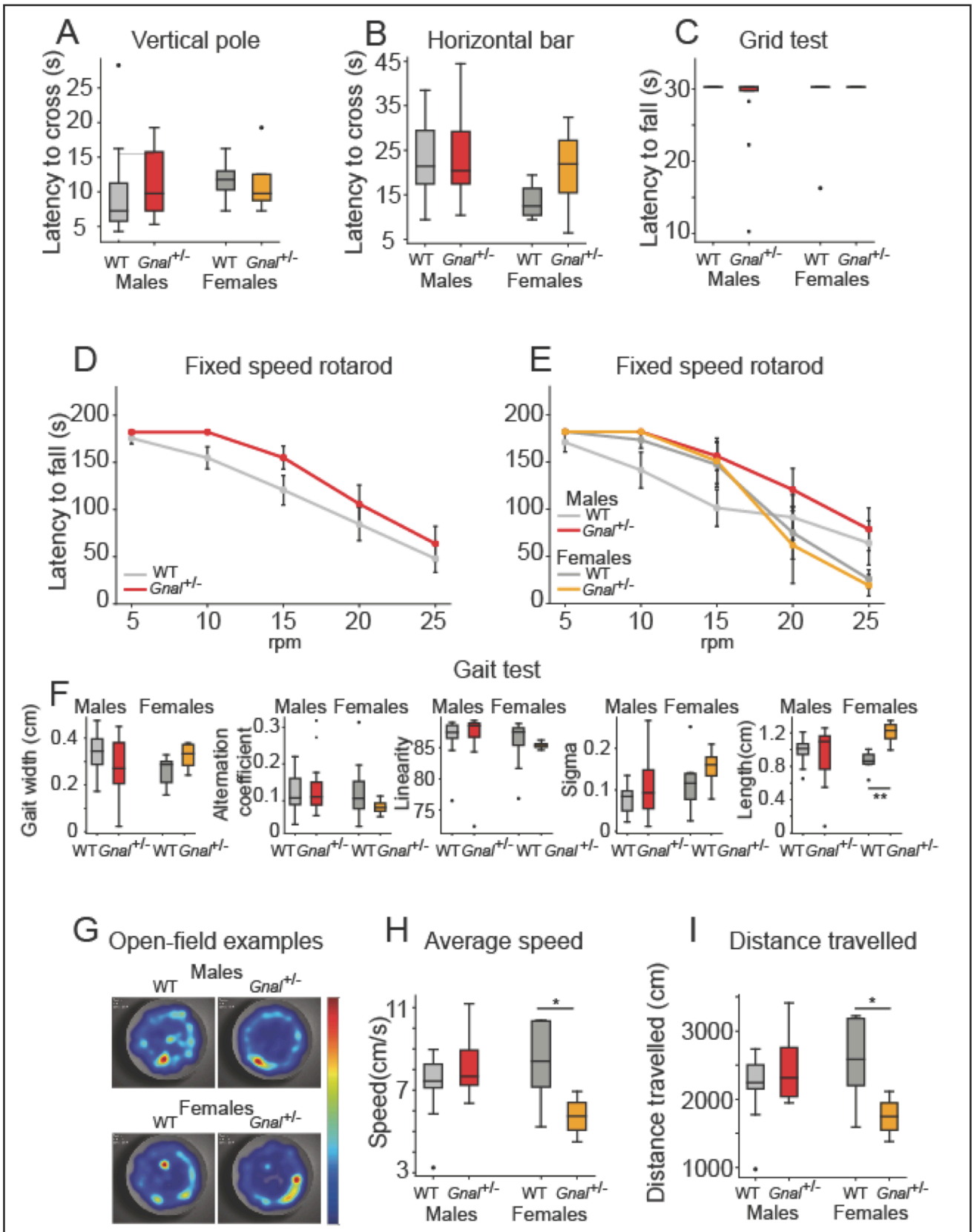


**Figure 1.** Locomotor activity and motor coordination in *Gnal*+/- mice. **(A)** Latency to cross the vertical pole; Mann-Whitney test. **(B)** Latency to cross the horizontal bar; Mann-Whitney test. **(C)** Latency to fall during the grid test with a 30s cut-off; Mann-Whitney test. **(D)** Latency to fall during the fixed speed rotarod test; Repeated measure ANOVA. **(E)** Latency to fall during the fixed speed rotarod test with groups separated by gender and genotype; Welch corrected Student's t test for each speed step, corrected for multitests using Bonferroni's method. **(F)** Gait width, alternation coefficient, movement linearity, sigma and stride length during the gait test; Mann-Whitney test *p<0.05; **p<0.01 **(G)** Example of heatmaps showing the position of mice during open-field sessions. Average speed **(H)** and total

**Thalamic and cortical activity, and coupling of the cerebellum to forebrain motor circuits in *Gnal*+/- mice**

The thalamus is the main gateway to the motor cortex and striatum, which are, together with the cerebellum, the main structures involved in dystonia. To examine the impact of the reduction of *Gnal* expression in the thalamus, we first examined the changes in neuronal activity in the motor thalamus (VAL), the striatum-projecting thalamus (CL) and the motor cortex (M1) in freely moving mice (Figure 2, Table 1). Saline injections in *Gnal*+/- mice did not induce abnormal motor patterns, consistent with previous observations (Pelosi et al., 2017). In these mice, we found no difference as compared to saline-injected wild type (WT) mice in the baseline firing rate of thalamic or cortical neurons (Figure 2E, ANOVA repeated measure VAL: $F(1,16)=0.19$, $p=0.67$, CL: $F(1,21)=0.21$, $p=0.65$, M1: $F(1,23)=0.033$, $p=0.86$; no difference was found when males and females were separated).

| | FR analysis | | | | Cb stim analysis | | | |
|---|---|---|---|---|---|---|---|---|
| | # cells | | # mice | | # cells | | # mice | |
| region | WT | HET | WT | HET | WT | HET | WT | HET |
| VAL | 179 | 221 | 8 | 10 | 23 | 21 | 3 | 4 |
| CL | 236 | 194 | 12 | 11 | 31 | 27 | 5 | 3 |
| M1 | 210 | 237 | 13 | 12 | 37 | 54 | 5 | 5 |

**Table 1**. Number of cells used in the analysis of baseline firing rate (Figure 2E) and of responses to cerebellar stimulation (Figure 3C,D,G,H).

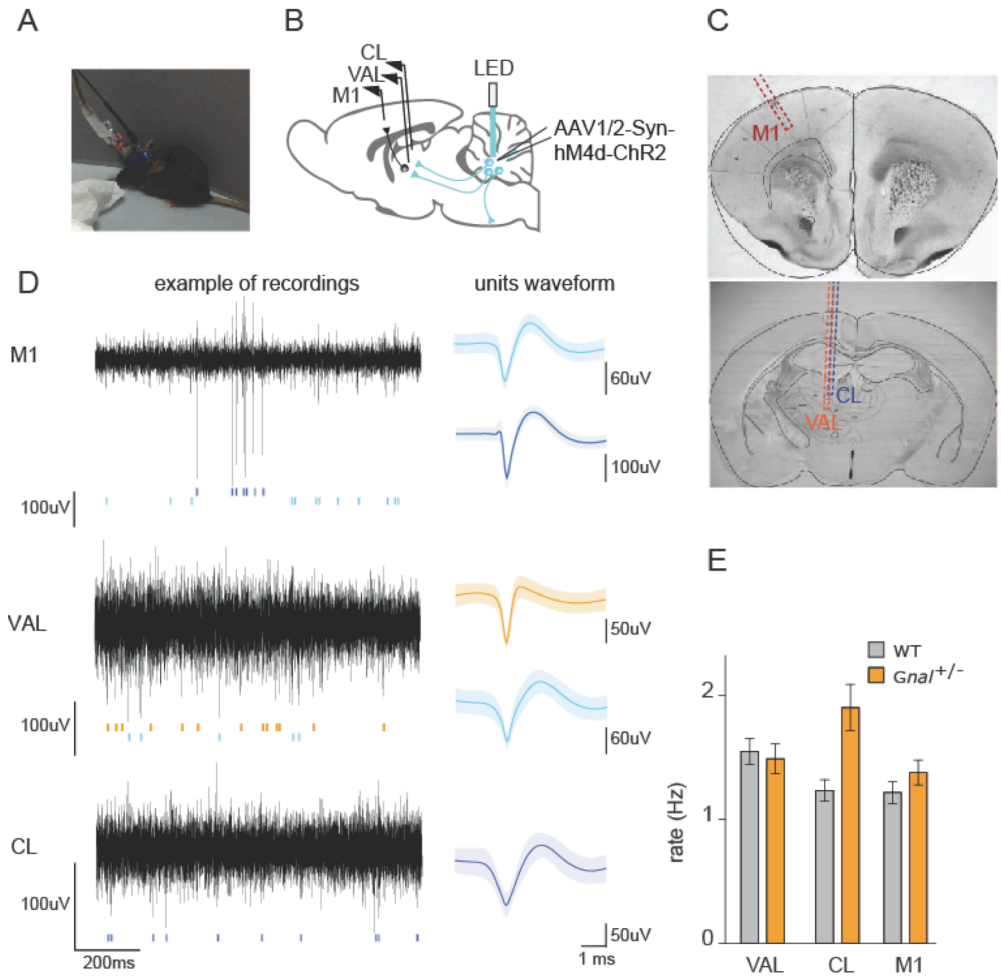


**Figure 2.** Electrophysiology recordings of ventro-lateral (VAL) and centro-lateral (CL) thalamic nuclei and motor cortex (M1). **(A)** Picture of a freely moving mouse during a recording coupled with optogenetic dentate (DN) stimulation. **(B)** Schematic of experimental design. Guide cannulas with bundles of electrodes were inserted in left M1 (motor cortex), CL (centro-lateral thalamus), VAL (ventro-lateral thalamus); an optic fibre was inserted in the right DN 3 weeks after AAV virus was injected. **(C)** Histology section showing the implantation sites. An atlas map is overlaid on the coronal sections to identify the targeted regions. **(D)** Left: excerpts of traces and spikes (colored bars); right: average ± SEM waveforms of VAL, CL and M1 neurons. **(E)** Average firing rate in freely moving WT and *Gnal*+/- mice.

To probe the functional drive of the cerebellum on these regions, we expressed channelrhodopsin 2 (ChR2) into DN neurons using an AAV viral strategy (AAV2/1.hSyn.ChR2(H134R)-eYFP.WPRE.hGH), and stimulated these neurons through an optical fibre implanted above the DN (Figure 2B, 2). We first applied simple low-frequency deep cerebellar stimulations (100ms, 0.25Hz,

156 0.9mW at the fibre entry), and we found an overall increase in firing rate of about 5 Hz during the
157 stimulation in all recorded regions in WT and in *Gnal*+/- saline-injected mice. We did not detect any
158 significant difference between the genotypes (Figure 3C, ANOVA with repeated measure in mice: CL:
159 $F(1,6)=1.057$, $p=0.343$), VAL: $F(1,5)=1.466$, $p=0.28$, M1: $F(1,8)=0.0395$, $p=0.847$). We then performed
160 oxotremorine M administration (0.1 mg/kg, i.p.) and observed an increase in the evoked responses to
161 cerebellar stimulation in all the structures studied in both the WT and *Gnal*+/- genotypes (Figure 3G,
162 Table 2).

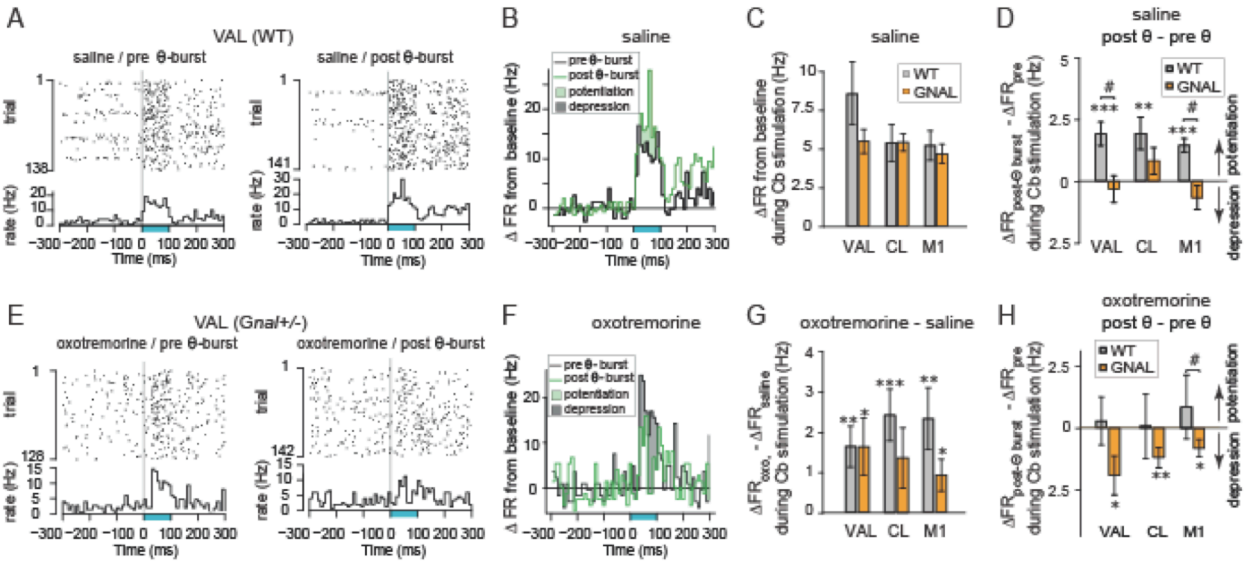


**Figure 3.** Effect of low-frequency and theta-burst cerebellar stimulations on the firing rate in saline and oxotremorine conditions in VAL, CL and M1 of WT and *Gnal+/-* mice. On the first day, we examined the effects of low frequency opto-stimulations (blue line, 100ms, 0.25Hz) on the firing rate of neurons in the various brain regions after saline and oxotremorine administrations. On the following day, the effects of the same low frequency stimulation were compared before and after θ-burst stimulations (20ms, 8,33Hz, applied for 2 x 40s with a 2 min pause in between) after saline and oxotremorine administrations. **(A)** Raster and peristimulus time histogram (PSTH, bin 10 ms) for one VAL neuron from a WT mouse before (left) and after (right) theta-burst stimulation in saline condition; the PSTH are normalized to express a firing rate (see Methods). **(B)** Overlay of the PSTHs from the panel A; the difference between the histograms is filled to evidence the potentiation or depression of the responses. In this case potentiation prevails. See Table 1 for number of cells/mice used. **(C)** Increase in firing rate (relative to the baseline firing rate) induced by 100 ms DN nucleus stimulations in WT and *Gnal+/-* animals. **(D)** Impact of theta-burst stimulations administered in saline condition on the response to 100 ms DN stimulation. Note the absence of potentiation in *Gnal+/-* mice. **(E) (F)** same as (A) and (B) respectively, for a VAL neuron from a *Gnal+/-* mouse before and after theta-burst stimulation in the oxotremorine condition. **(G)** effect of oxotremorine administration on the response to cerebellar stimulations. **(H)** Impact of theta-burst stimulations on the response to 100 ms DN stimulation (same as (D)) in the oxotremorine condition. See Table 2 for corresponding repeated measures ANOVAs. *p<0.05, **p<0.01, ***p<0.001 paired difference between conditions for the cells, #p<0.05 difference between *Gnal+/-* and WT mice. Error bars represent SEM.

To examine the plasticity of the cerebello-thalamic pathways, we then studied the impact of optogenetic theta-burst stimulations (given the limited number of cells, males and females were not

166 studied separately). In the saline condition, the response to low-frequency stimulations was significantly
167 increased in CL, VAL (Figure 3A,B) and M1 after theta-burst stimulations in the wild type mice, while no
168 significant change was found in the *Gnal*+/- mice (Figure 3D, Table 1 & 2). The difference between wild
169 type and Gnal+/- mice was clearly significant in VAL and M1 (Figure 3D, Table 1 & 2). In contrast,
170 following oxotremorine administration, the responses to cerebellar low-frequency stimulations were
171 not changed in wild type mice after theta-burst stimulations, while they were decreased in *Gnal*+/- mice
172 in all the structures considered : CL, VAL (Figure 3E,F) and M1 (Figure 3H, Table 1 & 2), suggesting a
173 weaker entrainment of the motor circuit by the cerebellum during dystonic-like attacks induced by
174 oxotremorine in *Gnal*+/- mice. The increase (potentiation) (Figure 3A,B) or decrease (depression) (Figure
175 3E,F) in firing rate were observed throughout the duration of the stimulation (Figure 3B,F).

| | | REGION RECORDED | | |
|---|---|---|---|---|
| TREATMENT | CONDITION | VAL | CL | M1 |
| Oxotremorine | WT | F(1,22)=10.38 P=0.003928 | F(1,30)=14.45 P=0.0006566 | F(1,36)=9.025 P=0.004824 |
| | GNAL +/- | F(1,20)=5.184 P=0.03394 | F(1,26)=3.301 P=0.08076 | F(1,53)=5.283 P=0.0255 |
| | Genotype ≠ | F(1,40)=0.1006 P=0.7527 | F(1,51)=1.214 P=0.2758 | F(1,80)=0.2567 P=0.6138 |
| Saline + θ-burst | WT | F(1,22)=16.11 P=0.0005835 | F(1,30)=8.812 P=0.005834 | F(1,36)=27 P=8.229e-06 |
| | GNAL+/- | F(1,20)=0.3588 P=0.5559 | F(1,26)=2.258 P=0.145 | F(1,53)=1.96 P=0.1674 |
| | Genotype ≠ | F(1,37)=4.791 P=0.03499 | F(1,48)=0.2916 P=0.5917 | F(1,78)=4.047 P=0.04771 |
| Oxo+ θ-burst | WT | F(1,22)=0.0858 P=0.7723 | F(1,30)=0.003561 P=0.9528 | F(1,36)=0.442 P=0.5104 |
| | GNAL+/- | F(1,20)=5.928 P=0.0244 | F(1,26)=8.154 P=0.008334 | F(1,53)=5.459 P=0.02329 |
| | Genotype ≠ | F(1,40)=2.681 P=0.1094 | F(1,53)=0.3898 P=0.5351 | F(1,84)=5.075 P=0.02688 |

**Table 2.** Repeated measure ANOVA for the increase in firing rate induced by low-frequency dentate stimulations in the VAL and CL thalamus, and motor cortex M1 in saline/oxotremorine conditions and before/after theta-burst stimulations.

176

177 **Beneficial effect on motor activity of the optogenetic stimulation in the cerebellar dentate nucleus of**
178 ***Gnal*+/- mice**

179 Taking advantage of chronic implanted animals, we then evaluated the dystonic behaviour in
180 *Gnal*+/- compared to WT mice using an abnormal motor score (Fremont et al., 2017; Pelosi et al., 2017;
181 White and Sillitoe, 2017). Saline-injected *Gnal*+/- and WT mice showed no signs of dystonia; in contrast,

the muscarinic cholinergic agonist, oxotremorine M (0.1 mg/kg), consistently induced abnormal postures such as extension of hind limbs from the body axis for >10 s, sustained hunched posture with little movements, slow walking with increased hind limb gait yielding maximal dystonia scores in all implanted *Gnal*+/- mice and only mild motor signs in wild type mice (Figure 4A,B). These observations are consistent with the previous observations in *Gnal*+/- mice (Pelosi et al., 2017) and indicate that the chronic implantation did not impact the development of dystonic-type motor abnormalities.

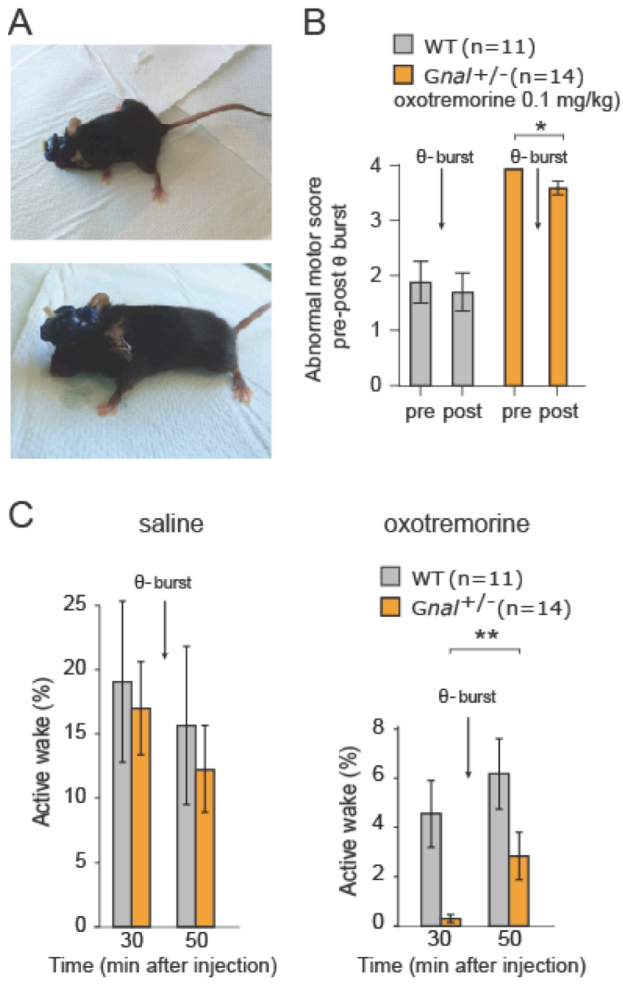


**Figure 4.** Motor behaviour of *Gnal*+/- (orange) and wild type (WT) mice (grey). **(A)** Examples of dystonic postures in *Gnal*+/- mice following oxotremorine administration. **(B)** Average dystonia scores in *Gnal*+/- and WT mice following oxotremorine administration before and after dentate nucleus (DN) theta burst stimulation **(C)** Change of average active wakefulness percentage after DN theta burst stimulation in *Gnal*+/- and WT mice after saline or oxotremorine administration. Data were analysed by Student t test. *p<0.05, **p<0.01 difference between pre and post theta-burst stimulations. Error bars represent SEM.

To test the impact of cerebellar stimulations on abnormal movements, the evolution of dystonic-like movements and postures was evaluated before and after the DN optogenetic theta stimulations (Figure 4A,B). DN optogenetic theta-burst stimulations decreased the abnormal motor behaviour in *Gnal*+/- mice following oxotremorine M challenge (Wilcoxon matched-pairs signed rank test; P=0.0313). To confirm these observations, we also evaluated the activity of the mice by measuring the percentage of time spent moving in an open-field ("active wakefulness") (Georgescu et al., 2018). In the saline-treated wild type mice, DN optogenetic theta burst stimulations had no significant effect (30 to 50 min after saline injection) on the active wake time. Similarly, in the saline-treated *Gnal*+/- mice, theta-burst stimulation did not significantly change the active wake time (Figure 4C). In contrast, in the oxotremorine condition, the average active wake time decreased in both wild type and *Gnal*+/- mice compared to saline, the effect being more marked in the mutant mice (Figure 4C). One session of DN optogenetic theta-burst stimulation was sufficient to significantly increase the wake time in *Gnal*+/- mice (p=0.0099) while the increase remained non-significant in wild type mice (Figure 4C). Overall, these results indicate that DN optogenetic theta-burst stimulations decrease the "dystonic" phenotype in oxotremorine-treated *Gnal*+/- mice regarding both the abnormal motor scores and locomotor activity deficit.

Overall, these results indicate a functional impairment of cerebello-thalamo-cortical pathway in *Gnal*+/- mice, which is revealed by a loss of potentiation following theta-burst stimulations in saline conditions. These stimulations decrease cerebello-thalamic connectivity during dystonic-like attacks in *Gnal*+/- mice and reduced the dystonic signs.

## *Discussion*

In the present study, we investigated the behaviour and functional coupling of the dentate (DN) nucleus of cerebellum to the thalamus and motor cortex M1 in basal condition and during dystonic-like state triggered pharmacologically in the *Gnal*+/- animal model. We confirmed the presence of dystonic-like movements and postures in these mutant mice after oxotremorine, a muscarinic cholinergic agonist. We found little if any change in locomotor activity or motor coordination and in baseline firing rate in the thalamus and M1 cortex between *Gnal*+/- and control mice. Theta-burst cerebellar DN stimulations induced potentiation of cerebello-thalamic pathways in wild type mice, but not in *Gnal*+/- mice suggesting a functional alteration of the cerebello-thalamic pathways in these mice. In contrast, theta-burst stimulation of cerebello-thalamic pathway induced a depression of the cerebello-thalamic connections after oxotremorine administration in G*nal*+/- mice (but not in WT mice). Such changes might prevent the propagation of the abnormal activity of the cerebellum to motor circuits in the *Gnal*+/- mice in oxotremorine condition. Indeed, theta-burst stimulation of the DN cerebellar nucleus decreased oxotremorine-induced dystonic-like motor abnormalities and increased normal active behaviour (active wakefulness) in *Gnal*+/- mice.

### Dystonia and cerebello-thalamic pathways

Despite the strength of the association between dystonia and basal ganglia (BG) demonstrated by numerous studies in both patients and animals (Köhling et al., 2004; Hallett, 2006; Fujita and Eidelberg, 2017; Simonyan et al., 2017; Huebl et al., 2018), the advances in neuroimaging approaches and electrophysiology have provided evidence that regions outside the BG are also involved. The dystonia should then be viewed as a “circuit disorder” (Lehéricy et al., 2013) spreading over a network

of brain motor regions. It is now established that the cerebellum is part of this network, since compelling evidence shows that disruption of cerebellar output causes dystonia (Pizoli et al., 2002; Raike et al., 2013). Abnormal cerebellar nuclei bursting activities were observed in several animal models of dystonia such as DYT1 (Fremont et al., 2017) Tewari et al., 2017), genetic disruption of the olivo-cerebellar circuit (White and Sillitoe, 2017) or Na+/K+-ATPase α3+/D801Y mutant mice (Fremont et al., 2015; Isaksen et al., 2017). These activities are thought to rely on a pathway joining the cerebellum to the CL thalamus and striatum to propagate pathological activities (Calderon et al., 2011). This cerebello-thalamo-striatal pathway seems to be a key player in such forms of dystonia: imaging studies in DYT1 and DYT6 gene carriers and patients suggested a decreased connectivity between the cerebellum and thalamus and a disruption of cerebellum output that could play a significant role in the appearance of the dystonia (Carbon et al., 2008; Argyelan et al., 2009). If cerebellar dysfunction may disrupt basal ganglia function, the reverse has received little attention so far.

Here we studied the *Gnal*+/- mouse model of the adult-onset dystonia DYT25 (Pelosi et al., 2017). The *Gnal* gene encodes the α subunit of the heterotrimeric G-protein Golf, which is an essential relay in dopamine and adenosine transmission onto the adenylyl cyclase in the striatum. Gnal+/- mice are also characterized by abnormal responses of striatal cholinergic interneurons (Eskow Jaunarajs et al., 2019). Despite the reduced production of striatal cAMP in these mice, we found no innate motor impairment in *Gnal*+/- mice for males and only a mild difference for females, in various motor tests (vertical pole, horizontal bar, grid test, fixed speed rotarod, gait test and open-field locomotor experiments). Therefore, these mice exhibit no overt motor deficit in baseline condition, which may correspond to a 'presymptomatic' state. Oxotremorine injections in these mice -performed either systemically or locally into the striatum- induce strong dystonic-like syndrome compared to wild type mice(Pelosi et al., 2017). Under oxotremorine, these mice are likely representing a model of dystonia

caused by striatal primary dysfunction, offering an opportunity to examine the function of the cerebello-thalamic connection in such model.

We did not find any differences in the spontaneous firing activity between wild type and *Gnal*+/- mice in CL and VAL thalamus or M1 cortex, indicating an absence of overt baseline deficits. Oxotremorine injections mildly increased the average firing rate in all structures, but there was no strong difference between wild type and *Gnal*+/- mice. Examining the activity evoked in these brain regions by cerebellar stimulation failed also to reveal overt differences, although changes in cerebello-thalamic efficiency might be concealed by the variability of parameters of the experiments (e.g. variability in ChR2 expression, in optical fiber positioning). Indeed, our plasticity experiments using theta-burst stimulations in the DN nucleus of the cerebellum revealed clear differences in the cerebello-thalamic pathway of *Gnal*+/- mice, with a lack of potentiation in the saline condition, and a depression - not observed in wild type mice- in the oxotremorine condition. These results suggest a saturation of potentiation of the cerebello-thalamic pathway of *Gnal*+/- mice, which could be reversed by stimulations in the oxotremorine condition. Such changes in plasticity and saturation are also found in the striatum in motor disorders (Calabresi et al., 2016). These anomalous plasticities might result from compensatory alterations to the striatal dysfunction induced by oxotremorine in *Gnal*+/- mice (Pelosi et al., 2017). Our results are consistent with those of White and Sillitoe (2017), who demonstrated in a model of dystonia caused by silencing the olivo-cerebellar transmission, that high frequency electrical stimulations of the interposed cerebellar nuclei decreased the dystonia-like behaviour of mice, an effect reproduced by cerebellar lidocaine inhibition consistent with an inhibitory effect of stimulations (White and Sillitoe, 2017).

***Cerebellar theta-burst stimulations and dystonia***

The rationale of using theta-burst stimulation derives from human studies, where lasting changes in excitability have been shown to be induced by such stimulations (Huang et al., 2005). Transcranial cerebellar stimulations are known to affect within few milliseconds both the inhibition and excitation in the motor cortex networks (Daskalakis et al., 2004), presumably via the di-synaptic excitatory connection linking the cerebellum to the motor cortex via the ventral thalamus (Allen and Tsukahara, 1974; Iwata and Ugawa, 2005). Theta-burst protocols applied to the cerebellum have then been found to induce long-lasting changes in motor response to motor cortex stimulations (Koch et al., 2008).

Cerebellar stimulations in dystonic patients have been mostly performed in the context of focal dystonia (cervical or hand) with good results for cervical dystonia. During a sham-controlled trial on cervical dystonic patients, Koch et al. have applied two-weeks of continuous theta-burst stimulation (TBS) and transcranial magnetic stimulation (TMS) and reported a clinical improvement of 15% at the end of the trial (Koch et al., 2014). No effect was observed in hand focal dystonia (Hubsch et al., 2013; Linssen et al., 2015; França et al., 2018), but an insufficient number of repetition may be responsible for the lack of effect (Meunier et al., 2015). The stimulations are administered on the cerebellar cortex, so the site(s) of plasticity responsible for the improvement of the patient's condition is unknown. In healthy individuals, transcranial cerebellar stimulations modulate the cortical plasticity in a paired-associative stimulation (PAS) paradigm (Hamada et al., 2012), and theta burst cerebellar stimulations may modulate the PAS remotely in time (Popa et al., 2013), indicating that the cerebellum controls cortical plasticity. Interestingly in patients with cervical dystonia, the impact of cerebellar manipulations on cortical plasticity was reversed compared to healthy controls (Popa et al., 2018). Our experiments suggest that theta-burst stimulations may also impact the cerebello-thalamic pathway, but as in cervical dystonia (Popa et al., 2018), stimulations reversing the cerebello-thalamic plasticity anomaly improve the mouse motor function, suggestive that manipulations aimed at recruiting cerebello-thalamic plasticity could be

a relevant therapeutic strategy.

***Control of striatal cholinergic interneurons by thalamo-striatal inputs (BG-CB interaction)***

The striatum has been shown to receive di-synaptic inputs from the cerebellum (Bostan et al., 2013), and these inputs are presumably relayed to a large part through the intralaminar thalamus CL (Ichinohe et al., 2000; Chen et al., 2014). These nuclei also send strong projections to the dorsal striatum while only modestly contributing to the innervation of the cerebral cortex (Smith et al., 2014). The principal synaptic targets of the thalamic nuclei in the striatum are the dendritic spines of the medium spiny neurons (MSNs), but they also engage cholinergic interneurons in a feed-forward regulation that differentially control the populations of MSNs expressing the D1 dopamine receptors and exerting pro-kinetic effect, and the MSNs expressing the D2 receptors and exerting an anti-kinetic effect (Ding et al., 2010). Brief stimulations of thalamic input generate in cholinergic interneurons, a burst-pause firing pattern that transiently suppresses cortical drive of the two types of MSNs and then creates a second-long period in which activity in D2-expressing MSNs is increased, producing a potent suppression of action. Since salient sensory stimuli activate intralaminar thalamic neurons, Surmerier and coll. proposed that these processes could be a key component of the physiological responses elicited in the striatum by salient sensory stimuli (Ding et al., 2010; Smith et al., 2014). These responses would produce a cessation of ongoing motor activity and later enable switching to different actions. Interestingly, in mice with the DYT1 dystonia mutation, brief stimulations of thalamo-striatal inputs, mimicking an effect of salient events, evoke abnormal responses in cholinergic interneurons, leading to an altered cortico-striatal synaptic activity of MSNs (Sciamanna et al., 2012). However, these abnormalities are probably related to a predisposition to dystonia rather than to dystonia manifestations since the animal model is essentially asymptomatic. In the *Gnal*+/- dystonia model, the dystonic state is induced by a cholinergic pharmacological activation (Pelosi et al., 2017), which likely produces a severe imbalance in the

329 activities of the two populations of MSNs. The "anti-dystonic" effects we induced by stimulations of
330 cerebellar output in the dentate nucleus of *Gnal*+/- mice might rely on a reduction of these alterations.
331 However, understanding the mechanisms at play will probably require solving the complex rules of
332 synaptic plasticity in the striatum (reviewed in Perrin and Venance, 2019).

333 In conclusion, our study investigates an original model of dystonia that mimics the genetic
334 alterations discovered in DYT25 dystonic patients, a subtype of dystonia that has not yet been studied in
335 detail. Despite the fact that the striatum is likely the primary origin of functional alterations (Pelosi et al.,
336 2017), our study revealed abnormalities in cerebello-thalamic pathways in *Gnal*+/- mice with different
337 plasticity properties in asymptomatic mice (in which dysfunctions are compensated) and during
338 dystonia-like state (in response to oxotremorine). The identification of patterns of cerebellar stimulation
339 maximizing the depression of the cerebello-thalamic pathway could thus potentially improve the
340 strategies for therapeutic interventions in patients.

## *References*

Albanese A, Bhatia K, Bressman SB, DeLong MR, Fahn S, Fung VSC, Hallett M, Jankovic J, Jinnah A, Klein C, Lang AE, Mink JW, Teller JK (2013) Phenomenology and classification of dystonia: A consensus update. Movement Disorders 28:863-873.

Allen GI, Tsukahara N (1974) Cerebrocerebellar. Cerebrocerebellar communication systems 54.

Argyelan M, Carbon M, Niethammer M, Ulug AM, Voss HU, Bressman SB, Dhawan V, Eidelberg D (2009) Cerebellothalamocortical Connectivity Regulates Penetrance in Dystonia. Journal of Neuroscience 29:9740-9747.

Bostan AC, Dum RP, Strick PL (2013) Cerebellar networks with the cerebral cortex and basal ganglia. Trends in Cognitive Sciences 17:241-254.

Breakefield XO, Blood AJ, Li Y, Hallett M, Hanson PI, Standaert DG (2008) The pathophysiological basis of dystonias. Nature Reviews Neuroscience 9:222-234.

Calabresi P, Pisani A, Rothwell J, Ghiglieri V, Obeso JA, Picconi B (2016) Hyperkinetic disorders and loss of synaptic downscaling. Nature neuroscience 19:868-875.

Calderon DP, Fremont R, Kraenzlin F, Khodakhah K (2011) The neural substrates of rapid-onset Dystonia-Parkinsonism. Nature neuroscience 14:357-365.

Campbell DB, North JB, Hess EJ (1999) Tottering mouse motor dysfunction is abolished on the Purkinje cell degeneration (pcd) mutant background. Experimental Neurology 160:268-278.

Carbon M, Ghilardi MF, Argyelan M, Dhawan V, Bressman SB, Eidelberg D (2008) Increased cerebellar activation during sequence learning in DYT1 carriers: an equiperformance study. Brain 131:146-154.

Chen CH, Fremont R, Arteaga-Bracho EE, Khodakhah K (2014) Short latency cerebellar modulation of the basal ganglia. Nature neuroscience 17:1767-1775.

Daskalakis ZJ, Paradiso GO, Christensen BK, Fitzgerald PB, Gunraj C, Chen R (2004) Exploring the connectivity between the cerebellum and motor cortex in humans. Journal of Physiology 2:689-700.

Ding JB, Guzman JN, Peterson JD, Goldberg JA, Surmeier DJ (2010) Thalamic gating of corticostriatal signaling by cholinergic interneurons. Neuron 67:294-307.

Dufke C, Sturm M, Schroeder C, Moll S, Ott T, Riess O, Bauer P, Grundmann K (2014) Screening of mutations in GNAL in sporadic dystonia patients. Movement Disorders 29:1193-1196.

Eskow Jaunarajs KL, Scarduzio M, Ehrlich ME, McMahon LL, Standaert DG (2019) Diverse Mechanisms Lead to Common Dysfunction of Striatal Cholinergic Interneurons in Distinct Genetic Mouse Models of Dystonia. J Neurosci 39:7195-7205.

França C, de Andrade DC, Teixeira MJ, Galhardoni R, Silva V, Barbosa ER, Cury RG (2018) Effects of cerebellar neuromodulation in movement disorders: A systematic review. Brain Stimulation.

Fremont R, Tewari A, Khodakhah K (2015) Aberrant Purkinje cell activity is the cause of dystonia in a shRNA-based mouse model of Rapid Onset Dystonia- Parkinsonism Rachel. Neurobiol Disorders 82:200-212.

Fremont R, Tewari A, Angueyra C, Khodakhah K (2017) A role for cerebellum in the hereditary dystonia DYT1. eLife.

Fuchs T, Ozelius LJ (2013) Genetics in dystonia: An update topical collection on movement disorders. Current Neurology and Neuroscience Reports.

Fuchs T, Saunders-Pullman R, Masuho I, Luciano MS, Raymond D, Factor S, Lang AE, Liang TW, Trosch RM, White S, Ainehsazan E, Hervé D, Sharma N, Ehrlich ME, Martemyanov KA, Bressman SB, Ozelius LJ (2013) Mutations in GNAL cause primary torsion dystonia. Nature Genetics 45:88-92.

Fujita K, Eidelberg D (2017) Imbalance of the direct and indirect pathways in focal dystonia: a balanced view. Brain 140:3069-3080.

Gallea C et al. (2013) Cerebellar rTMS stimulation may induce prolonged clinical benefits in essential tremor, and subjacent changes in functional connectivity: An open label trial. Brain Stimulation 6:175-179.

Georgescu EL, Georgescu IA, Zahiu DC, Morozan VP, Pana A, Zagrean A-m, Popa D, Zahiu CDM, Pană AŞ, Georgescu IA, Georgescu EL, Ştеopoaie AR, Popa D, Zăgrean A-M, Morozan VP (2018) Oscillatory cortical

activity in an animal model of dystonia caused by cerebellar dysfunction. Frontiers in Cellular Neuroscience 12:1-23.

Hallett M (2006) Pathophysiology of Dystonia. J Neural Transm (2006) 70:485-488.

Hamada M, Strigaro G, Murase N, Sadnicka A, Galea JM, Edwards MJ, Rothwell JC (2012) Cerebellar modulation of human associative plasticity. J Physiol 590:2365-2374.

Hendrix CM, Vitek JL (2012) Toward a network model of dystonia. Annals of the New York Academy of Sciences.

Hensch TK, Ogawa N, Hirono M, Yamada M, Miyamoto H, Hattori M, Yamaguchi N, Mikoshiba K, Hisatsune C, Ohshima T, Sugawara T, Ebisui E (2013) IP3R1 deficiency in the cerebellum/brainstem causes basal ganglia-independent dystonia by triggering tonic Purkinje cell firings in mice. Frontiers in Neural Circuits.

Huang YZ, Edwards MJ, Rounis E, Bhatia KP, Rothwell JC (2005) Theta burst stimulation of the human motor cortex. Neuron 45:201-206.

Hubsch C, Roze E, Popa T, Russo M, Balachandran A, Pradeep S, Mueller F, Brochard V, Quartarone A, Degos B, Vidailhet M, Kishore A, Meunier S (2013) Defective cerebellar control of cortical plasticity in writer's cramp. Brain : a journal of neurology 136:2050-2062.

Huebl J, Poshtiban A, Brücke C, Siegert S, Bock A, Koziara H, Kmiec T, Rola R, Mandat T, Kühn AA (2018) Subthalamic and pallidal oscillatory activity in patients with Neurodegeneration with Brain Iron Accumulation type I (NBIA-I). Clinical Neurophysiology.

Ichinohe N, Mori F, Shoumura K (2000) Short communication A di-synaptic projection from the lateral cerebellar nucleus to the laterodorsal part of the striatum via the central lateral nucleus of the thalamus in the rat. Brain Research 880:191-197.

Isaksen TJ, Kros L, Vedovato N, Holm TH, Vitenzon A, Gadsby DC, Khodakhah K, Lykke-Hartmann K (2017) Hypothermia-induced dystonia and abnormal cerebellar activity in a mouse model with a single disease-mutation in the sodium-potassium pump. PLoS Genetics 13.

Iwata NK, Ugawa Y (2005) The effects of cerebellar stimulation on the motor cortical excitability in neurological disorders: A review. Cerebellum 4:218-223.

Jannati A, Block G, Oberman LM, Rotenberg A, Pascual-Leone A (2017) Interindividual variability in response to continuous theta-burst stimulation in healthy adults. Clinical Neurophysiology 128:2268-2278.

Jinnah HA, Sepkuty JP, Ho T, Yitta S, Drew T, Rothstein JD, Hess EJ (2000) Calcium channel agonists and dystonia in the mouse. Mov Disord 15:542-551.

Kaji R, Bhatia K, Graybiel AM (2017) Pathogenesis of dystonia: is it of cerebellar or basal ganglia origin? Journal of Neurology, Neurosurgery & Psychiatry:jnnp-2017-316250.

Koch G, Porcacchia P, Ponzo V, Carrillo F, Cáceres-Redondo MT, Brusa L, Desiato MT, Arciprete F, Di Lorenzo F, Pisani A, Caltagirone C, Palomar FJ, Mir P (2014) Effects of two weeks of cerebellar theta burst stimulation in cervical dystonia patients. Brain Stimulation 7:564-572.

Koch G et al. (2008) Clinical Neurophysiology Changes in intracortical circuits of the human motor cortex following theta burst stimulation of the lateral cerebellum. Clinical Neurophysiology 119:2559-2569.

Köhling R, Koch UR, Hamann M, Richter A (2004) Increased excitability in cortico-striatal synaptic pathway in a model of paroxysmal dystonia. Neurobiology of Disease 16:236-245.

LeDoux MS, Lorden JF, Ervin JM (1993) Cerebellectomy eliminates the motor syndrome of the genetically dystonic rat. Exp Neurol 120:302-310.

LeDoux MS, Lorden JF, Meinzen-Derr J (1995) Selective elimination of cerebellar output in the genetically dystonic rat. Brain Res 697:91-103.

Lehéricy S, Tijssen MAJ, Vidailhet M, Kaji R, Meunier S (2013) The anatomical basis of dystonia: Current view using neuroimaging. Movement Disorders 28:944-957.

Linssen MW, Gaalen JV, Munneke MAM, Hoffland BS, Hulstijn W, Warrenburg BPCVD, Van Gaalen J, Munneke MAM, Hoffland BS, Hulstijn W, Van De Warrenburg BPC, Van De Warrenburg BPC (2015) A single session of cerebellar theta burst stimulation does not alter writing performance in writer's cramp. Brain : a journal of neurology:1-5.

Meunier S, Roze E, Kishore A, Hubsch C, Popa T, Hubsch C, Roze E, Kishore A (2015) Reply: A single session of cerebellar theta burst stimulation does not alter writing performance in writer's cramp. Brain 138:e356.

Neychev VK, Fan X, Mitev VI, Hess EJ, Jinnah HA (2008) The basal ganglia and cerebellum interact in the expression of dystonic movement. Brain 131:2499-2509.

444 Neychev VK, Gross RE, Lehéricy S, Hess EJ, Jinnah HA (2011) The functional neuroanatomy of dystonia. In:
445 Neurobiology of Disease.
446 Paz R, Pelletier JG, Bauer EP, Paré D (2006) Emotional enhancement of memory via amygdala-driven facilitation of
447 rhinal interactions. Nature neuroscience 9:1321-1329.
448 Pelosi A, Menardy F, Popa D, Girault J-A, Hervé D (2017) Heterozygous Gnal Mice Are a Novel Animal Model with
449 Which to Study Dystonia Pathophysiology. The Journal of Neuroscience 37:6253-6267.
450 Perrin E, Venance L (2019) Bridging the gap between striatal plasticity and learning. Curr Opin Neurobiol 54:104-
451 112.
452 Pizoli CCECCE, Jinnah HAH, Billingsley MLMML, Hess EEJ (2002) Abnormal cerebellar signaling induces dystonia in
453 mice. The Journal of neuroscience : 22:7825-7833.
454 Popa T, Russo M, Meunier S (2010) Long-lasting inhibition of cerebellar output. Brain Stimul 3:161-169.
455 Popa T, Velayudhan B, Hubsch C, Pradeep S, Roze E, Vidailhet M, Meunier S, Kishore A (2013) Cerebellar
456 processing of sensory inputs primes motor cortex plasticity. Cereb Cortex 23:305-314.
457 Popa T, Hubsch C, James P, Richard A, Russo M, Pradeep S, Krishan S, Roze E, Meunier S, Kishore A (2018)
458 Abnormal cerebellar processing of the neck proprioceptive information drives dysfunctions in cervical
459 dystonia. Scientific Reports.
460 Prudente CN, Hess EJ, Jinnah HA (2014) Dystonia as a network disorder: What is the role of the cerebellum?
461 Neuroscience 260:23-35.
462 Raike RS, Pizoli CE, Weisz C, van den Maagdenberg AMJM, Jinnah HA, Hess EJ (2013) Limited regional cerebellar
463 dysfunction induces focal dystonia in mice. Neurobiology of disease 49:200-210.
464 Sciamanna G et al. (2012) Cholinergic Dysfunction Alters Synaptic Integration between Thalamostriatal and
465 Corticostriatal Inputs in DYT1 Dystonia. Journal of Neuroscience 32:11991-12004.
466 Simonyan K, Cho H, Hamzehei Sichani A, Rubien-Thomas E, Hallett M (2017) The direct basal ganglia pathway is
467 hyperfunctional in focal dystonia. Brain 140:3179-3190.
468 Smith Y, Galvan A, Ellender TJ, Doig N, Villalba RM, Huerta- I, Wichmann T, Bolam JP (2014) The thalamostriatal
469 system in normal and diseased states. Systems neuroscince 8:1-18.
470 Suppa A, Huang YZ, Funke K, Ridding MC, Cheeran B, Lazzaro VD, Ziemann U, Rothwell JC (2016) Ten Years of
471 Theta Burst Stimulation in Humans : Established Knowledge , Unknowns and Prospects.
472 Ulug AM, Vo A, Argyelan M, Tanabec L, Schiffera WK, Deweya S, Dauerc WT, Eidelberg D (2011)
473 Cerebellothalamocortical pathway abnormalities in torsinA DYT1 knock-in mice. Proceedings of the
474 National Academy of Sciences 108:6638-6643.
475 Vemula SR, Puschmann A, Xiao J, Zhao Y, Rudzinska M, Frei KP, Truong DD, Wszolek ZK, LeDoux MS (2013) Role of
476 Galpha(olf) in familial and sporadic adult-onset primary dystonia. Hum Mol Genet 22:2510-2519.
477 White JJ, Sillitoe RV (2017) Genetic silencing of olivocerebellar synapses causes dystonia-like behaviour in mice.
478 Nat Commun 8:14912.

479

480

481

482

## *Materials & Methods*

### *Animals*

All experiments were performed in accordance with the guidelines of the European Community Council Directives. *Gnal*+/- mice were mated with C57BL/6J mice to produce male and female *Gnal*+/- and WT littermates. Animals (males and females *Gnal*+/- and WT aged 3 to 7-months-old) were kept at a constant room temperature and humidity on 12 h light/dark cycle and with *ad libitum* access to water and food. All the motor control experiments were performed in males and females and recordings were performed in freely moving mice.

### *Open-field activity*

Mice were placed in a circle arena made of plexiglass with 38 cm diameter and 15 cm height (Noldus, Netherlands) and video recorded from above. Each mouse was placed in the open-field for a period of 5 min with the experimenter out of its view. The position of centre of gravity of mice was tracked using an algorithm programmed in Python 3.5 and the OpenCV 4 library. Each frame obtained from the open-fields' videos were analysed according to the following process: Open-field area was selected and extracted in order to be transformed into a grayscale image. Then, a binary threshold was applied on this grayscale image to differentiate the mouse from the white background. To reduce the noise induced by the recording cable or by particles potentially present in the Open-field, a bilateral filter and a Gaussian blur were sequentially applied, since those components are supposed to have a higher spatial frequency compared to the mouse. Finally, the OpenCV implementation of Canny algorithm was applied to detect the contours of the mouse, the position of the mouse was computed as mouse's centre of mass. The distance travelled by the mouse between two consecutive frames was calculated as the variation of position of the mouse's centre point multiplied by a scale factor, to allow the conversion

from pixel unit to centimetres. The total distance travelled was obtained by summing the previously calculated distances over the course of the entire Open-field session. The speed was computed as the variation of position of centre points on two consecutive frames divided by the time between these frames (the inverse of the number of frames per seconds). This speed was then averaged by creating sliding windows of 1 second. After each session, faecal boli were removed and the floor was wiped clean with a damp cloth and dried after the passing of each mouse.

***Horizontal bar test***

Motor coordination and balance were estimated with the horizontal bar test which consists of a linear horizontal bar extended between two supports (length: 90 cm, diameter: 1.5 cm, height: 40 cm from a padded surface). The mouse is placed in one of the sides of the bar and released when all four paws gripped it. The mouse must cross the bar from one side to other and latencies before falling are measured in a single trial session with a 3-min cut-off period.

***Vertical pole test***

Motor coordination was estimated with the vertical pole test. The vertical pole (51 cm in length and 1.5 cm in diameter) was wrapped with white masking tape to provide a firm grip. Mice were placed heads up near the top of the pole and released when all four paws gripped the pole. The bottom section of the pole was fixated to its home-cage with the bedding present but without littermates. When placed on the pole, animals naturally tilt downward and climb down the length of the pole to reach their home cage. The time taken before going down to the home-cage with all four paws was recorded. A 20 sec habituation was performed before placing the mice at the top of the pole. The test was given in a single trial session with a 3-min cut-off period.

***Gait test***

Motor coordination was also evaluated by analysing gait patterns. Mouse footprints were used to estimate foot opening angle and hindbase width, which reflects the extent of muscle loosening. The mice crossed an illuminated alley, 70 cm in length, 8 cm in width, and 16 cm in height, before entering a dark box at the end. Their hind paws were coated with nontoxic water-soluble ink and the alley floor was covered with sheets of white paper. To obtain clearly visible footprints, at least 3 trials were conducted. The footprints were then scanned and examined with the Dvrtk software (Jean-Luc Vonesch, IGBMC). The stride length was measured with hindbase width formed by the distance between the right and left hind paws.

***Grid test***

The grid test is performed to measure the strength of the animal. It consists of placing the animal on a grid which tilts from a horizontal position of 0° to 180°. The animal is registered by the side and the time it drops is measured. The time limit for this experiment is 30 seconds. In those cases where the mice climbed up to the top of grid, a maximum latency of 30 seconds was applied.

***Fixed speed rotarod***

Motor coordination, postural stability and fatigue were estimated with the rotarod (mouse rotarod, Ugo Basile). Facing away from the experimenter's view, the mice placed on top of the plastic roller were tested at constant speeds (5, 10, 15, 20 and 25 r.p.m.). Latencies before falling were measured for up to 3 min in a single trial session.

***Surgery***

554 Two surgeries were performed. During the first surgery, AAV2/1.hSyn.ChR2(H134R)-eYFP.WPRE.hGH
555 (700nl) was injected into the deep cerebellar nuclei of the *Gnal*+/- and WT mice (dentate nucleus, DN:
556 −6 mm AP, ±2.3 mm ML, −2.4 mm depth from dura). After 3 weeks, implantation surgery was
557 performed. For both surgeries, the mice were anesthetized either with a mixture of ketamine/xylazine
558 or with a mixture of isoflurane and O2 (3% for induction, 1,7% for maintenance). Injections with
559 buprenorphine (0.05 mg/kg, s.c.) were performed to control pain, and core temperature (37°C) was
560 maintained with a heating pad. The mice were fixed in a stereotaxic apparatus (David Kopf Instruments,
561 USA). After a local midline lidocaine injection s.c. (2%, 1ml), a medial incision was performed exposing
562 the skull. Small craniotomies were drilled above the recording sites and above the optic fibre location
563 (above the virus injection site) and then the electrodes were stereotaxically lowered inside the brain.
564 This allowed us to record in the left motor cortex (M1) (AP +2 mm and -2 mm ML from the Bregma),
565 ventro-lateral thalamus (VAL) (-1.34 mm AP, ML=-1.00 mm and DV=-3.4 mm depth from the dura) and
566 centro-lateral thalamus (CL) (AP at -1.58mm, ML=-0.8mm, DV=-3.00mm depth from the dura). The mice
567 were implanted with bundles of extracellular electrodes for each recording site. The ground wire was
568 placed on the surface of the cerebellum. Super Bond (Dental Adhesive Resin Cement, Sun Medical CO,
569 Japan) was applied on the surface of the skull to strengthen the connection between the bone and the
570 cement. Then, the cannulas and ground wire were fixed with dental cement (Pi-Ku-Plast HP 36, Bredent
571 GmbH, Germany). The bundles of 8 electrodes were made in house by folding and twisting nichrome
572 wire with 0.005 inches diameter (Kanthal RO-800) (Menardy et al., 2019). The bundles were placed
573 inside guide cannulas (8-10 mm length and 0.16-0.18 mm inner diameter, Coopers Needle Works
574 Limited, UK) glued (Loctite universal glue) to an electrode interface board (EIB-16; Neuralynx, Bozeman,
575 MT, USA) with 1 wire for each channel and 4 channels for each brain region (M1, CL, VAL), extending 0.5
576 mm below the tube tip. Wires were then fixed to the EIB with gold pins (Neuralynx, Bozeman, MT, USA)

577 and then the EIB was secured in place by dental cement. A gold solution (cyanure-free gold solution,
578 Sifco, France) was used for gold plating and the impedance of each electrode was set to 200–500 kΩ.
579
580 ***Manipulations of cerebellar output***
581 Because the cerebellar nuclei sends projections in the contralateral thalamus that then connects with
582 the M1 (Teune et al., 2004) optogenetic stimulations were performed in the contralateral cerebellar DN
583 (left M1 and right DN). Light-induced excitation of the cerebellar-projection neurons was elicited by
584 using a LED driver (Mightex Systems®) through optical fibres radiating blue light (470 nm) unilaterally
585 implanted into the deep cerebellar nuclei (light intensity of ~1.5mW/mm2). Optogenetic stimulations of
586 the DN (1000 mA, 100ms, 0.25Hz or theta-burst stimulation 1000 mA, 20ms, 8,33Hz, applied for 2 x 40s
587 with a 2 min pause in between) were performed before and after triggering the dystonic attacks by an
588 oxotremorine methiodide (oxotremorine M) intraperitoneal injection.
589
590 ***Electrophysiological recordings***
591 The recordings begun after at least 3 days of recovery and were performed on awake freely moving
592 mice using a 16-channel acquisition system with a sampling rate of 25 kHz (Tucker Davis Technology
593 System 3, Tucker-Davis Technologies, Alachua, FL, USA). We performed 60 minutes baseline recording in
594 an open-field, followed by a 60 min recording after a saline injection. *Gnal*+/- and WT mice were then
595 injected intraperitoneally with oxotremorine methiodide (0.1 mg/kg, Sigma-Aldrich), dissolved in saline
596 (NaCl 0.9g/L) and recorded another 60 min with the same protocol as for saline. Optogenetic stimuli
597 were applied on the DN at low frequency stimuli of 100 ms, 1000 mA and 0.25 Hz. On the next day,
598 theta burst stimulations was implemented. The mice were recorded 60 min after the saline injection and
599 then 60 min after the oxotremorine M injection using the same protocol as in baseline day except that

after 30 minutes 2 theta-burst sessions of 40 sec each with 2 minutes pause in between were applied (a total of 600 pulses for each condition).

***Histological verification of the site of optical fibre in DN and verification of the position of the electrodes.***

The animals were sacrificed with a single dose of pentobarbital (100mg/kg, i.p.). Electrolytic lesions were performed to check the position of the electrodes, mice were perfused with paraformaldehyde and the brains were removed and kept in paraformaldehyde (4%). After slicing (using a vibratome at 90 µm thickness), all sites of the recordings were verified by superposing the atlas (Allen Brain Atlas) on slices, with the closest anatomical landmarks from our lesions used as reference points. *(Figure 1.D)*

***Behavioural Analysis***

Video recordings monitored the motor behaviour of *Gnal*+/- and WT mice in the open-field. Dystonia severity was estimated using a previously published abnormal movement scoring scale (Jinnah et al., 2000; Calderon et al., 2011; Pelosi et al., 2017) for every 10 min-long block of the recording, after the oxotremorine M injection was performed. The assessment was blinded for mouse genotype and was done by 2 members of the team. The scale uses the following scores: 0= normal motor behavior; 1=no impairment, but slightly slowed movements; 2. Mild impairment: occasional abnormal postures and movements; ambulation with slow walk; 3. Moderate impairment: frequent abnormal postures and movements with limited ambulation; 4. Severe impairment: sustained abnormal postures without any ambulation or upright position. In addition, total time of active wakefulness from the total time of recording (active wake percentages, AW%) was assessed for both states, pre and post oxotremorine and pre and post theta-burst stimulation. Active wake was considered as the state when the mouse is exploring the open-field by walking in any direction and is expressed as a percentage of the total time of

the recording (Georgescu et al., 2018). We evaluated the impact of theta-burst DN stimulation on the onset of dystonic-like symptoms in saline- and oxotremorine-treated *Gnal*+/- mice.

***Electrophysiological Analysis***

Spike sorting was completed using homemade Matlab scripts (Mathworks, Natick, MA, USA) that are based on *k-means clustering on PCA of the spike waveforms* (Paz et al., 2006). In order to evaluate the activity of the same cells in similar conditions during experiments, we investigated the change of the firing rate probability in the thalamus and M1 motor cortex during cerebellar DN 100ms stimulations after saline or oxotremorine M administration performed and analyses in one continuous session. The average increase in firing rate during the stimulation was determined by computing the peri-stimulus time histogram (bin: 10ms) of the spikes around the stimulation; the spike count in the histogram was divided by the duration of the stimulation and the number of stimulations administered to yield a firing rate. The acceleration of discharge due to the stimulation was taken as the average spike count during the stimulation subtracted by the baseline (taken as the 300ms that preceded the stimulation onset). The response to stimulation was only analysed in cells where at least one bin during the stimulation was larger than 4 times the standard deviation of the baseline values

***Statistics***

Figures represent the averages ± standard error of the mean (SEM). Student T test, Mann-Whitney test, repeated-measure ANOVA and multiple comparisons test was used as appropriate, after testing the normality of the data by D'Agostino and Pearson omnibus normality test.

***Figure legends:***

**Figure 1.** Locomotor activity and motor coordination in *Gnal*+/- mice. **(A)** Latency to cross the vertical pole; Mann-Whitney test. **(B)** Latency to cross the horizontal bar; Mann-Whitney test. **(C)** Latency to fall during the grid test with a 30s cut-off; Mann-Whitney test. **(D)** Latency to fall during the fixed speed rotarod test; Repeated measure ANOVA. **(E)** Latency to fall during the fixed speed rotarod test with groups separated by gender and genotype; Welch corrected Student's t test for each speed step, corrected for multitests using Bonferroni's method. **(F)** Gait width, alternation coefficient, movement linearity, sigma and stride length during the gait test; Mann-Whitney test *p<0.05; **p<0.01 **(G)** Example of heatmaps showing the position of mice during open-field sessions. Average speed **(H)** and total distance travelled **(I)** during an open-field session; Mann-Whitney test *p<0.05; **p<0.01.

**Figure 2.** Electrophysiology recordings of ventro-lateral VAL and centro-lateral CL thalami nuclei and M1 motor cortex. **(A)** Picture of a freely moving mouse during a recording coupled with optogenetic DN stimulation. **(B)** Schematic of experimental design. Guide cannulas with bundles of electrodes were inserted in left M1 (motor cortex), CL (centro-lateral thalamus), VAL (ventro-lateral thalamus); an optic fibre was inserted in the right DN 3 weeks after AAV2/1.hSyn.ChR2(H134R)-eYFP.WPRE.hGH virus was injected. **(C)** Histology section showing the implantation sites. An atlas map is overlaid on the coronal sections to identify the targeted regions. **(D)** Left: excerpts of traces and spikes (coloured bars); right: average ± SEM waveforms of VAL, CL and M1 neurons. **(E)** Average firing rate in freely moving WT and *Gnal*+/- mice.

**Figure 3.** Effect of low-frequency and theta-burst cerebellar stimulations on the firing rate in saline and oxotremorine conditions in VAL, CL and M1 of WT and *Gnal+/-* mice. On the first day, we examined the

671 effects of low frequency opto-stimulations (blue line, 100ms, 0.25Hz) on the firing rate of neurons in the
672 various brain regions after saline and oxotremorine administrations. On the following day, the effects of
673 the same low frequency stimulation were compared before and after θ-burst stimulations (20ms,
674 8,33Hz, applied for 2 x 40s with a 2 min pause in between) after saline and oxotremorine
675 administrations. **(A)** Raster and peristimulus time histogram (PSTH, bin 10 ms) for one VAL neuron from
676 a WT mouse before (left) and after (right) theta-burst stimulation in saline condition; the PSTH are
677 normalized to express a firing rate (see Methods). **(B)** Overlay of the PSTHs from the panel A; the
678 difference between the histograms is filled to evidence the potentiation or depression of the responses.
679 In this case potentiation prevails. See Table 1 for number of cells/mice used. **(C)** Increase in firing rate
680 (relative to the baseline firing rate) induced by 100 ms DN nucleus stimulations in WT and *Gnal*+/-
681 animals. **(D)** Impact of theta-burst stimulations administered in saline condition on the response to 100
682 ms DN stimulation. Note the absence of potentiation in *Gnal*+/- mice. **(E)** **(F)** same as (A) and (B)
683 respectively, for a VAL neuron from a *Gnal*+/- mouse before and after theta-burst stimulation in the
684 oxotremorine condition. **(G)** effect of oxotremorine administration on the response to cerebellar
685 stimulations. **(H)** Impact of theta-burst stimulations on the response to 100 ms DN stimulation (same as
686 (D)) in the oxotremorine condition. See Table 2 for corresponding repeated measures ANOVAs. *p<0.05,
687 **p<0.01, ***p<0.001 paired difference between conditions for the cells, $^{\#}$p<0.05 difference between
688 *Gnal*+/- and WT mice. Error bars represent SEM.
689
690 **Figure 4.** Motor behavior of *Gnal*+/- (orange) and WT mice (grey). **(A)** Examples of dystonic postures in
691 *Gnal*+/- mice following oxotremorine M administration. **(B)** Average dystonia scores in *Gnal*+/- and WT
692 mice following oxotremorine M administration before and after dentate theta-burst stimulation **(C)**
693 Change of average active wake percentage after one session of DN theta-burst stimulation in *Gnal*+/-
694 and WT mice. Data were analysed by repeated measure ANOVA. **p<0.01 difference between pre and

695 post theta-burst stimulations. Error bars represent SEM.

696

697 **Table 1**. Number of cells used in the analysis of baseline firing rate (Figure 2E) and of responses to
698 cerebellar stimulation (Figure 3C,D,G,H).

699

700 **Table 2.** Repeated measure ANOVA for the increase in firing rate induced by low-frequency DN
701 stimulations in the VAL and CL thalamus, and motor cortex M1 in saline/oxotremorine conditions and
702 before/after theta-burst stimulations.

Figure 1

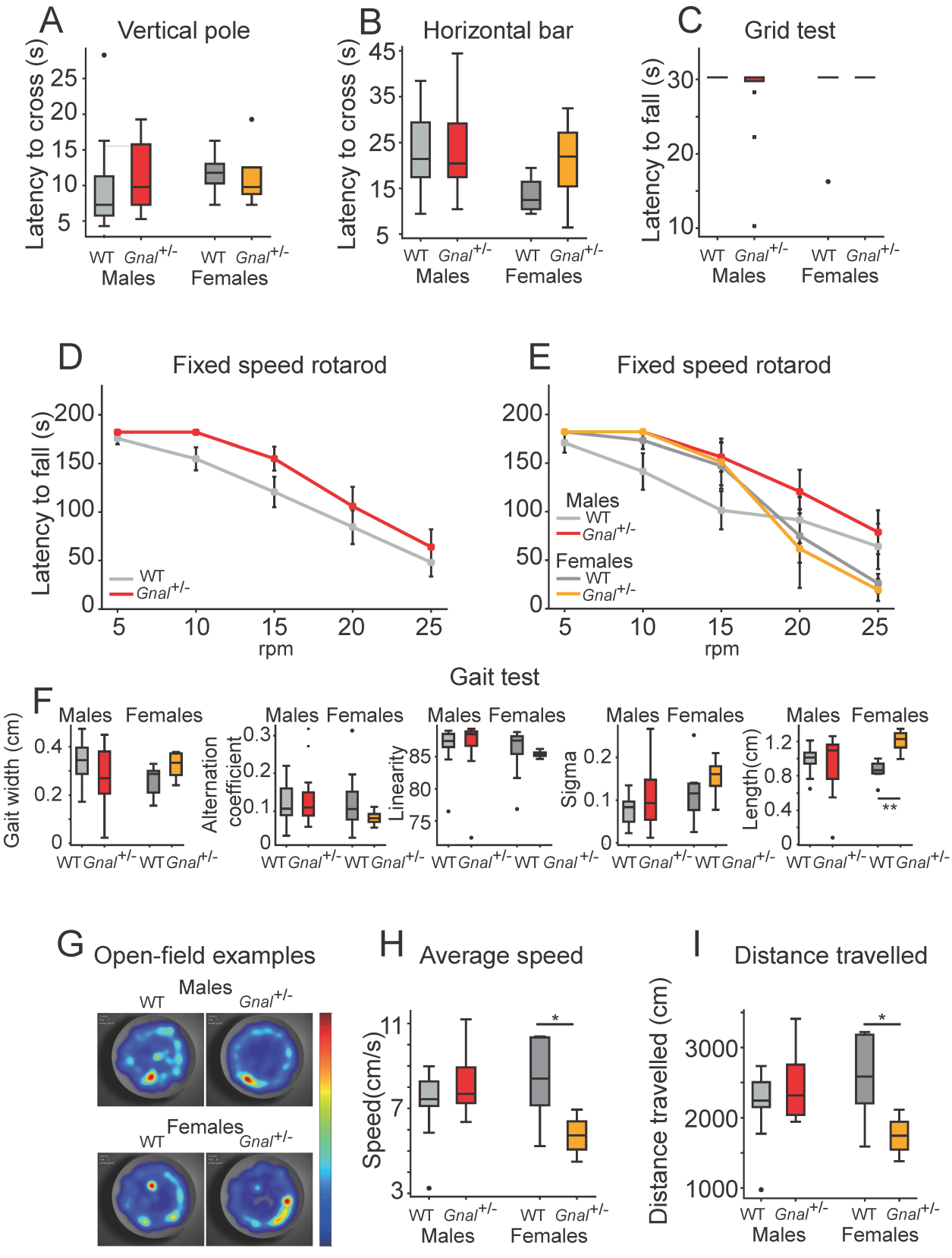

Figure 2

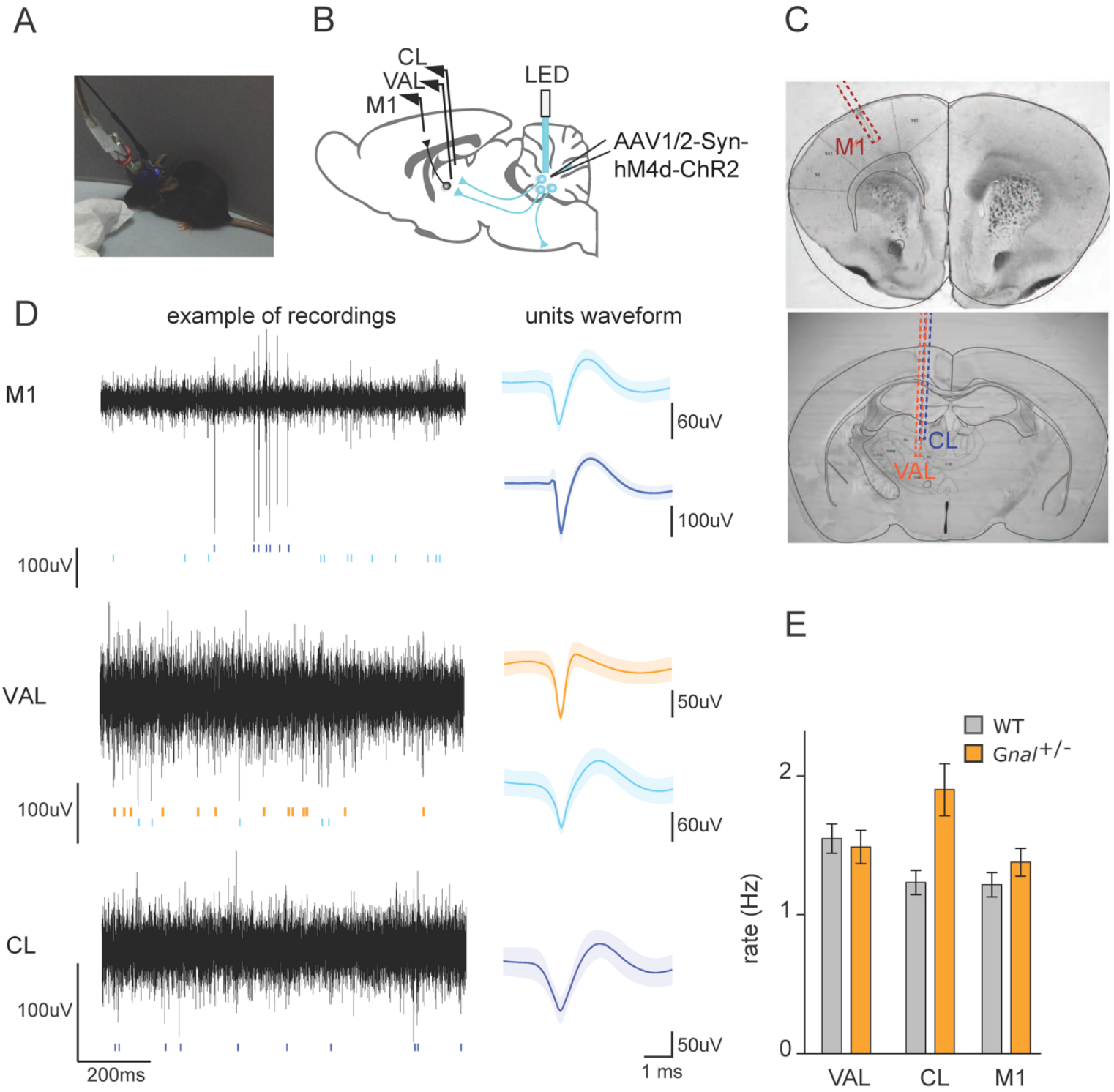

# Figure 3

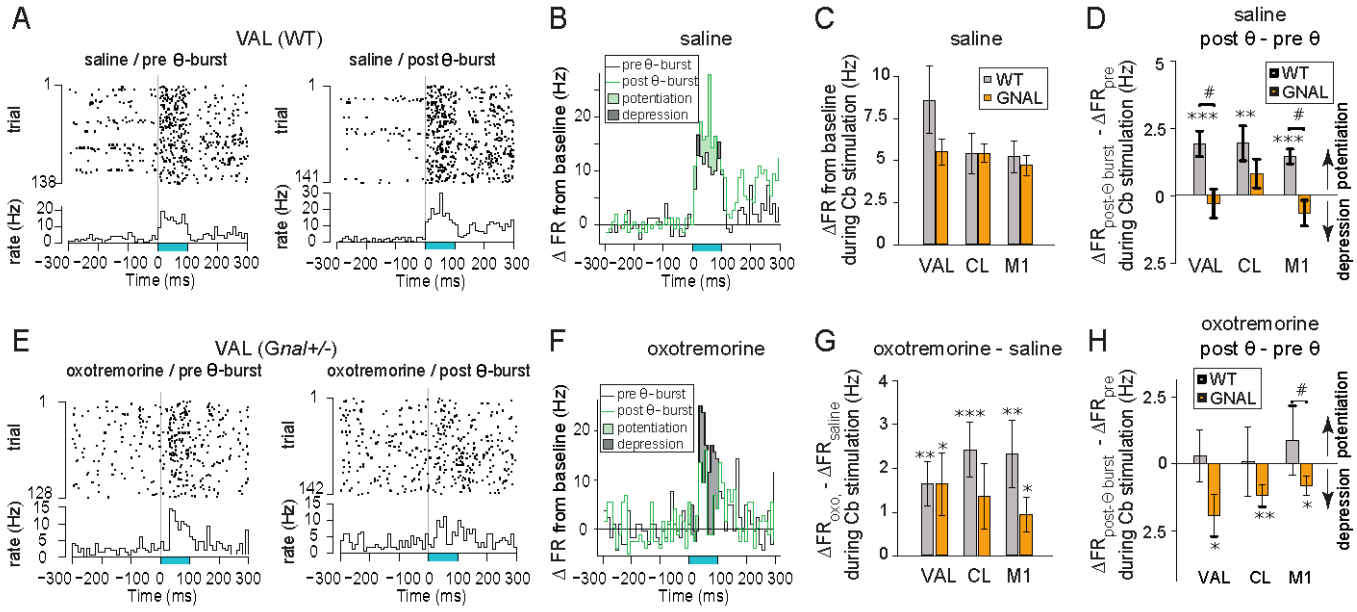

Figure 4

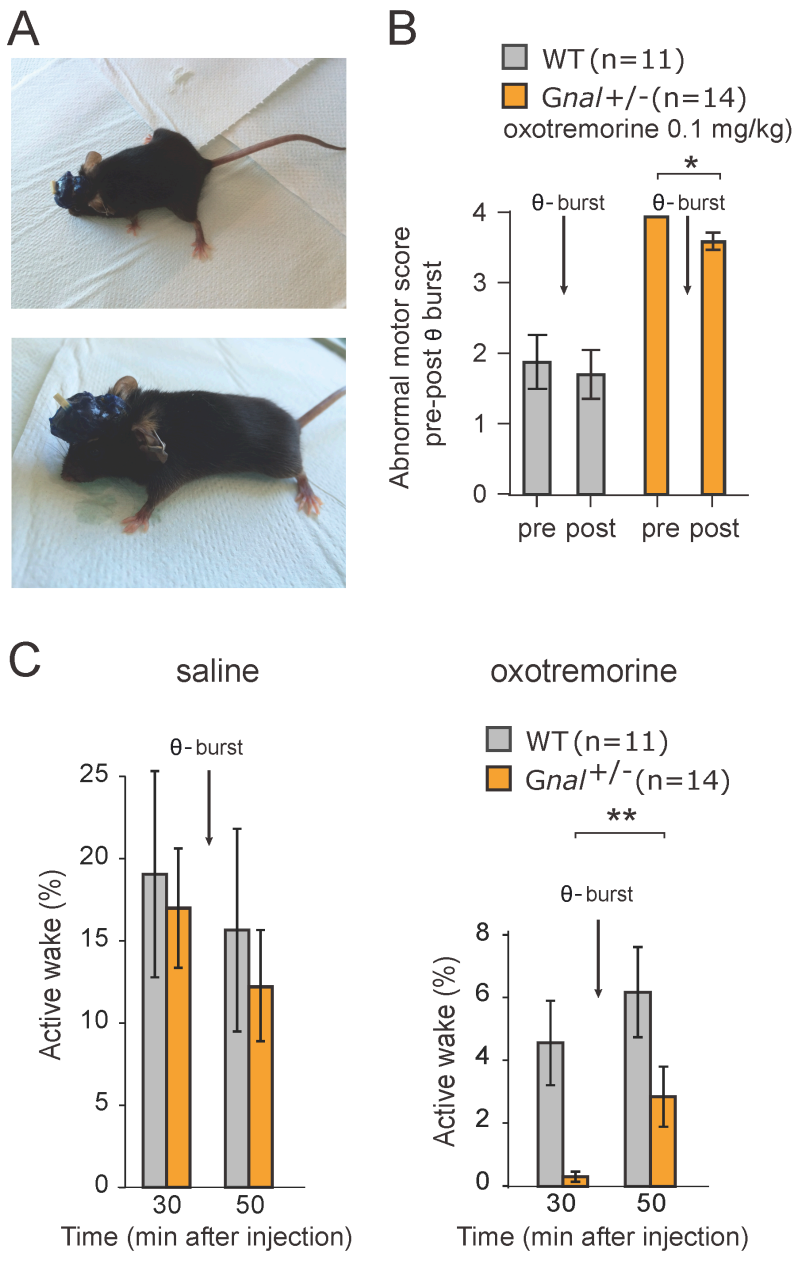

Table 1

| | FR analysis | | | | Cb stim analysis | | | |
|---|---|---|---|---|---|---|---|---|
| | # cells | | # mice | | # cells | | # mice | |
| region | WT | HET | WT | HET | WT | HET | WT | HET |
| VAL | 179 | 221 | 8 | 10 | 23 | 21 | 3 | 4 |
| CL | 236 | 194 | 12 | 11 | 31 | 27 | 5 | 3 |
| M1 | 210 | 237 | 13 | 12 | 37 | 54 | 5 | 5 |

Table 2

| | | REGION RECORDED | | |
|---|---|---|---|---|
| TREATMENT | CONDITION | VAL | CL | M1 |
| Oxotremorine | WT | F(1,22)=10.38 P=0.003928 | F(1,30)=14.45 P=0.0006566 | F(1,36)=9.025 P=0.004824 |
| | GNAL +/- | F(1,20)=5.184 P=0.03394 | F(1,26)=3.301 P=0.08076 | F(1,53)=5.283 P=0.0255 |
| | Genotype ≠ | F(1,40)=0.1006 P=0.7527 | F(1,51)=1.214 P=0.2758 | F(1,80)=0.2567 P=0.6138 |
| Saline + θ-burst | WT | F(1,22)=16.11 P=0.0005835 | F(1,30)=8.812 P=0.005834 | F(1,36)=27 P=8.229e-06 |
| | GNAL+/- | F(1,20)=0.3588 P=0.5559 | F(1,26)=2.258 P=0.145 | F(1,53)=1.96 P=0.1674 |
| | Genotype ≠ | F(1,37)=4.791 P=0.03499 | F(1,48)=0.2916 P=0.5917 | F(1,78)=4.047 P=0.04771 |
| Oxo+ θ-burst | WT | F(1,22)=0.0858 P=0.7723 | F(1,30)=0.003561 P=0.9528 | F(1,36)=0.442 P=0.5104 |
| | GNAL+/- | F(1,20)=5.928 P=0.0244 | F(1,26)=8.154 P=0.008334 | F(1,53)=5.459 P=0.02329 |
| | Genotype ≠ | F(1,40)=2.681 P=0.1094 | F(1,53)=0.3898 P=0.5351 | F(1,84)=5.075 P=0.02688 |

## RÉSUMÉ

Une acquisition sensorielle et une perception précises sont des éléments clés de la survie. Bien que de nombreux paramètres sous-jacents au traitement des informations sensorielles soient connus, plusieurs aspects sont encore mal compris, comme la contribution exacte de chaque structure cérébrale. Ici, nous analysons la contribution cérébelleuse au traitement sensoriel dans le système des vibrisses de la souris. Nous identifions une projection anatomique et physiologique disynaptique des noyaux cérébelleux vers le cortex sensoriel primaire, impliquant notamment le thalamus postérieur médian (POm). La modulation de cette projection cérébelleuse et thalamique de type "driver" induit un déficit dans une tâche de discrimination sensorielle fine, et sa co-activation avec des entrées périphériques induit le recrutement accru des projections du POm dans la couche I du cortex sensoriel. Dans leur ensemble, nos résultats montrent que le cervelet cible aussi des zones corticales non motrices et peut directement moduler le traitement sensoriel par l'intermédiaire d'un noyau thalamique d'ordre élevé, le POm.

## MOTS CLÉS

Neuroscience ; Cervelet ; Cortex ; Thalamus ; Système sensoriel ; Vibrisse ; Electrophysiologie ; Imagerie calcique ; Comportement ; Optogénétique ; Chemogénétique ; Anatomie ; Traçages viraux

## ABSTRACT

Accurate sensory acquisition and perception are key features to survival. Though many parameters underlying the processing of sensory information is known, several aspects are still poorly understood, such as the exact contribution of each cerebral structure. Here, we analyze the cerebellar contribution to sensory processing in the mouse whisker system. We identify an anatomical and physiological disynaptic projection from the cerebellar nuclei to the primary sensory cortex, involving notably by the posterior medial thalamus (POm). The modulation of this strong driver-like cerebello-thalamic projection induces an impairment in a fine sensory discrimination task, and its co-activation along with peripheral inputs induces the increased recruitment of POm projections to layer I of sensory cortex. Taken together, our results show that the cerebellum targets non-motor cortical areas and can directly modulate sensory processing through a higher order thalamic nucleus, the POm.

## KEYWORDS

Neuroscience ; Cerebellum ; Cortex ; Thalamus ; Sensory systems ; Whiskers ; Electrophysiology ; Calcium Imaging ; Behavior ; Optogenetic ; Chemogenetic ; Anatomy ; Viral tracings